RENEWABLE SOURCES BASED MICRO-GRID CONTROL SCHEMES AND RELIABILITY MODELING

RAZZAQUL AHSHAN

Renewable Sources Based Micro-grid Control Schemes and Reliability Modeling

by

©Razzaqul Ahshan, MEng.

A thesis submitted to the

School of Graduate Studies

in partial fulfillment of the

requirements for the degree of

Doctor of Philosophy

Faculty of Engineering and Applied Science

Memorial University of Newfoundland

April 2013

St. John's Newfoundland

Abstract

The micro-grid is a low rated, cost-effective, and multi-form micro-generation based modern power system. This system has many advantages such as the large scale integration of renewable power generation, the ability to provide power to rural and/or isolated communities and to maximize the usage of renewable power sources. This is because a micro-grid system can provide reliable power, improve the overall system efficiency, reduce system cost and increase the penetration level of renewable power in next generation power systems. The diverse combination of micro-generation in a micro-grid system makes the reliable operation and control of the system a remarkable challenge in stand-alone applications. A micro-grid system comprised of renewable micro-generation is presented in this thesis. Key issues such as the system's dynamic behaviour, continuous power adjustment in an isolated micro-grid system with and without wind power generation, micro-grid test set up and reliability assessment are investigated as part of this work.

An integrated dynamic model of a micro-grid system consisting of wind and hydro based micro-generation is first developed. This model is utilized to investigate the system behaviour under various modes of operations with the objective of revealing the nature of technical issues related to stable and reliable operation of the micro-grid system. The micro-grid control concepts are introduced to establish fast and accurate balance between micro-grid power generation and loads. An active power controller based on AC voltage control technique is developed to maintain real power equilibrium between generations and loads during the operating mode of an isolated micro-grid system with wind power generation.

A governor controlled pumped hydro storage system is also investigated for regulating system frequency during the operating mode of an isolated micro-grid

system without wind power generation. An alternative inverter interfaced storage control scheme for micro-grids in stand-alone and utility grid-connected modes of operation is introduced to achieve fast and accurate power balance between generation and loads. In addition, a micro-grid test set up is developed to verify and validate the controllers' performances obtained through simulation study.

Reliability assessment of the proposed micro-grid system is investigated. As part of this study, the reliability model of various sub-systems in a micro-generation unit is developed and used to formulate a model for the micro-grid system reliability study. It is found that the proposed micro-grid system is sufficiently reliable to generate and supply power during its various operational modes.

Acknowledgments

I would like to express my sincere gratitude and appreciation to Dr. Tariq Iqbal, Dr. George Mann and Dr. John Quaicoe for their invaluable guidance, advice and financial support throughout the course of this work. Without their help, this work would not be possible and I am grateful to them for their patience, support and friendly attitude. I thank Dr. Saleh Saleh for his suggestions and input.

Financial support for this project has been provided by the National Science and Engineering Research Council of Canada (NSERC), the Atlantic Innovation Fund (AIF) of the Atlantic Canada Opportunities Agency (ACOA), and the School of Graduate Studies, Memorial University of Newfoundland. I also wish to thank the Faculty of Engineering and Applied Science and Memorial University of Newfoundland, for providing much needed laboratory space, equipment and technical services to take this project from idea to implementation.

Special thanks and appreciation are expressed to my family, and to my wife, Nigar Sultana, for their great encouragement and support. Most of all, a deep appreciation and thanks to my parents, Jahurul Haque and Rabeya Khatun, whose love and encouragement is a key force in my life; without that, it would not be possible for me to ride on the path of my goal.

Finally, thanks to my little angel, Nameera Ahshan, who took me out of all my anxiety and made me laugh when I came home from my studies.

Dedication

To my little daughter (Nameera Ahshan), wife (Nigar Sultana), parents (Jahurul Haque and Rabeya Khatun).

Contents

List of Tables

List of Figures

List of Symbols

$(G_d)_{k,m}, G_{q(k,m)}, G_{0(k,m)}$ $dq0$ components of conductance

3ϕ	Three phase
α	Firing angle
α_s	Shear exponent
$\bar{P}_m$	Mechanical power in per unit
$\bar{q}_{nl}, \bar{q}_{fl}$	Per unit water flow at no load and full load
$\bar{S}_k$	Three phase apparent power
β	Pitch angle of rotor blades
ΔP	Deviated power at the micro-grid system
ΔT_{j_i}	Variation in junction temperature for i^{th} wind speed
ϵ	Power mismatch threshold
ϵ_a	Absolute roughness
η_{gt}	Generator-turbine efficiency
$\frac{\partial P}{\partial V_d}, \frac{\partial P}{\partial V_q}, \frac{\partial Q}{\partial V_d}, \frac{\partial Q}{\partial V_q}$	Elements of the Jacobian matrix

λ_i	Intermediate variable to calculate tip speed ratio
λ_{opt}	Optimal tip speed ratio of the wind turbine emulator
$(\omega_{rm})_{im}$	Mechanical angular speed of the induction motor rotor
$(\omega_{rm})_{sm}$	Mechanical angular speed of the synchronous machine
$(Q_k)_{max}$	Maximum reactive power for k^{th} bus
$(Q_k)_{min}$	Maximum reactive power for k^{th} bus
$\left(Q_k^{(n)}\right)_c$	Calculated reactive power for k^{th} bus at n^{th} iteration
$(T_{em})_{im}$	Electromagnetic torque of the induction motor
$(T_{em})_{sm}$	Electromagnetic torque of synchronous machine
$(T_m)_{sm}$	Mechanical torque of synchronous machine
$(T_m)_{wt}$	Wind turbine torque
$[Z_A], [Z_B], [Z_C]$	Coefficients of impedance matrix
$[\mathbf{Y}]$	Admittance matrix
$[\mathbf{Z}]$	Impedance matrix
$\mathbb{T}$	Transformation matrix
$\mathbb{Y}_{dq0}$	$dq0$ components of three phase admittance quantities
μ	Water viscosity
ω	System nominal angular frequency

ω_e	Speed of the synchronously rotating reference frame
ω_m	Angular velocity of turbine rotor
ω_r	Electrical angular speed of the rotor
$\omega_{wt,i}$	i^{th} wind turbine speed seen by the gear box
$\omega_{wt,m}$	Maximum operating speed of the wind turbine seen by the gear box
$\omega_{wt,s}$	Starting speed of the wind turbine seen by the gear box
ϕ	Micro-grid voltage angle
$\boldsymbol{\lambda^{(n)}}$	Bus voltage vector at n^{th} iteration
$\boldsymbol{\lambda}$	Bus voltage vector
ρ	Air density
ρ_w	Water density
$\tau_{ciw_C}, \tau_{ciw_C}$	Failure rates of a component in the interfacing power electronic system at cut-in and cut-out wind speed
τ_{ciw}, τ_{cow}	Failure rates of the interfacing power electronic system at cut-in and cut-out wind speed
τ_i	Failure rate of a component at i^{th} wind speed
θ	Inverter voltage angle
θ_{gb}, β_{gb}	Shape and scale parameter for the wind turbine speed seen by the gear box

θ_{gp}, β_{gp}	Shape and scale parameter for wind turbine generator power distribution
$\theta_{IPE_C}, \theta_{IPE_C}$	Shape parameter and scale factor for failure rate distribution of a component of an interfacing power electronic system
$\theta_{IPE}, \beta_{IPE}$	Shape parameter and scale factor for failure rate distribution of an interfacing power electronic system
θ_{tp}, β_{tp}	Shape and scale parameter for wind turbine power distribution
θ_{ws}, β_{ws}	Shape and scale parameter for wind speed data
$\varphi'_{dr}, \varphi'_{qr}$	d and q components of rotor flux linkage
$\varphi'_{dr}, \varphi'_{qr}$	d and q rotor flux linkage
φ'_{fd}	d-axis field winding flux linkage
$\varphi'_{kd}, \varphi'_{kq1}, \varphi'_{kq2}$	d and q-axis damper winding flux linkage
$\varphi_{ds}, \varphi_{qs}$	d and q components of stator flux linkage
φ_d, φ_q	d and q-axis components of stator flux linkage
$\varphi_{mds}, \varphi_{mqs}$	d and q-axis mutual flux linkage components
a, b	Coefficients of linear regression line
A_{pen}	Cross sectional area of the penstock
A_{SA}	Swept area covered by the turbine rotor
A_{TG}	Hydro turbine gain

$B_{d(k,m)}, B_{q(k,m)}, B_{0(k,m)}$	$dq0$ components of susceptance
C_{DC}	DC link capacitor
C_F	Capacitor for LCL filter
C_p	Power coefficient
C_q	Torque coefficient of the wind turbine emulator
d	Diameter of the pipe
D_c	Power variation coefficient
$e(t)$	Error between expected and actual control variable
E_A	Activation energy for typical semiconductor components
E_{on}, E_{off}	Turn-on and Turn-off energies of an IGBT
E_{sr}	Rated switching loss of energy
f	Friction factor for steel pipe
$F\left(\omega_{rm}\right)_{sm}$	Friction co-efficient of synchronous machine
f_{base}^{+}	Change in frequency in the system
f_{base}	Base frequency of the system
F_{crit}	Threshold test statistic value obtained from F-distribution curve
f_s	Switching frequency
F_{wg}	Friction co-efficient for wind generator

G	Gate position
g	Gravitational acceleration
g_1, g_2	Gate opening at full load and no load
H	Head at the turbine inlet
h_1	Height of the anemometer
h_2	Hub height
H_L	Head loss due to friction
H_s	Water column static head
H_t	Total head to lift water
i'_{dr}, i'_{qr}	d and q components of rotor current
i'_{fd}	d-axis field current component
$i'_{kd}, i'_{kq1}, i'_{kq2}$	d and q-axis components of damper winding current
$i_{agc}, i_{bgc}, i_{cgc}$	Current flow between the supply end converter and the grid
I_{Dc}, I_{Qc}	$d-q$-axis command currents
i_{dgc}, i_{qgc}	d and q components of current flow between the supply end converter and the grid
i_{ds}, i_{qs}	d and q components of stator current
i_d, i_q	d and q components of stator current of synchronous machine
I_{kd}, I_{kq}, I_{k0}	$dq0$ current components of the k^{th} bus

I_{mo}	Maximum output current of the inverter
J_{sm}	Total moment of inertia of synchronous machine
J_{wg}	Moment of inertia for wind generator
K	Gain which is equal to proportional gain of the PID controller
k	Discrete time step
K_B	Boltzmann constant
k_p, k_i	Proportional and integral gain of the active power controller
L	Length of the penstock
l	Length of the pipe
$L\left(T_{j_i}\right)$	Life time of a component for i^{th} wind speed
L'_{lfd}	Leakage inductance of the d-axis field winding
$L'_{lkd}, L'_{kq1}, L'_{kq2}$	d and q-axis components of leakage inductance of the damper winding
L_d, L_q	d and q-axis inductance due to leakage and magnetizing component
L_{ed}, L_{eq}	d and q-axis total equivlent inductance
L_G	Grid side inductor of the LCL filter
L_I	Inverter side inductor of the LCL filter
L_{lss}	Leakage inductance of the synchronous machine stator winding
L_{ls}, L'_{lr}	Leakage inductance of stator and rotor winding

L_{md}, L_{mq}	d and q-axis components of magnetizing inductance
L_m	Magnetizing inductance
L_o	Quantitative normal life measurement (assumed to be 10^6)
M	The test statistic value
m	Modulation index
M_i	Approximation of the test statistic value
N	Number of wind turbines in a wind power generation system
N_{shaft}	DC motor shaft speed
$P(v_\omega)$	Wind turbine real power output
p^+_{base}	Change in power due to change in frequency
p_0, p_1, p_2	Gain of the discrete controller
p_{base}	Power in a system at base frequency
P_{ciw}	Power at cut-in wind speed
$P_{cl,d}, P_{sl,d}$	Conduction and switching loss of a diode
$P_{cl,IGBT}, P_{sl,IGBT}$	Conduction and switching loss of an IGBT
P_{cow}	Power at cut-out wind speed
P_C, Q_C	Command active and reactive power
P_{DFIG}	Active power of the doubly-fed induction generator

$P_{g,ciw}, P_{g,cow}$	Generator power at cut-in and cut-out wind speed
$P_{g,i}$	Generator power for i^{th} wind speed
P_{gc}	Generation capacity of hydro storage unit
P_h	Active power output of the hydro unit
P_{imp}	Power required at the pump impeller
P_i	Power for i^{th} wind speed in between the cut-in and cut-out region
P_{L1}	Load active power
P_{l_i}	Power loss in a semiconductor component at the i^{th} wind speed
P_l	Power loss in a semiconductor component
P_{opt}	Optimal power output of the wind turbine emulator
P_o	Wind turbine rotor output power
P_r	Wind turbine rated output power
p_{sm}	Number of pole pairs of synchronous machine
$P_{tl,d}$	Total diode power losses in the interfacing power electronics system
$P_{tl,IGBT}$	Total switches power losses in the interfacing power electronics system
Q	Water flow rate
$Q(v_\omega)$	Wind turbine reactive power consumption
Q_{DFIG}	Reactive power of the doubly-fed induction generator

Q_h	Reactive power output of the hydro unit
Q_{L1}	Load reactive power
r	Total number of data in a test data set
r'_{fd}	d axis field winding resistance
$r'_{kd}, r'_{kq1}, r'_{kq2}$	d and q axis damper winding resistances
R_d	Diode resistance
R_e	Reynolds number
r_f, L_f	Filter resistance and inductance for the supply end converter
$R_{gb_{wt,i}}$	Reliability of the gear box for i^{th} turbine speed seen by the gear box
R_{gb}	Reliability of the gear box
R_g	Reliability of generating power by the wind turbine generator
R_{HGU}	Reliability of a hydro generation unit
R_{IPE_C}	Reliabilty of a component in the interfacing power electronic system
R_{IPE}	Reliability of an interfacing power electronic system
R_{ja}	Junction resistance at ambient temperature
$R_{MSR_{M1}}$	Micro-grid system reliability for Mode-I
$R_{MSR_{M2}}$	Micro-grid system reliability for Mode-II
$R_{MSR_{M3}}$	Micro-grid system reliability for Mode-III

R_{MSR}	Micro-grid system reliability
$R_{P_{g,i}}$	Reliability of generator power for i^{th} wind speed
R_{P_i}	Reliability of generating power at i^{th} wind speed
r_{ss}	Synchronous machine stator winding resistance
r_s, r'_r	Stator and rotor winding resistance of induction machine
R_{tp}	Reliability of generating power by the wind turbine rotor
R_t	Radius of turbine rotor
R_{UG}	Reliability of the utility grid
R_{WPGS}	Reliability of a wind power generation system
R_{wts}	Reliability of a wind turbine system
T_{av}	Average torque produced by the wind turbine emulator
T_a	Ambient temperature
T_D	Derivative time of the controller
T_I	Integral time of the controller
T_{j_i}	Junction temperature of a semiconductor component at the i^{th} wind speed
T_j	Junction temperature of a semiconductor device
T_o	Sampling time
$T_r(\theta)$	$\alpha\beta$ to dq transform matrix

T_{shaft}	Torque produced at the DC motor shaft
T_t	abc to $\alpha\beta$ transform matrix
T_w	Water time constant
$u(t)$	Output of the controller at any instant t
u_{cs}	Control signal for the active power controller
v	Water velocity
$V_{dr}'^*, V_{qr}'^*$	d and q components rotor voltage reference for generator side converter
V_{drcor}', V_{qrcor}'	Correction factor for d and q component rotor voltage reference for generator side converter
V_{dr}', V_{qr}'	d and q components of rotor voltage
V_{fd}'	d-axis field voltage component
$V_{kd}', V_{kq1}', V_{kq2}'$	d and q-axis components of damper winding voltages
$V_{ai}^s, V_{bi}^s, V_{ci}^s$	Voltages at the supply end converter
V_{di}^s, V_{qi}^s	d and q components of voltage at the supply end converter
V_α, V_β	$\alpha\beta$ components of micro-grid voltage
V_{ag}, V_{bg}, V_{cg}	Voltages at the grid terminal of the supply end converter
$V_{amg}, V_{bmg}, V_{cmg}$	Micro-grid three phase voltages
V_{CEO}, R_{ce}	IGBT threshold voltage and on-state resistance, respectively

v_{ciw}	Cut-in wind speed
v_{cow}	Cut-in wind speed
v_{cow}	Cut-out wind speed
V_{dc}, I_{dc}	Actual commutation voltage and current
V_{dg}, V_{qg}	d and q components of voltage at the grid terminal of the supply end converter
V_{ds}, V_{qs}	d and q components of stator voltage
V_d, V_q	d and q components of stator voltage of synchronous machine
V_D, V_Q	$d-q$-axis voltage components for command current calculation
V_{F0}	Diode threshold voltage
V_{kd}, V_{kq}, V_{k0}	$dq0$ voltage components of the k^{th} bus
V_{md}, V_{mq}, V_{m0}	$dq0$ voltage components of the m^{th} bus
V_M	Maximum voltage magnitude
$V_{ref,d}, I_{ref,d}$	Commutation voltage and current at rated switching loss of energy
$V_{ref,IGBT}, I_{ref,IGBT}$	Reference commutation voltage and current for an IGBT
v_{rw}	Rated wind speed
V_{TS}	Torque sensor output voltage
v_{w1}	Wind velocity at the anemometer height
v_{w2}	Wind velocity at the hub height

v_w	Wind velocity
$x_a(t)$, $x_b(t)$, $x_c(t)$	3ϕ quantities of voltages and currents
x_i, y_i	Variables defined by (6.7) and (6.8)
$Y_{d(k,m)}$, $Y_{q(k,m)}$, $Y_{0(k,m)}$	$dq0$ components of admittance
Z_0	Surface roughness
$\mathbf{J}_{dq}$	Jacobian matrix for $d-q$-axis power flow
$\mathbf{m_{dq}}$	Power mismatch vector
$\mathbf{P}_a$, $\mathbf{Q}_a$	Actual active and reactive power for buses
$\mathbf{P}_c^{(n)}$, $\mathbf{Q}_c^{(n)}$	Calculated active and reactive power for buses at n^{th} iteration
$\mathbf{\Delta P}$	Active power mismatch vector
$\mathbf{\Delta Q}$	Reactive power mismatch vector

List of Abbreviations

DG	Distributed generation
GEC	Generator end converter
HGU	Hydro generation unit
HSU	Hydro storage unit
IPE	Interfacing power electronics
IPE	Inverter interface storage
IGBT	Insulated gate bipolar transistor
MTS	Micro-grid test set up
MCFC	Molten carbonate fuel cell
MSR	Micro-grid system reliability
OLTC	On-load tap changing
PF	Power flow
PC	Power controller
PDF	Probability density function
PWM	Pulse width modulation
PAFC	Phosphoric acid fuel cell
PFMC	Power flow based micro-grid controller
RMS	Root mean square
RBD	Reliability block diagram

SEC	Supply end converter
SCR	Silicon control rectifier
SC	Storage controller
SOFC	Solid oxide fuel cell
SU	Storage unit
WT	Wind turbine
WTE	Wind turbine emulator
WPGS	Wind power generation system
WECS	Wind energy conversion system

Chapter 1

Introduction

1.1 Micro-Grid System

The environmental impact of fossil fuel based power generation has turned the attention of researchers, governments and commercial sectors from conventional power generation technology to renewable or alternative power generation technology. The demand for more power combined with interest in clean technologies have driven researchers to develop distributed power generation units using renewable energy sources [1–3]. However, the integration of a large number of distributed generations into distribution networks is restricted due to the capacity limitation of the distribution networks and their unidirectional power flow behaviour [2, 4, 5]. These barriers have motivated researchers to find alternative conceptual solutions to enhance distributed generation integration into the distribution network.

An alternative approach called "Micro-Grid" was proposed as a means of integrating distributed generation into distribution networks [5]. The micro-grid is a low power rated network that consists of a group of loads, micro-generation units,

central or individual storage systems, and associated power conditioning units operating as a single controllable system. The micro-grid system generally provides power or both power and heat to loads within the system [5–7]. A generic architecture of a micro-grid system is shown in Figure 1.1.

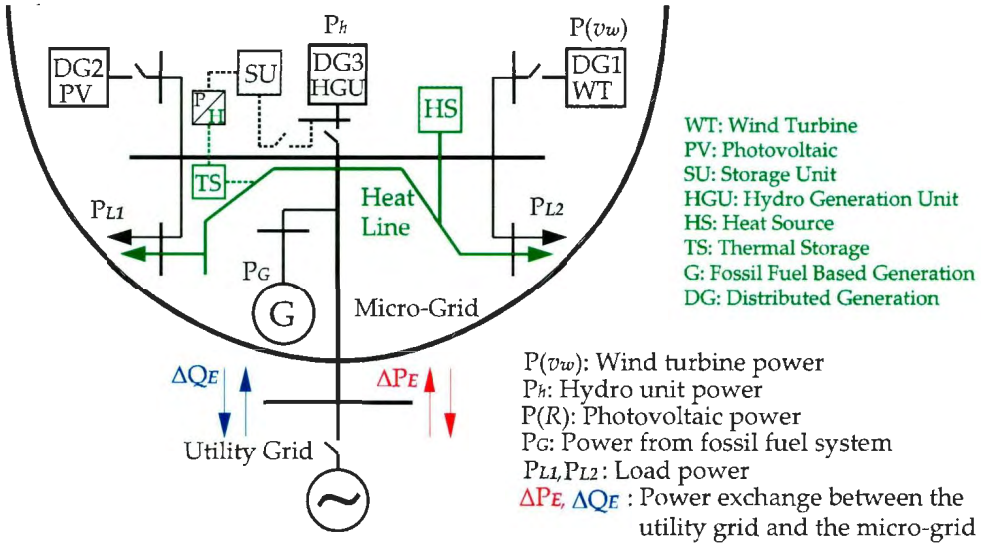

Figure 1.1: A typical micro-grid system.

The combination of micro-generation units in a micro-grid system can consist of either or both renewable and non-renewable energy sources [8]. Thus the use of diverse power sources in a small and low inertia micro-grid power system makes the operation, control and power management of the system more challenging. However, the employment of distributed generation in micro-grid systems can offer the following benefits to utility operators, distributed generation owners and consumers:

- Reliable Power Supply: Distributed generation units provide power to loads by means of grid connection near the load points. Any unexpected events,

such as grid faults occurring in the upstream power lines, result in a disconnection of the distributed generation unit from the grid, causing black-outs. However, if the utility grid is not available, the autonomous operation of a group of distributed generation units in a micro-grid system can provide power to local loads and this depends upon the generation capacity of the micro-grid.

- Power Loss Compensator: Many rural communities in Canada are generally connected to the central power stations through long transmission lines or obtain their power supply through diesel generators. Delivering power to such rural communities from a central power station produces a significant amount of loss. In Newfoundland, the power loss in the transmission system is about 9% [9]. Therefore, the formation of micro-grid systems near these rural areas can help to reduce a significant amount of power loss due to transmission, and also will help to reduce the cost of maintenance.

- Reduction in Transmission System Expansion: According to the Newfoundland and Labrador Hydro's (NLH) 2010 long term planning load forecast, power demand on this island is predicted to grow at 1.3 percent per year through 2029. As illustrated in Figure 1.2, the energy demand scenario in Canada also shows an increasing trend (Energy Handbook, Canada, 2011). The gradual increase in power demand requires more power transmission infrastructure, which may not be economically feasible because of the higher cost involved in new transmission lines installation and maintenance for rural areas. Therefore, the installation of a micro-grid system near the user load center can eliminate the requirement of re-designing or erecting new long transmission lines, thus resulting in cost savings.

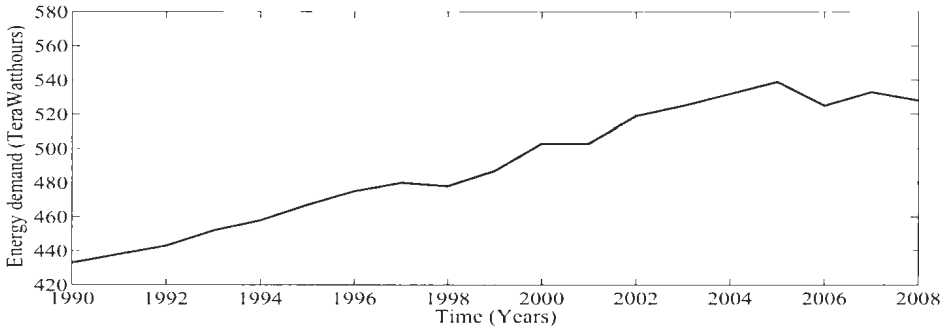

Figure 1.2: Energy demand in Canada.

- Enhancement of Renewable Power Penetration: In distributed networks containing wind generation, faults occurring in the upstream power line of the utility grid cause the disconnection of wind power generation from the grid, while wind power generation has the ability to deliver power. However, wind power generation in an isolated automated micro-grid operation can provide power to the loads when the grid is not available. Therefore, delivering power by wind power generation to the loads during grid unavailability implies the enhancement of renewable power penetration.

1.2 Thesis Motivations

When two or more micro-generation units are combined to create a micro-grid system, the overall system behaviour changes. In general, the characteristics of a micro-grid system depend on the size and nature of the micro-generation units in the micro-grid, as well as the site, and the availability of the primary energy resources. Such characteristics can be more unpredictable, especially if the micro-grid system with renewable power sources is included. The variation in micro-grid characteristics increases the complexity of the underlying challenges to the opera-

tion and control of micro-grid systems. Thus there is a need to investigate a micro-grid system that can be constructed with potentially available energy sources for particular sites.

A technological literature review conducted on micro-grid systems reveals that there exists a need to study a micro-grid system powered by renewable energy sources. Existing representations of micro-grid systems do not provide complete scenarios for several aspects of the system. These aspects include selection of the micro-grid system, the nature of micro-generation in the micro-grid, the type of storage systems and the capacity of renewable power generation units. These aspects also include micro-grid system modeling, operation and control, as well as protection strategies. On the other hand, the application of renewable power sources in a micro-grid can maximize the utilization of clean power for the power industry. An existing real system is considered to investigate the issues for micro-grid operation rather than working with a hypothetical system. The system investigated in this thesis is chosen based on potentially available renewable energy sources in Newfoundland Labrador, Canada. The system components and the available resources are found for the selected system based on a case study in Newfoundland, the island portion of the province.

1.3 Scope of Research

As an emerging alternative power system for integrating a large number of renewable energy technologies, the challenges to the micro-grid system are vast. The technical and non-technical issues related to micro-grid research may differ from one micro-grid architecture to another. This is because of the integration of a high number of micro-generations with diverse nature and size into a micro-grid sys-

tem. In this section, some of the challenges for the micro-grid system based on renewable energy sources are briefly outlined.

Resource Assessment

The first and foremost inquiry for micro-grid systems is to assess the available resources for specific sites where the micro-grid needs to be installed. Resource assessment is very important especially if the interest is to integrate renewable energy technologies into the micro-grid domain. A resourceful site can be identified based on annual energy yield by primary energy sources, and the availability of those sources over a large time duration. Such an assessment can help to choose renewable energy sources for a micro-grid system at a specific site. Although a site can be used for micro-grid system installation, however, the global databases are not sufficient to provide data for that particular site. Therefore, improvements in present global databases are required.

Economics

Cost of energy is another dominant factor, which may affect the success of any energy system. This factor may depend on capital cost, operations and maintenance cost, design simplicity, diversity of applications, modularity, material and labour engagement, and availability of the primary energy resources. Moreover, system operations under normal and abnormal conditions, visual impact, controls and system efficiency may also have a secondary influence on the cost of energy.

System Design and Components Selection

A simple cost effective design is desirable for a successful power system. However, the intermittent nature of renewable sources in a micro-grid system may require effective design and components selection for reliable power supply within the micro-grid domain. A generic view of a micro-grid system shown in Figure 1.1 consists of multiform energy sources in terms of availability, behaviour and energy harnessing techniques. Resource assessment at a site can easily inform the selection of energy sources for a particular micro-grid system; however, selecting, sizing and operating a storage system for a micro-grid system incorporates design challenges. This is because the storage system plays a vital role for efficient and reliable operation of a micro-grid system by storing excess power from the system or delivering deficit power into the system.

Operation, Control and Protection

Effective control and operation of a micro-grid system requires special attention in order to achieve stable and reliable operation along with optimal system performance. Selection of control strategies for control problems of any micro-grid may vary as the system is comprised of different sizes and a diverse group of micro-generations. Hence, operational and control problems for a micro-grid system with intermittent renewable generation can be formulated as follows:

- Identification of the operational modes of a micro-grid system:
  Operation of a micro-grid system depends on size, type, and operating conditions of micro-generation units, as well as the location where the micro-grid will operate. Also, the status of the utility grid or the distribution network can dictate the micro-grid operation. Thus preliminary investigation is required

to identify possible operational modes for the micro-grid system in order to study the system dynamic behaviour under various operating conditions.

- Balance between generation (real and reactive powers) and consumption (real and reactive powers):

  This is one of the most critical challenging issues for a micro-grid system powered by renewable energy sources for stable and reliable operation during stand-alone conditions. Two possible events are to be considered for power balance during islanded operation of the studied micro-grid system; namely, the isolated micro-grid system with wind power generation and the isolated micro-grid system without wind power generation. In the first event, the nature dependent wind power generation in the micro-grid system can deliver power to the micro-grid, which may be in excess of the micro-grid load and thus result in increasing the micro-grid frequency. The surplus power from the wind power generation (WPGS) needs to be managed economically and efficiently to maintain the micro-grid frequency within an acceptable range. At the same time, the micro-grid requires more reactive power due to the real power variation introduced by the WPGS. The tendency of the doubly fed induction generator in the WPGS to consume reactive power, coupled with the load reactive power variations, result in voltage deficiency. In the second event, the micro-grid load may demand real power, while the wind power generator is not able to deliver power to the micro-grid due to lack of sufficient wind, resulting in a decrease in micro-grid frequency. In addition, the micro-grid may also demand reactive power depending on the load requirement, resulting in a change in micro-grid voltage profile.

  On the contrary, high demand of reactive power by the WPGS and load is

delivered by the grid, while the micro-grid is in grid connected mode. However, the micro-grid can have the ability to provide high demand reactive power locally using a storage system. Therefore, attention is required to develop power control techniques for the proposed micro-grid system, which is able to maintain balance between generation and consumption, while the micro-grid is operational in isolated mode.

- Control Coordinator and Monitoring System:

  Continuous system monitoring and activating/deactivating, requiring control actions with minimal time are also challenges to achieving reliable and stable operation of a micro-grid system. Tasks of the control coordinator and monitoring system include detection of grid islanding and recovery, switching on and off controllers at different operational modes, and also grid synchronization.

- Micro-grid Test Setup:

  A scaled version micro-grid test setup is also vital to implement and test micro-grid controllers and the monitoring system. However, developing a complete micro-grid test setup has significant challenges because of the requirement to develop individual micro-generation in a micro-grid domain in the laboratory environment and then to integrate all the micro-generation to form a micro-grid in order to verify system performances in real time.

- Micro-grid Protection:

  The operation of micro-grid systems includes numerous critical factors, such as a considerable number of power electronic devices and components, nature dependent micro-generations, operating modes of a micro-grid, and

power exchange between the micro-grid and the utility grid. These factors introduce challenges to conventional protection systems, which are primarily designed for unidirectional power flow and a conventional utility grid. Thus there is a need of a protection system for reliable and stable operation of the micro-grid systems.

Micro-grid Reliability Assessment

The key primary energy sources of micro-generation in a micro-grid system comprised of renewable sources are nature dependent, as in wind, solar, hydro and ocean current energy conversion systems. Because of the stochastic nature of such energy sources, wind and solar always have uncertainty in wind speed and in solar insolation, respectively, which causes unpredictable power output of a wind turbine system or of a photovoltaic panel. Such variation in wind speed or in solar insolation also propagates through the other sub-systems in a wind energy conversion system (WECS) or in a photovoltaic (PV) system which eventually affects the power generation of such systems. Reliability of power generation with a renewable power generation system can be evaluated considering the effect of uncertainty in the primary energy sources such as wind or solar insolation. This assessment is required to ensure the ability to generate and supply power using the micro-grid system at an adequate reliability level.

The above discussion indicates both technical and non-technical challenges related to micro-grid systems. However, the scope of this work is limited to the technical challenges only.

1.4 Micro-Grid System Selected for the Study

Fermeuse (46°58′42″N 52°57′18″W), Port Kirwan (46°58′09″N 52°54′40″W), Renews-Cappahayden (46°51′36″N 52°56′37″W) and Cape Broyle (47°05′00″N 52°57′00″W) are small rural communities located on the southern shore of the Avalon Peninsula on the island of Newfoundland in the province of Newfoundland Labrador, Canada. The electricity demand of these communities is provided by a small hydro generation unit (HGU) located at Cape Broyle, which is connected to the Newfoundland grid through a 66 kV transmission line. The total average load demand of these communities is higher than the local hydro generation, and the excess demand comes from the upstream power lines. The small hydro generation unit (Fig. 1.3) is able to produce 5.3 MW. The available flow rate and head for the hydro generation unit are 14 m^3/s and 54.8 m respectively. The power generation from the hydro system hardly varies over a year which indicates that the hydro system is a firm power generation unit.

Figure 1.3: A view of the hydro generation unit

Recently, a 27 MW wind power generation system was installed at Fermeuse,

Newfoundland, which is about 20.12 kilometers away from the hydro generation unit. The wind power generation system, currently in operation, consists of nine 3 MW variable-speed, doubly-fed induction generator based wind turbines. A section of the wind farm and its transmission system is shown in Figure 1.4. The transmission system shown in Figure 1.4 is connected to the Newfoundland grid using a 12.5/66 kV, 45 MVA power transformer.

Figure 1.4: A view of the wind power generation system and its transmission line

The available wind resource (from May 2007- April 2008) recorded at the nearest possible site, which is scaled according to the tower height of 80 m, is shown in Figure 1.5. The average wind speed is 11.3 m/s.

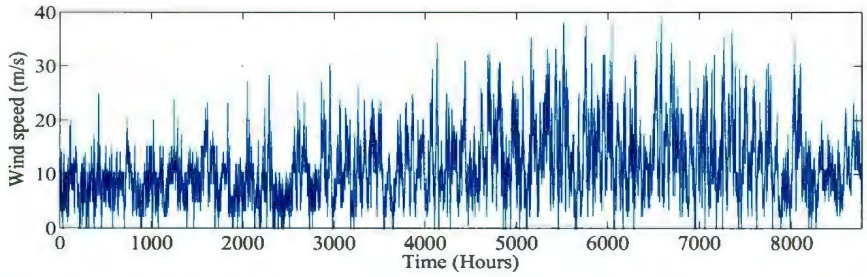

Figure 1.5: One year wind profile at the nearest site of the wind farm location

The total average load demand close to both wind and hydro generation systems is 6.76 MW, while the peak load is 14.8 MW. The load demand close to the hydro generation unit is referred to as Load-I (P_{L1}), and the load demand close to the wind power generation system is referred to as Load-II (P_{L2}). The yearly characteristics of the load demands for Load-I and Load-II are shown in Figures 1.6 and 1.7, respectively.

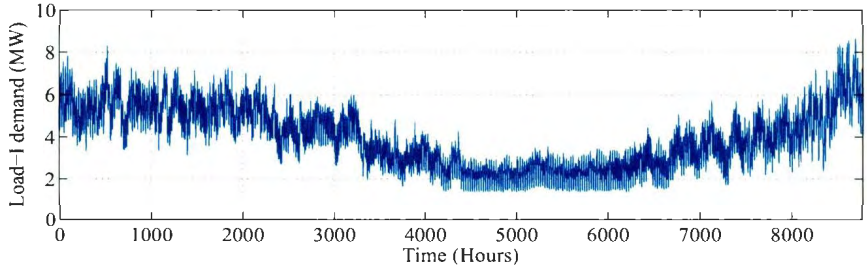

Figure 1.6: Load demand (P_{L1}) close to the hydro generation unit

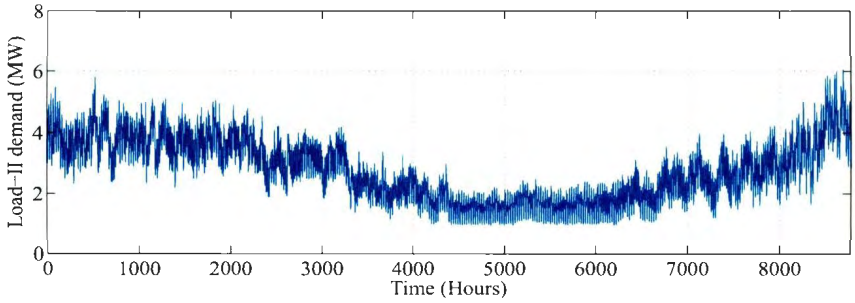

Figure 1.7: Load demand (P_{L2}) close to the wind power generation system

The system schematic shown in Figure 1.8 basically consists of a hydro generation unit (HGU) and a wind power generation system (WPGS), associated loads, a medium voltage transmission line, power transformers and the utility grid. The generated power by HGU and WPGS is delivered to the local loads and the utility

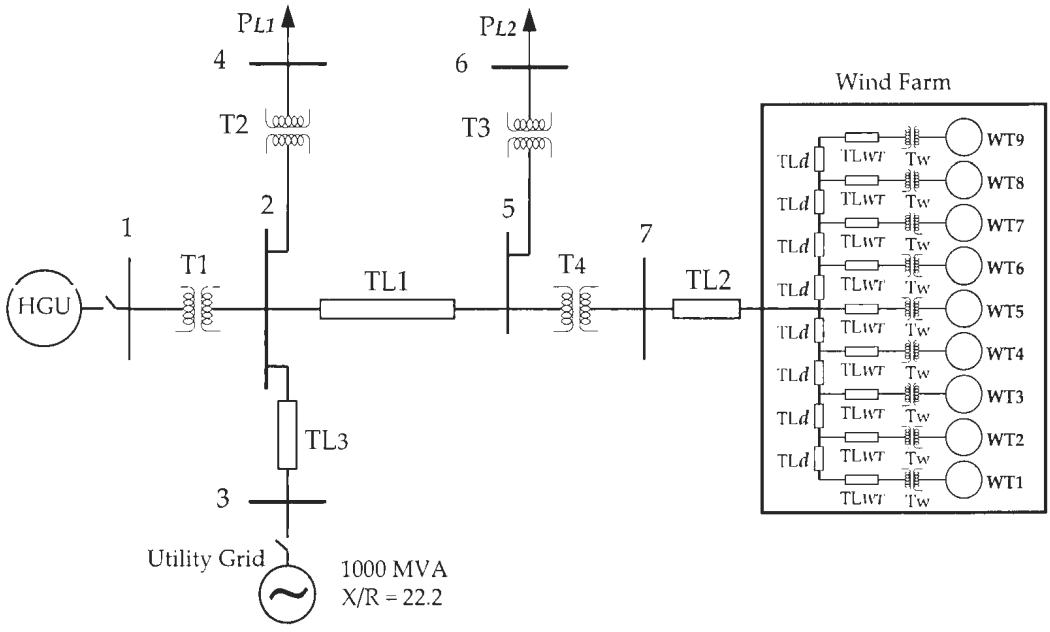

Figure 1.8: Selected system for micro-grid operation in Fermeuse, Newfoundland, Canada.

grid. The unavailability of the utility grid due to any faults in the upstream power line or regular maintenance first requires disconnecting WPGS from the grid. The operation of the HGU in isolated mode is not the current practice of the utility owner. In the event that the grid power is lost due to faults or scheduled maintenance, a black-out would result until the HGU comes into operation. Even with the HGU in operation, some load shedding is necessary since the HGU would not be able to meet the total average load demand. If the selected system can operate as an autonomous micro-grid system, then it will not only overcome the black-out problem for the site but will also create the motivation for constructing and operating micro-grids with only renewable sources for the utility owner. The motivation for this research arises from the need to develop controllers for stable and reliable

operation of a micro-grid system that is powered by renewable energy sources and is capable of delivering reliable power to the loads.

The system selected in this research is specific because the renewable sources considered and the proposed controllers are site specific. However, the concepts developed in this thesis can be applied to other micro-grid systems consisting of renewable sources such as solar, tidal and marine current micro-generation systems.

1.5 Thesis Objectives

Several micro-grid configurations with different types of micro-generations have been investigated. However, none of these micro-grid systems has the combination of popular and economically viable micro-generation such as a variable speed doubly-fed induction generator and a small hydro generator. On the other hand, the model of micro-generation in most of the micro-grid system is assumed to be a DC source, which utilizes an inverter to produce AC power for the grid. This modeling approach might be less effective when the model of the micro-generation has limited dynamical effects. Special attention needs to be paid to the power balance issue of the proposed micro-grid system under various operating conditions. Although considerable research has been devoted to studying the micro-grid system, rather less attention has been paid to the practical implementation and realization of the studied systems. In addition, since power supply by a micro-grid system consisting of stochastic renewable sources might be sensitive, the reliability assessment of the proposed micro-grid system is also an essential part of this research.

The first objective of this work is to develop a dynamic model of a micro-grid system based on renewable power generation units such as a variable speed doubly-fed induction generator and a small hydro generator. Development of such

a model is important to identify the operational modes and technical challenges, and also to utilize this model for further investigations.

The second objective of this work is to design and develop micro-grid controllers to maintain real and reactive power balance between generation and load during various operational modes of the proposed micro-grid system, and also to investigate the performances of the developed controller through simulation under different operating conditions.

The third objective of this work is to develop a micro-grid test set up. This objective also includes the implementation and experimental testing of the developed micro-grid controllers to verify the performances of the simulation study.

The final objective of this work is to develop a micro-grid system reliability model to assess the reliability level of generating and supplying power by the proposed micro-grid system. Also, this objective includes the modeling and reliability assessment of each subsystem of variable speed wind generators.

1.6 Thesis Outline

Chapter 1 introduces a broad overview of micro-grid systems, their significance and the possible candidates for selecting a system for micro-grid operation. Finally, the research areas for a micro-grid system based on renewable power generation units are discussed, and proposed research objectives are laid out.

A review of distributed generation units, micro-grid configurations and their control techniques is presented and discussed in chapter 2. The power sharing strategy of the micro-grid system using an inverter interfaced system is reviewed. In addition, a survey of the micro-grid test set up in a laboratory environment for testing the designed controller is also provided. Finally, the reliability analysis

for a micro-grid system based on renewable power generation is reviewed and presented.

Chapter 3 provides a dynamic model of the proposed micro-grid system. Also, the simulation of the developed model and the analysis of the results obtained through simulation are presented. In addition, an outline of the additional necessities for stable and reliable operation of the proposed micro-grid system is discussed. This model will be utilized to design and test the controller for the proposed micro-grid system.

An overview of the micro-grid control concept is presented in chapter 4. The frequency regulation scheme for an isolated micro-grid system with wind power generation is called the active power controller. The design and development of the active power controller based on AC voltage control concept along with a heating load/dump load is also presented in this chapter. Frequency regulation of the isolated micro-grid system without wind power generation using a pumped hydro storage system is also presented. The performances of the designed controllers are investigated through simulation study, and the results are presented and discussed. Finally, the formulation of the micro-grid power controller using power flow analysis is described. The simulation of the developed controller employing power flow analysis with the Matlab/Simulink tool is also presented in this chapter.

In chapter 5, a real-time implementation of the micro-grid test set up for experimental testing is developed. This chapter also presents the implementation of the active power controller and micro-grid controller for various modes of operation. The control algorithms are realized using Matlab coding in the Matalab/Simulink environment for the $dSPACE\ ds1104$ controller board. Experimental tests are car-

ried out on various operating conditions of a micro-grid system based on renewable energy sources.

The reliability assessment of generating and supplying power using a micro-grid system that consists of renewable energy sources is provided in chapter 6. The reliability model of various sub-systems in a distributed generation unit such as a wind energy conversion system is also presented. The sub-systems include wind turbine rotor, gear box, generator and interfacing power electronics system, and the impact of stochastically varying wind speed is considered in developing the sub-systems reliability model. Chapter 6 also presents a micro-grid system reliability (MSR) model by integrating the reliability models of individual distributed generation units using the system reliability concept. The implementation of the developed MSR model through numerical simulation using Matlab coding in the Matlab/Simulink package is also presented and discussed.

The final chapter, chapter 7, summarizes and concludes the research work. Also, it provides a description of the main contributions and future scope of this work in various aspects.

Chapter 2

Literature Review

The literature review for the current study is discussed in three sections of this chapter. The first section covers the issues related to the integration of conventional distributed generation into distribution networks. The second section discusses existing micro-grid configurations and their technical challenges and methods proposed in the past to address them. This section also reviews the reliability assessment of a micro-grid system comprised of renewable micro-generation. Finally, a summary of further important research considerations relevant to the micro-grid system based on renewable micro-generations is discussed.

2.1 Distributed Generation

Distributed generation (DG) is defined as a small electric power generation unit connected to the distribution network or a user site of the network [10, 11]. The benefits of utilizing DG units are as follows:

- Support deregulation policy of the power industry.

- Introduce emission free, smaller size and environmentally friendly energy sources.
- Provide local electricity production for remote areas, where there is no grid connection.

DG technology is comprised of solar, wind, small or micro or mini hydro, geothermal, ocean, bio-mass, internal combustion engine, combined cycle, reciprocating engine, combustion turbines, micro-turbines and fuel cells etc. [8]. DG technologies can be in different forms such as dispatchable and non-dispatchable systems. Dispatchable systems generate power according to the power demand whereas the non-dispatchable systems generate power based on the availability of the primary energy source.

2.1.1 Integration of distributed generation into distribution networks

While DG technology provides benefits and opportunities, a large integration of distributed generation into distribution networks introduces several technical issues in the operation of the distribution network. Some of the issues are [3, 12–14]:

- A change in the system voltage profile occurs due to the variation in the amount and/or direction of power flow throughout the system;
- Transient voltage variation may occur due to the connection/disconnection of generators or even as a result of their operations;

- Due to the presence of DG units, angle and voltage stability of the system will be affected in the event of loss of a large central power generation;
- Power quality may be affected due to the large number of converter interfaced DG units, if the harmonic injection by the DG units is not within an acceptable range;
- Re-designing the protection system may be required due to the increase in short circuit possibility;
- Control co-ordination will be required between the DG units for proper operational planning which increases the degree of system complexity.

Voltage profile in the system refers to the voltage dip and voltage rise. Voltage dip occurs due to motor starting, transformer energizing and short circuits in the transmission system [12, 15, 16], and voltage rise occurs due to the integration of distributed generation and the rising variation occuring along the distributed line with respect to the distance of a consumer from the primary substation [17]. The voltage dip issue has been addressed by several researchers. Some methods have utilized DGs to inject reactive power into the system to minimize the voltage dip [18, 19]. A dynamic voltage restorer technique has also been proposed to mitigate the voltage dip [16]. The approaches found in the literature to address the voltage rise issue include reducing the primary substation voltage; allowing the distributed generation system to import reactive power; resetting the voltage along the line using more auto transformers; increasing the conductor size, and imposing a constraint for distributed generation production during low demand to minimize this voltage variation [17, 20, 21].

The voltage fluctuation issue, either short term or long term, is raised when wind turbine based DG systems are connected to low voltage distribution feeders [22]. A fixed speed induction generator utilizing a 5-step, no-load compensation capacitor bank is used to manage the flicker induced in the system during the wind turbine's continuous operation [22]. Soft-starters are used to connect the fixed speed wind turbines with the grid to reduce short term fluctuations [23, 24].

Loss of a large central power generation means a severe disturbance in the utility grid. In that case, IEEE Standard 1547-2003 [24] and IEEE Standard 929-2000 [25] suggest disconnecting the DGs from the AC line. DG operation in islanding mode can improve the system reliability and reduce the outage cost from loss of supply [27]. The impact of islanding operation of distributed generation connected to a radial sub transmission system has been studied and it has been shown that appropriately planned protection and operation schemes are required for an intentional islanding operation [28].

Integration of DGs introduces harmonics into the system by means of electronic interfaces. The capacitances at the interface of small generation units cause a shift in resonance frequencies. The additional capacitance moves the resonance closer to the lower order harmonics [29, 30]. Harmonic compensation techniques using shunt active filters have been proposed in [31, 32].

A coordinated voltage controller has been proposed to increase the share of DG in the distribution network [33]. The author also commented that the coordinated voltage control technique presents a complex structure where different devices (e.g. DG units, OLTC transformers, etc.) are operated according to the network situation. To develop such a complex structure, a relatively high investment cost is expected.

In summary, a continuous effort with respect to control, power quality, and stability and protection issues for DG integration is found in the literature. However, re-designing the protection system, and the unidirectional power flow nature of the existing distribution network, may limit the integration of a large number of DGs [3, 14].

2.2 Micro-Grid Concepts

The limitations of the host distribution network and the interest in utilizing diverse DG units near each other electrically have brought about the idea of the micro-grid [13, 34]. A micro-grid is a smaller power network at the distribution level, comprising multiple DG units which are adequately capable of supplying power to the loads in that network.

2.2.1 Micro-Grid Architectures

A review of the existing literature reveals that the first micro-grid architecture was proposed by R. H. Lasseter [5], and was called the Consortium for Electric Reliability Technology Solutions or CERTS micro-grid. The CERTS micro-grid generally assumes power electronic interfaced distributed generation units that are based on both renewable and non-renewable power sources. Each distributed generation unit has its own battery based storage system connected to the DC link of an inverter. An autonomous control system for each converter-interfaced micro-generation is developed, and the proposed system is tested in a laboratory prototype. The capacity of each distributed generation is 60kW and is driven by natural gas [123].

Barnes et al [35, 36] also proposed a micro-grid system under the frame of the European project "Micro-grids". The European micro-grid architecture consists of two photovoltaic generators, one wind turbine, battery storage, controllable loads and a controlled interconnection to the local low voltage grid. The crucial component of this micro-grid system is the battery inverter which is controlled to maintain the desired voltage and frequency during isolated operation. Such a storage system may not be feasible for a micro-grid system where the power requirement is very high for a short period. Moreover, the selection of micro-grid storage is also dependent on the type of micro-generation units within the micro-grid system as well as on economic factors.

The New Energy and Industrial Technology Development Organization (NEDO) in Japan proposed three micro-grid projects in 2003 [37, 38]. The first NEDO micro-grid (1.7MW) system is comprised of different kinds of fuel cells such as MCFC, PAFC, SOFC, and a PV system and battery storage. In the first NEDO micro-grid, only 18 percent of the power is generated by renewable energy sources. The second NEDO micro-grid (610kW) configuration consists of PV, WT, biomass, battery storage and a biomass boiler. The main feature of this configuration is the combination of different kinds of renewable energy sources. The third NEDO micro-grid (750kW) system consists of PV, WT, MCFC, biogas gen-sets and battery bank, and has a low percentage (66 percent) of renewable energy generation.

Micro-grid research in Canada started in universities with the cooperation of the CANMET energy technology center at Varennes [37]. This research group has identified industry cases, such as the isolated Ramea wind-diesel micro-grid system, and the Fortis Alberta grid-tied micro-grid system, for investigation. Ramea's wind-diesel micro-grid system consists of six 65 kW fixed speed WTs and diesel

generators. An additional three 100 kW rated WTs are currently being installed for integration with the existing system. The Fortis-Alberta grid-tied system consists of 3 MW run-of-river based hydro and 3.78 MW fixed speed wind turbine generation units [3]. Canada's micro-grid research and development also evolved to develop a test bed for industrial-grade prototype testing and performance evaluation [37].

A study of micro-grid dynamic behaviour and the control of the micro-generation units is performed by F. Kateraie [39]. This micro-grid system is based on the benchmark system of the IEEE Standard 399-1997 [40], which consists of three generation units comprising a diesel generator or a gas turbine generator, an electronically interfaced distributed generation and a fixed speed wind power generator. Research on micro-grid systems is also found in the literature, where hypothetical generation units and loads are assumed [41–43].

The dynamic model of a micro-grid system comprised of photovoltaic cell, wind turbines and hydro turbines is developed using the electromagnetic transient program (EMTP) [44]. A wind-hydro-pumped storage hybrid power station is proposed to integrate with Greece's Ikaria Island system in order to increase renewable power penetration. An operating strategy is proposed for the overall generation system of Ikaria Island to assess the expected benefits from the operation of the system [45]. A micro-grid system comprised of a fuel cell and an inverter interfaced induction generator is developed in the laboratory environment [123]. However, the requirement of energy storage in this micro-grid system has not discussed.

2.2.2 Control of Micro-Grid System

Distributed generation unit control in a grid-connected system is straightforward; however, significant difficulties appear in the micro-grid mode of operation. A reliable and robust operation of a micro-grid system strongly depends on an efficient control and power sharing scheme of micro-grid components. The control objective in a micro-grid is to achieve proper power sharing while maintaining close regulation of the micro-grid voltage magnitude and frequency. Voltage and frequency regulation for different micro-grid architectures found in a literature survey are as follows.

An energy management system, which receives the terminal information of each inverter and loads to dispatch the inverter units in different load conditions, is proposed in [46]. The frequency deviation in each inverter unit is controlled by controlling the power angle between the inverter terminal voltage and the micro-grid voltage. The voltage regulation is performed by controlling the reactive power component of each inverter unit. The local voltage and frequency controller of each inverter unit receives the reference reactive and real power for a new operating point from the energy management system. The successful laboratory test of a micro-grid system is presented in reference [46] and is performed and reported in [53]. The application of non-inverter interfaced DG units and storage systems in these micro-grid systems is also studied [53]. This centralized management approach may require high bandwidth communication infrastructure to share the dynamic sharing information from each inverter and load terminal. In addition, it is also required to send new set points to each storage system controller associated with each micro-generation unit. This may not be a cost effective solution in the micro-grid case, because a large number of inverter-interfaced micro-generation

units requires long connection distances between them and the energy management system.

A DC/AC pulse width modulated inverter interfaced battery storage system that is used to maintain the micro-grid frequency is presented in [47]. The battery-inverter arrangement is controlled to regulate the magnitude and frequency of its voltage output during the isolated operation of the micro-grid system, according to the power-frequency droop curve [35, 47]. The battery unit power electronics interface consists of a Cuk DC/DC converter and a voltage source PWM inverter, both bi-directional, permitting charging and discharging of the batteries. However, this control approach is for a single phase low power micro-grid system.

The voltage and frequency regulation scheme for NEDO micro-grids is also based on regulating the active and reactive power component of the inverter-interfaced battery storage system [48, 49]. In the first NEDO micro-grid, MCFC and SOFC power generation sources operate to meet the system base load while PAFC power generation sources operate as the load following unit. In the second NEDO micro-grid, three 170kW controllable gensets burning sewage digester gas are used as a biomass generation system. In the third NEDO micro-grid system, a gas engine with 400kW and an MCFC with 250kW capacity are used with other small capacity PV (50kW) and WT (50kW) generation systems. Due to the nature of generation units in the NEDO micro-grid, frequency and voltage regulation are not solely dependent on battery storage system control. In addition, the control duration of the battery inverter is only a few seconds, and is used as backup until the gas engine system responds to operate in controlling voltage and frequency of the system. However, these cases may not be applicable to the micro-grid system under investigation in this research.

Frequency and voltage control in a micro-grid system is studied in [50]. A distributed generation unit represented by an equivalent DC source model with no dynamics related to the input source is interfaced using a PWM voltage source inverter to the micro-grid. The active and reactive power component of the inverter is controlled using droop methods to manage frequency and voltage of the micro-grid system. The assumptions considered for distributed generation modeling are not very accurate for the nature dependent renewable source based distributed generation unit such as the DFIG, unless a storage system is considered at the DC link. In addition, as the wind generator is not allowed to deliver reactive power to the system, which is the case in the proposed micro-grid system, the voltage control idea in [50] may not be applicable if the distributed generation unit is DFIG.

A control approach to provide both voltage and frequency regulation capabilities for a variable-speed DFIG in micro-grid application is proposed in [41]. The frequency control is integrated into the rotor-side speed control loop using the power-frequency droop method. The droop coefficient is used to determine a change in the active power injected by the DFIG when a system frequency variation occurs. This generated active power requires a new operating point of the DFIG. The new operating point is implemented by converting the required active power to equivalent reference electromechanical torque for the rotor side converter. Similarly, the reactive power-voltage droop is used to determine the reference reactive power for the grid side converter. This reactive power is directly dependent on the rotor current component, while stator resistance is neglected, and the current component is used to regulate the reactive power in the micro-grid system [41]. The control approach is applicable as long as sufficient wind is available to deliver load demand. However, if there is no wind, the micro-grid voltage and frequency

will not be regulated by the proposed control approach along with the DFIG. In addition, controlling DFIG in this approach basically forces the wind generator to extract as much power from the wind as the micro-grid needs. This technique limits the extraction of maximum power from the wind, which is not desired for power extraction from renewable energy sources.

A central automatic control system based on an estimated load curve is proposed for the diesel-photovoltaic-battery storage micro-grid system [49]. The battery is charged by photovoltaic during daytime while the PV generation exceeds the micro-grid load demand. Each generation has its local control unit, which controls the generation units either by turning 'on' or 'off' depending on the micro-grid frequency state. Turning 'on' and 'off' a generation unit puts the micro-grid frequency in a preset range. If the micro-grid frequency is above the preset value, the diesel governor system is used to maintain the constant frequency of the micro-grid system.

A control strategy based on the droop method is proposed for load sharing between parallel converters connected in a micro-grid and supplied by distributed generators [51]. The control of the distributed generation units is emphasized to compensate for the effect of imbalance and non-linearity of the local loads. The distributed generation control compensator shows better system response in terms of total harmonic distortion of the micro-grid voltages. To account for nonlinear load sharing, the harmonic droop controller is also presented in [52]. However, the distributed generation unit represented by an equivalent DC source model with no dynamics related to the input source is considered in these investigations.

A dynamic fuzzy PI frequency controller is proposed for a micro-grid system [54]. The proposed dynamic control is used for the fuel cell and electrolyzer hy-

brid system to ensure real power balance between generation and consumption. An objective function for frequency control in the micro-grid system is formulated using the difference between power generation and consumption in the micro-grid system. However, the efficiency of the electrolyzer system is not satisfactory compared to other types of storage systems. An aggregate load-frequency controller is presented [55], that regulates the frequency of a micro-grid system consisting of a hydro unit and a fixed speed wind generator unit. Such a controller has features of frequency control as well as of imbalance compensation between the three micro-grid phases.

A power sharing strategy using the droop characteristic is proposed for an inverter-interfaced micro-turbine, PV and FC power generation based micro-grid system [56]. The flywheels and batteries are modeled as a DC source for storage systems, which are interfaced to the micro-grid using a voltage source inverter (VSI). The inverter of the power generation units is controlled to supply a given active and reactive power set-point. On the contrary, the VSI of the storage system is controlled to maintain real and reactive power with pre-defined values for frequency and voltage. However, the proposed control strategy shows a slow response to regulate micro-grid frequency which has been claimed to be due to the slow response of micro-turbines and FC. A dynamic model of a hybrid system along with an optimal control issue for real time operation is discussed and presented in [57].

Power sharing technique among multiple DGs in a micro-grid system is also presented and discussed, where DGs are assumed to be inverter interfaced with dispatchable energy sources [58]. In [58], one of the limitations of feeder flow control introduced in [46] is addressed to achieve improved power sharing among DGs

which are connected to a common feeder in series during the transition between the grid-connected and island system. This limitation is solved by employing a method of determining the new droop coefficients during the transition period. The droop based parallel inverter control concept is also adopted to achieve frequency regulation in a wind-solar power source based micro-grid system [59].

A potential function based secondary control of inverter interfaced DG units for the operation of a micro-grid is proposed in [60]. However, the potential function based approach is not applicable for primary control because of its high computational burden and signal transmission delays. In [61], a parallel inverter control concept using droop methods is proposed for micro-grid application where the issues of circulating current flow between the inverters is taken into account. A control scheme for an isolated photovoltaic-diesel micro-grid system is proposed in [62]. The objective of this controller is to track maximum power from the photovoltaic panel, regulate the load voltage, compensate the load imbalances and control the diesel-engine speed. An alternative control strategy that employs micro-grid voltage versus dc-link voltage and real power versus the micro-grid voltage droop characteristic for power sharing among the multiple inverters in a micro-grid is presented in [63]. A voltage sensitivity analysis-based control scheme is presented to regulate micro-grid voltage of a target bus. This scheme provides adjustment in reactive power based on active power generation by the wind generator [64].

Control and operation of a DC micro-grid for both the grid connected and isolated mode are presented in [65]. The power balance in this micro-grid is achieved by controlling the battery energy storage and the grid inverter in grid-connected mode. During the stand-alone operating condition, the power balance is obtained

through a coordinated control strategy for the battery system, wind turbine and load managment system.

The preceeding literature review indicates that the parallel inverter control technique based on droop methods has been extensively used to regulate frequency and voltage in the micro-grid system. However, it has been reported in [66] that because of the droop characteristics, the system frequency may drop to a value where all micro-generation units will be operating at a newer operating frequency, which may differ from the nominal frequency of the micro-grid system. Thus, a power sharing strategy using static droop characteristics and an adaptive transient droop function is investigated in [66]. In addition, a comprehensive survey of micro-grids suggests careful application of frequency versus real power and voltage versus reactive power droop methods in control because of the fact that the impedance of the line in isolated micro-grid is predominantly resistive [67]. Furthermore, the impact of frequency and voltage droop on micro-grid stability has been reported recently in [68].

2.2.3 Reliability Assessment of Micro-Grid System

Reliability assessment of a micro-grid system is a concern when the micro-grid contains renewable sources. Because the ability to generate and deliver power by the renewable sources highly depends on the primary energy sources. Reliability evaluation is a quantitative measure of the ability to generate and supply power by the renewable sources in a micro-grid. It also indicates the viability of constructing a renewable source based micro-grid at a specific site.

A reliability study of a micro-grid system is presented in [69], where the concentration is given for the power quality aspect based on the assumption that the

micro-grid system is a large virtual generator which has the ability to generate sufficient power for loads in various operating conditions. Reliability based coordination between the wind and hydro system is investigated, which shows adequacy benefits due to the coordination between them when an appropriate number of hydro units are engaged to follow the wind speed changes based on the wind power penetration [70]. A wind speed modeling approach is considered to evaluate the reliability of a wind integrated electric power system with the emphasis on various wind speed modeling techniques [71]. However, the effect of wind speed variation on various sub-systems of a wind energy conversion system is not considered for reliability assessment. It is found from literature that while micro-grid architectures, control and power sharing issues are investigated a fair amount, reliability evaluation of micro-grid systems has not been explored yet.

Reliability assessment of the wind turbine generator in the power system application has been studied by several researchers [72–79]. The application of two-state and multi-state models for wind turbine systems are investigated in [72–74]. However, in [72–74], the stochastic variation and interactions of wind speed and thus time dependent wind power effects are avoided [80]. A Monte Carlo simulation based method is then used to evaluate wind generation system reliability in [70, 75–78]. All these past studies evaluate reliability of the wind turbine system by determining the available power output using (2.1), while the effects of other sub-systems such as gear box, generator, and interfacing power electronics have

not been considered.

$$P_o = \begin{cases} 0 & 0 \leq v_w \leq v_{ciw} \\ (A + Bv_w + Cv_w^2)P_r & v_{ciw} \leq v_w \leq v_{rw} \\ P_r & v_{rw} \leq v_w \leq v_{cow} \\ 0 & v_w \geq v_{cow} \end{cases} \tag{2.1}$$

where, P_o and P_r are rotor output power and rated power of the WT, respectively. v_{ciw}, v_{rw}, and v_{cow} are cut-in, rated and cut-out wind speed, respectively, and the parameters A, B, and C are the functions of cut-in, rated and cut-out wind speed.

Moreover, such an approach of determining available power only provides power at the output of the WT rotor. A reliability evaluation, carried out only for an interfacing power electronics sub-system to compare performances of small (1.5 kW) wind energy conversion systems is presented in [81], while the consideration of all sub-systems is considered in reference [79] with an assumption that the wind generator is 100 percent reliable. Furthermore, the reliability assessment of the interfacing power electronics sub-system is carried out for a single operating condition, the rated wind speed condition. However, operating conditions of a WECS can vary between cut-in to cut-out wind speed due to the stochastic behaviour of wind speed. Hence, a reliability evaluation of generating power by the wind energy conversion system is important to carry out, considering both the operating conditions due to stochastic wind variation as well as the impact of stochastic wind behaviour on different sub-systems in a wind energy conversion system. This consideration is important to achieve a better reliability estimation regarding the ability of the micro-grid system to generate and supply reliable power.

2.3 Summary

Based on the literature survey, the following issues relevant to the micro-grid system have been identified.

- The micro-grid system with a combination of a hydro generation unit and a wind farm consisting of variable speed doubly-fed induction generator based wind turbines has not been investigated yet. In past study, the combination of DG units in a micro-grid system was found as (DC source interfaced by an inverter) [5, 50, 51], (PV, WT and battery storage) [35, 36], (MCFC, PAFC, SOFC, WT and a PV) [37, 38], (wind-diesel) [37], (run-of-river hydro and fixed speed WT) [3], (a diesel generator, DC source interfaced inverter and a fixed speed WT) [40], (PV, fixed speed WT and hydro) [44], (Diesel, PV and battery) [49].

- The previous research on micro-grid systems has been carried out based on hypothetical systems or on bench mark systems, where loads, type of micro-generations and their capacities are assumed arbitrarily [5, 35, 40–43, 50, 51]. This type of selection may not be applicable for a particular site, because the capacity of micro-generations depends on availability of renewable sources which varies from one site to another. Also, the effective operation of renewable micro-generations depends on the frequency and amplitude of the available renewable sources at a particular site. Thus this study has considered micro-generations available at Fermeuse, Newfoundland, Canada, and investigations are carried out on the issues while the micro-generations operate in a micro-grid system.

- The components model of the micro-grid system is required to study the sys-

tem dynamic behaviour during transient and steady state operation. However, the detail components model of the micro-grid system is not presented in past research [3, 5, 35, 38, 40, 50, 52]. This study has developed an integrated model of the micro-grid system that is comprised of all components model of the micro-grid system. This model technically provides better system dynamic behaviour than the model that does not contain the dynamics of the components in that model.

- Real and reactive power control of micro-generation units is designed without considering the dynamics and uncertainties of the input energy sources [50, 52, 58]. Droop based real and reactive power control are proposed for inverter interfaced micro-generation units in a micro-grid system [35, 41, 46–48, 50–52, 56, 59, 61, 68]. If a number of inverter interfaced micro-generation units operate in parallel and are primary candidates for frequency and voltage regulation, because of the droop characteristics, the system frequency and voltage might drop to such a value that all micro-generation units will be operating at a new lower frequency and voltages that are different from the nominal values [66]. Thus an alternative power control scheme without the employment of droop characteristics is an important research consideration.

- The micro-grid test set up development is required to test and verify conclusions obtained through simulation study. Most of the past research on the micro-grid system has been carried out based on simulation study [41, 46–48, 50–52, 56, 59, 61, 66, 68]. Thus the micro-grid test bench development is an important consideration of this research.

- The proposed micro-grid system has stochastically varying, nature dependent energy sources. Thus technically, the evaluation of adequate power generation capacity by such sources in micro-grid operational modes cannot be avoided. However, the literature survey indicates very little research has been conducted to assess the reliabilty of the micro-grid system containing renewable micro-generations [69, 70]. Therefore, reliability evaluation of the proposed micro-grid system in order to provide reliable power to micro-grid loads is essentially considered a good candidate for further investigation.

Chapter 3

Micro-Grid Behaviour Analysis

A renewable source based micro-grid is defined as a pliable combination of a group of loads, which only consists of renewable micro-generations with central or distributed storage units operating as a single controllable system. The objective of this chapter is to investigate operational modes and system dynamic behaviour of a micro-grid system comprised of renewable source based power generation units. In order to carry out this investigation, the micro-grid system dynamic model is developed, which is the integration of the dynamic model of various sub-systems and components in the selected system. The developed model is then verified through simulation study using the Matlab/Simulink software tool. The analysis of the simulation results are presented and discussed. Finally, technical issues revealed through simulation study and concepts for addressing these issues in the proposed micro-grid system are briefly outlined for further investigation in the subsequent chapters.

3.1 The Proposed Micro-Grid System

The single-line diagram of the proposed micro-grid system is shown in Figure 3.1. The diagram is a representation of the real system located at Fermeuse, Newfoundland, Canada. The system consists of a Hydro Generation Unit (HGU), nine Wind Turbines (WTs), power transformers (T1, T2, T3, T4 and T_W), short transmission lines (TL1, TL2, TL3, TL_d and TL_{WT}) and two load areas represented as Load-I (P_{L1}) and Load-II (P_{L2}).

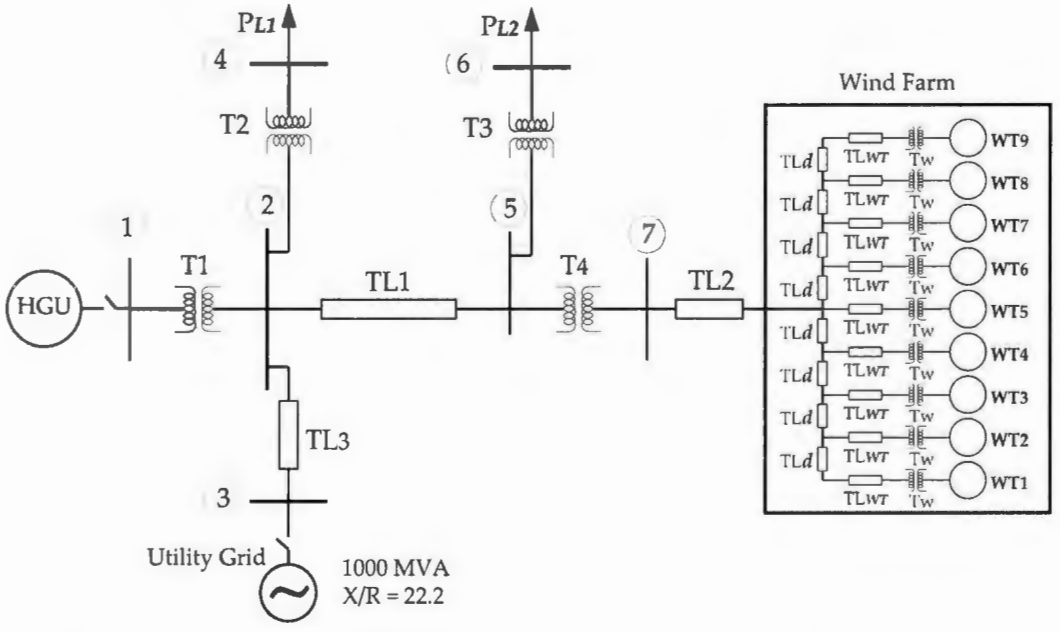

Figure 3.1: The single-line diagram of the proposed system for micro-grid operation located at Fermeuse, Newfoundland, Canada.

The nine WTs together are called the wind power generation system (WPGS) that will be used throughout the thesis. Each of the WTs in the WPGS is a 3 MW variable-speed, doubly-fed induction generator wind turbine. The distance

between each wind turbine generator is represented by a transmission line, TL_d. Each wind turbine generator is connected to the line, TL_d through a transformer, T_W and a transmission line, TL_{WT}. The transmission line (TL2) of the WPGS is connected to a common bus (bus 7), which is eventually connected to bus 2 using a power transformer, T4. Load bus 6 (P_{L2}) is connected to bus 5 and the power is delivered to the load using a power transformer, T3. Load bus 4 (P_{L1}) is connected to the bus 1 and the power is delivered to the load using a power transformer, T2. The two load areas are connected through a transmission line, TL1. The HGU is connected to bus 1 using a power transformer, T1. A conventional synchronous generator, equipped with an IEEE standard excitation and governor system, is used for the HGU. The two generating systems (WPGS and HGU) are connected through the transmission lines, TL1 and TL2. Also, the proposed system includes a link for utility-connection. It is important to note that the distributed generation (DG) units in the micro-grid system employ renewable energy sources (wind and hydro). Data for the buses of the proposed system are provided in Table 3.1. Also, the data for transmission lines and transformers are also provided in Appendix A.1.

Table 3.1: Fermeuse Micro-Grid System: Buses

Bus	P [MW]	Q [MVAR]	V [kV]
1	7.3	6.8	6.9
2	ΔP_E	ΔQ_E	66
3	ΔP_E	ΔQ_E	66
4	3.94	0.95	12.5
5	0	0	66
6	2.82	0.6	12.5
7	27	12	12.5

The active and reactive powers balance in the proposed micro-grid system can be stated as:

$$\Delta P_E = P(v_\omega) + P_h - P_{L1} - P_{L2} \tag{3.1}$$

$$\Delta Q_E = Q(v_\omega) + Q_h - Q_{L1} - Q_{L2} \tag{3.2}$$

where v_ω is the wind speed, P_h and Q_h are active and reactive power outputs of the hydro unit, $P(v_\omega)$ and $Q(v_\omega)$ are active and reactive power outputs of the WT, and P_{L1}, Q_{L1}, P_{L2} and Q_{L2} are active and reactive powers of loads $L1$ and $L2$ respectively. In order to achieve reliable and stable operation of the proposed system, the excess active power, ΔP_E and the excess reactive power, ΔQ_E must be managed technically and effectively. At any time, t the excess powers, $\Delta P > 0$ and $\Delta Q > 0$ can be managed by supplying them to the utility grid, while $\Delta P < 0$ and $\Delta Q < 0$ can be managed by delivering from the utility grid, if the system is connected to the utility grid. However, if the utility grid is not available, and when $\Delta P > 0$ and $\Delta Q > 0$, the excess power needs to be accommodated continuously to maintain balance between generation and load, and when $\Delta P < 0$ due to low wind speed availability, more than one wind turbine is required to be used to supply power demand along with load. Moreover, if the utility grid is not available and there is no power generation by the WT because of insufficient wind speed, and when $\Delta P < 0$ and $\Delta Q < 0$, additional power is required to be supplied to the micro-grid system using HGU and SU. The various scenarios derived from (3.1) and (3.2) define the following operational modes of the proposed micro-grid system.

1. Grid connected system (Mode-I), and conceptually shown in Figure 3.2.

2. Isolated system with wind power generation (Mode-II), and conceptually

shown in Figure 3.3.

3. Isolated system without wind power generation (Mode-III), and conceptually shown in Figure 3.4.

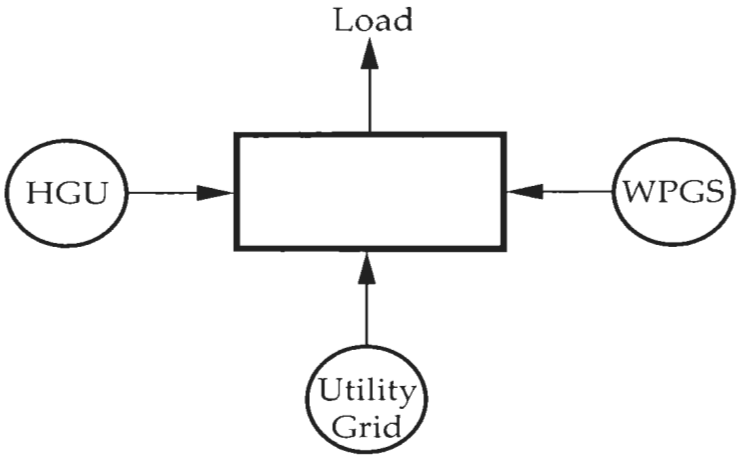

Figure 3.2: Simplified model of the grid-connected micro-grid system (Mode-I)

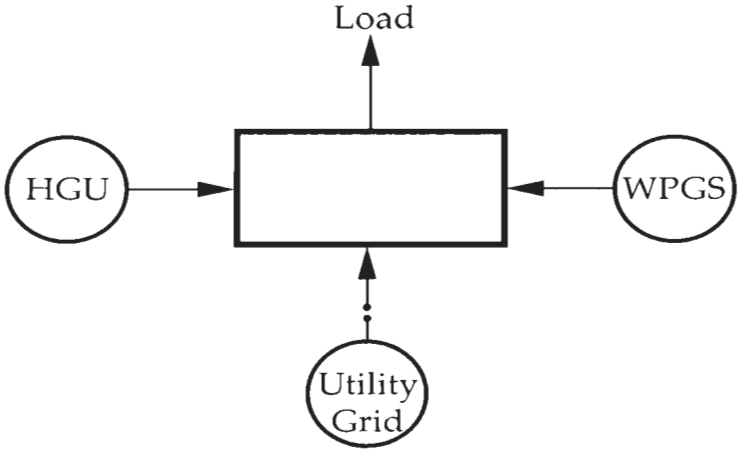

Figure 3.3: Isolated system with wind power generation (Mode-II)

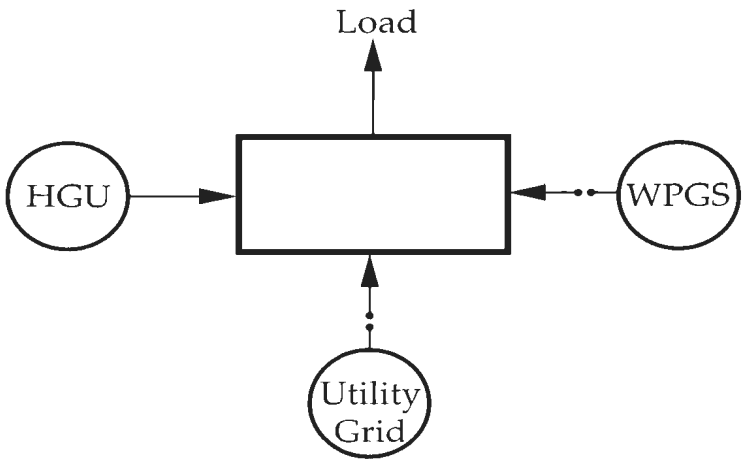

Figure 3.4: Isolated system without wind power generation (Mode-III)

3.2 Component Model of the Micro-Grid System

In order to study the dynamic behaviour of the proposed micro-grid system in various operational modes (Figs. 3.2, 3.3, 3.4), the development of the mathematical model of the proposed system is essential. This section describes the various component models of the proposed system, and finally, all the component models are integrated to produce the model of the proposed micro-grid system.

3.2.1 Wind Power Generation System Model

The WPGS model consists of 9 dynamic models of variable-speed, doubly-fed induction generator based wind energy conversion systems (WECS). Each variable-speed, doubly-fed induction generator contains the model of a variable pitch wind turbine rotor and a wound rotor asynchronous generator. The rotor winding is connected to the grid using a back-to-back pulse width modulated (PWM) voltage source converter (GEC and SEC), where the stator is directly connected to the grid.

The Vestas-90 WECS is utilized in the proposed micro-grid system. The topology utilized in the Vestas-90 wind power converter in order to extract energy from the wind is shown in Figure 3.5. The decouple control technique is incorporated to control the converters in the rotor side [82]. Thus the model of the WECS including the converter control is developed according to the topology shown in Figure 3.5, and is presented sequentially in the following subsections.

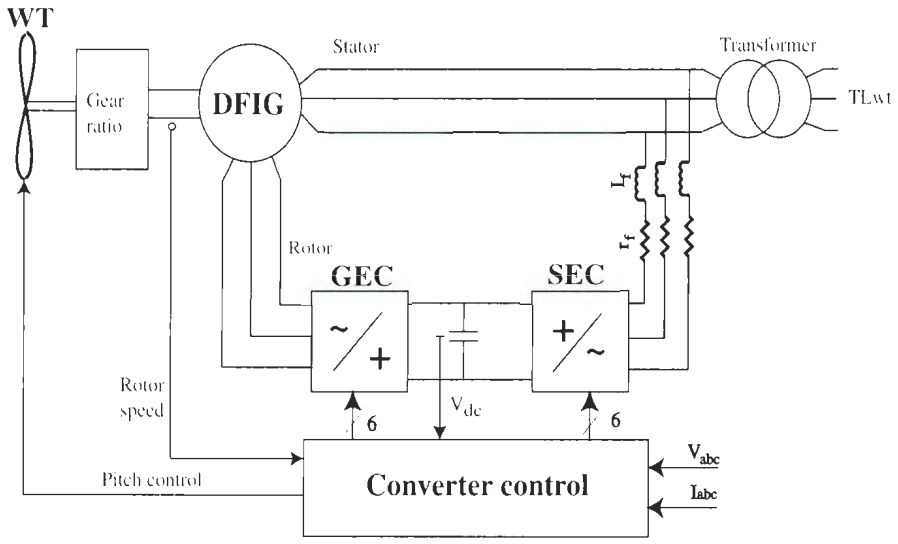

Figure 3.5: Schematic of a variable speed doubly-fed induction generator based wind energy conversion system

Wind Turbine Rotor

The aerodynamic power output at the wind turbine rotor is expressed as

$$P_{ro} = 0.5\rho A_{SA} C_p(\lambda, \beta)\, v_w^3 \tag{3.3}$$

where A_{SA} is the swept area covered by the turbine rotor, C_p is the power coefficient and is a function of the tip speed ratio (λ) and the pitch angle of the rotor blades

(β), and v_w is the wind velocity. Tip speed ratio, λ is the quotient of linear speed of the tip of the blades to the rotational speed of the WT and it is expressed as [83]

$$\lambda = \frac{\omega_m R_t}{v_w} \tag{3.4}$$

The effects of the different $C_p - \lambda$ curves for various types of wind turbines are very small and negligible, while the electrical behaviour of a system is of interest [83]. Therefore, the analytical approximation of the $C_p - \lambda$ characteristics is considered for rotor modeling as [84]

$$C_p(\lambda, \beta) = 0.5176\left(\frac{116}{\lambda_i} - 0.4\beta - 0.5\right)\exp\left(\frac{-21}{\lambda_i}\right) + 0.0068\lambda \tag{3.5}$$

and

$$\frac{1}{\lambda_i} = \frac{1}{\lambda + 0.08\beta} - \frac{0.035}{\beta^3 + 1} \tag{3.6}$$

Wind Generator

The dynamic equivalent ($d-q$) circuit of a doubly-fed induction machine in a synchronously rotating reference frame is represented in Figure 3.6. Using $d-q$-axis transformation in the synchronously rotating reference frame, the output voltages for the doubly-fed induction generator are written as [85]

$$V_{ds} = r_s i_{ds} - \omega_e \varphi_{qs} + \frac{d\varphi_{ds}}{dt} \tag{3.7}$$

$$V_{qs} = r_s i_{qs} + \omega_e \varphi_{ds} + \frac{d\varphi_{qs}}{dt} \tag{3.8}$$

$$V'_{dr} = r'_r i'_{dr} - (\omega_e - \omega_r)\,\varphi'_{qr} + \frac{d\varphi'_{dr}}{dt} \tag{3.9}$$

$$V'_{qr} = r'_r i'_{qr} + (\omega_e - \omega_r)\,\varphi'_{dr} + \frac{d\varphi'_{qr}}{dt} \tag{3.10}$$

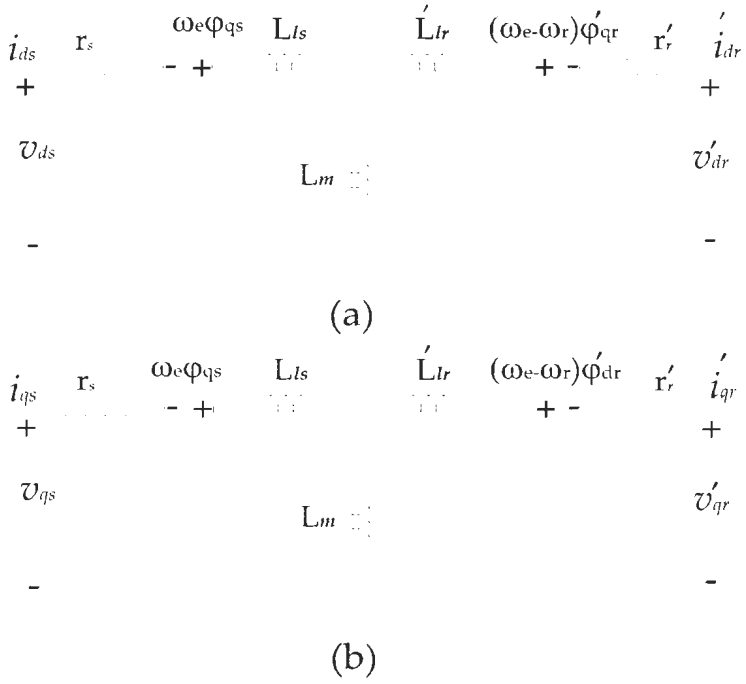

Figure 3.6: Equivalent circuit representation of an induction machine in synchronously rotating referenced frame: (a) d-axis, (b) q-axis.

After rearranging (3.7), (3.8), (3.9) and (3.10), the flux linkages developed in the generator are expressed as

$$\varphi_{ds} = \int \left[V_{ds} - r_s i_{ds} + \omega_e \varphi_{qs}\right] dt \tag{3.11}$$

$$\varphi_{qs} = \int \left[V_{qs} - r_s i_{qs}) - \omega_e \varphi_{ds}\right] dt \tag{3.12}$$

$$\varphi'_{dr} = \int \left[V'_{dr} - r'_r i'_{dr} + (\omega_e - \omega_r)\, \varphi'_{qr}\right] dt \tag{3.13}$$

$$\varphi'_{qr} = \int \left[V'_{qr} - r'_r i'_{qr} - (\omega_e - \omega_r)\, \varphi'_{dr}\right] dt \tag{3.14}$$

Flux linkages developed in the induction machine are also expressed in terms of self and mutual inductances, and the $d-q$-axis current components as

$$\varphi_{ds} = L_{ls} i_{ds} + L_m \left(i_{ds} + i'_{dr}\right) \tag{3.15}$$

$$\varphi_{qs} = L_{ls} i_{qs} + L_m \left(i_{qs} + i'_{qr}\right) \tag{3.16}$$

$$\varphi'_{dr} = L'_{lr} i'_{dr} + L_m \left(i_{ds} + i'_{dr}\right) \tag{3.17}$$

$$\varphi'_{qr} = L'_{lr} i'_{qr} + L_m \left(i_{qs} + i'_{qr}\right) \tag{3.18}$$

The $d-q$ components, φ_{md} and φ_{mq} of the mutual flux are written as

$$\varphi_{md} = L_m \left(i_{ds} + i'_{dr}\right) \tag{3.19}$$

$$\varphi_{mq} = L_m \left(i_{qs} + i'_{qr}\right) \tag{3.20}$$

Further manipulations of (3.15), (3.16), (3.17) and (3.18) produce the $d-q$-axis current relations as

$$i_{ds} = \frac{1}{L_{ls}} \left(\varphi_{ds} - \varphi_{md}\right) \tag{3.21}$$

$$i_{qs} = \frac{1}{L_{ls}} \left(\varphi_{qs} - \varphi_{mq}\right) \tag{3.22}$$

$$i'_{dr} = \frac{1}{L'_{lr}} \left(\varphi'_{dr} - \varphi_{md}\right) \tag{3.23}$$

$$i'_{qr} = \frac{1}{L'_{lr}} \left(\varphi'_{qr} - \varphi_{md}\right) \tag{3.24}$$

The mutual flux components in $d-q$ axis can also be expressed in terms of flux linkages developed in the machine as

$$\varphi_{md} = L_{ed}\left(\frac{\varphi_{ds}}{L_{ls}} + \frac{\varphi'_{dr}}{L'_{lr}}\right) \tag{3.25}$$

$$\varphi_{mq} = L_{eq}\left(\frac{\varphi_{qs}}{L_{ls}} + \frac{\varphi'_{qr}}{L'_{lr}}\right) \tag{3.26}$$

where

$$L_{ed} = L_{eq} = \frac{1}{\left(\frac{1}{L_m} + \frac{1}{L_{ls}} + \frac{1}{L'_{lr}}\right)} \tag{3.27}$$

The flux linkages developed in the induction generator can be obtained by substituting (3.21–3.24) into (3.7–3.10) as follows

$$\varphi_{ds} = \int \left[V_{ds} - \frac{r_s}{L_l s}\left(\varphi_{ds} - \varphi_{md}\right) + \omega_e \varphi_{qs}\right] dt \tag{3.28}$$

$$\varphi_{qs} = \int \left[V_{qs} - \frac{r_s}{L_l s}\left(\varphi_{qs} - \varphi_{mq}\right) - \omega_e \varphi_{ds}\right] dt \tag{3.29}$$

$$\varphi'_{dr} = \int \left[V'_{dr} - \frac{r_r}{L'_{lr}}\left(\varphi'_{dr} - \varphi_{md}\right) + \left(\omega_e - \omega_r\right)\varphi'_{qr}\right] dt \tag{3.30}$$

$$\varphi'_{qr} = \int \left[V'_{qr} - \frac{r_r}{L'_{lr}}\left(\varphi'_{qr} - \varphi_{mq}\right) - \left(\omega_e - \omega_r\right)\varphi'_{dr}\right] dt \tag{3.31}$$

The electromagnetic torque is defined as

$$\left(T_{em}\right)_{im} = \frac{3}{2} p \left(\varphi_{ds} i_{qs} - \varphi_{qs} i_{ds}\right) \tag{3.32}$$

The equation of motion of the rotor is given by

$$\frac{d\left(\omega_{rm}\right)_{im}}{dt} = \frac{1}{J_{wg}}\left(\left(T_{em}\right)_{im} - \left(T_m\right)_{wt} - F\left(\omega_{rm}\right)_{im}\right) \tag{3.33}$$

The power generated by the doubly-fed induction generator can be expressed as follows:

$$P_{DFIG} = \frac{3}{2}\left(V_{ds}i_{ds} + V_{qs}i_{qs} + V'_{dr}i'_{dr} + V'_{qr}i'_{qr}\right) \tag{3.34}$$

$$Q_{DFIG} = \frac{3}{2}\left(V_{qs}i_{ds} - V_{ds}i_{qs} + V'_{qr}i'_{dr} - V'_{dr}i'_{qr}\right) \tag{3.35}$$

Wind Generator Converter Control

The rotor side of the doubly-fed induction generator based wind generator system is connected to the grid through a back-to-back PWM voltage source converter. The converter connected to the generator rotor winding is referred to as the generator end converter (GEC) and the inverter connected between the DC link and the grid is referred to as the supply end converter (SEC). The purpose of the GEC is to maintain the variable speed operation of the generator while that of the SEC is to regulate the DC bus voltage. The models of the converter controls are derived in the following subsections.

Generator End Converter (GEC)

The generator end converter is utilized to control rotor speed for achieving variable speed operation with maximum power extraction by the wind turbine system. A tip speed ratio is kept at a value that leads to the optimal power coefficient, while keeping the rotor speed within limits of the turbine. From the actual value of the rotor speed, the wind speed that would correspond to the optimum value of the power coefficient is calculated. Then, the power that would be generated at this

wind speed is calculated by substituting the wind speed in (3.3), together with the optimum value of the power coefficient. This amount of power is then drawn from the generator by controlling the rotor current accordingly. The resulting power versus rotor speed characteristic is called the tracking characteristics and is shown in Figure 3.7.

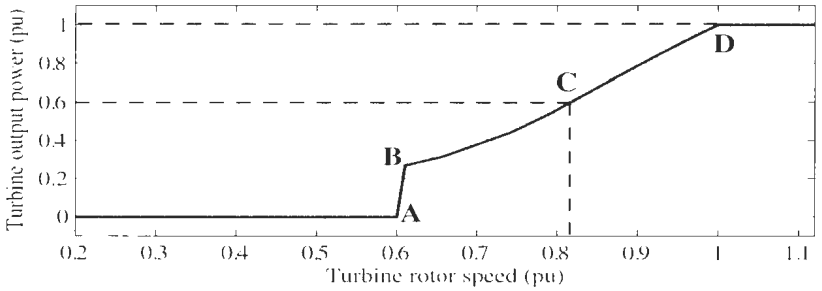

Figure 3.7: Maximum power tracking characteristic employed in the generator side converter

The tracking characteristics is defined by four points: A, B, C and D. From zero speed to the speed of point, A, the reference power is zero. Between point A and point B the tracking characteristics is a straight line. Between point B and point C the tracking characteristics is the locus of the maximum power of the turbine. The tracking characteristics is a straight line from point C to point D. The power at point D is one per unit. Beyond point D the reference power is a constant equal to one per unit. The actual speed of the rotor is measured and the corresponding power is determined using a predefined tracking characteristics. The electrical (stator and rotor resistance loss) and mechanical (frictional loss) power losses are subtracted from the power determined from the tracking characteristics to obtain the reference power which is used to determine the torque of the generator. The generator torque and the estimated flux are used according to equations (3.36)-(3.40) to generate reference rotor current in q-axis. The actual q-axis component

of rotor current is compared with the reference rotor current component and the error is reduced by a current regulator. The reactive power can be controlled by controlling the d-component of the rotor current.

Due to the stator flux-orientation vector along the d-axis of the rotating reference frame, the q-axis component of stator flux and the d-axis component of stator voltage are zero [86]. Hence,

$$i_{qs} = -\frac{L_m}{L_m + L_{ls}} i'_{qr} \tag{3.36}$$

$$(T_{em})_{im} = -\frac{3}{2} p \left(\frac{L_m}{L_m + L_{ls}} \right) \varphi_{ds} i'_{qr} \tag{3.37}$$

The stator flux can be calculated as [86]

$$\varphi_{ds} = \int (V_{ds} - r_s i_{ds})\, dt \tag{3.38}$$

$$\varphi_{qs} = \int (V_{qs} - r_s i_{qs})\, dt \tag{3.39}$$

$$|\varphi_{ds}| = |\varphi_s| = \sqrt{\varphi_{ds}^2 + \varphi_{qs}^2} \tag{3.40}$$

Assuming that the stator flux is practically constant, its derivative can be neglected [86]. The governing equations for the generator side converter are as follows:

$$V'^{*}_{dr} = V'_{drcor} - (\omega_e - \omega_r)(L'_{lr} + L_m) i'_{qr} + (\omega_e - \omega_r) L_m i_{qs} \tag{3.41}$$

where $V'_{drcor} = r'_r i'_{dr} + (L'_{lr} + L_m) \frac{di'_{dr}}{dt}$

$$V'^{*}_{qr} = V'_{qrcor} - (\omega_e - \omega_r)(L'_{lr} + L_m) i'_{dr} + (\omega_e - \omega_r) L_m i_{ds} \tag{3.42}$$

where $V'_{qrcor} = r'_r i'_{qr} + (L'_{lr} + L_m) \frac{di'_{qr}}{dt}$

In (3.37), the torque is related to the current, i'_{qr} and hence the torque is controlled by regulating the current, i'_{qr}. Similarly, the rotor excitation current is also controlled using d-axis current component, i'_{dr}. However, it is assumed that all reactive power to the machine is provided through the stator. The errors in two current regulators are processed by PI controllers to obtain V'_{drcor} and V'_{qrcor}. To achieve better tracking of these currents, compensation terms are added to obtain the reference voltages V'^{*}_{dr} and V'^{*}_{qr}. The analysis above results in the control loop for the GEC shown in Figure 3.8.

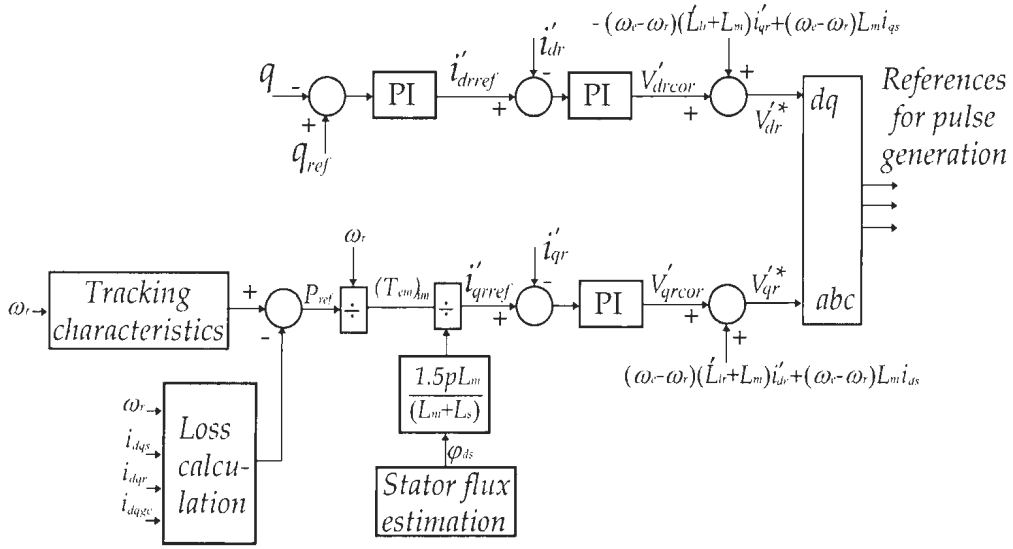

Figure 3.8: Schematic of the generator end converter control

Supply End Converter (SEC)

The supply end converter is used to regulate the voltage of the DC bus capacitor. The SEC interface arrangement is shown in Figure 3.9.

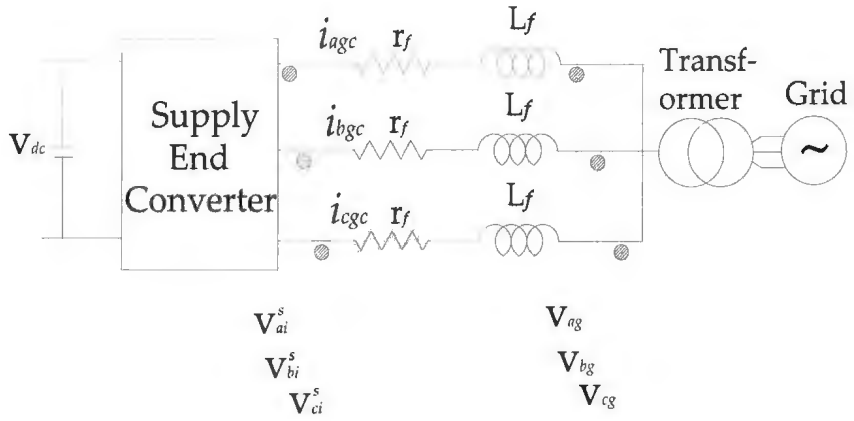

Figure 3.9: Supply end converter arrangement for the rotor side of the generator.

Voltage balance equations across the inductor are

$$V_{ag} = r_f i_{agc} + L_f \frac{di_{agc}}{dt} + V^s_{ai} \tag{3.43}$$

$$V_{bg} = r_f i_{bgc} + L_f \frac{di_{bgc}}{dt} + V^s_{bi} \tag{3.44}$$

$$V_{cg} = r_f i_{cgc} + L_f \frac{di_{cgc}}{dt} + V^s_{ci} \tag{3.45}$$

Voltage balance equations across the inductors in $d-q$ axis can be expressed as

$$V_{dg} = r_f i_{dgc} + L_f \frac{di_{dgc}}{dt} - \omega_g L_f i_{qgc} + V^s_{di} \tag{3.46}$$

$$V_{qg} = r_f i_{qgc} + L_f \frac{di_{qgc}}{dt} + \omega_g L_f i_{dgc} + V^s_{qi} \tag{3.47}$$

Equations (3.46) and (3.47) indicate that current components i_{dgc} and i_{qgc} are coupled through terms $-\omega_g L_f i_{qgc}$ and $\omega_g L_f i_{dgc}$. The coupling can be eliminated by

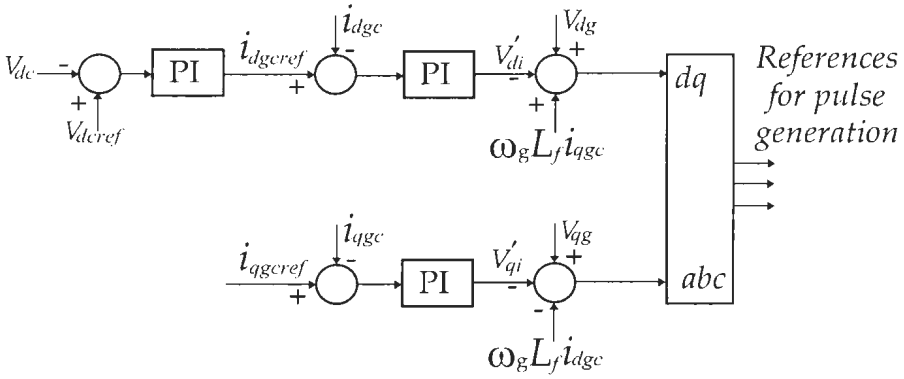

Figure 3.10: Supply end converter control

introducing intermediate variables V'_{di} and V'_{qi} as defined by

$$V'_{di} = V_{dg} - V^s_{di} + \omega_g L_f i_{qgc} \tag{3.48}$$

$$V'_{qi} = V_{qg} - V^s_{qi} - \omega_g L_f i_{dgc} \tag{3.49}$$

The decoupling current components are modeled by putting, V'_{di} and V'_{qi} into (3.46-3.47), resulting in

$$\frac{di_{dgc}}{dt} = -\frac{r_f}{L_f} i_{dgc} + \frac{V'_{di}}{L_f} \tag{3.50}$$

$$\frac{di_{qgc}}{dt} = -\frac{r_f}{L_f} i_{qgc} + \frac{V'_{qi}}{L_f} \tag{3.51}$$

Figure 3.10 shows the conceptual diagram of the decoupled current controller for the supply end converter. In Figure 3.10, an outer control loop consisting of a DC voltage regulator sets the reference current i_{dgcref} for the inner control loop. The current component i_{dgc} controls the active power flow into the grid using an inner PI controller. The other PI controller is used to control i_{qgc} to regulate the

desired voltage at the grid bus. As the WPGS connected to the grid is not allowed to regulate the grid voltage, the current component i_{qgcref} is set to zero.

3.2.2 Hydro Generation Unit Model

The hydro generation unit consists of the model of a synchronous generator, a hydro turbine, and turbine governor and excitation system. The synchronous machine is modeled with the dynamics of stator, rotor and damper windings [85]. A hydro turbine is modeled according to [87]. The synchronous generator is equipped with an IEEE standard governor and excitation system and is obtained from [87, 88].

Hydro Generator

The synchronous machine electrical system is represented by the dynamic equivalent, $(d-q)$ circuit in Figure 3.11. Voltage equations in $d-q$ axis rotor reference frame are expressed as [85]

$$V_d = r_{ss} i_d - \omega_r \varphi_q + \frac{d\varphi_d}{dt} \tag{3.52}$$

$$V_q = r_{ss} i_q + \omega_r \varphi_d + \frac{d\varphi_q}{dt} \tag{3.53}$$

$$V'_{fd} = r'_{fd} i'_{fd} + \frac{d\varphi'_{fd}}{dt} \tag{3.54}$$

$$V'_{kd} = r'_{kd} i'_{kd} + \frac{d\varphi'_{kd}}{dt} \tag{3.55}$$

$$V'_{kq1} = r'_{kq1} i'_{kq1} + \frac{d\varphi'_{kq1}}{dt} \tag{3.56}$$

$$V'_{kq2} = r'_{kq2} i'_{kq2} + \frac{d\varphi'_{kq2}}{dt} \tag{3.57}$$

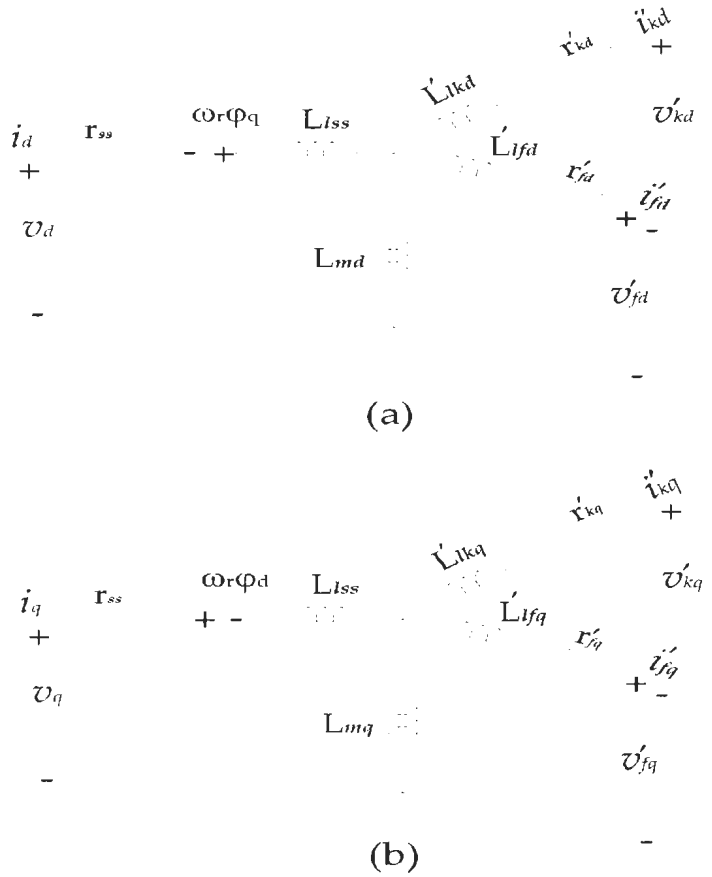

Figure 3.11: Equivalent circuit representation of a synchronous machine in rotor reference frame: (a) d-axis, (b) q-axis.

After rearranging (3.52), (3.53), (3.54), (3.55), (3.56), and (3.57), the flux linkages developed in the generator are expressed as

$$\varphi_d = \int \left[V_d - r_{ss} i_d + \omega_r \varphi_q\right] dt \tag{3.58}$$

$$\varphi_q = \int \left[V_q - r_{ss} i_q - \omega_r \varphi_d\right] dt \tag{3.59}$$

$$\varphi'_{fd} = \int \left[V'_{fd} - r'_{fd} i'_{fd}\right] dt \tag{3.60}$$

$$\varphi'_{kd} = \int \left[V'_{kd} - r'_{kd} i'_{kd}\right] dt \tag{3.61}$$

$$\varphi'_{kq1} = \int \left[V'_{kq1} - r'_{kq1} i'_{kq1}\right] dt \tag{3.62}$$

$$\varphi'_{kq2} = \int \left[V'_{kq2} - r'_{kq2} i'_{kq2}\right] dt \tag{3.63}$$

Flux linkages developed in the synchronous machine are also expressed in terms of machine inductances as

$$\varphi_d = L_d i_d + L_{md}\left(i'_{fd} + i'_{kd}\right) \tag{3.64}$$

$$\varphi_q = L_q i_q + L_{mq}\left(i'_{kq1} + i'_{kq2}\right) \tag{3.65}$$

$$\varphi'_{fd} = L_{md} i_d + L_{md} i'_{kd} + \left(L'_{lfd} + L_{md}\right) i'_{fd} \tag{3.66}$$

$$\varphi'_{kd} = L_{md} i_d + L_{md} i'_{fd} + \left(L'_{lkd} + L_{md}\right) i'_{kd} \tag{3.67}$$

$$\varphi'_{kq1} = L_{mq} i_q + L_{mq} i'_{kq2} + \left(L'_{lkq1} + L_{md}\right) i'_{kq1} \tag{3.68}$$

$$\varphi'_{kq2} = L_{mq} i_q + L_{mq} i'_{kq1} + \left(L'_{lkq2} + L_{md}\right) i'_{kq2} \tag{3.69}$$

where $L_d = L_{md} + L_{lss}$, and $L_q = L_{mq} + L_{lss}$.

The mutual flux components for the d axis, φ_{mds} and the q axis, φ_{mqs} are expressed as

$$\varphi_{mds} = L_{md}\left(i_d + i'_{fd} + i'_{kd}\right) \tag{3.70}$$

$$\varphi_{mqs} = L_{mq}\left(i_q + i'_{kq1} + i'_{kq2}\right) \tag{3.71}$$

The current equations are derived as

$$i_d = \frac{1}{L_{lss}}\left(\varphi_d - \varphi_{mds}\right) \tag{3.72}$$

$$i_q = \frac{1}{L_{lss}}\left(\varphi_q - \varphi_{mqs}\right) \tag{3.73}$$

$$i'_{fd} = \frac{1}{L'_{lfd}}\left(\varphi'_{fd} - \varphi_{mds}\right) \tag{3.74}$$

$$i'_{kd} = \frac{1}{L'_{lkd}} \left(\varphi'_{kd} - \varphi_{mds}\right) \tag{3.75}$$

$$i'_{kq1} = \frac{1}{L'_{lkq1}} \left(\varphi'_{kq1} - \varphi_{mqs}\right) \tag{3.76}$$

$$i'_{kq2} = \frac{1}{L'_{lkq2}} \left(\varphi'_{kq2} - \varphi_{mqs}\right) \tag{3.77}$$

Now, the mutual flux components φ_{mds} and φ_{mqs} are expressed as

$$\varphi_{mds} = L_{ed} \left(\frac{\varphi_d}{L_{lss}} + \frac{\varphi'_{fd}}{L'_{lfd}} + \frac{\varphi'_{kd}}{L'_{lkd}}\right) \tag{3.78}$$

$$\varphi_{mqs} = L_{eq} \left(\frac{\varphi_q}{L_{lss}} + \frac{\varphi'_{kq1}}{L'_{kq1}} + \frac{\varphi'_{kq2}}{L'_{kq2}}\right) \tag{3.79}$$

where $L_{ed} = \left(\frac{1}{L_{md}} + \frac{1}{L_{lss}} + \frac{1}{L'_{lfd}} + \frac{1}{L'_{lkd}}\right)^{-1}$, and $L_{eq} = \left(\frac{1}{L_{mq}} + \frac{1}{L_{lss}} + \frac{1}{L'_{kq1}} + \frac{1}{L'_{kq2}}\right)^{-1}$. The flux linkages developed in the synchronous generator can be obtained by substituting (3.72–3.77) into (3.58–3.63) as follows

$$\varphi_d = \int \left[V_d - \frac{r_{ss}}{L_{lss}} \left(\varphi_d - \varphi_{mds}\right) + \omega_r \varphi_q\right] dt \tag{3.80}$$

$$\varphi_q = \int \left[V_q - \frac{r_{ss}}{L_{ss}} \left(\varphi_q - \varphi_{mqs}\right) - \omega_r \varphi_d\right] dt \tag{3.81}$$

$$\varphi'_{fd} = \int \left[V'_{fd} - \frac{r'_{fd}}{L'_{lfd}} \left(\varphi'_{fd} - \varphi_{mds}\right)\right] dt \tag{3.82}$$

$$\varphi'_{kd} = \int \left[V'_{kd} - \frac{r'_{kd}}{L'_{lkd}} \left(\varphi'_{kd} - \varphi_{mds}\right)\right] dt \tag{3.83}$$

$$\varphi'_{kq1} = \int \left[V'_{kq1} - \frac{r'_{kq1}}{L'_{lkq1}} \left(\varphi'_{kq1} - \varphi_{mqs}\right)\right] dt \tag{3.84}$$

$$\varphi'_{kq2} = \int \left[V'_{kq2} - \frac{r'_{kq2}}{L'_{lkq2}} \left(\varphi'_{kq2} - \varphi_{mqs}\right)\right] dt \tag{3.85}$$

The electromagnetic torque produced by the synchronous machine is

$$(T_{em})_{sm} = \frac{3}{2} p_{sm} (\varphi_d i_q - \varphi_q i_d) \tag{3.86}$$

The equation of motion of the rotor is

$$\frac{d(\omega_{rm})_{sm}}{dt} = \frac{1}{J_{sm}} ((T_m)_{sm} - (T_{em})_{sm} - F(\omega_{rm})_{sm}) \tag{3.87}$$

The synchronous machine operates as a generator when $(T_m)_{sm}$ is positive.

Hydro Turbine

The mathematical representation of a single penstock is as follows [87]:

$$\frac{dq}{dt} = (H_s - H - H_L) \frac{gA_{pen}}{L} \tag{3.88}$$

and

$$q = G\sqrt{H} \tag{3.89}$$

Assuming that the base flow and base head for rated power output are q_{base} and H_{base}, respectively, the per unit representation of (3.88) and (3.89) are

$$\bar{q} = \bar{G}\sqrt{\bar{H}} \tag{3.90}$$

$$\frac{d\bar{q}}{dt} = \left(1 - \bar{H} - \bar{H}_L\right) \frac{gA_{pen}H_{base}}{Lq_{base}} \tag{3.91}$$

$$\frac{d\bar{q}}{dt} = \frac{\left(\left(1 - \bar{H} - \bar{H}_L\right)\right)}{T_w} \tag{3.92}$$

where the water time constant T_w is expressed as

$$T_w = \frac{Lq_{base}}{gA_{pen}H_{base}} \tag{3.93}$$

The relation between the turbine output power and water flow from no load (q_{nl}) to full load (q_{fl}) is expressed as follows:

$$\tilde{P}_m = A_{TG}\tilde{H}\left(\bar{q}_{fl} - \bar{q}_{nl}\right) \tag{3.94}$$

The turbine gain A_{TG} is defined by the actual gate position (g_1) and the effective gate position (g_2) as follows:

$$A_{TG} = \frac{1}{g_2 - g_1} \tag{3.95}$$

The speed deviation damping due to gate opening is represented by a supplementary term $GD\Delta\omega$, which is subtracted from the output of the turbine model.

3.2.3 Other Components Model

Other components such as line, transformer and load models are also used. The transmission lines are presented by series connected $R-L$ branches in each phase. A constant impedance load model is used [89], where the active and reactive power injections at a given load bus vary directly with the square of the magnitude of the bus voltage. The 3ϕ transformer model is also used according to [89].

3.3 Simulation of the Micro-Grid System

Simulation is the basic and fundamental methodology to observe the dynamic behaviour of any system that is represented by system dynamic equations. The proposed micro-grid system dynamic model is realized by integrating all component models presented in section 3.2. In order to study the behaviour of the proposed micro-grid system in various operational modes, a simulation study is performed and the simulation results are presented in the subsequent sections. The measurements presented in the simulation results are in per unit, while using a base power of 27 MVA. The simulation was performed for a 60 second interval. The results are presented without initial transients and indicate the steady state operation of the system in the grid connected operating condition.

The WPGS operates with one, nine or without any wind turbines during the operation of an isolated micro-grid with wind power generation, grid connected micro-grid or isolated micro-grid without wind power generation system, respectively. The wind speed profile shown in Figure 3.12 is utilized by the wind turbine rotor and is generated using the wind field model in [90]. WPGS with no output power represents insufficient wind velocity to generate electric power. The number of wind turbines in operation in the WPGS in isolated mode depends on the micro-grid load demand and the wind availability, and to be determined by the control coordinator. The Vestas-90 wind turbine parameters are used to develop the wind turbine rotor model [91], and the generator parameters are given in Appendices A.2 and A.3 [91, 92].

The HGU model is the combination of the model of synchronous generator, hydro turbine and turbine governor system and excitation system. The synchronous machine parameters are obtained from Newfoundland Power, Canada and are

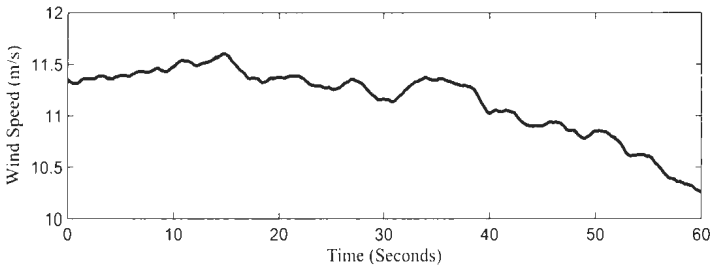

Figure 3.12: Wind speed profile used in simulation.

given in Appendix A.4 [93, 94]. The parameters for the hydro turbine and penstock are obtained from Newfoundland Power, Canada. The initial parameter settings for the governor and excitation system are obtained from [95, 96] and are modified for the system requirements in this research. The utility grid is represented by an equivalent model of 66 kV three phase voltage source with short-circuit capacity of 1000 MVA and reactance to resistance ratio of 22.2 [88]. The parameter information about the line, transformer and load are obtained from the utility company Newfoundland Power, Canada and is given in Appendix A.1. In the simulation, it is assumed that the grid is isolated from the system because of a fault in the grid transmission system (unintentional islanding) or regular maintenance (intentional islanding). The fault is simulated using a three phase circuit breaker with the fault time set at t = 5 seconds.

3.4 System Simulation Results and Discussions

The micro-grid system shown in Figure 3.13 is simulated using Matlab/simulink software. The complete Matlab/Simulink model of the micro-grid system is given in Appendix B. The overall model of the micro-grid system is comprised of detailed models of the HGU and WPGS. For example, the modeling of a WT generator is

developed by integrating the models of WT, induction generator and back-to-back PWM voltage source inverter. The developed model of the WT generator opposes the model of the WT generator that is represented by an equivalent DC source with no dynamics of the input primary sources.

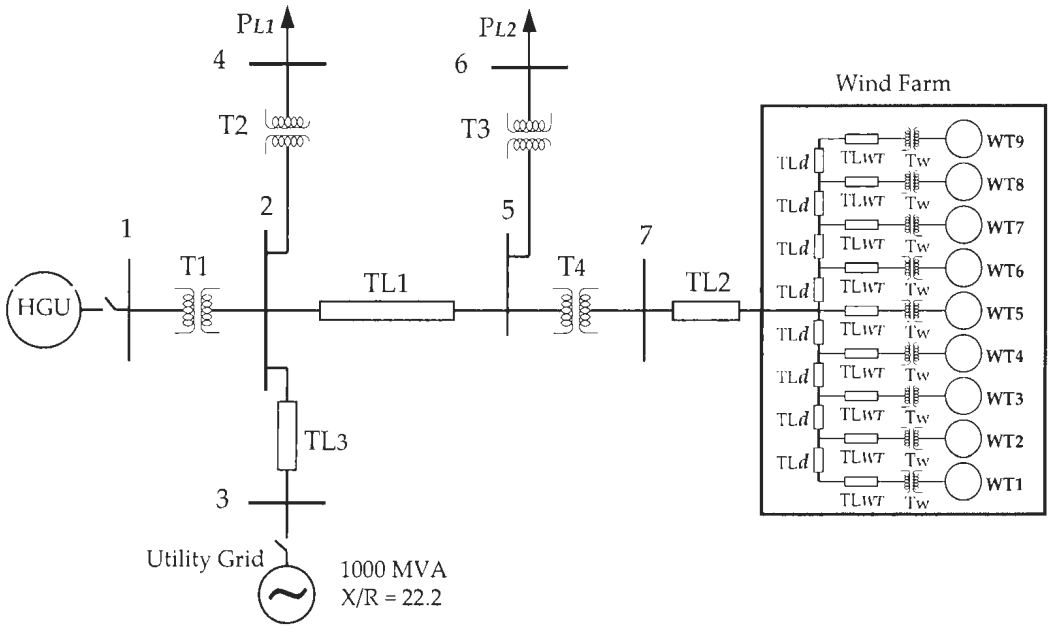

Figure 3.13: The single-line diagram of the micro-grid system that is simulated using Matlab/Simulink.

3.4.1 Mode-I: Grid connected system

The simulation results for Mode-I are represented in Figures 3.14(a-k). During this mode the WPGS and HGU are connected to the grid system (Figure 3.2). It can be seen from Figure 3.14(a) that the system frequency is at the rated value. Figures 3.14(b) and 3.4.1(c) show the real power generated and reactive power consumed by the WPGS, while nine WTs are in operation. The output of the WPGS varies

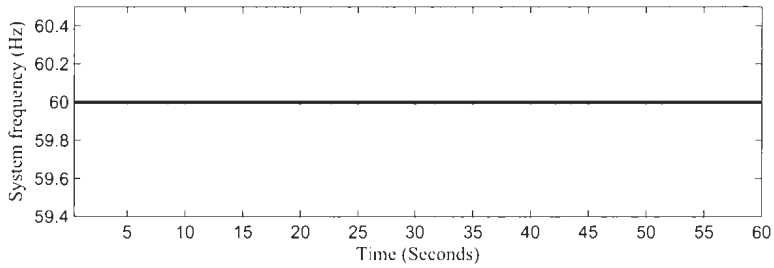
System frequency (Hz)
60.4
60.2
60
59.8
59.6
59.4
5 10 15 20 25 30 35 40 45 50 55 60
Time (Seconds)

(a)

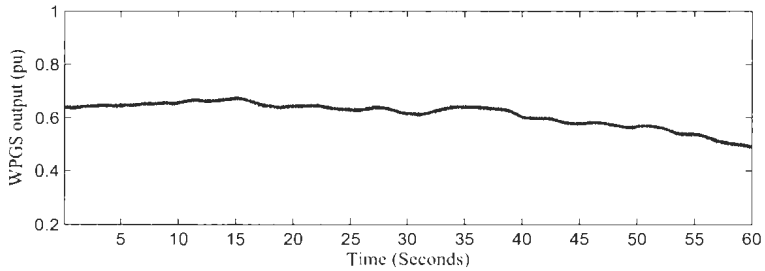
WPGS output (pu)
1
0.8
0.6
0.4
0.2
5 10 15 20 25 30 35 40 45 50 55 60
Time (Seconds)

(b)

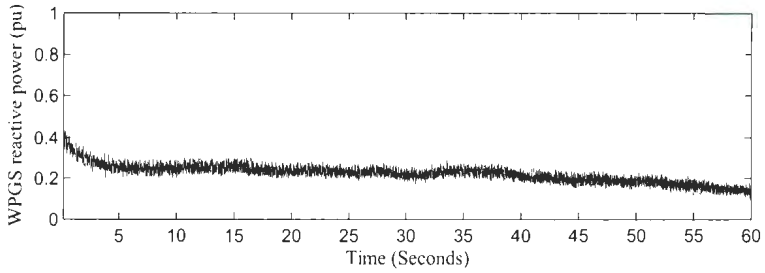
WPGS reactive power (pu)
1
0.8
0.6
0.4
0.2
0
5 10 15 20 25 30 35 40 45 50 55 60
Time (Seconds)

(c)

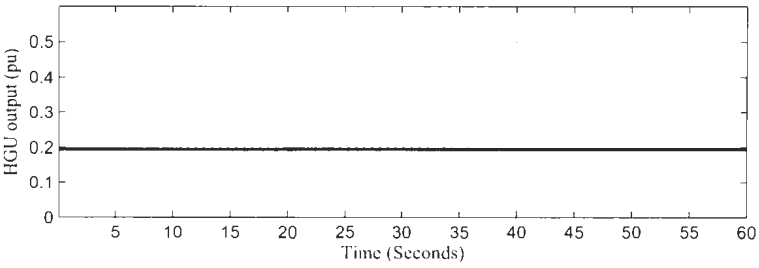
HGU output (pu)
0.5
0.4
0.3
0.2
0.1
0
5 10 15 20 25 30 35 40 45 50 55 60
Time (Seconds)

(d)

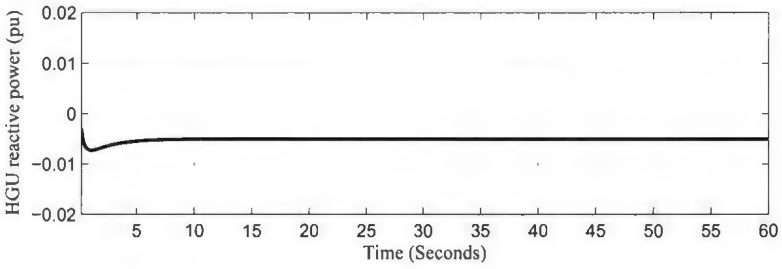
HGU reactive power (pu)
0.02
0.01
0
−0.01
−0.02
5 10 15 20 25 30 35 40 45 50 55 60
Time (Seconds)

(e)

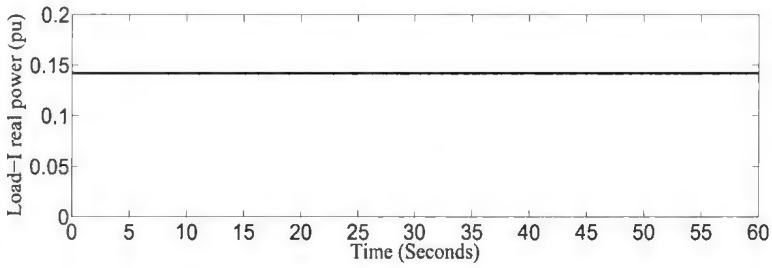
Load−I real power (pu)
0.2
0.15
0.1
0.05
0
0 5 10 15 20 25 30 35 40 45 50 55 60
Time (Seconds)

(f)

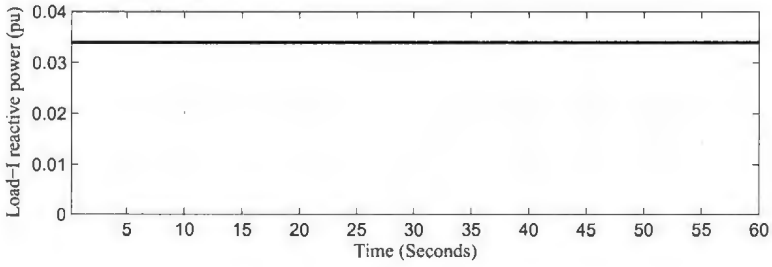
Load−I reactive power (pu)
0.04
0.03
0.02
0.01
0
5 10 15 20 25 30 35 40 45 50 55 60
Time (Seconds)

(g)

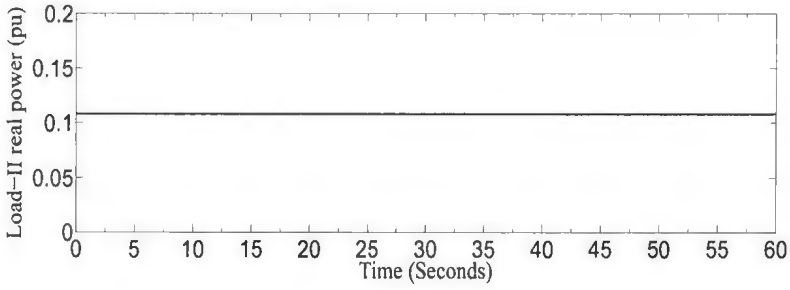
Load−II real power (pu)
0.2
0.15
0.1
0.05
0
0 5 10 15 20 25 30 35 40 45 50 55 60
Time (Seconds)

(h)

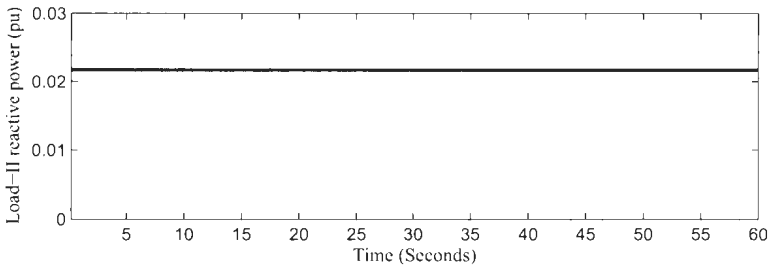

(i)

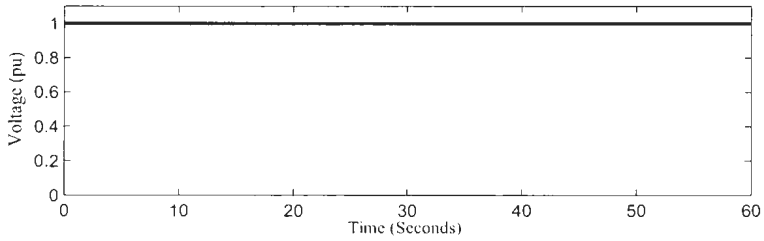

(j)

Figure 3.14: Grid connected system: (a) System frequency, (b-c) WPGS real and reactive power (d-e) HGU real and reactive power, (f-i) Load-I and Load-II real and reactive power demand, (j) Voltage at bus-2

due to wind speed variation. The reactive power consumed by the WPGS is high because all nine wind turbines in the WPGS are operating. The real and reactive power generated by the HGU is shown in Figures 3.14(d) and 3.14(e). Load-I real and reactive power demand supplied by the grid is shown in Figures 3.14(f) and 3.14(g). Figures 3.14(h)-3.14(i) represent the load-II real and reactive power demand. The voltage at bus 2 is shown in Figure 3.14(j). The voltage at bus 2 of the system is at its rated value. These results indicate that the operation of the HGU and WPGS in grid connected mode is dictated by the grid with the expected system voltage and frequency. In other words, the system variables such as voltage and frequency are not affected due to the variation in WPGS real power output.

3.4.2 Mode-II: Isolated system with wind power generation

The system operation follows Mode-I until t = 5 seconds. At t = 5 seconds, the grid is isolated from the system. Figure 3.15(a) shows the micro-grid frequency variation, which indicates that the power generation and consumption is not balanced during this mode of operation. It is to be noted that the frequency deviation is such that the generator will trip because of the system protection. However, such deviation is presented to show extreme conditions and check the exact frequency deviation during the transition from Mode-I to Mode-II. Figures 3.15(b) and 3.15(c) show the real power contribution and reactive power consumption by the WPGS during this mode when only one wind turbine is in operation in the WPGS. The variation in WPGS real and reactive power affects the total power generation in the micro-grid system, which can be seen from Figures 3.15(d) and 3.15(e). The real and reactive power consumed by Load-I is shown in Figures 3.15(f-g), while the real and reactive power consumed by Load-II is shown in Figures 3.15(h-i). It indicates that the load power is reduced by a small amount after grid isolation because of the reduction in system voltages caused by the lack of sufficient reactive power in the isolated micro-grid system. The lack of sufficient reactive power in the micro-grid system results in reduced voltage levels at the micro-grid system bus 2 (Figure 3.15(j)). Since the system variables such as frequency and voltage are impacted significantly, this would lead the system to an unstable operation during this operating mode. Figure 3.14(k) shows the current response which confirms the grid disconnection at t=5 seconds. More than one wind turbine operating in the WPGS will deliver more active power in the micro-grid system than the load demand. The reactive power demand will also increase in the micro-grid system which may result in further reduction in voltage level at different buses in the

micro-grid system.

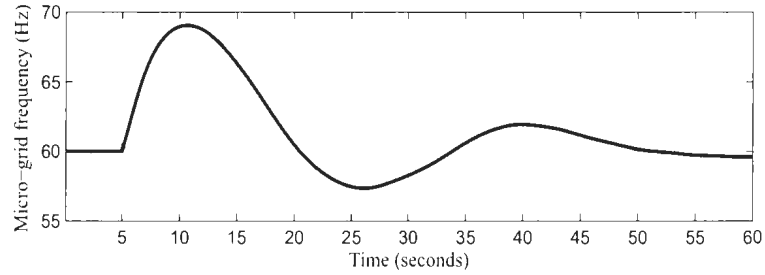

(a)

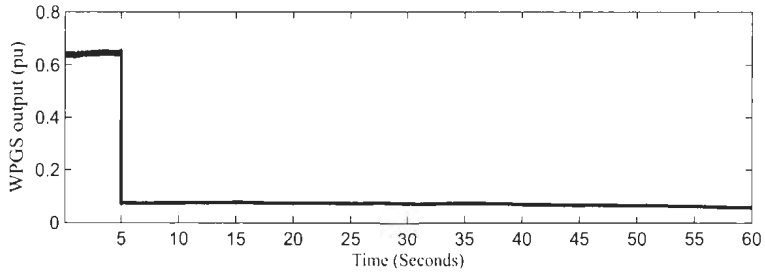

(b)

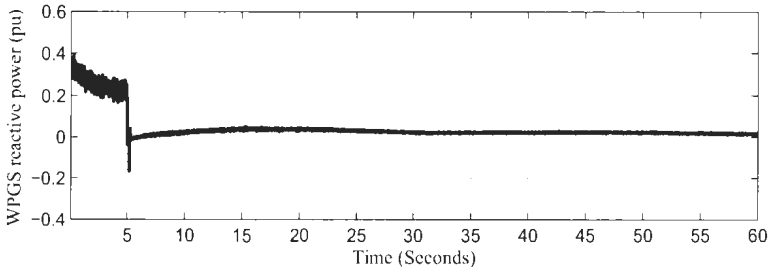

(c)

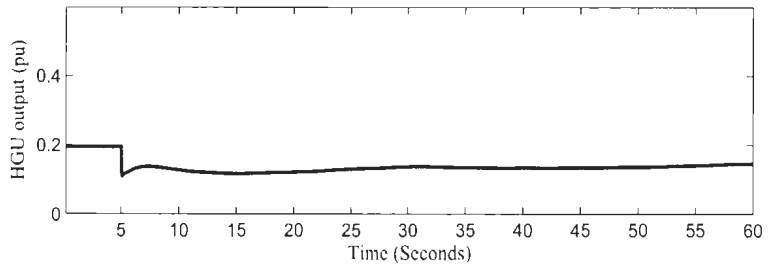

(d)

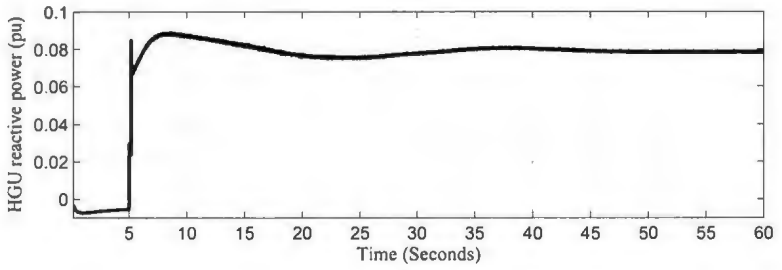
HGU reactive power (pu)
0.1
0.08
0.06
0.04
0.02
0
5 10 15 20 25 30 35 40 45 50 55 60
Time (Seconds)

(e)

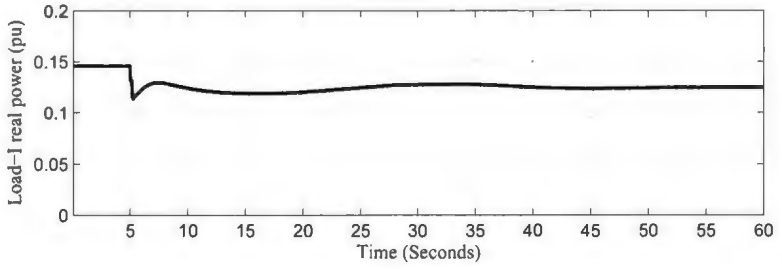
Load−I real power (pu)
0.2
0.15
0.1
0.05
0
5 10 15 20 25 30 35 40 45 50 55 60
Time (Seconds)

(f)

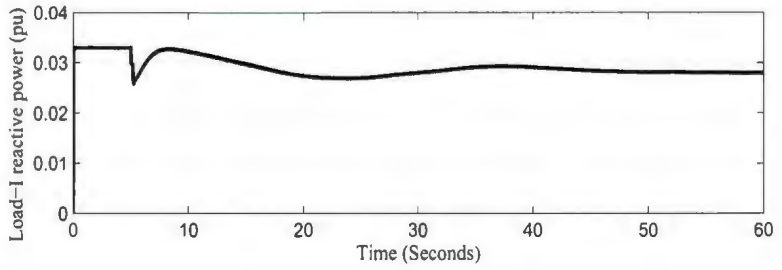
Load−I reactive power (pu)
0.04
0.03
0.02
0.01
0
0 10 20 30 40 50 60
Time (Seconds)

(g)

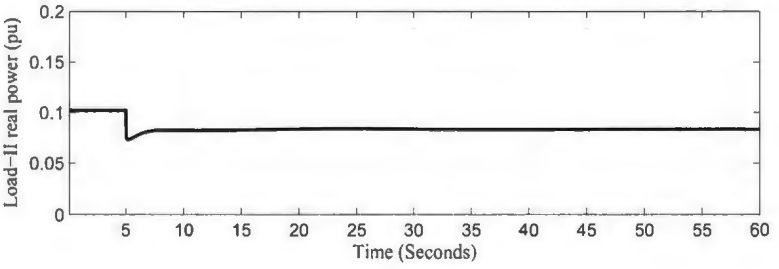
Load−II real power (pu)
0.2
0.15
0.1
0.05
0
5 10 15 20 25 30 35 40 45 50 55 60
Time (Seconds)

(h)

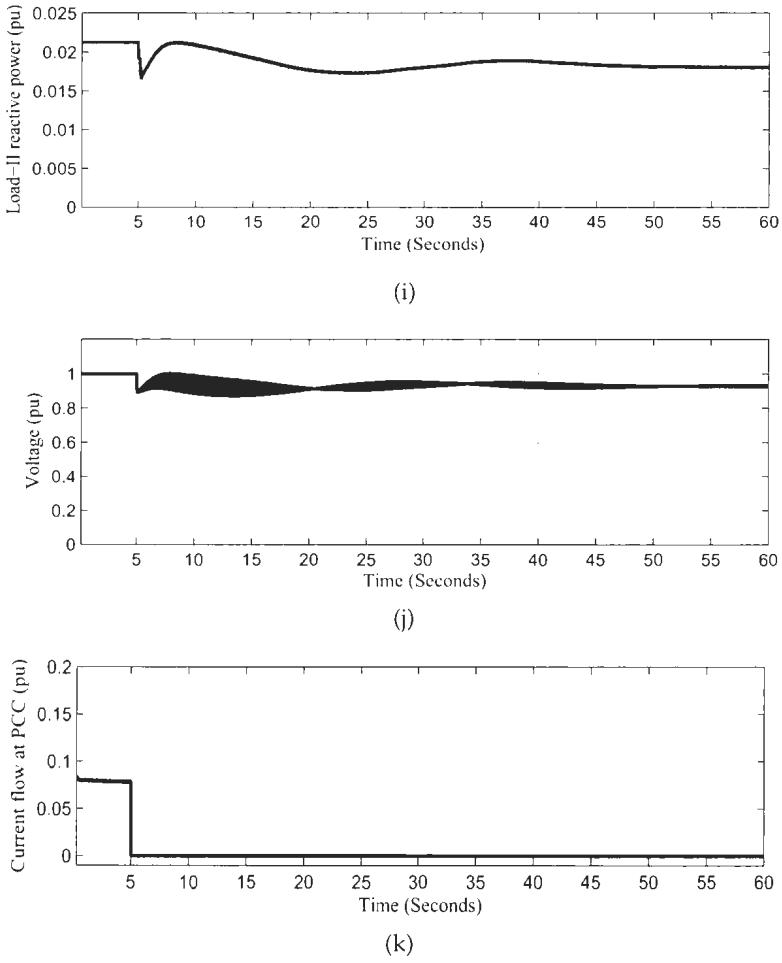

Figure 3.15: Isolated system with wind power generation: (a) System frequency, (b-c) WPGS real and reactive power (d-e) HGU real and reactive power, (f-i) Load-I and Load-II real and reactive power demand, (j) Voltage at bus 2, (k) Current flow at the Point of Common Coupling (PCC).

3.4.3 Mode-III: Isolated system without wind power generation

The system operation follows Mode-I until $t = 5$ seconds. However, at $t = 5$ seconds, the grid is isolated from the system. Concurrently, the WPGS has no output power as there is insufficient wind resource to produce electricity. This mode of operation is simulated, and the results are shown in Figures 3.16(a-l). Figure 3.16(a) shows the micro-grid frequency deviation after grid isolation, which is not in a tolerable range for micro-grid operation. This variation in system frequency occurs due to the fact that there is a shortage of real power generation in the micro-grid system. This is observed from the power out responses of the WPGS and HGU. Figures 3.16(b) and 3.16(c) represent the real power generation and reactive power consumption by the WPGS, which shows zero output power after isolation. The real and reactive powers generated by the HGU are shown in Figures 3.16(d) and 3.16(e). The HGU generates rated value real power because this is the only real power generation unit in the micro-grid, and also the reactive power demand is lower than for Mode-II. The load power shown in Figures 3.16(f-i) is lower than that of the Mode-II, as the power supplied by the micro-grid system is less than the load demand. This implies the requirement of additional power from a reliable storage system. The effect of insufficient reactive power in the micro-grid system is also observed from the voltage level at the system buses. The reduced level of voltage at different buses shown in Figures 3.16(j) and 3.16(k) indicates the requirement for reactive power in the micro-grid system. Thus it is found that the system variables such as frequency and voltage are affected while the system is disconnected from the utility grid and in subsequent operation. The current flow at the Point of Common Coupling (PCC) is shown in Figure 3.16(l), which shows zero current and confirms the grid isolation.

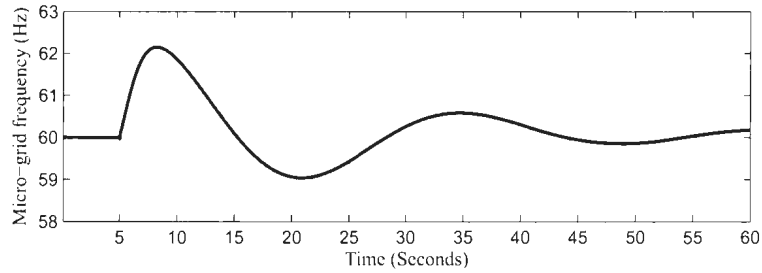
Micro-grid frequency (Hz)
63
62
61
60
59
58
5 10 15 20 25 30 35 40 45 50 55 60
Time (Seconds)

(a)

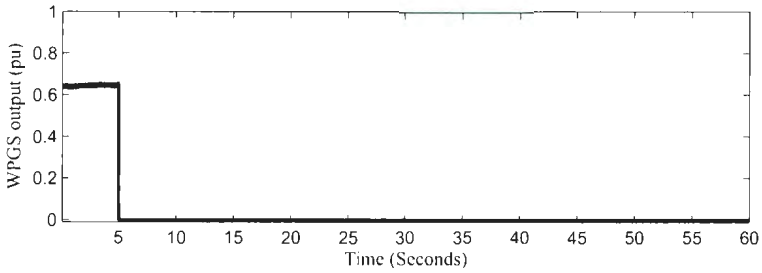
WPGS output (pu)
1
0.8
0.6
0.4
0.2
0
5 10 15 20 25 30 35 40 45 50 55 60
Time (Seconds)

(b)

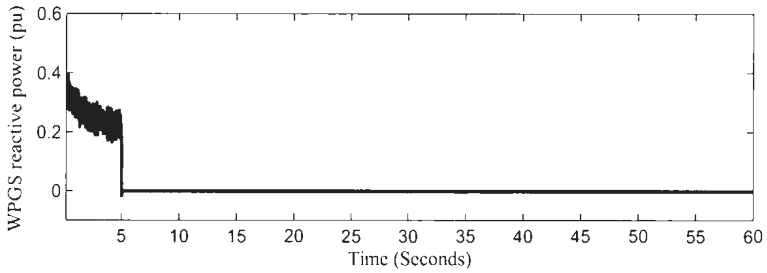
WPGS reactive power (pu)
0.6
0.4
0.2
0
5 10 15 20 25 30 35 40 45 50 55 60
Time (Seconds)

(c)

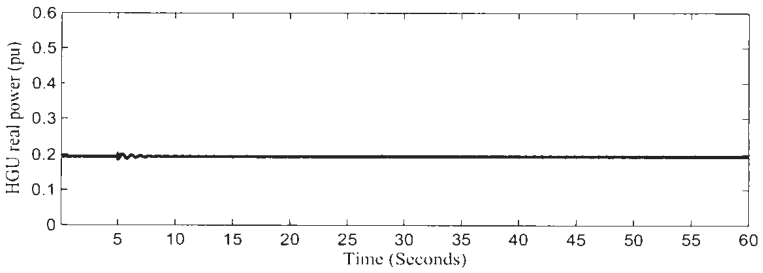
HGU real power (pu)
0.6
0.5
0.4
0.3
0.2
0.1
0
5 10 15 20 25 30 35 40 45 50 55 60
Time (Seconds)

(d)

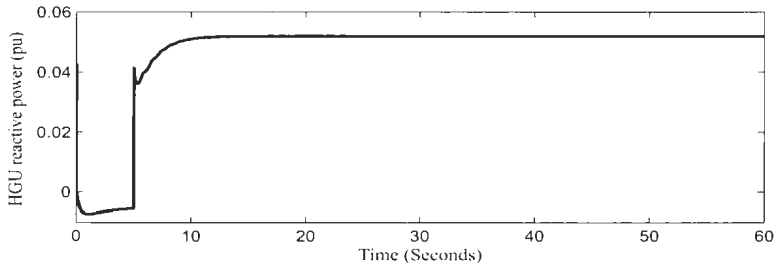
HGU reactive power (pu)
0.06
0.04
0.02
0
0
10
20
30
40
50
60
Time (Seconds)

(e)

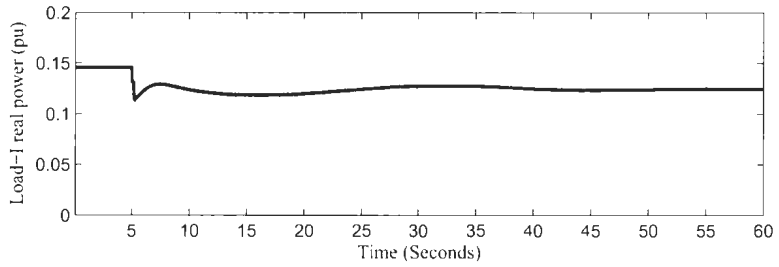
Load−I real power (pu)
0.2
0.15
0.1
0.05
0
5
10
15
20
25
30
35
40
45
50
55
60
Time (Seconds)

(f)

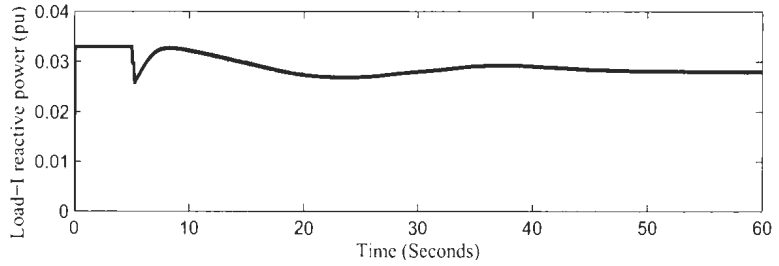
Load−I reactive power (pu)
0.04
0.03
0.02
0.01
0
0
10
20
30
40
50
60
Time (Seconds)

(g)

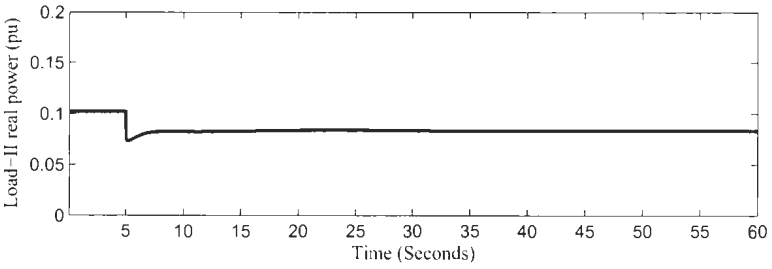
Load−II real power (pu)
0.2
0.15
0.1
0.05
0
5
10
15
20
25
30
35
40
45
50
55
60
Time (Seconds)

(h)

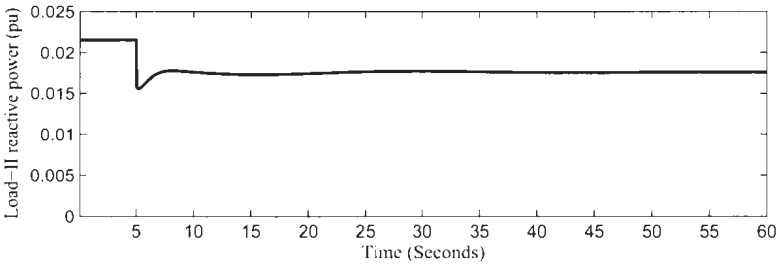

(i)

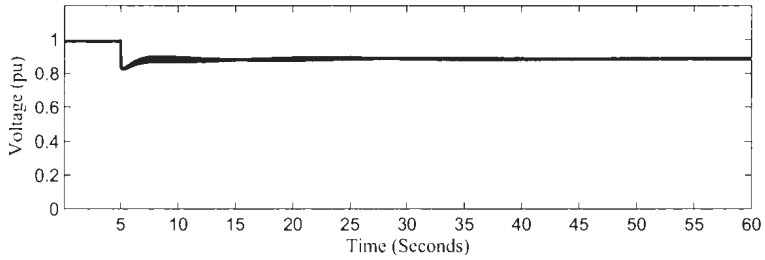

(j)

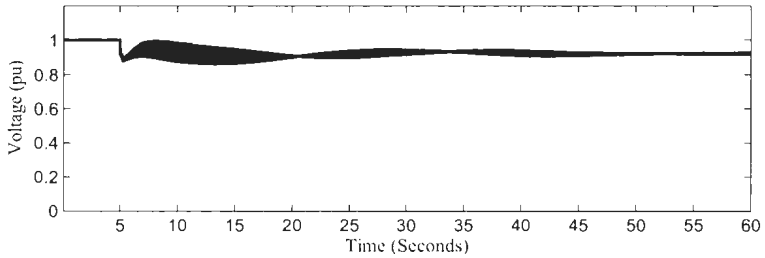

(k)

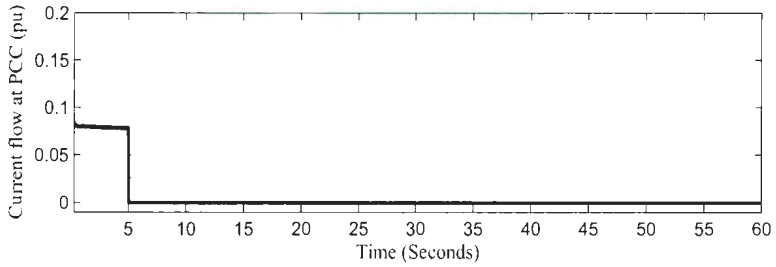

(l)

Figure 3.16: Isolated system without wind power generation: (a) Micro-grid frequency, (b-c) WPGS real and reactive power, (d-e) HGU real and reactive power, (f-i) Load-I and Load-II real and reactive power demand, (j-k) Voltage at bus-2 and Load bus-I, (l) Current flow at the PCC.

The analysis and discussion of the simulation study explore the problems related to the stable and reliable operation and control of the proposed micro-grid system based on renewable power generation. These are summarized as:

- Active power imbalance between generation units and loads in isolated micro-grid mode when wind power is available.
- Active power imbalance between generation units and loads when wind power is not available in isolated micro-grid mode.
- Reactive power is required during isolated micro-grid operation to maintain the expected voltage level at different buses in the micro-grid system.
- Need for reliable energy storage in isolated micro-grid mode.

A dump load will also be needed to maintain the active power balance between generation and loads in isolated micro-grid mode when wind power is available. The reactive power demand can be provided by STATCOM during isolated mode with wind power generation and by storage unit during isolated system without wind power generation mode.

3.5 Additional Requirements for Micro-Grid Operation

The system frequency and the required voltage level for the load are decided by the utility grid during the utility grid-connected operation. Any abnormal condition occurring in the up stream power line which is not cleared within the fault

clearing time set by the utility grid will result in system isolation. For reliable operation of the proposed micro-grid system during isolated mode, additional components such as a storage system, STATCOM, dump load as well as control strategies will be required. The isolated micro-grid system with additional components is represented conceptually in Figure 3.17.

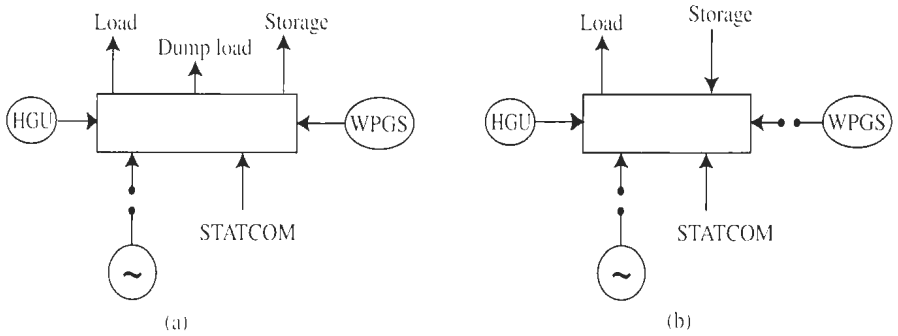

Figure 3.17: Functional block diagram of the proposed micro-grid operating modes: (a) Isolated micro-grid system with wind generator, (b) Isolated micro-grid system without wind generator.

Moreover, a voltage and frequency controller, control coordinator and monitoring system would be required to ensure reliable operation of the micro-grid system. During the isolated mode, the number of wind turbines in operation depends on the load demand and wind availability, which is determined by the control coordinator. Functions of the control co-ordinator and monitoring system can be performed based on the state diagram shown in Figure 3.18. This diagram shows the possible conditions for which the control co-ordinator and monitoring system may enable the system controllers to put the micro-grid system in different operating modes. The possible conditions include the availability of the grid power, P_{grid}; HGU power, P_h; cut-in wind speed of the wind turbine, v_{ciw}; and cut-out wind speed of the wind turbine, v_{cow}. In order to ensure reliable operation of the micro-

grid system over the entire range of operation, a control concept is proposed. Figure 3.19 shows the block diagram representation of the proposed control concepts for reliable and stable operation of the proposed wind-hydro micro-grid system.

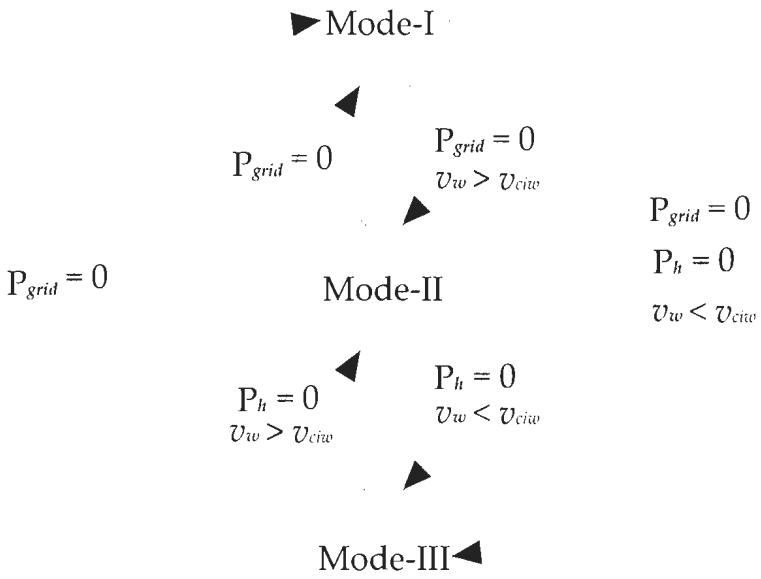

Figure 3.18: State diagram for operational modes of the micro-grid system.

- Control coordinator and system monitoring: The main functions of this subsystem are to: (i) detect the system islanding, (ii) activate the operating modes of the micro-grid system with the proper frequency and voltage controller, (iii) manage the wind turbine operation in the WPGS, (iv) monitor grid recovery and, (v) synchronize the grid. A load flow based micro-grid monitoring and control coordinator scheme is chosen to determine the power status at the buses of the proposed micro-grid system. Load flow problems for a

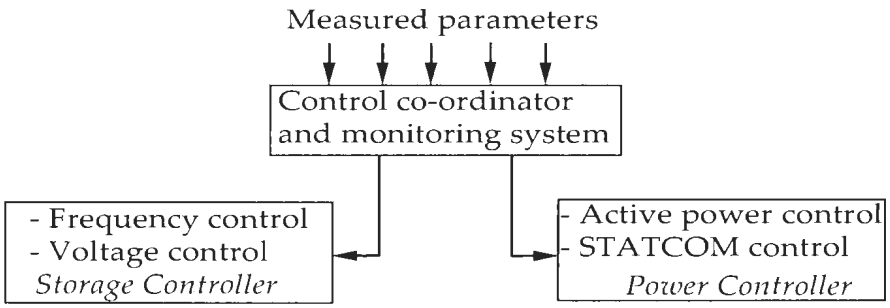

Figure 3.19: Proposed control and micro-grid system management concepts.

micro-grid system with few buses can be solved with fewer computational complexities.

- Active power controller: The objective of this control subsystem is to maintain the micro-grid frequency between 59.5-60.3Hz, while the HGU and WPGS deliver power to the micro-grid. The controller will maintain frequency by balancing the active power between the generation and load either by dumping power into the dump load or releasing power from it, and/or by storing energy using motor-pump units for pumping water into the upper reservoir.

- Storage system control: The objective of this control subsystem is to maintain the micro-grid frequency between 59.5-60.3Hz, while the micro-grid generated power, without wind power generation, is less than the load demand. The controller will maintain frequency by balancing the active power between the generation and load using a pumped hydro storage system or another fast response power electronic interface storage system.

- Voltage controller: The objective of this control subsystem is to maintain the micro-grid voltage at a desired level. The controller will maintain voltage level by balancing the reactive power in the micro-grid system. The control subsystem will ensure that during isolated mode with wind power generation the STATCOM will provide reactive power balance in the system. Similarly, during isolated mode without wind power generation the storage unit or STATCOM will provide reactive power balance in the micro-grid system.

3.6 Summary

The system behaviour analysis of a micro-grid consisting of renewable micro-generations and the observations derived from the investigations are presented and discussed in this chapter. Firstly, a micro-grid system based on available renewable energy sources is proposed. The key operational modes of the proposed micro-grid system are identified through analytical analysis. Secondly, an integrated dynamic model of the proposed micro-grid system is developed, which includes the dynamic models of various systems and sub-systems of the micro-grid system. Thirdly, the developed micro-grid system model is simulated in the Matlab/Simulink environment that reveals numerous issues regarding the operation and control of the proposed micro-grid system. Some of the key issues for operation of the isolated micro-grid system with wind power generation and the isolated micro-grid system without wind power generation are explained in this chapter in detail. Finally, an outline of solutions for some of the issues indicated in this chapter are also briefly proposed and will be examined in the subsequent chapters.

Chapter 4

Design and Development of Micro-Grid System Controllers

The aim of this chapter is to present the design and development of controllers for the stable and reliable operation of a micro-grid operating with renewable micro-generation. This chapter starts with an overview of the proposed control strategies of the micro-grid system under study. The purpose of the proposed control is to regulate the frequency and the voltage during micro-grid operation in a continuous fashion. The conceptual demonstrations of frequency and voltage regulation schemes in various operational modes are provided. The frequency regulation scheme used during the operating mode of an isolated micro-grid system with wind power generation is called the active power controller. The active power controller is designed based on AC voltage control concepts along with a heating load/dump load. The system frequency regulation using a pumped hydro storage unit during the operating mode of an isolated micro-grid system without wind power generation is also presented. The design, model and simulation of the frequency regulation schemes for both operational modes are presented and

discussed. Then the limitations of the pumped hydro storage in controlling the frequency for an isolated micro-grid system without wind power generation are also outlined. The limitations of the hydro storage system lead to the idea of utilizing inverter interfaced storage for the proposed micro-grid system. Therefore, a control scheme for an inverter interfaced storage system called the micro-grid power controller is presented. Finally, the formulation of the micro-grid power controller using power flow analysis is described. This controller is simulated using the Matlab/Simulink tool, and the simulation results are presented in this chapter.

4.1 Micro-Grid Control Concepts

The analysis of the micro-grid system behaviour presented in chapter 3 reveals the necessities and arrangements for controlling the operation of the micro-grid system. The outcome of the study shows that there is a need to develop controllers for two operational modes of the proposed micro-grid system. These operating modes are the isolated micro-grid with wind power generation and the isolated micro-grid without wind power generation. The overview of the control concepts for such operational modes is demonstrated in the following subsections. The basic schematic of the micro-grid control concepts for two operational modes are shown in Figures 4.1(a) and 4.1(b), respectively.

4.1.1 Isolated Micro-Grid with Wind Power Generation

The isolated micro-grid system with wind power generation is one of the modes of operation of the proposed micro-grid system where the system is isolated from the utility grid and consists of a hydro generation unit as well as a wind power

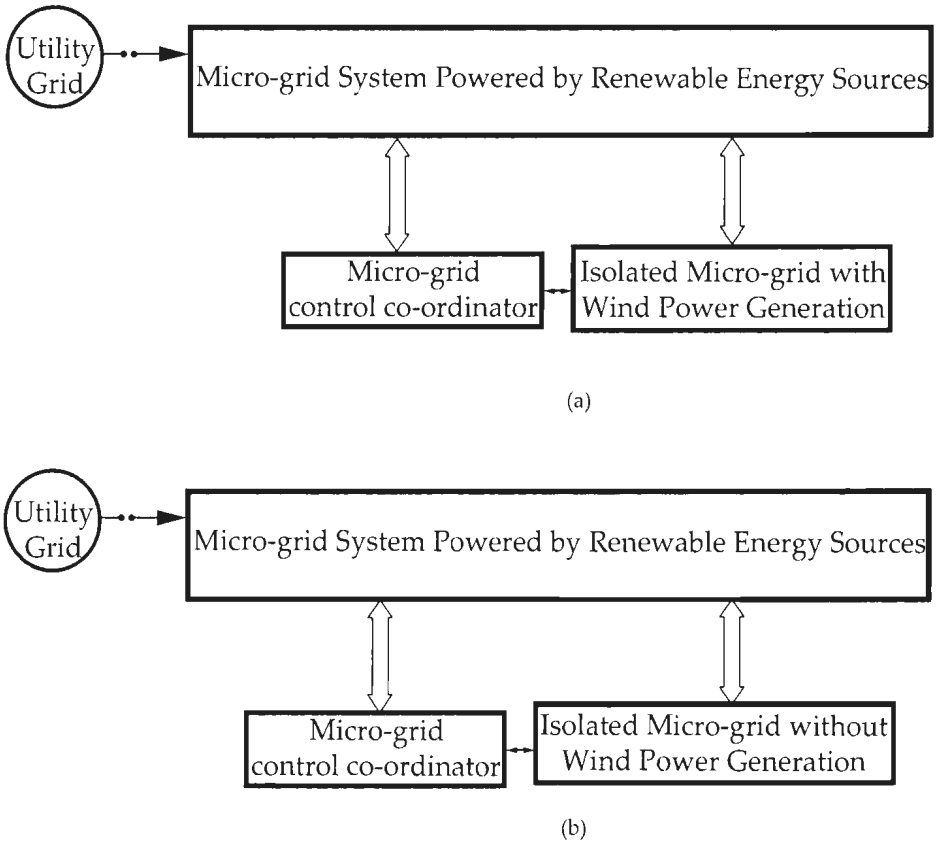

Figure 4.1: Conceptual diagram of the control concepts for the proposed micro-grid system.

generation system. The control for this mode of operation is referred to here as the Power Controller (PC). The basic layout of the PC during this operating mode is shown in Figure 4.2. The PC is comprised of two controllers, in order to regulate frequency and voltage of the micro-grid system. The frequency regulation scheme in the PC is called the active power controller, and the voltage regulation scheme in the PC is referred to here as the reactive power controller. Thus the objectives of the PC shown in Figure 4.2 are to control frequency and voltage of an isolated

micro-grid system while wind power generation is connected to the system.

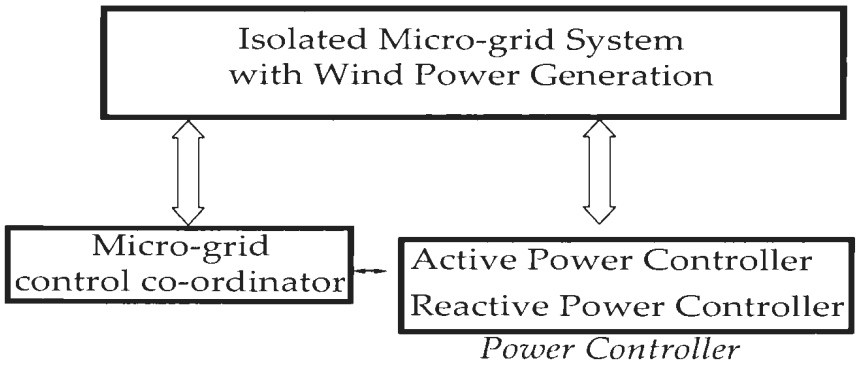

Figure 4.2: Power controller along with isolated micro-grid system while wind power generation is connected to the system

During this operating mode, the control principle of the active power controller has two purposes. One is to store energy in the upper reservoir and the other is to shape excess energy using a dump load such as a heating load. Due to the availability and opportunity to use an existing reservoir at the selected site (Fermeuse, NL, Canada), a pumped hydro storage system is proposed for the micro-grid operation. A motor equivalent load is used in the system to represent a motor-pump set during this operational mode. However, as the wind power varies stochastically and a motor-pump set consumes a finite amount of power, the isolated micro-grid system will still have excess active power which is required to be shaped continuously to maintain the system frequency in an acceptable range (59.5-60.3 Hz). In this work the focus is on the design, development and experimental testing of an active power controller for the micro-grid system based on renewable energy sources.

The reactive power controller in the PC is also required during the operating

mode of an isolated micro-grid with a wind power generation system. During this mode, the reactive power demanded by the wind power generator varies as long as there is a change in the wind velocity. Moreover, there is also a demand for reactive power by the micro-grid loads. Since the hydro generation unit is operated at its rated power, the reactive power generated by the hydro generation unit may not be sufficient to meet the reactive power demand. This reactive power demand can be met by utilizing a STATCOM based reactive power controller or an inverter interfaced storage controller.

4.1.2 Isolated Micro-Grid without Wind Power Generation System

The isolated micro-grid system without wind power generation is the mode of operation of the proposed micro-grid system where the system is isolated from the utility grid, as well as the wind power generation system being disconnected from the micro-grid due to insufficient wind speed. The control for this mode of operation is referred to here as the Storage Controller (SC). The basic block diagram representation of the SC during the operation of this mode is shown in Figure 4.3. The SC is comprised of two controllers whose objectives are to regulate frequency and voltage of the micro-grid system while wind turbines are not in operation within the system. One is a hydro storage control, that is investigated for frequency regulation of the proposed micro-grid system. The other control scheme is an inverter interfaced control.

For the hydro storage control, a conventional droop based governor control system is designed to regulate the frequency of the isolated micro-grid system. The synchronous generator equipped with a governor and excitation system is utilized

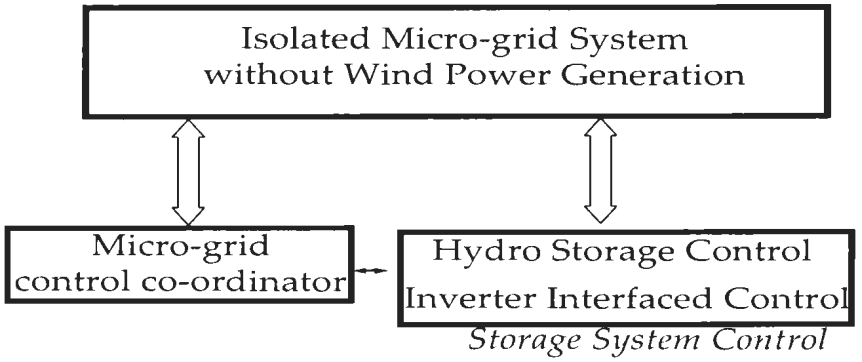

Figure 4.3: Basic schematic of the isolated micro-grid system without wind power generation along with storage controller.

as a hydro storage system. The performance results of such a controller show that the frequency regulation capability of the governor control scheme is acceptable; however, the response time is higher. Such a response characteristic may not be effective for an isolated micro-grid operation. Therefore, an inverter interfaced control scheme is designed and developed for the storage unit. The power electronic interfaced storage unit for the isolated micro-grid system without wind power generation is represented in Figure 4.4.

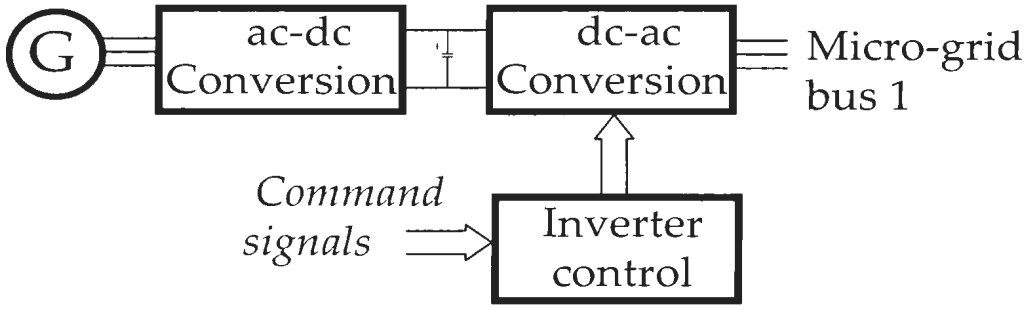

Figure 4.4: Schematic of the inverter interfaced storage unit for the isolated micro-grid system without wind power generation.

The output of the storage is assumed to be converted to DC using a rectifier/-converter which is then fed to the micro-grid using a controlled inverter. The demand of real and reactive power in the micro-grid system is utilized as the command values for the inverter controller. The inverter controller is required to maintain the command power flow from the storage unit to the micro-grid system. It is assumed that the storage unit is capable of providing sufficient power to meet the command power of the inverter controller. In this control scheme, the focus is given to the inverter control to manage real and reactive power of the micro-grid system based on a power flow analysis technique. Therefore, the storage unit and storage side converter are assumed to be a DC source, which is interfaced with the micro-grid bus 1 using a controlled inverter.

4.2 Power Controller

Power balance between generation and consumer loads is a critical issue for the stable and reliable operation of micro-grid systems. This issue becomes more critical when a micro-grid system contains distributed generation of a stochastic nature such as wind and solar because their output power changes non-uniformly. In order to achieve accurate and fast power balance in such a micro-grid system, power in the system has to be regulated continuously. Therefore, the aim is to design and develop a power controller scheme comprised of an active power controller and a reactive power controller for the operating mode of an isolated micro-grid system with wind power generation. The design, development and performance testing of the active power controller through simulation study are presented in the following subsections.

4.2.1 Active Power Controller

The main objective of the proposed active power control scheme is to maintain a continuous and smooth active power balance between generation and micro-grid load. It is worth mentioning that during the operating mode of an isolated micro-grid with wind power generation system, the active power generation in the system varies due to the stochastic variation in wind speeds. Moreover, the power balance in such a micro-grid system has to be achieved by allowing the wind generator to operate with optimal power extraction criteria rather than forcing the wind generator to produce power with a limited capacity of generation. Forcing wind turbines to generate power less than their available power will reduce turbine efficiency, as well as requiring additional time to get payback, which may not be an attractive option for investors. Therefore, an active power controller is required to be designed in a micro-grid system that contains renewable energy sources such as wind turbines by allowing them to operate in their maximum power extraction characteristic so that wind generators can produce power at their optimal efficiency.

Figure 4.5 shows the active power control strategy for the operating mode of an isolated micro-grid system with WPGS. The micro-grid control co-ordinator monitors the grid status by observing the current flowing between the micro-grid and the utility grid. The absence of the utility grid identified by the micro-grid control co-ordinator sends a signal to activate the active power controller. The active power controller always senses the system 3ϕ voltages to carry out the controller functions. The controller generates pulses for switching devices to maintain the power balance in the micro-grid. The micro-grid control co-ordinator also monitors the power, ΔP consumed by the dump load. Depending upon the value of

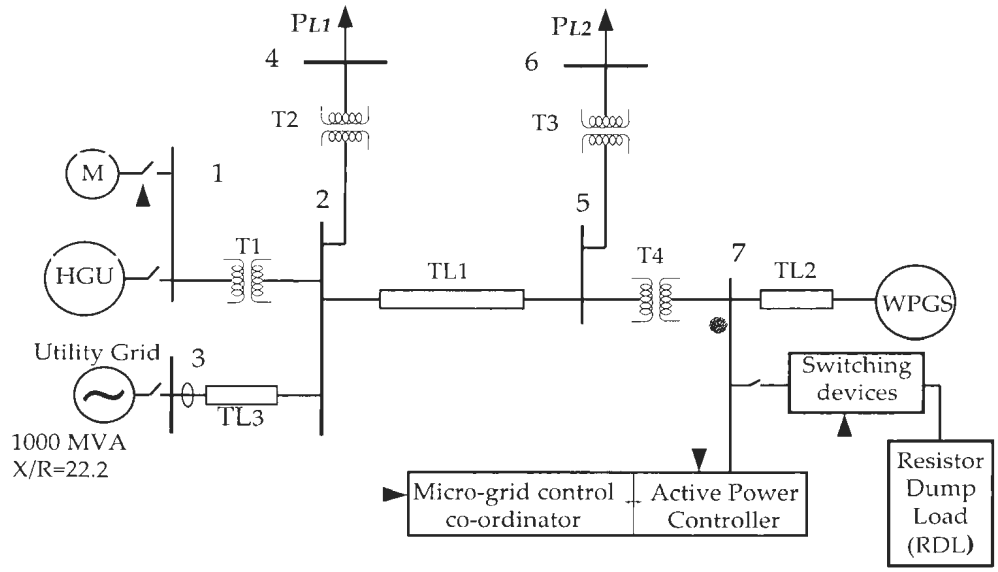

Figure 4.5: Conceptual diagram of the active power controller along with the micro-grid system.

ΔP, the control co-ordinator starts the motor-pump set to pump water. On the other hand, when the power ΔP is not sufficient to operate the motor-pump set, the control co-ordinator takes action to disconnect the motor-pump set from the system.

The functional block diagram of the developed controller is shown in Figure 4.6. The controller is comprised of a phase locked loop, droop calculator, proportional-integral regulator, firing angle calculator, firing pulse generator, switching devices, and resistive dump load. Two thyristor switches are connected in anti-parallel and used in one phase to achieve bi-directional operation. The thyristor switches are selected because of their capability to operate in high power applications [97].

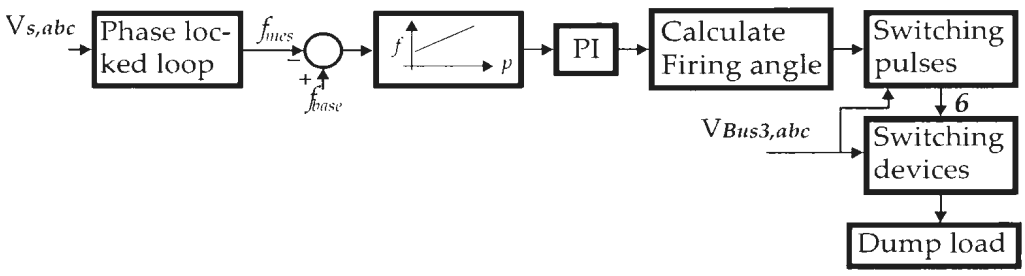

Figure 4.6: Functional block diagram of active power controller

Phase locked loop

The 3ϕ system voltages $V_{s,abc}$ are utilized in a phase locked loop to measure the micro-grid frequency. The measured frequency is compared with the micro-grid base frequency and it is utilized in the frequency-active power droop characteristics.

Real power and frequency droop characteristic

The frequency control of a system dynamically controls the power angle that basically leads to the regulation of the active power in the system. Thus the adjustment of real power is the key to maintain the micro-grid frequency at its rated value. Such an adjustment is performed using the droop characteristic between active power and frequency along with the alternating current control technique. The droop characteristic between active power and the system frequency is shown in Figure 4.7, and is defined as

$$p_{base} - p^{+}_{base} = \Delta P = -\frac{1}{D_c}\left(f_{base} - f^{+}_{base}\right) \tag{4.1}$$

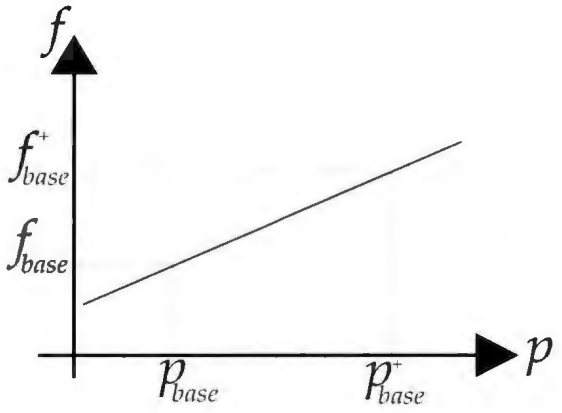

Figure 4.7: Frequency versus active power droop characteristic

where p^{+}_{base} is the power deviation in the micro-grid system, f^{+}_{base} is the frequency deviation due to the variation in active power, D_c is the power variation coefficient and f_{base} is the nominal micro-grid frequency at the nominal power p_{base} and ΔP is the power variation in the micro-grid that causes the change in the micro-grid nominal frequency. Thus the deviated power at a bus in the micro-grid system due to the change in frequency is determined by

$$\Delta P = -\frac{1}{D_c}\left(f_{base} - f_{mes}\right) \tag{4.2}$$

where f_{mes} is the frequency measured from the system.

Proportional-integral regulator

The active power deviation due to the frequency change in the micro-grid system, ΔP is calculated using (4.2), where the power variation coefficient, D_c is predefined. The power variation coefficient (D_c = 4.02) is determined based on the steady state power requirement at a bus while the isolated micro-grid system operates at its base frequency. The amount of deviated power or power error, ΔP obtained

using (4.2) must be absorbed or released by the dump load to maintain constant frequency in the micro-grid system. The deviated power, ΔP is passed through a proportional-integral regulator, which derives the control signal for silicon control rectifier switches. The control signal is expressed as

$$u_{cs} = \Delta P \left(k_p + \frac{k_i}{s} \right) \tag{4.3}$$

where k_p and k_i are the proportional and integral gain of the PI regulator. The controller is designed by looking at responses at the output of the firing angle estimator. The designed controller parameters (k_p=0.075, k_i=0.65) are chosen so that the response starts with a lower value of the firing angle and reaches the steady state value with a minimum rise time and settling time.

Firing angle estimation for switching devices

The control signal derived from the PI regulator is used to estimate the firing angle of the silicon controlled rectifier (SCR) switches for controlling the current flow into the dump load. The variation in the control signal creates the variation in the firing angles for the switches, which results in a change in the conduction angle of the SCR switches. The change in conduction angle of the SCR switches causes a change in the RMS value of the current flowing into the dump load, and thus results in a change in the amount of the real power going into the dump load. The firing angle estimator is represented by a linear equation using the fact that the higher value of the control signal, and hence more power going into the dump load, requires a lower value of firing angle and vice versa. Conceptually, higher value control signals represent larger error or larger power deviation in the micro-grid system, which require absorbing more power from the micro-grid system and vice versa.

As illustrated in Figure 4.8, the relation between firing angle and control signal is expressed as follows according to the principle of the SCR based three phase full wave AC voltage controller [97].

$$\alpha = \begin{cases} -69 \times u_{cs} + 87^0 & \text{for } 1 \geq u_{cs} \geq 0 \\ 69 \times u_{cs} + 87^0 & \text{for } 0 \geq u_{cs} \geq -1 \end{cases} \tag{4.4}$$

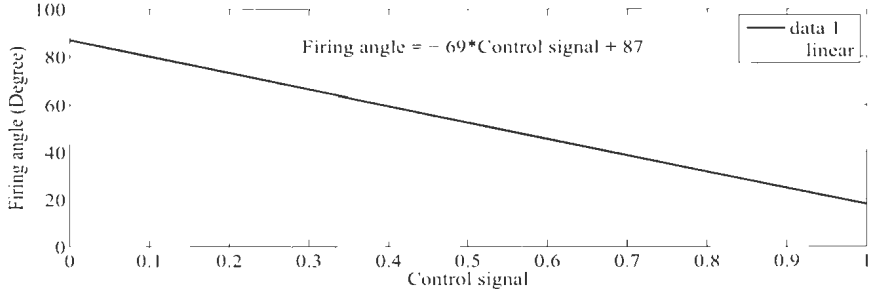

Figure 4.8: Relationship between the firing angle and the control signal

Firing pulse generation

A model of a pulse generation unit in Simulink is used to generate firing pulses for the silicon control rectifier switches. The firing angles determined by the firing angle estimator, and three phase voltages to be applied to the dump load, are taken as inputs to the pulse generation unit. The pulse generation unit generates synchronized firing pulses with these three phase voltages, which are sent to the gate of the SCR switches.

4.2.2 Modeling and Simulation

The designed active power control scheme described in the preceding section is modeled and simulated in the Matlab/Simulink environment in order to observe its performance. The available model of a phase locked loop and a firing pulse generation unit in the Simpower system library are used in this simulation. The models of power variation coefficient, control signal and firing angle estimator are developed using the available components in Simulink. The simulation is performed for a 20 second interval. The results are presented in pu at base power of 27 MVA. The HGU was operating at its rated power of 5.3 MW, and the WPGS was running with one wind power generator turbine while wind speed variation occurred according to Figure 3.12. In this case, the total maximum power generation possible in the micro-grid system is 8.3 MW. As the total load demand in the micro-grid system is 6.78 MW, a 2 MW dump load is used to absorb the surplus power from the micro-grid system. The designed control scheme is also simulated for this case, while a step load is applied to or released from the micro-grid system. The amount of load for a step change is equivalent to a load of a motor-pump set. Since it is necessary to run motor-pump sets to pump water into the upper reservoir for generating power using the stored water, a load equivalent to a motor-pump set is used for step change in the simulation. The simulation for a step load change is also a 20 second interval. The grid disconnection occurs at $t = 5$ seconds due to a fault or regular maintenance.

4.2.3 Simulation Results and Discussions

A simulation study is carried out on a system consisting of the active power controller along with the micro-grid system based on renewable power generation

shown in Figure 4.5, and the performance results are presented in Figures 4.9 and 4.11–4.21. The performances of the designed controller are observed for various operating conditions. These conditions are utility grid disconnection and subsequent operation, variable power generation by the wind generators, and step increase and decrease in loading conditions. The micro-grid frequency using the proposed active power controller and without the controller are shown in Figures 4.9 and 4.10, respectively. Until $t = 5$ seconds, the system frequency remains at its rated

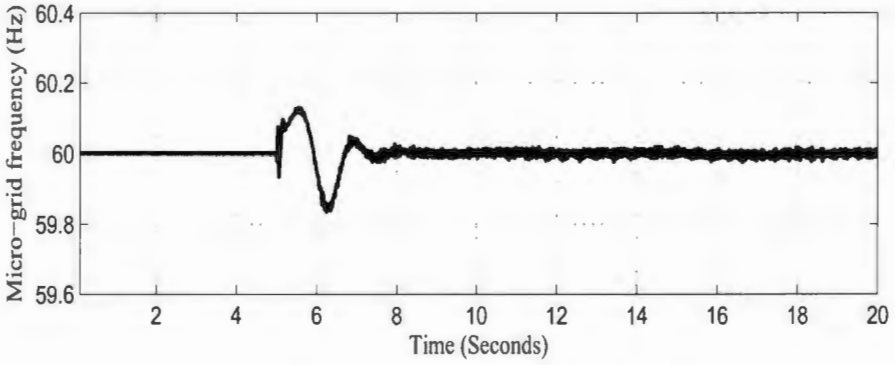

Figure 4.9: Micro-grid frequency using active power controller

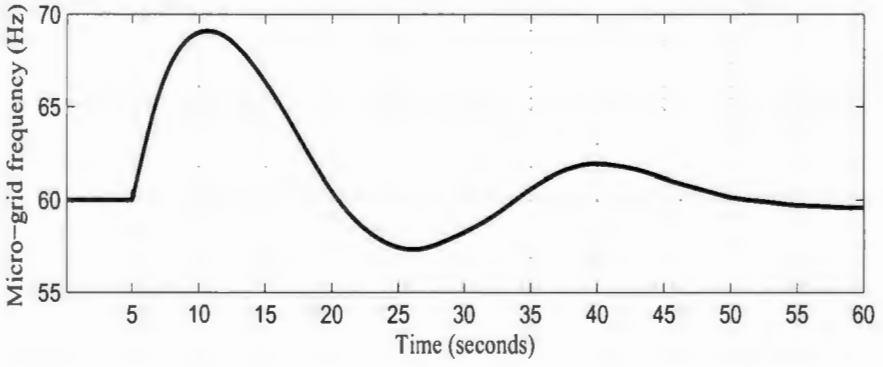

Figure 4.10: Micro-grid frequency without active power controller

value as the micro-grid system is connected to the utility grid. At $t = 5$ seconds,

the utility grid is disconnected from the micro-grid system and the designed active power controller is activated for the operating mode of an isolated micro-grid system with wind power generation. The frequency of the isolated micro-grid system during utility grid disconnection and in subsequent operation while wind power generation system is connected is shown in Figure 4.9. Due to the control action of the active power controller, the micro-grid frequency settles to its nominal value after a smooth dynamic change during the time of transistion from grid-connected to isolated micro-grid operation. On the other hand, the frequency of the isolated micro-grid system with wind power generation and without an active power controller, shown in Figure 4.10, starts with a large overshoot at the time of grid disconnection. This overshoot occurs as no control action is applied to the system. Thus the system frequency response indicates a significant ability of the developed controller to maintain an active power balance between the generation and the loads in the isolated micro-grid system with wind power generation.

During the operation of the isolated micro-grid system with wind power generation mode, the power consumed by Load-I and Load-II is shown in Figures 4.11 and 4.12. After isolating the utility grid, the load powers are reduced because of the reduction in voltage level (4.13) at the load buses in the system. The firing angle for the thyristor switches that is derived from control signals at the proportional-integral regulator output, and the average value of the current flowing into the dump load, are shown in Figures 4.14 and 4.15, respectively. Figure 4.14 illustrates that there is a fast, smooth and wide range of change in the firing angles at the beginning of the grid disconnection. These changes allow the controller to be able to accommodate the initial power mismatches during the transition from the utility connection to the isolated mode of operation. The rest of the time, t=10-20 seconds,

the firing angle varies dynamically to adjust the power in the micro-grid system that is supplied by the wind power generation system, since the power generation by the wind generator varies according to the change of the wind speed. Furthermore, Figure 4.15 demonstrates the change in the current flow into the dump load with the variation in firing angles. The variation in the average value of the current flow dictates the variation in power delivered to the dump load, which results in an active power balance in an isolated micro-grid system with wind power generation.

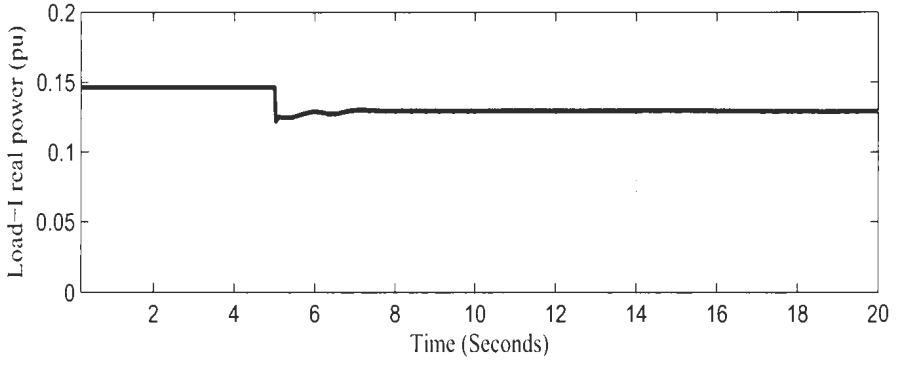

Figure 4.11: Power consumed by Load-I

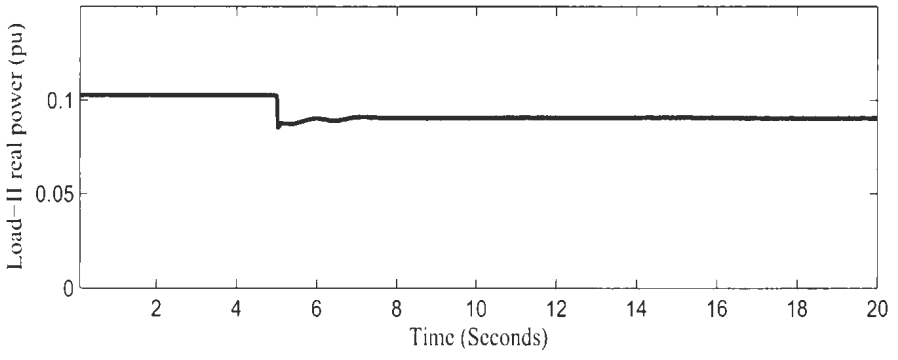

Figure 4.12: Power consumed by Load-II

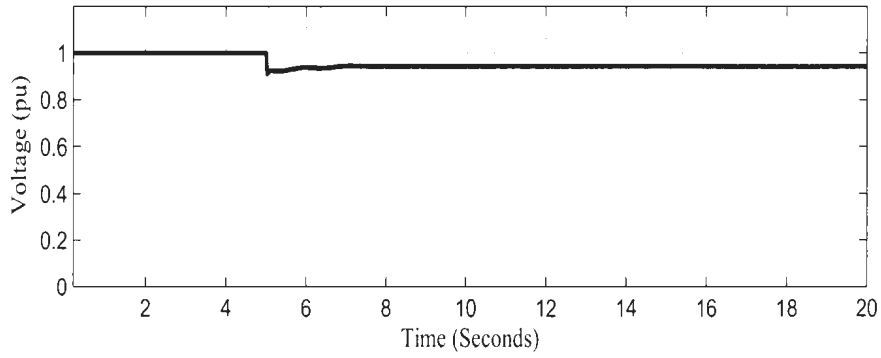

Figure 4.13: Voltage at load bus 1

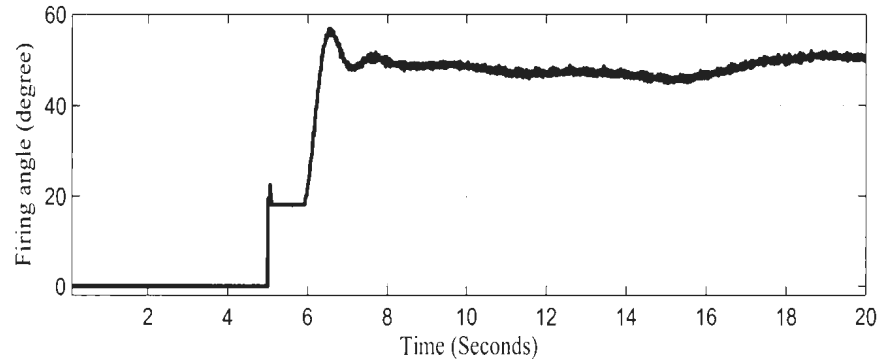

Figure 4.14: Firing angle for SCR switches

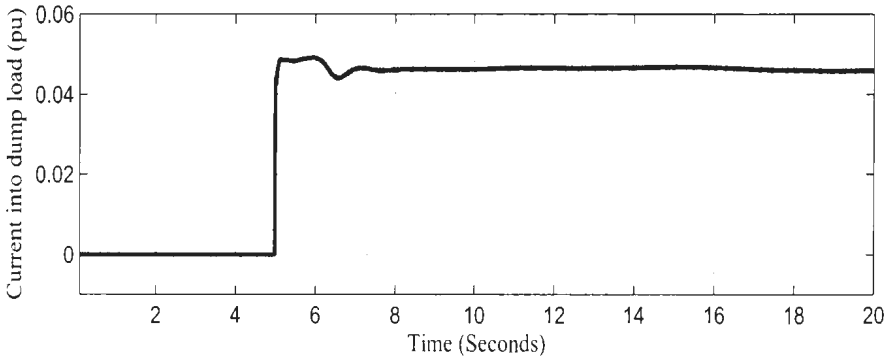

Figure 4.15: Current flowing into dump load

The active power controller performances are also verified using step changes in the loading condition, and the simulation results are presented in Figures 4.16-4.19 and 4.20-4.21. During the utility grid disconnection at t=5 seconds, the system frequency varies and then settles down to its rated value smoothly. An increase step change in load is applied to the system at t = 10 seconds in an amount of 7.4 percent of the total load demand of the micro-grid system. Similarly, a decrease step change in load is also created in the system at t = 15 seconds in the same quantity of the load. These step changes in load are applied at the same bus where load-II is connected and are shown in Figure 4.17. The selection of step change in load is chosen according to the load variation characteristics in the system, which are shown in Figure 4.18. The vertical axis of Figure 4.18 shows the amount of load change in percentage in every hour over a year. The actual change in load in each hour is more than 7.4 percent; however, in simulation 7.4 percent load change is chosen for every 5 seconds, which may be the worst case load change scenario in the proposed micro-grid system.

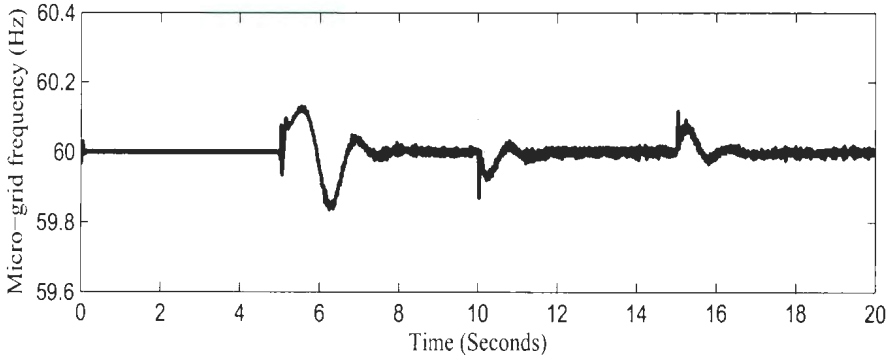

Figure 4.16: Micro-grid frequency using active power controller with step changes in load

The frequency of the isolated micro-grid system with wind power generation

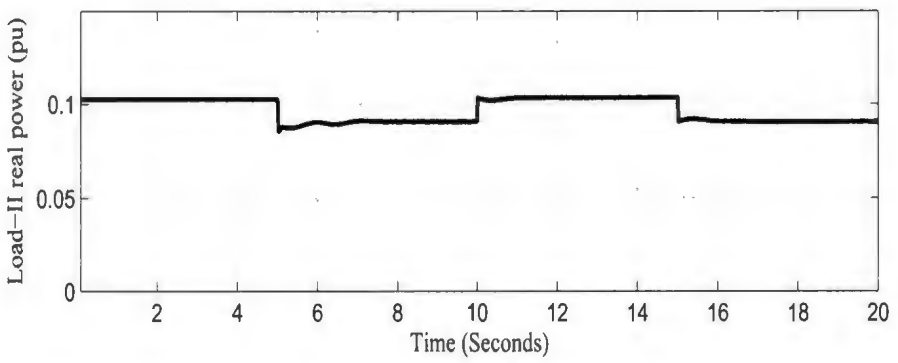

Figure 4.17: Power consumed by Load-II during step change in micro-grid load

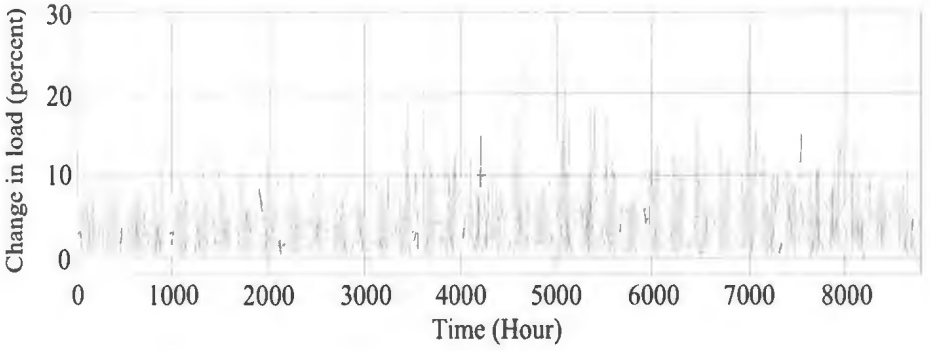

Figure 4.18: Variation in load on an hourly basis

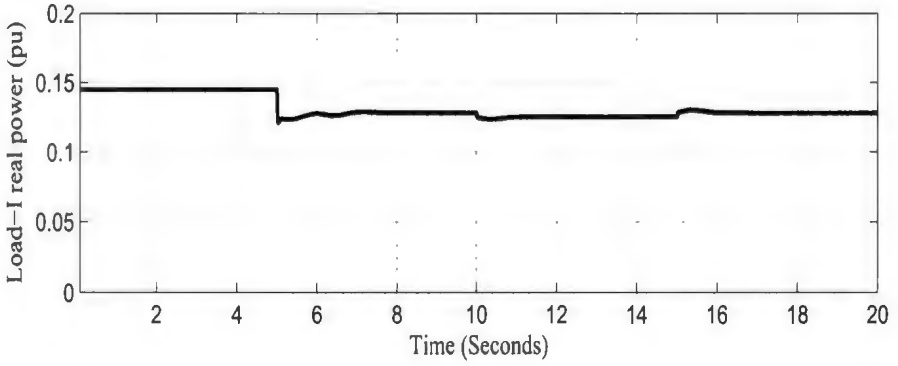

Figure 4.19: Power consumed by Load-I during step change in micro-grid load

along with the active power controller is recorded during step changes in load and is shown in Figure 4.16. The figure illustrates that a dip in system frequency occurs due to the change in load demand every time; however, after a short while the frequency settles back to its rated value. Frequency regulation in these operating conditions by adjusting the active power in the system also indicates a significant ability of the designed controller in the isolated micro-grid operation. Furthermore, the firing angles for thyristor switches derived from control signals and the current flowing into the dump load during step changes in the load are also shown in Figures 4.20 and 4.21, respectively.

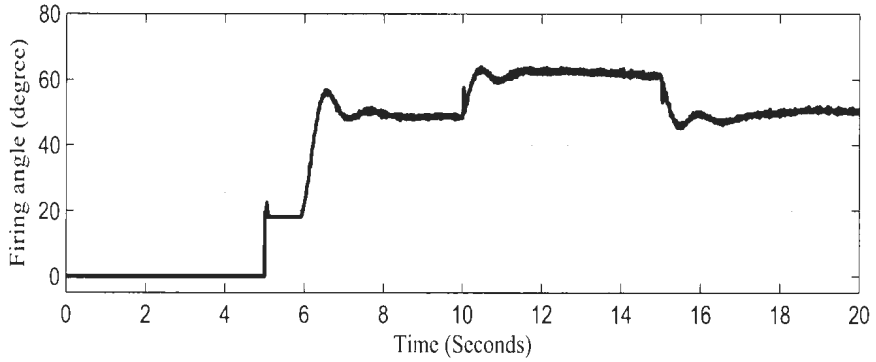

Figure 4.20: Variation in firing angle for thyristor switches during step changes in load

Figure 4.20 illustrates that the firing angle increases at t = 10 seconds because the micro-grid load demand increases. This condition indicates that there is a requirement to send less power into the dump load. This requirement is achieved by the action of the designed controller and is shown in Figure 4.21 because less power is supplied to the dump load starting at t = 15 seconds . Figure 4.20 also illustrates that the firing angle decreases at t = 15 seconds because micro-grid load demand decreases. This case indicates that there is a need to deliver more power

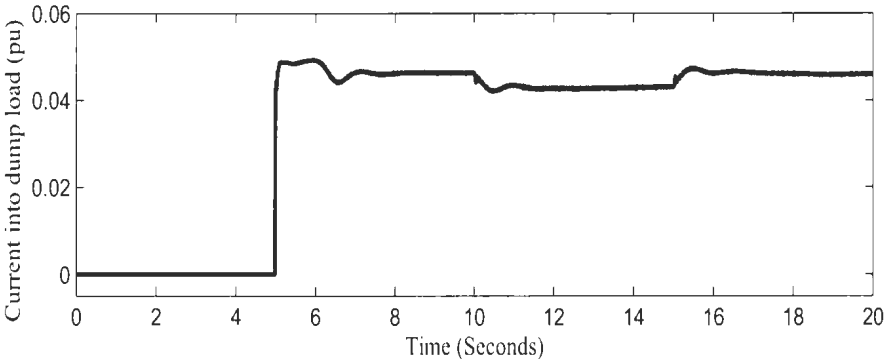

Figure 4.21: Change in current flow into the dump load during step changes in load

into the dump load. This goal is reached by applying the developed controller action and is shown in Figure 4.21, because more power is delivered into the dump load starting at t = 15 seconds.

4.3 Storage Controller

In chapter 3, it was observed that the power balance issues for the isolated micro-grid system without wind power generation are technically different from those of the isolated micro-grid system with wind power generation. The technical differences include the additional needs of reliable power generation sources and the control scheme to maintain the balance between generation and consumer loads. A storage unit, pumped hydro storage, is considered a reliable power generation source during the operation of the isolated micro-grid system without wind power generation. In addition, to maintain the balance between generation and loads, it is also desirable to design and develop a control scheme for the storage unit. The following section describes the primary design of the pumped hydro storage system, a controller for frequency regulation and a summary of the outcome obtained

by utilizing such a storage unit.

4.3.1 Pumped Hydro Storage

One of the major challenges of installing pumped hydro storage is the availability of a suitable land site to create a water reservoir because such an arrangement requires a significant amount of investment of the utility company. The opportunity to use the existing water reservoir in the selected site, and to utilize wind power to pump water into the water reservoir are the key reasons to choose pumped hydro storage for the operation of the proposed micro-grid in isolated conditions. The pumped hydro storage system basically consists of motor-pump sets to pump water into the upper reservoir and a hydro turbine generator to generate electricity using water's potential energy from the upper reservoir. The motor-pump sets are utilized in order to pump water into the upper reservoir using the excess power generated by the wind generator during the operating mode of an isolated micro-grid system with wind power generation. However, during the time when the wind generators are not available due to the lack of sufficient wind speed, the hydro turbine generator in the hydro storage system is employed to deliver power to the micro-grid. The hydro turbine generator (generator and turbine) is referred to here as a hydro storage unit (HSU). The isolated micro-grid system with the HSU is represented in Figure 4.22, where a motor-pump set is shown by an equivalent motor load, M.

Design of Pumped Hydro Storage System

The pumped hydro storage system is designed based on the power requirement of the isolated micro-grid system. The total average load demand in the micro-grid

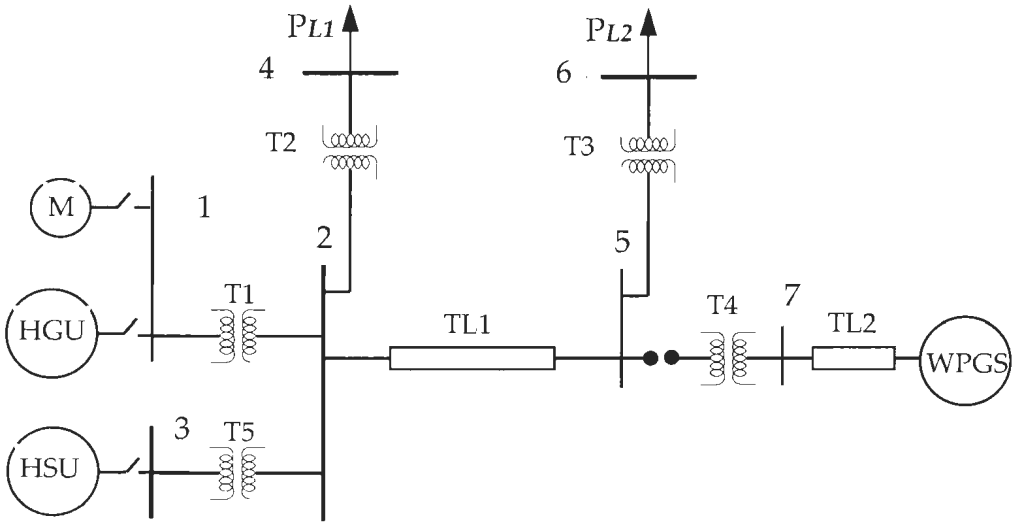

Figure 4.22: Isolated micro-grid system with hydro storage unit

system is 6.78 MW. The HGU is a firm generation system and has the ability to produce 5.3 MW. The shortage of power demand in the isolated micro-grid system while WPG is not available is 1.48 MW. Therefore, it is necessary to make up for the shortage of power using the HSU. The power requirement for motor-pump sets to store water in the upper reservoir, and power generation capacity supplied by the HSU using reserved water are calculated as follows.

Power Required for Motor-pump Sets:

It is assumed that a 1 m diameter steel pipe is used to pump water at a 54.8 m height with a 4 m^3/s flow rate. The water velocity is determined as

$$v = \frac{4Q}{\pi d^2} = 5.1 \ m/s \tag{4.5}$$

where Q is the flow rate of the water, and d is the diameter of the pipe.

The Reynolds number, R_e for a steel pipe is found by

$$R_e = \frac{\rho_w v d}{\mu} = 5.1 \times 10^6. \tag{4.6}$$

Relative roughness of the steel pipe is calculated as

$$\frac{\epsilon_a(mm)}{d(m)} = 0.5 \times 10^{-4}. \tag{4.7}$$

The Reynolds number and the relative roughness of the steel pipe are fitted into the Moody's diagram, and thus the friction factor for the selected pipe is found to be 0.017.

The head loss, H_L is thus determined as

$$H_L = \frac{f l v^2}{2gd} = 1.23 \ \ m. \tag{4.8}$$

Hence, the total head required for lifting water by the motor is

$$H_t = (54.8 + 1.23) = 56.03 \ \ m. \tag{4.9}$$

Power required at the pump impeller, P_{imp} is calculated as

$$P_{imp} = \frac{9.8 Q H_t}{0.75} = 2.92 \ \ MW. \tag{4.10}$$

Assuming that the motor efficiency is 90 percent, the power required at motor input, P_m is 3.25 MW.

The power required to run the motor-pump set is obtained from the isolated micro-

grid system while the micro-grid has surplus power. A motor-pump set is required to turn on, depending on how much surplus power is available in the isolated micro-grid system with wind power generation. The amount of surplus power in the isolated micro-grid system depends on wind speed availability and will vary over a time period. An arrangement that consists of at least seven parallel motor-pump sets, each rated at 460 kW, is preferred, rather than choosing a bigger motor-pump set which requires more power to turn on. If the isolated micro-grid system has surplus power of about 500 kW, one motor-pump set is required to turn on. Similarly, other motor-pump sets have to be turned on individually depending upon the available power. Such an arrangement keeps open an opportunity to add more motor-pump sets in future to store an extra amount of water to produce a higher amount of electricity. Switching on and off a 460 kW motor-pump set also implies a step change in load which is equivalent to 6.8 percent of the total load. It is to be noted that the active power controller described in section 4.2 is simulated with a 7.4 percent step change in load, and the performance results indicate the stable operation of the micro-grid system under such operating conditions.

Generation Capacity

The power generation capacity of the hydro turbine generator in the hydro storage system is determined using a flow rate of 4 m^3/s and a head of 54.8 m. Considering the efficiency of the generator-turbine as 72 percent, the power generation capacity of the hydro turbine generator is

$$P_{gc} = 9.8 \times \eta_{gt} \times Q \times H = 1.55 \ MW. \tag{4.11}$$

Reservoir Availability and Back up Duration

The area of the water reservoir that is currently available to store water is approximately 3.1 km^2. It is decided that the water level of the reservoir can be raised by 0.5 m with the extra amount of water pumped by the motor-pump set. The total volume of water that can be stored in the reservoir is 1,550,000 m^3. Since the discharge rate of water for generating power is 4 m^3/s, the designed storage system can generate power for 107 hours at its rated value of 1.55 MW.

4.3.2 Control System for the Hydro Storage Unit

The concept of energy conversion of a hydro storage unit (HSU) is similar to a conventional hydro generation unit (HGU). The combination of a synchronous generator coupled to a hydro turbine is utilized as the HSU in this thesis. The topological similarities between the HSU and HGU are the main motivation to choose the conventional governor and excitation control for the HSU. However, the differences between the HGU and the HSU are in their generation capacities, as well as the operation of the HSU being only on a demand basis and in discrete time. The difference in generation capacities is a result of the differences between the water flow rates and the penstock dimension in the HSU and HGU. The on-demand and discrete time factors demonstrate that the HSU needs to operate when wind power generation is not available, which can happen at any point of time. Such differences in the operation of the hydro storage system create a challenge to design a control system for storage. However, the similarities between the HGU and HSU allow the conventional governor and excitation control to be applied to the HSU. The function of the governor system in the HSU is to control the frequency of the isolated micro-grid system using the speed and power variation informa-

tion acquired from the system, while the excitation system is used to control the generator terminal voltage by controlling the excitation voltage in the field of the synchronous generator. The governor and the excitation system for the HSU are adopted according to [87, 88]. The parameter for the generator unit is obtained from [6]. In addition, the initial parameter settings for the governor and excitation system are obtained from [89, 98] and are modified according to the requirements of the system utilized in this thesis.

4.3.3 System Modeling and Simulation

Simulation of the isolated micro-grid system with the HSU (Fig. 4.22) is performed and the simulation results are presented in the subsequent section. The simulation results are presented in per unit on a base power of 27 MVA. The simulation is performed for a 100 second interval. It is assumed that the HSU starts up before grid isolation. The grid is isolated from the system at t = 5 seconds because of a fault or regular maintenance in the upstream power line. As the WPGS is not in operation during this operational mode, at t = 5 seconds, the HSU is connected to the system to meet the power demand of the micro-grid load. During this operational mode, the frequency of the micro-grid system is managed by the governor control of either the HGU or HSU. As both generation units use the same reservoir to generate power, the power shortage in the micro-grid during this mode can be met by either generation unit. The control scheme is also simulated for a case while a step load is applied or released from the micro-grid system. The amount of load used for a step change is about 2-7.5 percent. The simulation for step load change is performed for a 150 seconds interval. The grid disconnection occurs at t = 5 seconds, and load rejection and addition occurs at t = 50 seconds and t = 100 seconds,

respectively.

4.3.4 System Simulation Results and Discussions

The simulation results for operation of an isolated micro-grid with storage are presented in Figures 4.23 and 4.25-4.34. The performance of the system frequency during the operation of the isolated micro-grid with hydro storage system control and without hydro storage control are shown in Figures 4.23 and 4.24. The system frequency remains at its rated value until t = 5 seconds due to the grid connected operation of the micro-grid system. At t = 5 seconds, the utility grid is disconnected from the system and the storage unit is connected for operation of the isolated micro-grid system without wind power generation. Figure 4.23 shows that the isolated micro-grid system with a storage unit operates at a desired frequency level because of the power contribution from the storage unit. However, the system frequency of the isolated micro-grid system without a storage unit shown in Figure 4.24 deviates in an undesirable magnitude. The power generated by the HGU and HSU, generator load angles, power consumed by loads and voltage at the load bus are shown in Figures 4.25, 4.26, 4.27, and 4.28, respectively.

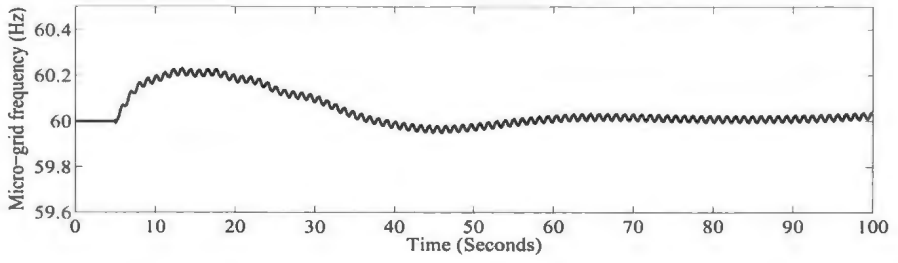

Figure 4.23: Micro-grid frequency using governor control in hydro storage system

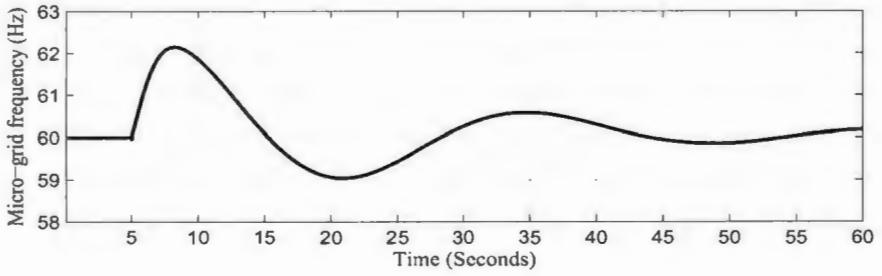

Figure 4.24: Micro-grid frequency without storage system

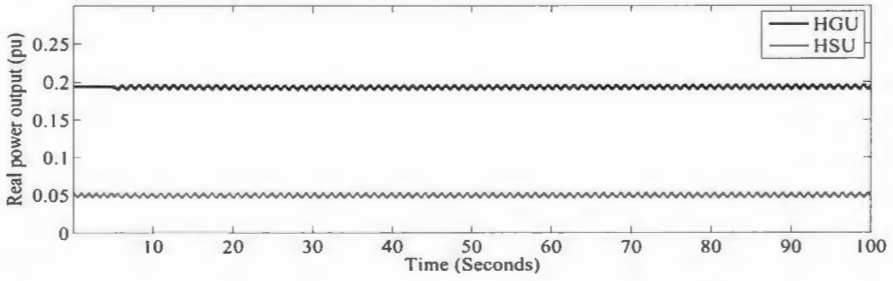

Figure 4.25: Active power generated by the hydro generation unit and hydro storage unit

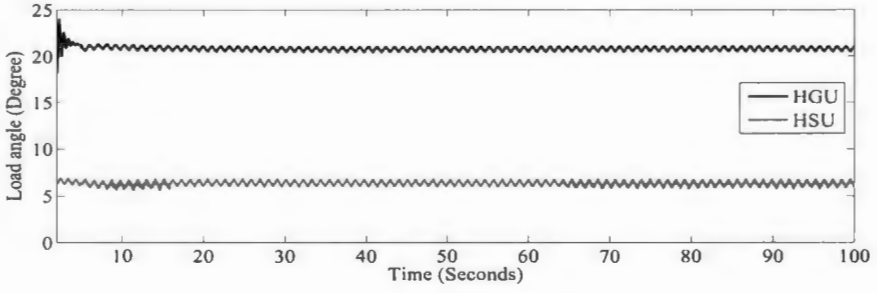

Figure 4.26: Load angle of hydro generation and hydro storage unit

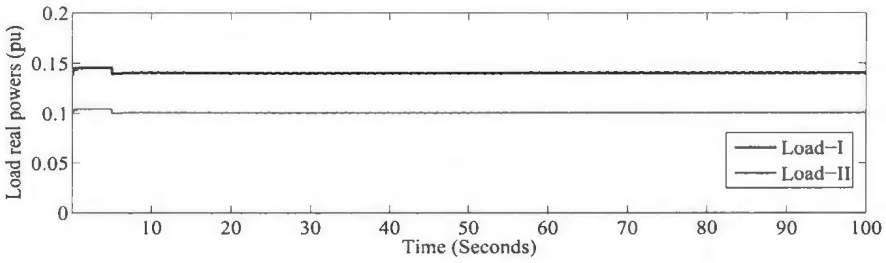

Figure 4.27: Power consumed by Load-I and Load-II

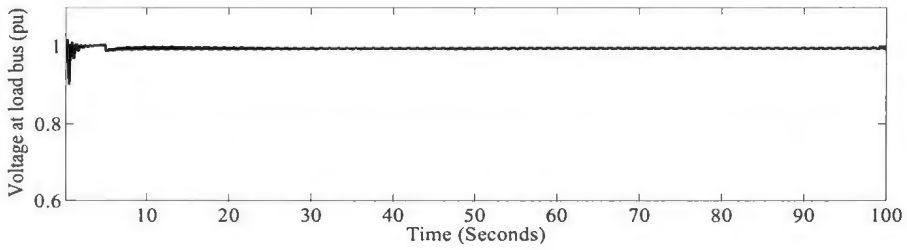

Figure 4.28: Voltage at load bus 1

The control of the storage system is also verified while a step change in load occurs in an isolated micro-grid operation, and the simulation results are shown in Figures 4.29-4.32. A decreased step change in load occurs at t = 50 seconds in an amount of 2 percent of the total load demand while an increased step change in load occurs at t = 100 seconds in the same amount. The step change in load is shown in Figure 4.32. After the step change in load, the frequency of the isolated micro-grid system with storage system control remains in an acceptable range and is shown in Figure 4.29.

The performance of the micro-grid grid system is also tested using a hydro storage unit while another step load change, 7.5 percent of the total micro-grid load

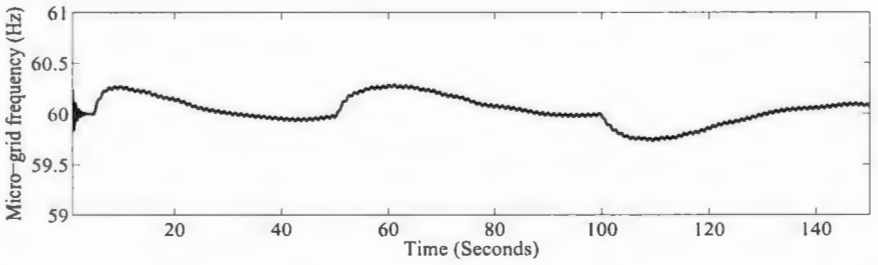

Figure 4.29: Micro-grid frequency using storage control with a step change in load

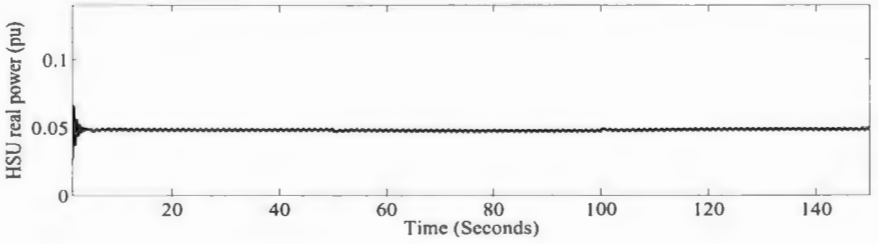

Figure 4.30: Active power generated by hydro storage unit during step change in load

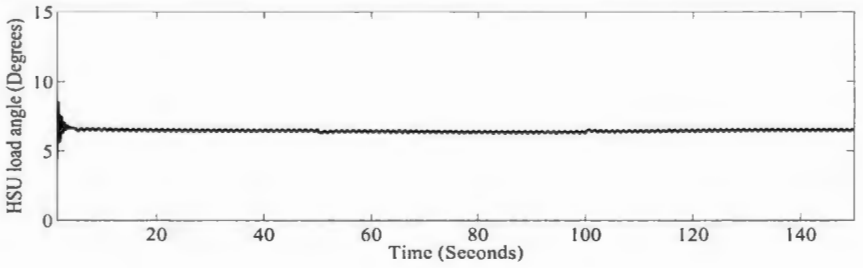

Figure 4.31: Load angle of hydro storage unit during step change in load

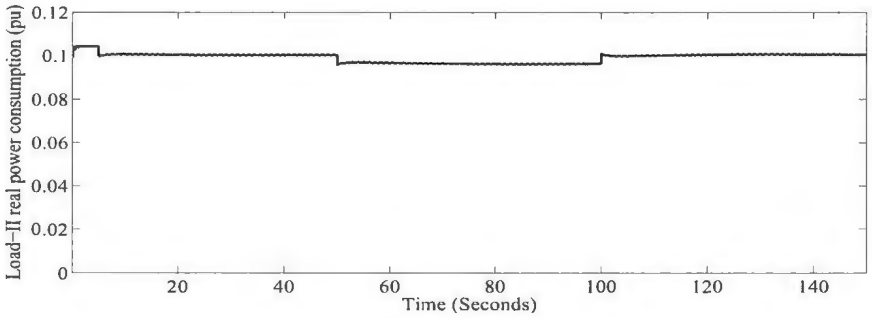

Figure 4.32: A step (2 percent) decrease in load at t = 50, and a step (2 percent) increase in load at t = 100 seconds

demand, is applied. The performance results obtained through simulation study are presented in Figures 4.33 and 4.34. The simulation results indicate that the storage system equipped with a conventional governor control is able to maintain the isolated micro-grid system frequency between 59.5-60.3 Hz while step changes in load are 2 percent and 7.5 percent of the total load demand. However, the initial frequency deviations at two different step changes in load are different, where a higher percent step change in load creates a higher overshoot in the isolated micro-grid frequency. In addition, the decaying time from maximum overshoot to a desired level (59.5-60.3) is longer, which may not be sufficient for an effective operation of an isolated micro-grid system with the hydro storage unit.

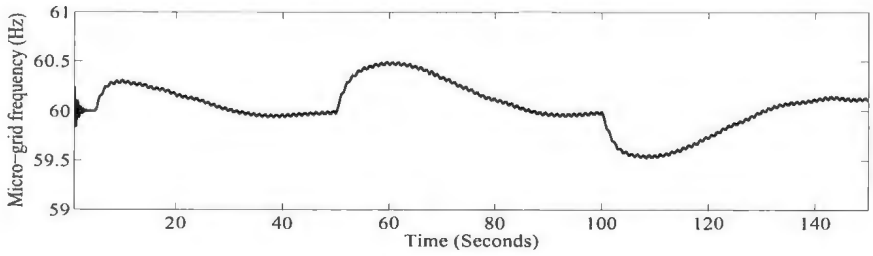

Figure 4.33: Micro-grid frequency while a step change in load is 7.5 percent

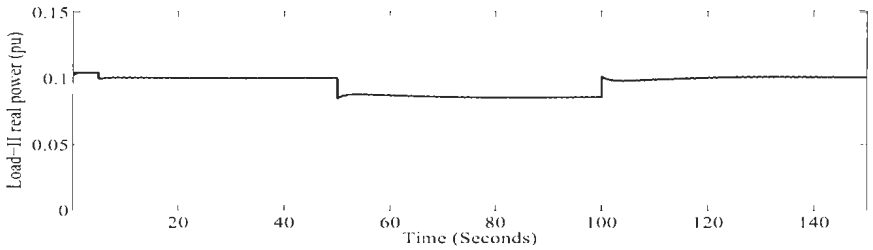

Figure 4.34: A step (7.5 percent) decrease in load at t = 50, and a step (7.5 percent) increase in load at t = 100 seconds

4.4 Power Flow Based Micro-Grid Controller

The frequency regulation performance in an isolated micro-grid system using the developed active power controller is encouraging because of its ability to achieve fast, reliable and accurate power balance in the system. On the other hand, the performance in regulating the system frequency using conventional governor control may be acceptable but may not be very promising because fast and accurate responses are required by the micro-grid system. Thus this section aims to develop an alternative control scheme for micro-grid systems. The developed control scheme is realized by employing the $d-q$-axis power flow analysis. Utilizing the $d-q$-axis power flow in such a controller provides instantaneous values for the command active and reactive power delivered from generator(s), renewable energy source(s), storage system(s) and/or the utility grid. Also, results obtained from the $d-q$-axis power flow analysis are used for monitoring the power exchange between the micro-grid system and the utility, as well as the status of storage system(s). The developed controller can be operated both in utility-connected or stand-alone modes of operation.

4.4.1 The Micro-Grid Control Scheme

The developed control scheme for both the stand-alone and the utility grid-connected modes of operation of micro-grid systems is referred to here as a power flow based micro-grid controller (PFMC). The conceptual diagram of the developed power flow based micro-grid controller is shown in Figure 4.35. The PFMC

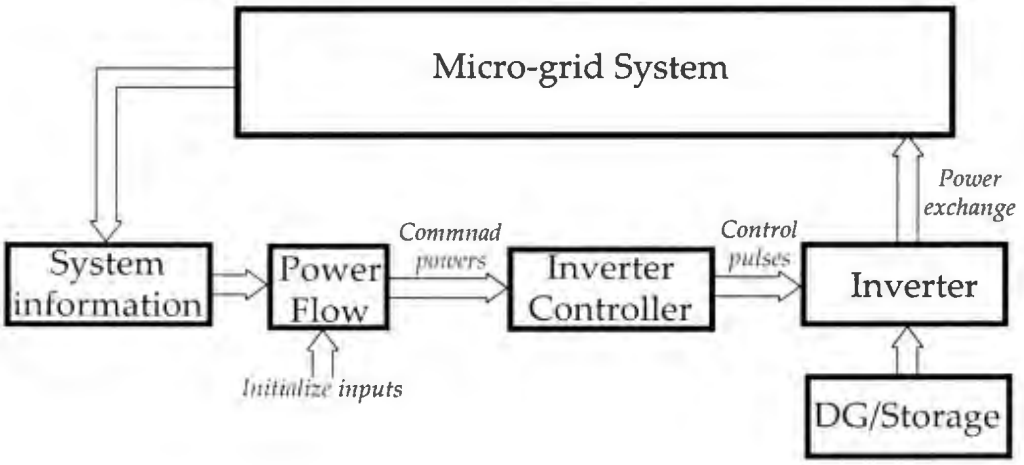

Figure 4.35: Basic structure of the micro-grid controller using power flow and controlled inverter

is comprised of the micro-grid power flow calculation, inverter controller, and inverter interfaced storage or distributed generation units. It is important to monitor the current status of the micro-grid system continuously in order to establish the balance between the power generation and the load demand in a continuous fashion. The information acquired from the system is utilized as the input to the power flow calculation of the micro-grid system. The power flow calculation converges to a solution for a balanced condition between generation and load, and the outcome of the calculation provides powers required at various buses for the same balanced condition. These powers are utilized to determine the command currents

for the inverter controller. The inverter is controlled so that the command powers are delivered by the DG/storage unit to the micro-grid system.

4.4.2 $d-q$-Axis Power Flow

Power flow (PF) analysis is among the widely used numerical tools for determining values for voltages (both magnitude and phase), active power and reactive power of all buses in a power system. There are several methods to formulate and solve PF problems, among which are Gauss–Seidel (GS), Newton–Raphson (NR), decoupled, fast decoupled and DC methods. In general, a PF formulation assumes that at each load bus (PQ bus), the active power P_L and reactive power Q_L are known. Also, a PF formulation assumes that for each generator bus (PV bus) the real power generated P_G and the voltage magnitude $|V|$ are known, except for the swing bus, where the voltage magnitude $|V|$ and phase δ are known. Furthermore, the aforementioned assumptions describe three phase (3ϕ) quantities of load powers, generator powers and bus voltages. In order to validate the common approach of the single-line system-based PF, analyzed power systems are assumed to be perfectly balanced 3ϕ systems in steady state [50, 66, 99–102]. Although power flow formulation and solution methods are well developed in defining states of stable power system operation, assumptions about their validity may not be accurate for buses with DG units in various modes of operation. The reason for such an inaccuracy is that power produced by the DG units may change based on wind speed, available sunlight, etc. [100, 103]. Therefore, the balance between system power generation and load demand may not be secured at all modes of operation. In addition, the stochastic natures of the primary energy sources for DG units can also lead to bus type conversion (PV to PQ and vice versa). Furthermore, the active and reactive

power for buses with DG units can be determined based on the $d-q$-axis voltage and current components on the output side of the utilized grid-connected converters. This correlation between active and reactive power delivered from buses with DG units and the $d-q$-axis voltage components suggests the formulation of power flow employing $d-q$-axis voltage components.

A mathematical transformation called the abc-to-$dq0$ transform converts the three AC quantities into three quantities, namely the direct or the d-axis component, quadrature or the q-axis component, and the zero or the 0-axis component. The abc-to-$dq0$ transform is stated mathematically as [104].

$$\begin{bmatrix} x_d \\ x_q \\ x_0 \end{bmatrix} = \mathbb{T} \begin{bmatrix} x_a(t) \\ x_b(t) \\ x_c(t) \end{bmatrix} \tag{4.12}$$

where $x_a(t)$, $x_b(t)$ and $x_c(t)$ are 3ϕ quantities (voltages and currents), and $\mathbb{T}$ is the abc-to-$dq0$ transform matrix that is given by:

$$\mathbb{T} = \sqrt{\frac{2}{3}} \begin{bmatrix} \cos(\omega t) & \cos(\omega t - 2\pi/3) & \cos(\omega t + 2\pi/3) \\ \sin(\omega t) & \sin(\omega t - 2\pi/3) & \sin(\omega t + 2\pi/3) \\ \frac{1}{\sqrt{2}} & \frac{1}{\sqrt{2}} & \frac{1}{\sqrt{2}} \end{bmatrix} \tag{4.13}$$

where ω is the system nominal angular frequency.

Formulation of $d-q$-Axis Power Flow

The power flow formulation in the $d-q$-axis is initiated using the simple 2-bus system shown in Figure 4.36, where all voltages and currents are phasor quantities. The mesh equations for the three phase quantities of this 2-bus system are stated

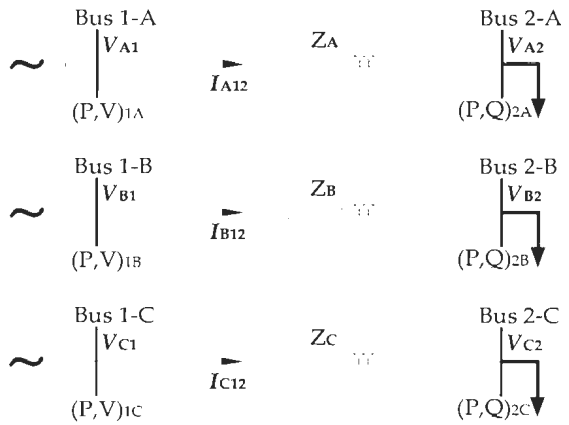

Figure 4.36: The circuit diagram of a simple 2-bus power system.

as:

$$\begin{bmatrix} V_{A1} \\ V_{B1} \\ V_{C1} \end{bmatrix} = [\mathbf{Z}] \begin{bmatrix} I_{A12} \\ I_{B12} \\ I_{C12} \end{bmatrix} + \begin{bmatrix} V_{A2} \\ V_{B2} \\ V_{C2} \end{bmatrix} \tag{4.14}$$

where $[\mathbf{Z}]$ is defined as

$$[\mathbf{Z}] = \begin{bmatrix} R_A + j\omega_s L_A & 0 & 0 \\ 0 & R_B + j\omega_s L_B & 0 \\ 0 & 0 & R_C + j\omega_s L_C \end{bmatrix} \tag{4.15}$$

where ω_s is the angular frequency of the system in rad./sec.. After rearranging (4.14):

$$\begin{bmatrix} V_{A1} - V_{A2} \\ V_{B1} - V_{B2} \\ V_{C1} - V_{C2} \end{bmatrix} = [\mathbf{Z}] \begin{bmatrix} I_{A12} \\ I_{B12} \\ I_{C12} \end{bmatrix} \tag{4.16}$$

Applying the abc-to-$dq0$ transformation on both sides of (4.16) as [105] generates

$$\begin{bmatrix} V_{d1} - V_{d2} \\ V_{q1} - V_{q2} \\ V_{01} - V_{02} \end{bmatrix} = [\mathbf{Z}] \begin{bmatrix} I_{d12} \\ I_{q12} \\ I_{012} \end{bmatrix} \tag{4.17}$$

The $d-q$-axis current components in (4.17) can be expressed as

$$\begin{bmatrix} I_{d12} \\ I_{q12} \\ I_{012} \end{bmatrix} = [\mathbf{Z}]^{-1} \begin{bmatrix} V_{d1} - V_{d2} \\ V_{q1} - V_{q2} \\ V_{01} - V_{02} \end{bmatrix} \tag{4.18}$$

Since $[\mathbf{Z}]^{-1} = [\mathbf{Y}]$, (4.18) is expressed as

$$\begin{bmatrix} I_{d12} \\ I_{q12} \\ I_{012} \end{bmatrix} = [\mathbf{Y}] \begin{bmatrix} V_{d1} - V_{d2} \\ V_{q1} - V_{q2} \\ V_{01} - V_{02} \end{bmatrix} \tag{4.19}$$

The impedance matrix, $[\mathbf{Z}]$ is a diagonal matrix, thus $[\mathbf{Z}]$ can be generalized for a multi-bus system as

$$[\mathbf{Z}] = \begin{bmatrix} [Z_A] & 0 & 0 \\ 0 & [Z_B] & 0 \\ 0 & 0 & [Z_C] \end{bmatrix} \tag{4.20}$$

where $[Z_A]$, $[Z_B]$, and $[Z_C]$ are the Z-bus metrices of three phase quantitites. Since the matrix, $[\mathbf{Z}]$ is a diagonal matrix, its inverse can be obtained as

$$[\mathbf{Z}]^{-1} = \begin{bmatrix} [Z_A]^{-1} & 0 & 0 \\ 0 & [Z_B]^{-1} & 0 \\ 0 & 0 & [Z_C]^{-1} \end{bmatrix} \tag{4.21}$$

The diagonal sub-matrices in (4.21), are sub matrices of the Y-bus metrices as

$$[\mathbf{Z}]^{-1} = [\mathbf{Y}] = \begin{bmatrix} [Y_A] & 0 & 0 \\ 0 & [Y_B] & 0 \\ 0 & 0 & [Y_C] \end{bmatrix} \tag{4.22}$$

Let $\mathbb{Y}_{dq0}$ be defined as

$$\mathbb{Y}_{dq0} = [\mathbf{Y}] = \begin{bmatrix} [Y_d] & 0 & 0 \\ 0 & [Y_q] & 0 \\ 0 & 0 & [Y_0] \end{bmatrix} \tag{4.23}$$

The nodal equations in the $d-q$-axis for bus k can be expressed utilizing (4.22) as

$$[I_{kd}] = \sum_{m=1}^{N} V_{md} Y_{d(k,m)} = \sum_{m=1}^{N} V_{md} \left(G_d + jB_d\right)_{(k,m)} \tag{4.24}$$

$$[I_{kq}] = \sum_{m=1}^{N} V_{mq} Y_{q(k,m)} = \sum_{m=1}^{N} V_{mq} \left(G_q + jB_q\right)_{(k,m)} \tag{4.25}$$

$$[I_{k0}] = \sum_{m=1}^{N} V_{m0} Y_{0(k,m)} = \sum_{m=1}^{N} V_{m0} \left(G_0 + jB_0\right)_{(k,m)} \tag{4.26}$$

The significance of representing a 3ϕ system in its $dq0$ components as in (4.24), (4.25) and (4.26) is the ability to accommodate unbalanced 3ϕ systems. This ability originates from the fact that using the $d-q$-axis components, three independent circuits are created, each of which has its own voltage source, impedance (or admittance) and current.

The instantaneous 3ϕ apparent power, $\bar{S}$ for bus k can be stated using the $d-q$-axis components of voltage and current as [101, 106],

$$\bar{S}_k = \mathbf{V_k I_k^*} = \left(\begin{bmatrix} V_{kd} \\ V_{kq} \\ V_{k0} \end{bmatrix} \cdot \begin{bmatrix} I_{kd}^* & I_{kq}^* & I_{k0}^* \end{bmatrix} \right) \tag{4.27}$$

Substituting (4.24), (4.25) and (4.26) into (4.27), and taking the real and imaginary parts, provide the active and reactive power for bus k as

$$P_k = \frac{3V_{kd}}{2} \sum_{m=1}^{N} V_{md} \left(G_d\right)_{(k,m)} + \frac{3V_{kq}}{2} \sum_{m=1}^{N} V_{mq} \left(G_q\right)_{(k,m)} + \frac{3V_{k0}}{2} \sum_{m=1}^{N} V_{m0} \left(G_0\right)_{(k,m)} \tag{4.28}$$

$$Q_k = \frac{3V_{kq}}{2} \sum_{m=1}^{N} V_{md} \left(B_d\right)_{(k,m)} - \frac{3V_{kd}}{2} \sum_{m=1}^{N} V_{mq} \left(B_q\right)_{(k,m)} - \frac{3V_{k0}}{2} \sum_{m=1}^{N} V_{m0} \left(B_0\right)_{(k,m)} \tag{4.29}$$

Equations (4.28) and (4.29) are non-linear, and obtaining their solution requires the use of numerical techniques. The Newton-Raphson (NR) method for solving a system of non-linear equations is utilized to solve the power equations and obtain values of V_d and V_q for each bus. The formulation of the $d-q$-axis power flow can be stated as

$$\mathbf{m}_{dq} = \mathbf{J}_{dq} \Delta \boldsymbol{\lambda} \tag{4.30}$$

where the vector $\mathbf{m_{dq}}$ is the power mismatches as

$$\mathbf{m}_{dq} = [\mathbf{\Delta P}, \mathbf{\Delta Q}]^T \tag{4.31}$$

The matrix $\mathbf{J}_{dq}$ is the Jacobian matrix, which is determined as

$$\mathbf{J}_{dq} = \frac{3}{2} \begin{bmatrix} \left[\frac{\partial \mathbf{P}}{\partial \mathbf{V_d}}\right] & \left[\frac{\partial \mathbf{P}}{\partial \mathbf{V_q}}\right] \\ \\ \left[\frac{\partial \mathbf{Q}}{\partial \mathbf{V_d}}\right] & \left[\frac{\partial \mathbf{Q}}{\partial \mathbf{V_q}}\right] \end{bmatrix} \tag{4.32}$$

Also, the vector $\boldsymbol{\lambda}$ is the voltage vector defined as

$$\boldsymbol{\lambda} = [\mathbf{V}_d, \mathbf{V}_q]^T \tag{4.33}$$

The elements of the Jacobian matrix $\mathbf{J_{dq}}$ are evaluated as

- For the elements with $m \neq k$:

$$\frac{\partial P_k}{\partial V_{md}} = V_{kd} \left(G_d\right)_{(k,m)} \tag{4.34}$$

$$\frac{\partial P_k}{\partial V_{mq}} = V_{kq} \left(G_q\right)_{(k,m)} \tag{4.35}$$

$$\frac{\partial Q_k}{\partial V_{md}} = V_{kq} \left(B_d\right)_{(k,m)} - V_{kq} \left(B_q\right)_{(k,m)} \tag{4.36}$$

$$\frac{\partial Q_k}{\partial V_{mq}} = V_{kd} \left(B_d\right)_{(k,m)} - V_{kd} \left(B_q\right)_{(k,m)} \tag{4.37}$$

- For the elements with $m = k$:

$$\frac{\partial P_k}{\partial V_{kd}} = 2V_{kd}\left(G_d\right)_{(k,k)} + \sum_{m=1,m\neq k}^{N} V_{md}\left(G_d\right)_{(k,m)} \tag{4.38}$$

$$\frac{\partial P_k}{\partial V_{kq}} = 2V_{kq}\left(G_q\right)_{(k,k)} + \sum_{m=1,m\neq k}^{N} V_{mq}\left(G_q\right)_{(k,m)} \tag{4.39}$$

$$\frac{\partial Q_k}{\partial V_{kd}} = V_{kq}\left(B_d\right)_{(k,k)} - \sum_{m=1,m\neq k}^{N} V_{mq}\left(B_q\right)_{(k,m)} \tag{4.40}$$

$$\frac{\partial Q_k}{\partial V_{kq}} = V_{kd}\left(B_q\right)_{(k,k)} - \sum_{m=1,m\neq k}^{N} V_{md}\left(B_d\right)_{(k,m)} \tag{4.41}$$

Elements of the developed Jacobian matrix derived in equations (4.34) through (4.41) show a high degree of symmetry, which can reduce the numerical computations required by the proposed $d-q$-axis power flow, as well as simplify its implementation.

Implemention of the $d-q$-axis Power Flow in Micro-Grid Controller

The $d-q$-axis PF method described above can be implemented to generate active and reactive power command values P_C and Q_C for each generator bus (PV bus). Figure 4.37 shows a schematic diagram of a grid connected inverter, where the P_C and Q_C are fed as inputs to the inverter controller.

In order to implement the $d-q$-axis power flow method, the following step-by-step procedure can be used to structure the required computations.

STEP 1: Set the value for the tolerance ϵ, initialize the iteration counter as $n = 0$, and initialize the bus voltage vector $\boldsymbol{\lambda}^{(0)}$ as

$$\boldsymbol{\lambda}^{(0)} = [\mathbf{V}_d^{(0)}, \mathbf{V}_q^{(0)}]^T \tag{4.42}$$

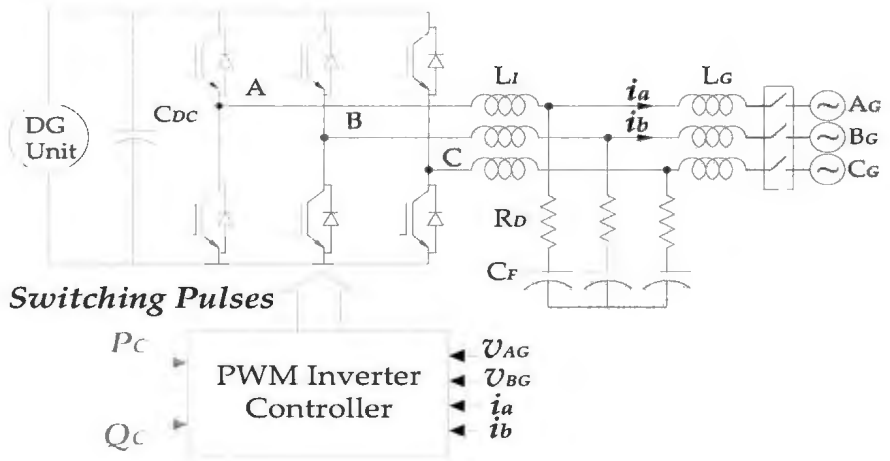

Figure 4.37: The schematic diagram for a grid-connected inverter for utilizing the generated power of a DG unit.

where

$$\mathbf{V}_d^{(0)} = \sqrt{2}[1, 1, 1, \ldots, 1]^T$$

$$\mathbf{V}_q^{(0)} = [0, 0, 0, \ldots, 0]^T$$

STEP 2:

- Read elements of the Y-bus matrix and determine $[\mathbf{Y}_d]$ and $[\mathbf{Y}_q]$ using equation (4.23).
- Read buses actual active and reactive power $\mathbf{P}_a$ and $\mathbf{Q}_a$.

STEP 3: Calculate active and reactive power for each bus $\mathbf{P}_c^{(n)}$ and $\mathbf{Q}_c^{(n)}$ using equations (4.28) and (4.29) for bus voltages at iteration n using bus voltages $\boldsymbol{\lambda}^{(n)}$.

STEP 4: For all PV buses, check reactive power limits as

- If $\left(Q_k^{(n)}\right)_c \leq (Q_k)_{max}$, Go to *STEP 5*.

- If $\left(Q_k^{(n)}\right)_c > (Q_k)_{max}$, then convert the PV bus k into PQ bus k and set $\left(Q_k^{(n)}\right)_c = (Q_k)_{min}$.

STEP 5: Calculate the mismatches in buses' active and reactive power $\mathbf{m_{dq}}$ in iteration n as

$$\mathbf{m_{dq}^{(n)}} = [\mathbf{\Delta P^{(n)}}, \mathbf{\Delta Q^{(n)}}]^T \tag{4.43}$$

where:

$$\mathbf{\Delta P}^{(n)} = \mathbf{P}_a - \mathbf{P}_c^{(n)} \tag{4.44}$$

$$\mathbf{\Delta Q}^{(n)} = \mathbf{Q}_a - \mathbf{Q}_c^{(n)} \tag{4.45}$$

STEP 6:

- If $\epsilon \geq \max\left(|\mathbf{m_{dq}^{(n)}}|\right)$, then the solution is reached. Stop iterations.
- If $\epsilon \ngeq \max\left(|\mathbf{m_{dq}^{(n)}}|\right)$, then evaluate the Jacobian Matrix $\mathbf{J}_{dq}\left(\boldsymbol{\lambda}^{(n)}\right)$ using equations (4.34) through (4.41), and determine its inverse $\left[\mathbf{J}_{dq}\left(\boldsymbol{\lambda}^{(n)}\right)\right]^{-1}$.

STEP 7: Solve equation (4.30), and evaluate the vector $\mathbf{\Delta\lambda}^{(n)}$.

STEP 8: Update the voltage vector $\boldsymbol{\lambda}$ for the next iteration $(n+1)$ as:

$$\boldsymbol{\lambda}^{(n+1)} = \boldsymbol{\lambda}^{(n)} + \mathbf{\Delta\lambda}^{(n)} \tag{4.46}$$

Increase the iteration counter $n = n + 1$, and Go to *STEP 3*.

The generated command power values P_C and Q_C in *STEP 3* are used as inputs for current-controlled inverters, which are used to interface with the DG units.

Moreover, P_C and Q_C can also be used as inputs for governor and excitation controllers in synchronous generator units.

4.4.3 Inverter Controller

Distributed generation units are interfaced with the utility grid using an AC-DC-AC link for the purpose of energy conversion. The AC-DC-AC link may consist of a diode rectifier and/or voltage source converter, DC link capacitor and a voltage source inverter with filter. The interface of any generation units through the AC-DC-AC link may require control either in generator or grid side converters, or both generator and grid side converters. The control of the generation side of the storage unit has not been a focus in this research. The power generation and conversion from the storage unit to an input of the micro-grid side inverter is approximated by a DC source [56] and is shown in Figure 4.37. This is because the focus in this research is to control the micro-grid side inverter according to the command power coming from power flow calculation. The inverter controller senses the micro-grid voltage, and current going from storage to the micro-grid. Real and reactive power commands are sent to the inverter controller from the power flow solution. The modified control structure is shown in Figure 4.38, which is implemented as an inverter-interfaced storage control scheme to provide commanded real and reactive power to the micro-grid system.

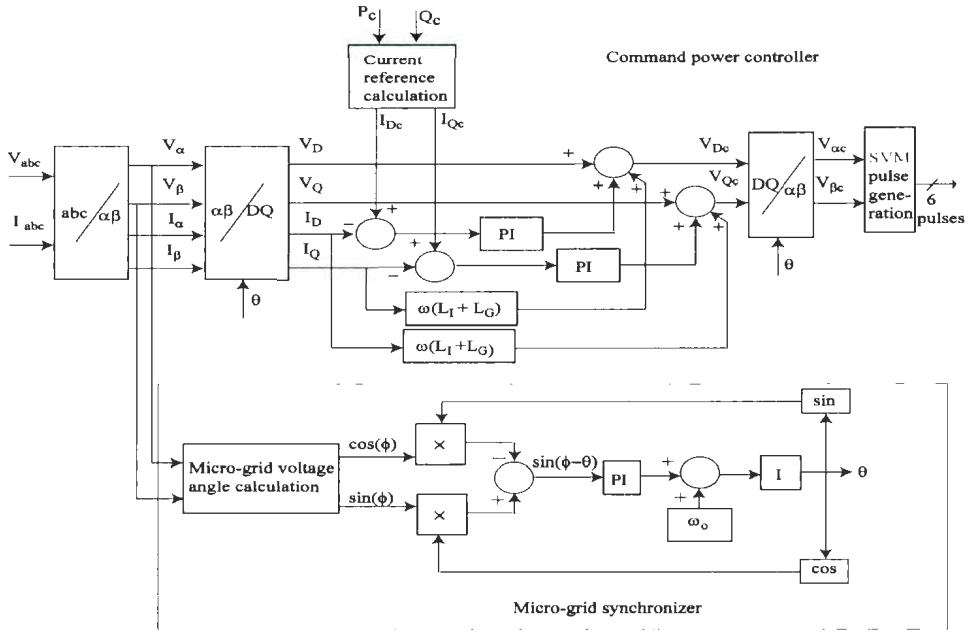

Figure 4.38: Schematic of the current controller for the inverter

The micro-grid three phase voltages are expressed as:

$$V_{amg} = V_M cos\phi \tag{4.47}$$

$$V_{bmg} = V_M cos\left(\phi - \frac{2\pi}{3}\right) \tag{4.48}$$

$$V_{bmg} = V_M cos\left(\phi + \frac{2\pi}{3}\right) \tag{4.49}$$

The three phase micro-grid voltages can be expressed in $\alpha - \beta$ reference frame as follows [107, 108]:

$$V_{\alpha\beta} = T_t V_{abcmg} \tag{4.50}$$

where

$$V_{\alpha\beta} = \begin{bmatrix} V_\alpha \\ V_\beta \end{bmatrix} \tag{4.51}$$

$$V_{abcmg} = \begin{bmatrix} V_{amg} \\ V_{bmg} \\ V_{cmg} \end{bmatrix} \tag{4.52}$$

and

$$T_t = \frac{2}{3}\begin{bmatrix} 1 & -0.5 & -0.5 \\ 0 & -\frac{\sqrt{3}}{2} & \frac{\sqrt{3}}{2} \end{bmatrix} \tag{4.53}$$

The $\alpha\beta$ voltage components in (4.50) are converted to the $d-q$-axis components as [108],

$$V_{DQ} = T_r(\theta)V_{\alpha\beta} \tag{4.54}$$

where

$$V_{DQ} = \begin{bmatrix} V_D \\ V_Q \end{bmatrix} \tag{4.55}$$

and

$$T_r(\theta) = \frac{2}{3}\begin{bmatrix} cos\theta & -sin\theta \\ sin\theta & cos\theta \end{bmatrix} \tag{4.56}$$

The $d-q$-axis components of 3ϕ current going from the storage unit to the micro-grid system are also obtained using (4.50) and (4.54).

$$P_c = V_{Dc}I_{Dc} + V_{Qc}I_{Qc} \tag{4.57}$$

$$Q_c = V_{Dc}I_{Qc} - V_{Qc}I_{Dc} \tag{4.58}$$

The reference current for the current control loop for the inverter is determined

using (4.57) and (4.58) as

$$I_{Dc} = \frac{P_c - V_Q I_{Qc}}{V_D} \tag{4.59}$$

$$I_{Qc} = \frac{Q_c V_D + P_c V_Q}{V_D^2 + V_Q^2} \tag{4.60}$$

The adjustment in current flow due to the change in command power is regulated by the proportional-integral current control loop. The coupling effect of the output filter is resolved using cross-coupling of the $d-q$-axis current components [107, 109]. The output obtained from the current regulator, with the addition of the filter effect, is the $d-q$-axis components of command voltages corresponding to the command powers. These voltage components are further converted to $\alpha - \beta$ components, which are the voltage reference for space vector modulation that generates pulses for the switches of the micro-grid side inverter.

The phase-locked loop technique is utilized for synchronization between the inverter voltage and the micro-grid voltage. The conceptual diagram of the micro-grid synchronizer is shown in Figure 4.38. The micro-grid voltage angle, ϕ is obtained using the $\alpha - \beta$ voltage components of the micro-grid voltage and is expressed as [107, 108]

$$cos\phi = \frac{V_\alpha}{V_\alpha^2 + V_\beta^2} \tag{4.61}$$

$$sin\phi = \frac{V_\beta}{V_\alpha^2 + V_\beta^2} \tag{4.62}$$

The concept of the phase-locked loop based synchronizer is that $sin(\phi - \theta)$, where ϕ is the micro-grid voltage angle and θ is the inverter voltage angle, can be reduced to a value that allows synchronization. The phase difference between the voltages, $\Delta\theta$

that allows the synchronization is obtained using a proportional-integral controller based on the fact that

$$sin(\phi - \theta) \cong (\phi - \theta) = \Delta\theta \tag{4.63}$$

4.4.4 Modeling and Simulation of the Developed Controller

The performances of the developed inverter-interfaced storage controller are investigated through simulation using the Matlab/Simulink software tool. The step-by-step procedure for implementing the $d-q$-axis power flow is realized using a Matlab code, while the inverter control is accomplished using the Simulink model created using the available components of the simulation tool. Two tests, namely the open loop and closed loop test, are performed in this investigation. The open loop study is conducted only with the employment of the $d-q$-axis power flow. On the other hand, the closed loop study is carried out by employing the $d-q$-axis power flow and the control of the inverter. Two modes of operation of the proposed micro-grid system are investigated through the open loop and closed loop simulation tests. The open loop study reveals micro-grid system information such as bus voltages, real and reactive power and load angle for various buses under the equilibrium condition. On the other hand, the closed loop study is performed to represent the dynamic condition of the micro-grid system along with power adjustments in the system in order to maintain the system voltage and frequency at their rated value under various operating conditions.

4.4.5 Simulation Results and Discussion: Open-loop Conditions

The simulation results for the utility-connected and the isolated micro-grid system in open loop condition are presented and discussed in the following subsections.

Stand-alone mode of operation:

During this mode of operation, the test micro-grid is disconnected from the utility grid, where $P_{grid} = 0$, and the developed $d-q$-axis power flow sets bus 1 as the swing bus since the storage unit (SU) is connected to Bus 1. Table 4.1 summarizes open loop performance results of the developed control method for the stand-alone mode of operation.

Table 4.1: Power Flow Calculation Results for Fermeuse Micro-Grid: Stand-Alone

Bus	P [MW]	Q [MVAR]	V [P.u]	δ°
1 (Swing Bus)	4.28	3.87	1.0	0
2 (PQ Bus)	0	0	1.0	-0.1
3 (PQ Bus)	0	0	1.0	-0.1
4 (PQ Bus)	3.94	1.3	1.0029	-0.2
5 (PQ Bus)	0	0	1.0197	-0.01
6 (PQ Bus)	2.82	0.62	1.0111	-0.01
7 (PV Bus)	3.00	-1.65	0.9865	-0.86

The data presented in Table 4.1 show that the SU connected to Bus 1 is storing energy. The energy stored in the SU is the result of high power generation at bus 7, where the wind turbines are connected. It is to be noted that the swing bus stores active power (in the storage unit) and generates reactive power using the HGU connected to the same bus. The operating conditions provided in this research indicate that a combination of a storage unit and a hydro unit can act like a swing bus.

Grid-connected mode of operation:

During this open loop performance test, the micro-grid is connected to the utility grid ($P_{Grid} \neq 0$) and the grid bus (Bus 3) is set as the swing bus. Table 4.2 summarizes the open loop results of the $d-q$-axis PF during the utility-connected mode of operation. The data in Table 4.2 indicate that the micro-grid is able to deliver power

Table 4.2: Power Flow Calculation Results for Fermeuse Micro-Grid: Utility-Connected

Bus	P [MW]	Q [MVAR]	V [P.u]	$\delta°$
1 (PV Bus)	4	3.26	1.0	-0.05
2 (PQ Bus)	0	0	1.0	-0.05
3 (Swing Bus)	-0.78	0.22	1.0	0
4 (PQ Bus)	3.94	1.3	1.006	-0.32
5 (PQ Bus)	0	0	1.003	-0.09
6 (PQ Bus)	2.82	0.6	1.00	-0.03
7 (PV Bus)	2.92	-1.43	0.9946	-0.65

to the utility grid during this mode of operation due to high power generation at bus 7, where the wind turbines are connected.

4.4.6 Simulation Results and Discussion: Closed-loop Conditions

The performance of the developed power flow based control scheme is tested for the proposed micro-grid system presented in this thesis. Although the proposed system has 7 buses, the system can be conceptually represented as a 4 bus system and is shown in Figure 4.39. Performance tests are carried out using Matlab/Simulink software for different operating conditions. The considered operating conditions include varying the power generation and load demand for standalone and utility grid-connected modes. The variation of power generation is re-

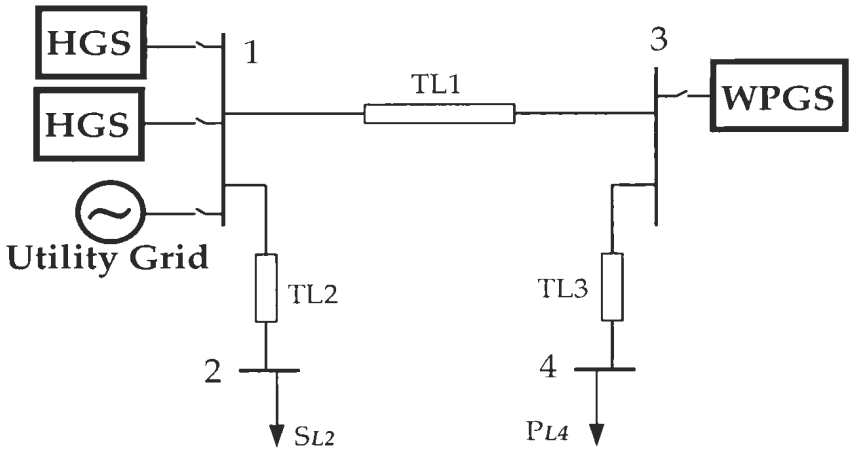

Figure 4.39: Micro-grid system with a reduced number of buses

alized through operating the wind farm, which is connected at bus 3, for variable wind speed. In addition, the variations of the load power demand are made possible through timed connection of an additional load at bus 2. The tested operating conditions are presented in the following subsections.

Isolated Micro-Grid with Wind Power Generation

This test is performed for the operating mode of an isolated micro-grid system, while the WPGS is operated in variable wind speed conditions. Figures 4.40 and 4.41 show the results of this test, where both simulated and calculated per-unit active and reactive powers are plotted on the same axis. Simulated per-unit $d-q$-axis components of bus voltages are also provided in Figure 4.41 for this mode of operation.

The test results of Figures 4.40 and 4.41 show close matches between simulated and calculated active and reactive powers for all buses of the test micro-grid system. Such close matches provide support to the features of the proposed control approach in which accurate adjustments in the generated power of the slack bus

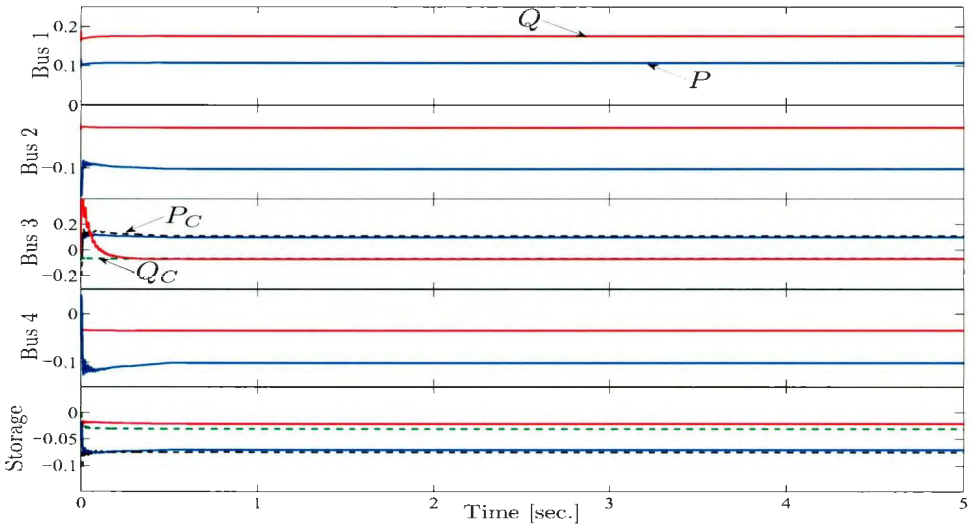

Figure 4.40: Simulation (——) and calculation (– – –) results for real and reactive power in stand-alone with variable wind speed operation for the wind farm at bus 3.

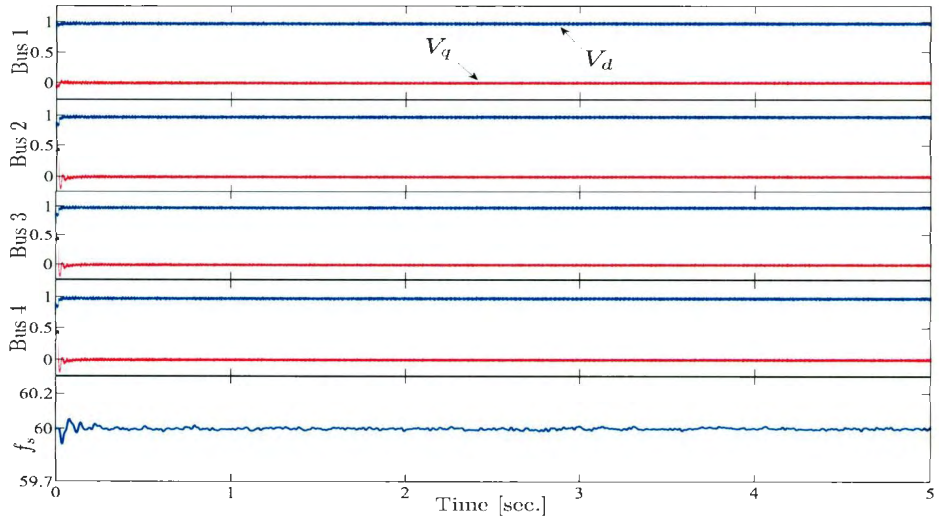

Figure 4.41: Simulation and calculation results for $d-q$-axis voltage components at micro-grid buses in stand-alone with variable wind speed operation for the wind farm at bus 3.

are achieved. Moreover, as the wind farm at bus 3 is operated in variable wind speed condition, changes in the generated power are accommodated by the controller so that stable active and reactive power generation and delivery are maintained at all buses of the micro-grid system. In addition, the stability of the active and reactive power generation and delivery can be observed through bus $d-q$-axis voltage components shown in Figure 4.41, where close-to-unity V_d and close-to-zero V_q values are observed at all buses. Also, the frequency during this operating mode, as shown in Figure 4.41, confirms the balance between the power generation and demand within the micro-grid domain, as it does not show any significant variations.

Utility Grid Connection-Disconnection and Variable Wind Speed

The performance of the proposed power flow based control for the proposed micro-grid system is investigated as the utility grid is connected at time t=2 seconds and disconnected at time t=4 seconds. During this test, the wind power generation is operated at variable wind speed. Performance results of this test are shown in Figures 4.42 and 4.43, where simulated and calculated per-unit active and reactive powers, along with $d-q$-axis voltage components for all buses, are presented.

Test results in Figure 4.42 for active and reactive powers show a decrease in the active power supplied by the storage unit, while the power generated at bus 1 remains unchanged after connecting with the utility grid (bus 1) at time t=2 seconds. These changes are initiated due to the fact that power demands within the micro-grid are met by the utility grid, hydro generator and WPGS. Also, the storage unit stores power as a result of the excess power in the micro-grid during grid-

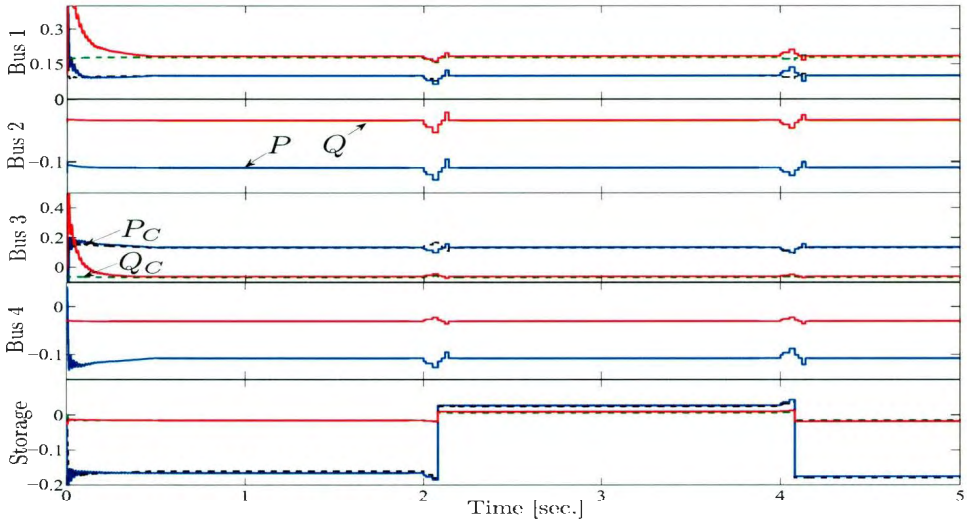

Figure 4.42: Simulation (——) and calculation (− − −) results for real and reactive power at micro-grid buses before and after grid connection (at time t=2 seconds) and disconnection (at time t=4 seconds) with variable wind speed operation for the wind power generation system at bus 3.

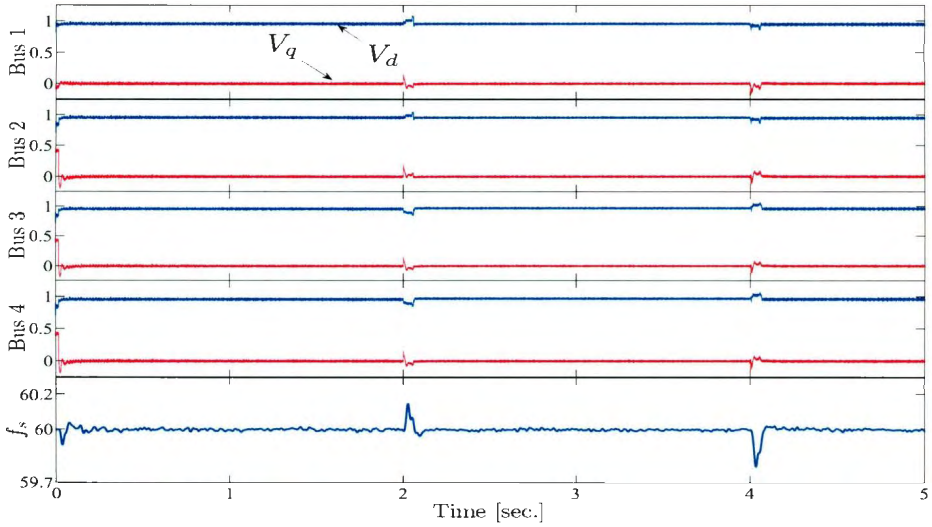

Figure 4.43: Simulation and calculation results for $d-q$-axis voltage components at micro-grid buses before and after grid connection (at time t=2 seconds) and disconnection (at time t=4 seconds) with variable wind speed operation for the wind farm at bus 3.

connection operation. The fast settling of buses 1 and 3 active and reactive power after the grid connection at time t=2 seconds, as well as after the grid disconnection at time t=4 seconds, is achieved by the control actions of the developed power flow based controller. Furthermore, the voltages at all buses are maintained at close-to-unity V_d and close-to-zero V_q values. The system frequency is also maintained at its rated value after a dynamic change during the grid connection and disconnection.

Isolated Micro-Grid with Wind Power Generation Disconnection

The ability of the $d-q$-axis PF based control scheme to function, as the micro-grid has limited power generation, is investigated as the micro-grid is operated in a stand-alone mode with WPGS disconnected at time t=2.5 seconds. Figures 4.44 and 4.45 show the results of this test including simulated and calculated per-unit active and reactive powers and $d-q$-axis components of bus voltages.

Performance results in Figure 4.44 show that the generated active power of the hydro unit increases, while the generated reactive power of the hydro is decreased in response to the disconnection of the wind farm (bus 3) at t=2.5 seconds. The simulated and calculated bus active and reactive power show an almost identical match. The active power delivered from the storage unit is increased as the WPGS is disconnected. The changes in active and reactive power generated at bus 1 (slack bus) are initiated to ensure that load power demands within the micro-grid are met by the hydro and storage units. The changes in active and reactive power at bus 1 after the disconnection of the wind farm at t=2.5 seconds are performed with minor overshoots and without steady-state errors as shown in Figure 4.44. Finally, these changes in reactive powers at bus 1 are initiated in order to maintain bus voltages in their close-to-unity per-unit values. The effects of changing the reactive power

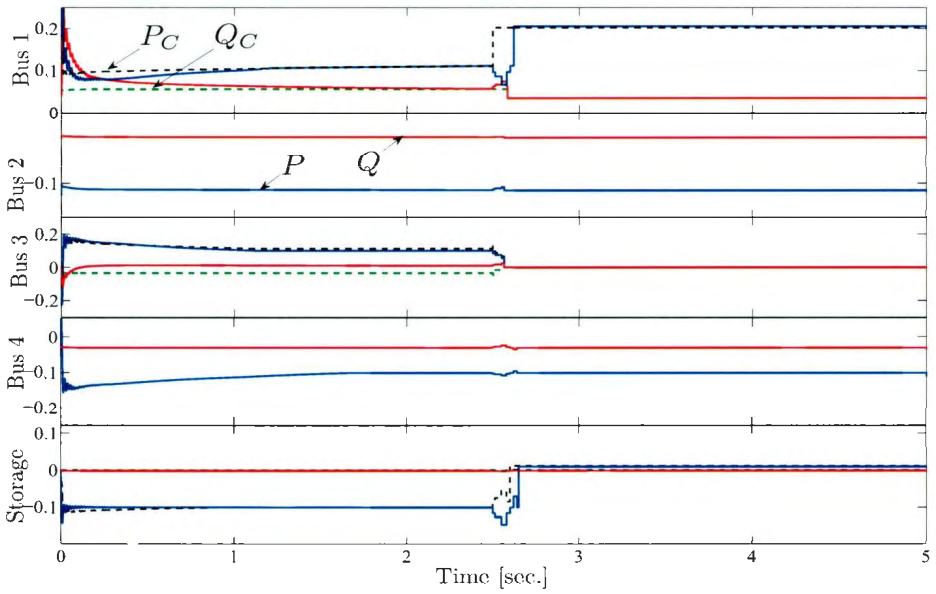

Figure 4.44: Simulation (—) and calculation (− − −) results for real and reactive powers at micro-grid buses before and after wind generator disconnection (at time t=2.5 seconds) as the micro-grid is operated in a stand-alone mode.

are clear in the bus voltages, where close-to-unity V_d and close-to-zero V_q values are maintained at all buses and are shown in Figure 4.45.

Isolated Micro-Grid with Step Increase in Load Power Demand

The performances of the $d-q$-axis power flow based control are investigated for an isolated micro-grid, variable wind speed conditions, and, at time t=3 seconds, when the load active power at bus 4 P_4 is increased from 2.82 to 3.82 MW. The per-unit simulated and calculated per-unit active and reactive power and the $d-q$-axis components of bus voltages for all buses in the test micro-grid power system are presented in Figures 4.46 and 4.47, respectively.

Test results for the step increase in the load active power demand at bus 4 are provided in Figure 4.46, where an increase in the power generated at bus 1 (slack

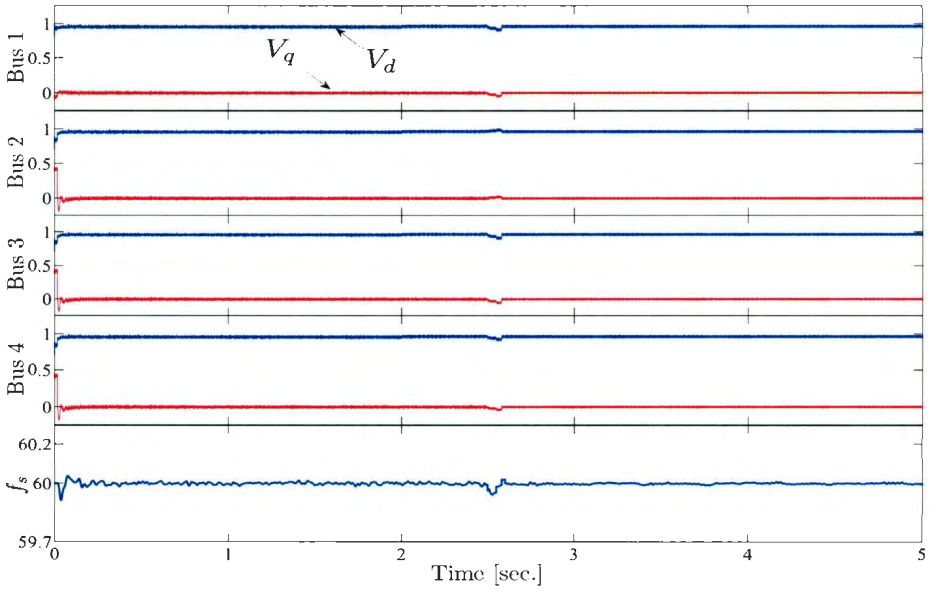

Figure 4.45: Simulation and calculation results of the $d-q$-axis voltage components at micro-grid buses before and after wind power generation disconnection (at time t=2.5 seconds) as the micro-grid is operated in a stand-alone mode.

bus) is observed at t=3 seconds to meet the increase in bus 4 active power demand. Also, the power stored in the SU decreases as the load demand increases at bus 4. The rest of the micro-grid buses maintain their active and reactive powers unchanged as an indication of the stability of the micro-grid under step increase in its power demand in an isolated mode of operation. An additional indication for the stability of the test micro-grid is observed from the close-to-unity V_d and close-to-zero V_q values before and after the step increase in P_4. Finally, the micro-grid system frequency response shown in Figure 4.47 is not affected by the step increase in P_4, which indicates a stable power generation to meet changing load demands. These indications are ingredients for stable power generation and delivery, as well as showing significant capability of the proposed power flow based control to initiate adjustments in response to increases in power demands.

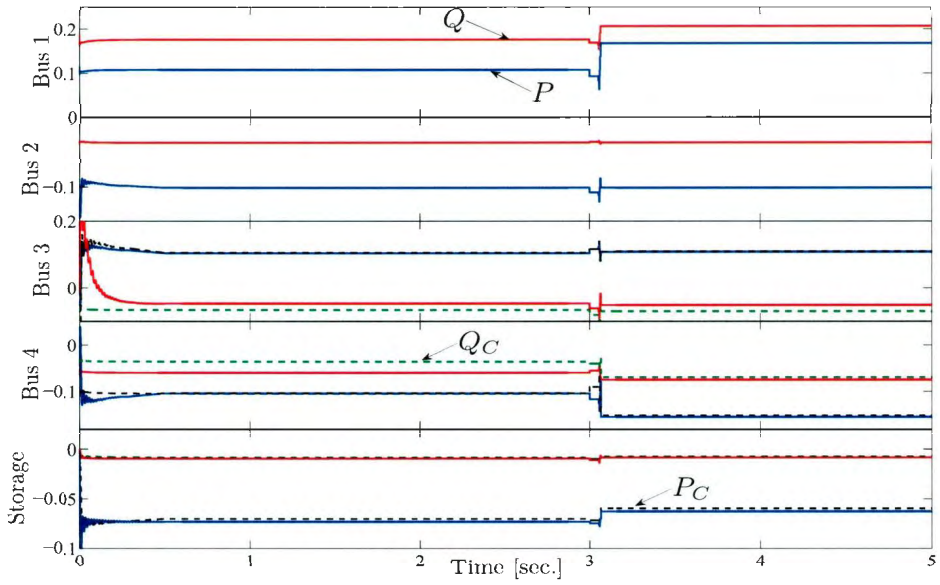

Figure 4.46: Simulation (—) and calculation (– – –) results for real and reactive power for micro-grid buses in stand-alone with step increase in bus 4 power.

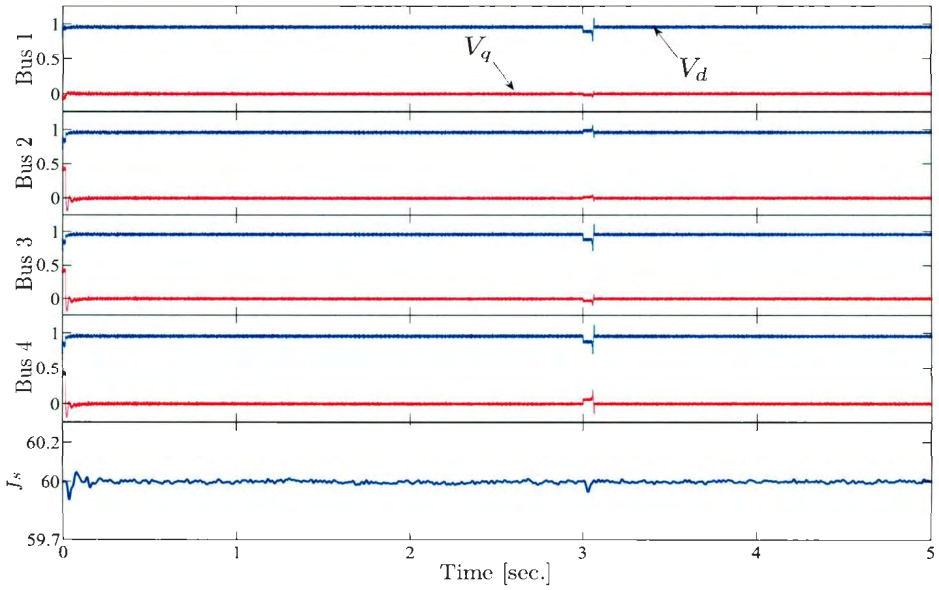

Figure 4.47: Simulation and calculation results of the $d-q$-axis voltage components for micro-grid buses in stand-alone with step increase in bus 4 power.

Utility Grid-Connected with Unbalanced Load at Bus 2

In this test, the $d-q$-axis power flow based controller is tested for the micro-grid operated in utility grid connection, with variable wind speed, and with a step change in the load active and reactive power supplied through phase B (i.e. an unbalanced power change). The changes in phase B active P_{2B} and reactiveQ_{2B} are increased from 3.94 to 4.94 MW and 1.3 to 1.75 MVAR respectively for the time $2 \geq t \geq 4$. Figures 4.48 and 4.49 provide the results of this test including both simulated and calculated per-unit active and reactive power, as well as $d-q$-axis voltage components for all buses in the test micro-grid.

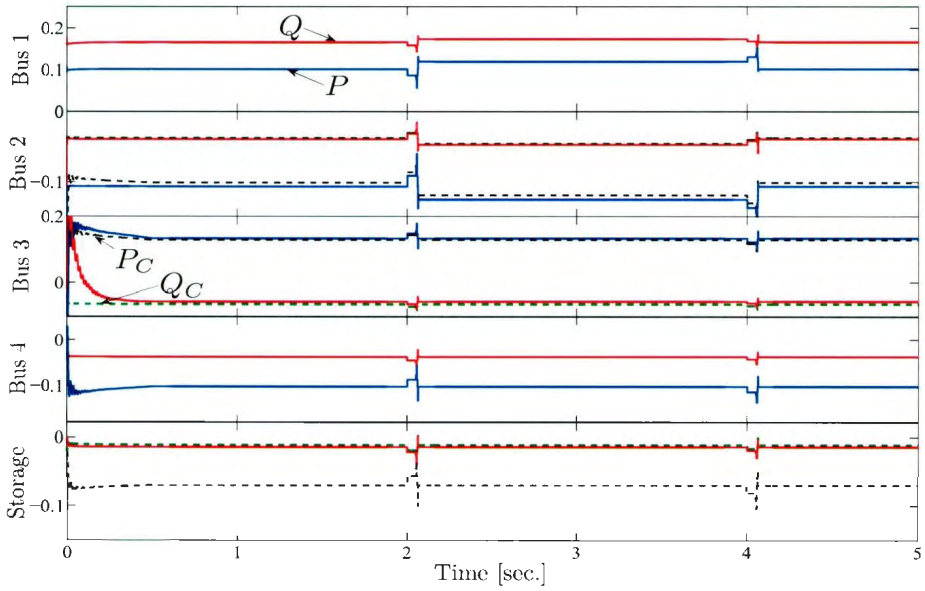

Figure 4.48: Simulation (—) and calculation (− − −) results for real and reactive power for micro-grid buses in utility grid-connected and unbalanced load changes at bus 2 for the time $2 \geq t \geq 4$.

In this test, the proposed $d-q$-axis power flow based controller demonstrates significant abilities for adjusting active and reactive power generated at bus 1 in response to the step change in phase B active and reactive power at bus 2 for

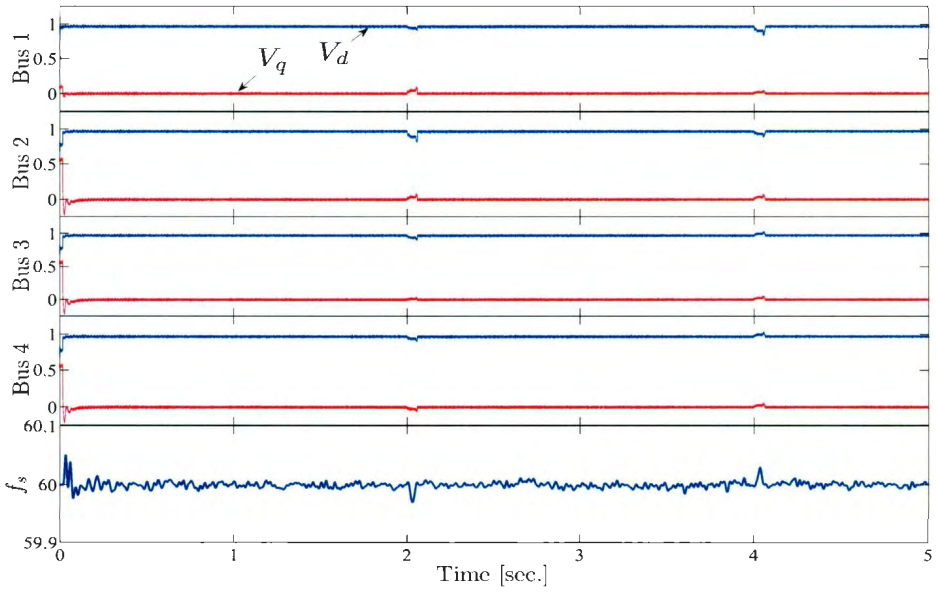

Figure 4.49: Simulation and calculation results for $d-q$-axis voltage components for micro-grid buses in utility grid-connected and unbalanced load changes at bus 2 for the time $2 \geq t \geq 4$.

the time $2 \geq t \geq 4$. The loading conditions before and after the change at bus 2 are capable of delivering active power to the utility grid, while importing reactive power from the utility grid. It is to be noted that possible variations in the active and reactive powers at bus 3 (due to the variable wind speed conditions) are handled by the controller of each wind turbine in the WPGS. The performance results show high agreement between the simulation results and the power calculated results, where such an agreement indicates that accurate control actions are initiated to maintain the stability of the micro-grid under the aforementioned conditions. Moreover, these results demonstrate that the proposed $d-q$-axis power flow based controller is able to function without sensitivity to the unbalanced change in the power demand of bus 2. Finally, Figure 4.49 shows that $d-q$-axis components of all bus voltages are maintained with close-to-unity V_d and close-to-zero V_q values

as a good indication of stable power generation and delivery under changes in bus power that could be of an unbalanced nature.

4.5 Summary

In this chapter, the design, development and performance analysis of the micro-grid controllers are presented in detail. Firstly, the design of an active power controller during the operation of an isolated micro-grid system with wind power generation is presented. The performances of the controller are analyzed and discussed based on simulation results. It is found that the developed active power controller is capable of maintaining a power balance between generation and load during utility grid disconnection and in subsequent operation of the micro-grid system comprised of renewable energy sources. Secondly, the operation of an isolated micro-grid system with a storage unit using a conventional governor control is studied and simulated. While the governor control of the hydro storage unit shows satisfactory performances, an alternative control scheme is also developed in order to achieve an effective and fast power adjustment. Finally, the development of a power flow based control scheme for micro-grids in stand-alone and utility grid-connected modes of operation is presented. The developed control scheme is realized using a power flow analysis, which simplifies the required calculations to determine command values of active and reactive power for both generation and delivery under various changes in operating conditions. In addition, an inverter controller is also employed in this control scheme to maintain the flow of the command powers between the micro-generations and the micro-grid buses. Performance results of the proposed power flow based control for micro-grid systems demonstrate good abilities to initiate control actions to quickly and effectively

maintain stable and reliable operation of the micro-grid for various modes of operation, and for changes in its operating conditions. Through all performance tests, the $d-q$-axis power flow based control scheme successfully initiates accurate and fast actions to adjust the power generation and delivery in response to changes in either power generation or demand. Moreover, the accuracy of such control actions is observed from the micro-grid system frequency response and bus voltages through all tested operating conditions, where close-to-unity V_d and close-to-zero V_q values have been maintained.

Chapter 5

Experimental Setup and Testing of the Micro-Grid System

In Chapter 4 the development of the micro-grid controllers for various modes of operation of the micro-grid consisting of renewable micro-generation was presented. The performances of the developed controllers were also investigated and presented in Chapter 4 through simulation using the Matlab/Simulink software tool. It was found that the developed micro-grid controllers were able to provide and maintain stable operation of the micro-grid system under various operating conditions. In order to verify the performances of the micro-grid controllers concluded through simulations, an experimental test bench for the micro-grid system is constructed and detailed tests are carried out. Firstly, a wind turbine emulator is developed that represents the wind power generator in the micro-grid system. Then the hardware of the other components is integrated into the system in order to complete the micro-grid test bench. Secondly, the implementation and hardware arrangments for the micro-grid active power controller and the power flow based micro-grid controller are described. Finally, the experimental results and the

relevant outcomes are presented and discussed.

5.1 Micro-Grid Test Setup

The literature review reveals that the majority of investigations of micro-grid issues was based on simulations. It is obvious that simulation yields introductory analysis and foresight of any system behaviours. However, laboratory testing is required in order to verify the outcome obtained by the simulation. In this thesis, an attempt has been made to validate the simulation results by developing the Micro-grid Test Setup (MTS) for the system presented in Figure 3.1. It is also worth mentioning that the development of the test setup is accomplished within the lab facilities using the equipment available in the lab. The basic organizations of the MTS are shown in Figure 5.1. The following sections describe each major component of the developed MTS.

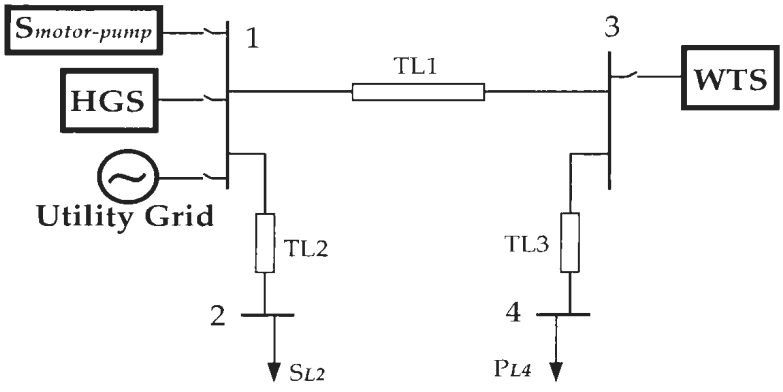

Figure 5.1: Conceptual layout of a micro-grid test setup

5.2 Wind Turbine Emulator

One of the major components in the proposed micro-grid system is the wind power generator. In order to incorporate a wind turbine system into the developed MTS, a wind turbine emulator (WTE) is developed in this thesis. The generic configuration of a WTE, as shown in Figure 5.2, consists of a programming platform to implement the model and characteristics of the wind turbine, an electrical drive to represent the rotor of the wind turbine, signal sensors and conditioning system, data acquisition, and power electronic devices to control the electrical drives.

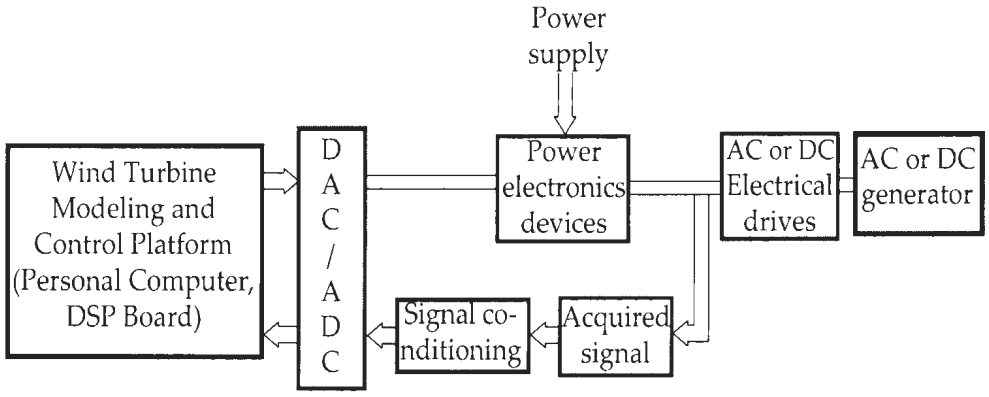

Figure 5.2: Typical conceptual diagram of a wind turbine emulator

While the basic structure of the WTE remains the same, different components may be used to implement the structure. For example, an AC or DC drive can be used to represent the wind turbine rotor. In the past, DC drives had significant advantages over AC drives for adjustable speed drive applications. Currently, AC drives are attractive due to the benefits of low cost and little or no maintenance, in contrast to a DC drive [110]. Moreover, the DC drive may be bulky and costly. However, the following are the main reasons to select a DC drive as the representation of the wind turbine rotor in this research [111].

- Speed or torque control of AC drives is more complex and requires expensive power electronics. DC drive is easy to understand and it has precise torque and speed control properties without sophisticated power electronics.
- DC drives are not limited to operate at any speed level within their operating speed range. On the contrary, AC drives are not suitable to operate below one third of their base speed.
- Torque and speed of the DC motor can be controlled using armature current and voltage, respectively.
- The cost of controlling equipment for the DC motor is lower than that of the AC motor.

A personal computer (PC) with a DSP board is utilized as the programming and control platform for the developed WTE. The characteristics of the wind turbine and associated controls are implemented into the DSP board to emulate the DC motor drive as a wind turbine rotor in the laboratory environment.

5.2.1 The Developed Emulator

A separately excited DC motor is used to represent a wind turbine rotor. The DC motor represents a horizontal axis wind turbine that follows the theoretical rotational torque of the wind turbine rotor. The inertia of the DC motor and induction generator is assumed as the inertia of the wind turbine rotor. A DSP board incorporated into a PC is utilized to implement the steady state wind turbine model and characteristics. The torque and speed information of the DC motor are acquired by torque and speed sensors. The aerodynamic torque produced by the wind turbine rotor is calculated from the rotational speed of the DC motor using wind turbine

model equations. This calculated torque is considered as the reference torque of the WTE. Based on the reference torque and the torque produced by the motor, a control signal is generated by the controller implemented in the DSP board. The control signal coming out from the DSP board is then applied to the phase control relay/analog input power controller in order to control the voltage applied to the armature of the DC motor. The basic outline of the developed WTE is shown in Figure 5.3.

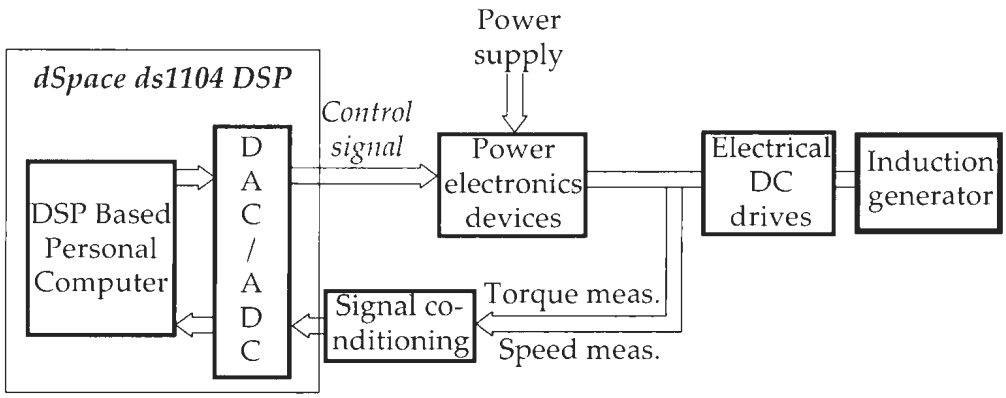

Figure 5.3: Basic outline of the developed wind turbine emulator

Wind Turbine Model

In general, the wind turbine model defines the output characteristics of the wind turbine as well as its failure and repair processes [112]. The output of a wind turbine can be characterized by the non-dimensional curves of the performance coefficient such as (a) torque coefficient C_q, or (b) power coefficient C_p, as a function of tip speed ratio λ. The desired output from the wind turbine model utilized for the developed WTE is the torque. Thus, the aerodynamic model of the wind turbine rotor in this research is based on the C_q versus λ curve. Such a curve is very useful

in the modeling of a small wind turbine, because the wind turbine torque is not zero even if the rotor is at standstill condition [113].

The actual mechanical power at the output of the wind turbine rotor can be expressed as

$$P_{mech} = \frac{1}{2}\rho A v_w^3 C_p(\lambda) \tag{5.1}$$

where ρ is the air density in kg/m^3, A is the area swept out by the turbine blades in m^2, v_w is the wind velocity in m/sec, $C_p(\lambda)$ is the dimensionless power coefficient that is a function of tip speed ratio λ.

Tip speed ratio λ is the ratio of the linear speed of the tip of the blades to the rotational speed of the wind turbine, and it can be expressed as

$$\lambda = \frac{\omega_m r_t}{v_w} \tag{5.2}$$

where ω_m is the angular velocity of the turbine rotor in rad/sec, r_t is the radius of the rotating turbine in m.

The average torque produced by the wind turbine is given by

$$T_{av} = \frac{P_{mech}}{\omega_m} \tag{5.3}$$

After manipulation, the average torque in (5.3) becomes

$$T_{av} = \frac{\frac{1}{2}\rho A v_w^2 C_p(\lambda) r_t}{\lambda} \tag{5.4}$$

The average torque in (5.4) can be further simplified as

$$T_{av} = \frac{1}{2}\rho A v_w^2 C_q(\lambda) r_t \tag{5.5}$$

where the torque coefficient, C_q can be expressed as the ratio of the power coefficient, C_p and the tip speed ratio, λ, i.e $c_q(\lambda) = \frac{C_p(\lambda)}{\lambda}$.
The relationship between the torque coefficient and the tip speed ratio can be characterized as follows [111]:

$$C_q = -0.02812 + 0.038576\lambda - 0.0045912\lambda^2 + 0.0001489\lambda^3 \tag{5.6}$$

Expected Rotor Torque for the Emulator

The reference torque for the developed WTS is determined by the wind turbine model in (5.5). The gear ratio is used to calculate the wind turbine rotor speed using the speed information measured from the DC motor shaft. The estimated wind turbine rotor speed is then fed to the wind turbine model to calculate the theoretical reference torque of the wind turbine rotor using (5.5).

Torque Control Algorithm Design

The proportional-integral-derivative (PID) is an extensively used controller for many applications because of the ease of implementation, cost effectiveness and the requirement of less computing power. In order to implement such a controller in developing the WTE, the discrete form of the controller is required. Thus the time domain PID controller is converted to a discrete form with a sample time T_0. The digitized form of the discrete controller in Appendix D is called a non-recursive controller that is not suitable for computer implementation, because such a controller calculates the actual desired output at every calculation period. On the contrary, recursive type algorithms are more suitable for programming on computers because they calculate a change in the output for each calculation period. It

can be seen from the derivation and expression of the recursive type PID controller presented in Appendix D, that the current change in the control variable, Δu_k is calculated based on the current manipulated variable, u_k and the previous manipulated variable, $u_{(k-1)}$. This algorithm provides the following advantages over the non-recursive algorithm:

- It is suitable for micro-processor based design.
- The previous control can be set to any reasonable arbitrary value which makes it easier to tune.
- It has the anti-integral wind up property because it never uses the summations of errors to calculate the contribution of the integral term.

Thus the recursive type control algorithm is selected for the developed WTE. However, because of the simplicity in implementation and the nature of the system (electrical motor coupled with the generator), a proportional-integral (PI) recursive type control algorithm is selected and designed for the developed WTE. Moreover, the derivative control gain might be affected by the noise from the electrical systems and interfacing circuitry in the case of a PID controller. Also, the PI controller has the ability to make the steady-state error zero, and is less complex to tune. Therefore, a PI type recursive controller is designed and implemented for the developed WTE.

Optimum Power Controller Design

The task of an optimum power controller in a wind energy conversion system is to continuously tune the system so that it draws maximum power from the wind regardless of wind speed. The developed wind turbine emulator incorporates an

optimum power controller in order to extract maximum power for a particular wind speed. The aim of the optimum power controller (OPC) is to establish the angular speed, ω_m of the WT to an optimum value, ω_{mopt} at which the power captured by the WT is maximum. The dynamic power captured by the WT at various angular rotational speeds of the turbine is shown in Figure 5.4.

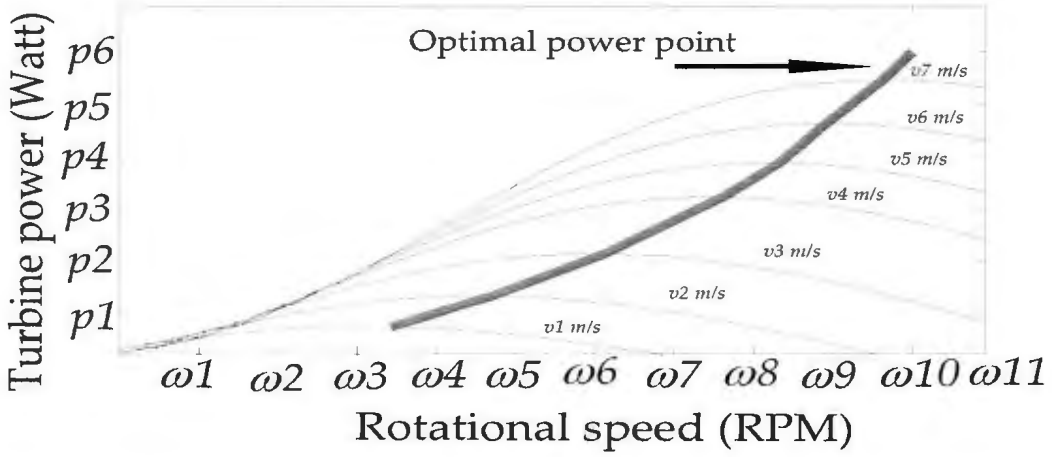

Figure 5.4: Power captured along maximum power point locus by the wind turbine at various rotational speeds

It can be seen from the Figure 5.4 that the power captured by the WT is maximum when the turbine rotor rotates at an optimal angular speed, ω_{mopt}. Thus the optimal tip speed ratio can be expressed at the optimum angular speed of the wind turbine as

$$\lambda_{opt} = \frac{\omega_{mopt} r_t}{v_w} \tag{5.7}$$

In order to ensure optimum power generation, the operation of the WT rotor needs to be established at an optimal tip speed ratio, λ_{opt}. The power coefficient at the optimal tip speed ratio is defined as $C_{p,opt}$. Therefore, the optimum power, P_{opt}

extracted from the WT rotor can be expressed as

$$P_{opt} = \frac{1}{2}\rho A v_w^3 C_{p,opt}(\lambda) \tag{5.8}$$

A PI type tip speed ratio controller is designed to operate the wind tubine rotor at its optimal rotor speed. The value of the optimum tip speed ratio for the modeled WT is used as the reference tip speed ratio of the controller. The actual tip speed ratio is then calculated based on the wind speed input to the WT model and the rotor speed acquired from the system. The error between the values of these two tip speed ratios is corrected by the designed PI controller. The output of the controller is utilized to generate the switching pulses for controlling the final element in the system that makes sure the WT operates at the reference tip speed ratio. The conceptual block diagram of the tip speed ratio controller is shown in Figure 5.5.

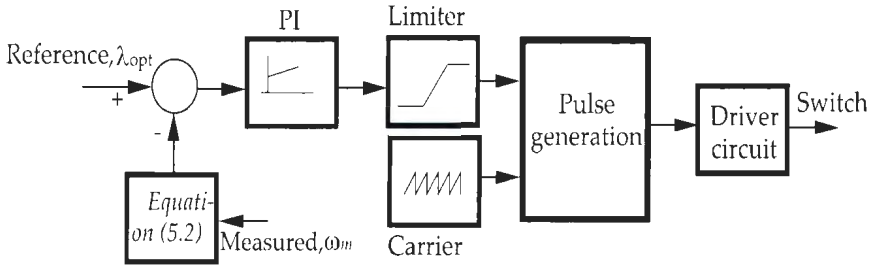

Figure 5.5: Conceptual diagram of the optimum power controller employed in the developed wind turbine simulator

5.2.2 Implementation of the Developed Wind Turbine Emulator

The characteristics and the various features of the developed WTE are implemented in the laboratory environment. The overall experimental layout of the developed WTE is shown in Figure 5.6. A combination of both hardware and soft-

ware is utilized for the implementation of the developed simulator. The implementation procedure is sequentially discussed in this section. A separately-excited

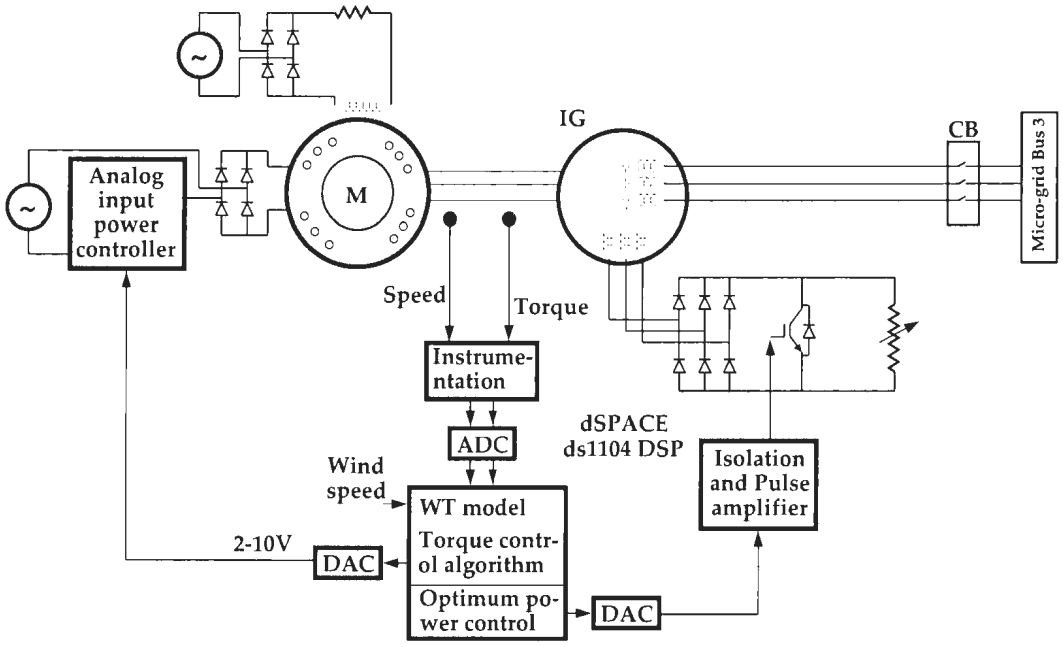

Figure 5.6: Laboratory arrangement for the wind turbine emulator

DC motor is utilized to represent the wind turbine rotor. The field of the DC motor is excited by a single phase AC supply using a full wave bridge rectifier along with power resistors in series with the field coil. The field circuit of the DC motor is supplied with a constant voltage, while the armature voltage is controlled in order to operate the DC motor at a variable speed to simulate the wind turbine characteristics. The nameplate data of the DC motor is given in the Appendix C.

As part of the implementation procedure, two system parameters, speed and torque, are measured using speed and torque sensors built into the system. The

output of the speed sensor is an AC signal which passes through the root mean square (RMS) to a DC converter integrated circuit. The DC output from the integrated circuit is then passed through a differential amplifier to achieve better resolution of the measured signal. Torque sensor output is fed through a high gain instrumentation amplifier because of the low output of the sensor. The amplified output voltages from the instrumentation amplifier and the differential amplifier are acquired by the dSPACE ds1104 DSP board. Calibration equations for speed and torque of the DC motor are given by (5.9) and (5.10) respectively, where N_{shaft} is the speed of the DC motor, v_s is the voltage output of the speed sensor, T_{shaft} is the torque of the DC motor, and V_{TS} is the output voltage of the torque sensor. These equations are set in the DSP memory to acquire the original speed and torque information measured from the system. RC filters are used in conjunction with the current and voltage sensors to reduce the noise level introduced by the system measuring instruments.

$$N_{shaft} = 154.17 \times v_s + 1358.3 \tag{5.9}$$

$$T_{shaft} = (V_{TS} - 0.28) \times 1.4546 \tag{5.10}$$

The acquired speed information of the DC motor shaft as well as the wind velocity stored in a file are plugged into the wind turbine model, (5.2), (5.6), and (5.4), to generate reference torque for the DC motor. The generated reference torque is compared with the torque information acquired from the system. The error between the target and the measured torque is passed through a recursive discrete PI controller that is also called the torque controller. This controller generates a

control signal that is sent to the input of the analog input power controller/phase control relay through a digital to analog converter of the DSP board. The output of the phase control relay is passed through a bridge rectifier and applied across the armature of the DC motor. The armature control voltage is passed through a fuse to avoid unexpected situations.The control signal at the input of the analog input power controller essentially controls the voltage applied to the armature of the DC motor. The control action generated by the torque controller ensures that the DC motor shaft follows the wind turbine reference torque derived from the wind turbine model. A Ziegler-Nichol's (ZN) closed loop tuning method is used to obtain the primary guess about the value of controller parameters. A change in the wind velocity causes the change in the reference torque produced by the wind turbine. The torque controller shows its ability to track and maintain the reference torque that is changed due to the wind velocity. The implementation of the wind turbine model and the recursive torque controller are accomplished using Matlab coding on a dSPACE ds1104 DSP board in a PC. The following step-by-step procedure for laboratory implementation of the developed WTE can be stated as:

STEP 1: Variable declaration, and initialize the value of the controller gains, K_p (0.396), T_I (1.843) and T_o (0.031).

STEP 2: Calculate parameters, p_o, p_1 and p_2 of the recursive discrete PI controller.

STEP 3: WT constant and gear ratio initialization.

STEP 4:

- Read DC motor speed information from the system through DSP analog to digital (ADC) port.
- Read wind speed data from the file stored in the DSP memory.

STEP 5: Calculate the tip speed ratio, the torque coefficient and the reference torque from the WT model

STEP 6: Read the actual torque information of the motor from the system through DSP analog to digital (ADC) port.

STEP 7: Calculate the error between the reference torque and the actual torque.

STEP 8: The error passes through the designed controller, and the controller generates control action.

STEP 9: Write the control value to the DSP digital to analog (DAC) port.

Moreover, the developed WTE is featured with an optimum power controller that is implemented through rotor side control. The DC motor simulated as the WT rotor is coupled with an induction generator as shown in Figure 5.6. The stator of the induction generator is directly connected with the grid, while the rotor of the generator is connected with a variable resistor through a 3ϕ uncontrolled bridge rectifier and a switching device. In order to maintain the topological similarity of the wind generator utilized in the simulation, the generator rotor must be connected back to the grid through a back to back PWM voltage source converter. However, the topology (Fig. 5.6) utilized for the sake of lab implementation is for the following reasons.

- The capacity of the available machine in the lab is low, for example 3.75 kW.
- The power output at the rotor side of this machine at low wind speed is also low. This low power conversion through a back to back PWM converter is not technically and economically beneficial.

- Moreover, it is to be noted that the topological change made for the lab implementation does not compromise the effect of the wind generator in the micro-grid system.

Thus the rotor side arrangement of the generator shown in Figure 5.6 is utilized to implement the optimum power controller for the developed WTS. An optimum tip speed ratio controller is designed and implemented as an optimum power controller in order to extract maximum power available in the wind. This control objective is achieved based on continuous adjustment of the power-speed characteristics of the generator. The external resistor connected to the rotor side of the induction generator is utilized in order to make these changes to the power-speed characteristcs of the generator. The 3ϕ AC voltage coming out from the rotor side is converted to a DC value using a 3ϕ diode bridge rectifier. The DC voltage at the rectifier output is applied across the external resistor followed by a switching device. The variation in the rotor resistance is made through the changes of the duty cycle of the switch utilized between the bridge rectifier and the external resistor. The adjustment in the duty cycle due to the wind speed variation is achieved by implementing the designed controller shown in Figure 5.5. This variation in the duty cycle occurs under varying wind speed conditions, causing the continous changes in rotor resistance so that the wind turbine operates at the maximum tip speed ratio. WT operation at optimum tip speed ratio ensures the maximum power extraction through the stator of the wind generator. The implementation of the optimum tip speed ratio controller is accomplished in the Matlab/Simulink environment using a dSPACE ds1104 DSP board. The photograph of the developed WTE based WECS for micro-grid research in the energy lab is shown in Figure 5.7.

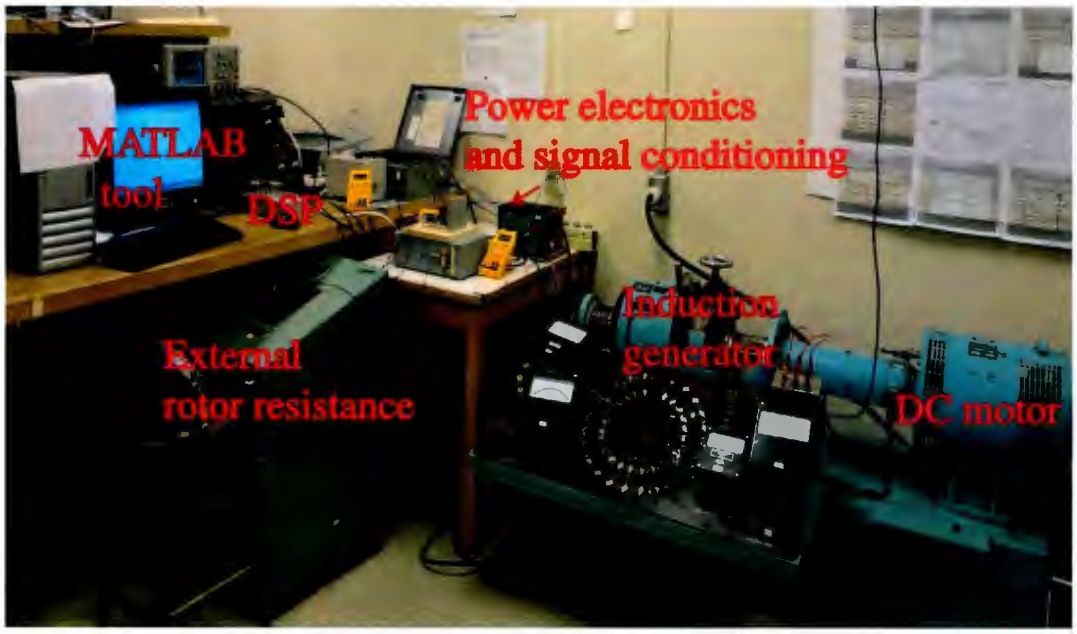

Figure 5.7: A photograph of the laboratory wind turbine system

5.3 Other Hardware Components of the Micro-Grid Test Setup

The other major component in the MTS is the hydro generation unit (HGU). A 3ϕ synchronous generator coupled with a shunt DC machine are used to represent the HGU. The synchronous generator is generally equipped with excitation and field control in order to maintain the rated voltage and frequency of the generator output under variable speed operation of the prime mover. Since the HGU in the micro-grid system is assumed to operate at its rated power due to the availability of invariant water potential at the selected site, the synchronous generator coupled with the DC machine is operated at constant speed and constant field voltage. Furthermore, it is also intended to maintain the micro-grid system voltage at its rated value by controlling the real and reactive power from the storage unit.

This fact basically leads to the decision to maintain the constant field voltage of the synchronous generator. The laboratory layout of the HGU is shown in Figure 5.8.

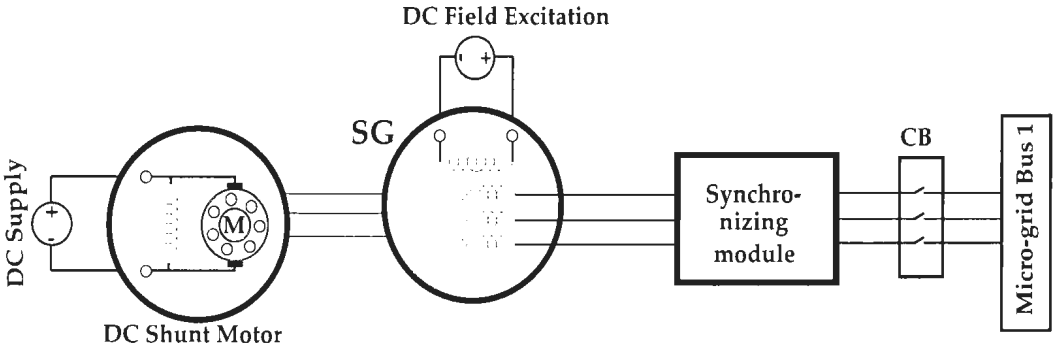

Figure 5.8: Laboratory arrangement for hydro generation unit

A 3ϕ, 208 V, 60 Hz supply available in the lab is used as the utility grid. The connection link between the MTS and the utility grid is done through a 3ϕ circuit breaker. The proposed micro-grid system has a short transmission line between the HGU and the WPGS. The line, $TL1$ is utilized in the MTS between the HGU and WTS. Moreover, two other lines $TL2$ and $TL3$ are used to represent the line between bus 1 and load $PL2$, and bus 3 and $PL4$. The parameters of the lines employed in the MTS are as follows:

- TL1=6m and Z1=(0.00341+j0.00413) Ω
- TL2=2m and Z2=(0.00143+j0.00212) Ω
- TL3=2.5m and Z3=(0.00161+j00271) Ω

Three different loads are employed in the micro-grid test setup. Load $PL2 = (750 + j251)$ W is connected to load bus 2, and load $PL4 = 1.24$ kW is connected to load bus 4. Loads $PL2$ and $PL4$ represent the regular consumer loads in the micro-grid

system. The other load, $S_{motor-pump} = 0.5$ kVA is utilized as the load equivalent to a motor-pump set in the MTS.

5.4 Implementation of the Micro-Grid Active Power Controller

The experimental arrangement of the active power controller along with the laboratory micro-grid test setup are shown in Figure 5.9. The overall controller ar-

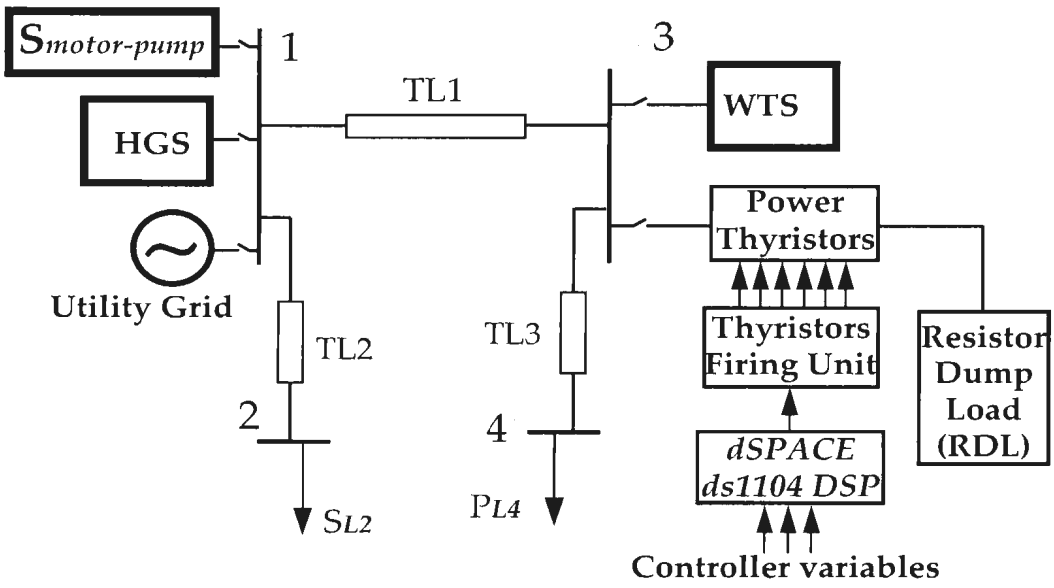

Figure 5.9: Schematic of the active power controller with the micro-grid test setup in the energy lab

rangement is comprised of a digital signal processing (DSP) board installed in a PC, thyristor firing unit, thyristor switching module, driver circuit, and resistive dump load connected with the micro-grid test setup. The control variables and

measured system variables are the input to the dSPACE ds1104 DSP board where the designed controller algorithm is implemented. The controller generates the control action based on the design criteria and the signal is sent out to the thyristor firing unit. The firing pulses generated by the thyristor firing unit trigger the thyristor switches in the power thyristor module. This control allows the dynamic change in the current flow through the dump load.

The detailed hardware implementation of the developed active power controller is presented in Figure 5.10. The input to the active power controller from

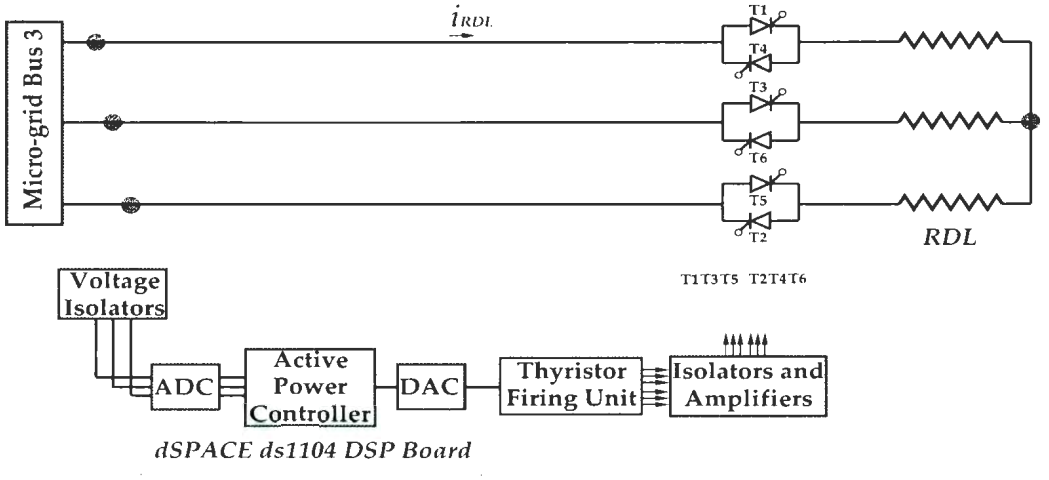

Figure 5.10: Implementation detail of the developed active power controller in the laboratory environment

the MTS is the 3ϕ voltage. This voltage can be obtained from any of the buses in the MTS. Since bus 3 is closer to the location of the power controller, the 3ϕ voltage of bus 3 is utilized as the input to the power controller. The micro-grid 3ϕ voltages at bus 3 are acquired using voltage isolator sensors which take input $\pm$300V AC or DC and provide $\pm$10V AC or DC as the output. The output of the sensor is taken to the DSP board through the dSPACE built-in analog-to-digital converter. This

signal is utilized as the input to the phase locked loop (PLL) in the active power controller algorithm that is shown in Figure 5.11. The Simulink model of the PLL is

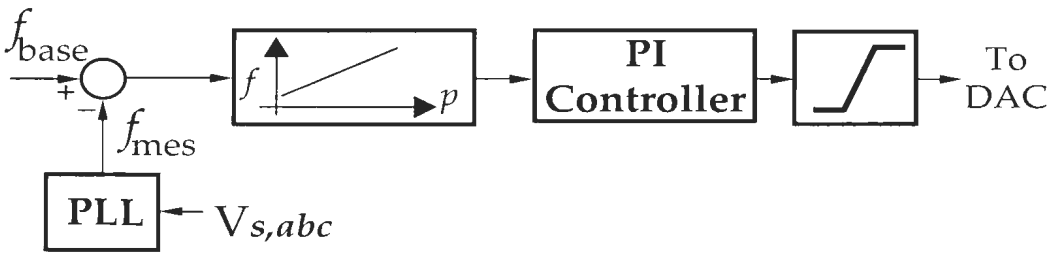

Figure 5.11: Active power control algorithm implemented in the DSP memory

utilized in the designed controller. The output of the PLL is the system frequency that is called system measured frequency, f_{mes}. The micro-grid system nominal frequency, f_{base} is then subtracted from the system measured frequency, f_{mes}, in order to calculate the frequency deviation in the system. This frequency deviation is utilized to determine the power deviation in the system using the pre-defined droop coefficient. The power deviation in the system is then passed through the PI controller that generates the control signal, u_{cs}. The signal, u_{cs}, is limited by the limiter to maintain the control signal in the range ($\pm 10V$) of input to the thyristor firing unit. This signal is sent to the thyristor firing unit through the dSPACE built-in digital-to-analog converter. The thyristor firing unit converts the input voltage $\pm$10V to $\pm$180 degrees. At any time, t, the angle corresponding to the input voltage of the firing unit, is the firing angle for the thyristor switches. In addition, the thryristor firing unit also requires input reference voltage from the system which is shown in Figure 5.10. The thyristor firing angle corresponding to the control signal and the reference voltage are utilized by the firing unit to generate synchronizing firing pulses. These firing pulses are sent to the thyristors' switching module. The

thyristor switching module consists of isolator and pulse amplifier, and switching devices. The firing pulses from the firing unit are passed through the isolation and pulse amplifier circuit before being sent to the gate of the switch. The pulses trigger the switches in such a way that the current flowing into the dump load, i_{RDL}, changes smoothly in order to maintain the power balance between the generation and load. The lab-volt thyristor firing unit, pulse amplifier and thyristor switching modules are integrated in this hardware arrangement. Furthermore, a 1.5 kW resistance box and a 0.5 kVA resistive-inductive load are used to represent a resistive dump load (RDL) and the load equivalent of the motor pump set, $S_{motor-pump}$, respectively. The photograph of the micro-grid test set up along with the active power controller hardware arrangement is shown in Figure 5.12.

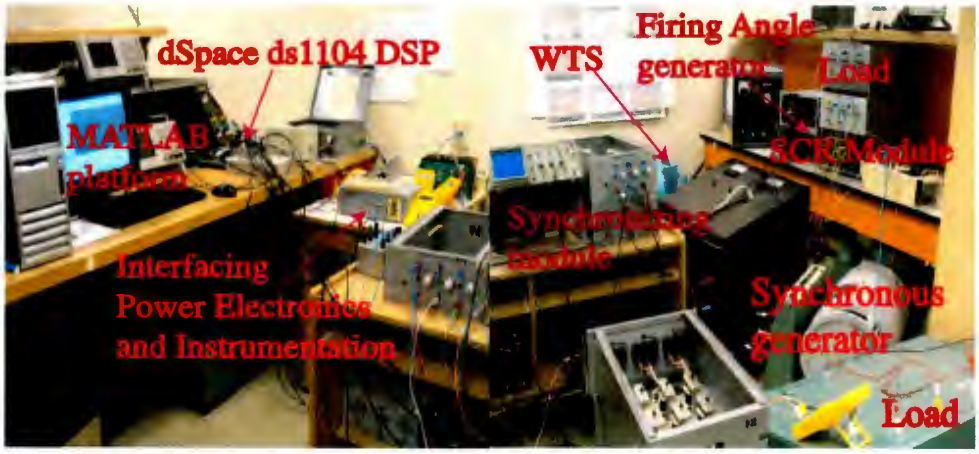

Figure 5.12: A photograph of the micro-grid test setup for the experimental testing

5.5 Implementation of the Power Flow Based Micro-Grid Controller

The experimental arrangement of the power flow based micro-grid controller along with the laboratory micro-grid test setup are shown in Figure 5.13. The micro-grid system variables are measured and used as input to the power flow algorithm. The power flow calculates the power at various buses for the equilibrium condition between power generation and load. The calculated powers can be utilized as the command power for the micro-generation in the micro-grid test setup in order to control power generation by the DGs. However, it is important to mention that only the command power for the inverter interfaced storage (IIS) unit is generated to calculate the current reference for the inverter controller in this thesis. This is because of the purpose of using the storage unit to deliver power to the micro-grid during the operating mode of an isolated micro-grid without wind power generation. The reference current is then regulated by the current controlled inverter to maintain the power balance between the micro-grid generation and load during the operation of an isolated micro-grid when the wind power generation system is not available.

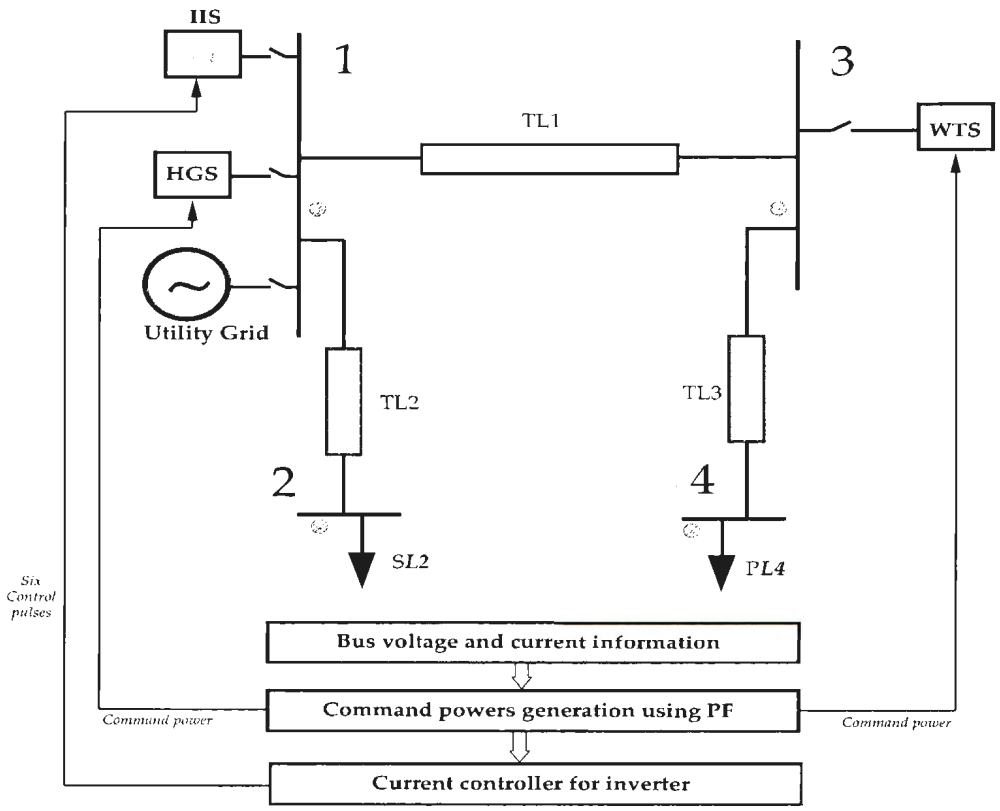

Figure 5.13: Schematic of the active power controller with the micro-grid test setup.

The detailed hardware implementation of the developed inverter interfaced micro-grid controller is shown in Figure 5.14. The hardware setup in the labo-

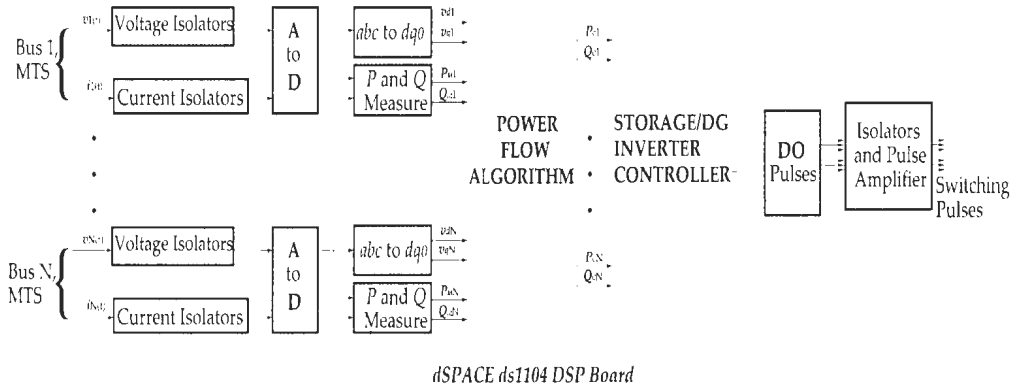

Figure 5.14: Hardware detail of inverter interfaced micro-grid controller for experimental testing.

ratory is comprised of a DSP board installed in a PC, voltage and current isolators, isolation and pulse amplifier circuit, an inverter, filter, a DC source, capacitors and synchronizing modules. The two phase voltages and currents for each bus are measured and then the third phase voltages and currents are calculated. The micro-grid voltages are acquired using voltage isolator sensors which take input $\pm$300V AC or DC and provide $\pm$10V AC or DC as the output. Similarly, the current isolator sensors are used to measure current that takes $\pm$10 ampere AC or DC current and provides $\pm$10V AC or DC. The output of the sensor is sent to the DSP board through the dSPACE built-in analog-to-digital converter port. After determining the third phase of the voltages and currents, the 3ϕ AC voltages and currents are converted to $d-q$-axis components using (4.12). The $d-q$-axis voltages and current components are utilized to determine the measured real and reactive power using

(4.57) and (4.58), respectively. The $d-q$-axis voltage components and the measured power are used as input to the power flow algorithm. The power flow algorithm is implemented in the DSP board according to the step-by-step procedure decribed in chapter 4, sub-section 4.4.2. The solution of the power flow equation determines the power required for each bus in order to maintain the rated system voltage at each bus of the system. The calculated power obtained from the power flow solution (present state) is compared with the measured power (previous state) in order to determine the value of command powers for the inverter controller.

The command powers derived from the power flow are used to calculate the reference signals for the inverter current controller using (4.59) and (4.60). The 3ϕ voltage and current at bus 1 are also acquired for the controller. This voltage and current are converted to $\alpha-\beta$ and then $d-q$-axis components. The current components are used as feedback information for the current controller, while the voltage components are used to generate the reference voltage signal for the space vector modulation. After comparing the reference and feedback current signal, the error is passed through the proportional-integral controller to minimize the error between the reference and the feedback current. The current controller is also employed in the cross coupling of the filter components in order to minimize the coupling effects of the filter at the inverter output. The signals from the controller are converted to $\alpha-\beta$ in order to use them as input to the space vector modulation block. This block also takes the angle θ to generate the reference signal for the space vector modulation. The space vector modulation block available in the Simulink library is utilized in order to generate the control pulses for the inverter switches. The generated pulses are then sent out through the digital output port of the DSP board. The control pulses are passed through a pulse amplifier before driving the

gate of the insulated gate bipolar transistors in the inverter module. The pulse amplifier provides an isolation between the system and the DSP board as well as amplifying the pulses to a required voltage level for driving the switches. A PLL based micro-grid synchronizer shown in Figure 4.38 is also implemented with the inverter controller to synchronize the storage system with the micro-grid. The photograph of the inverter interfaced micro-grid controller along with the micro-grid test setup is shown in Figure 5.15.

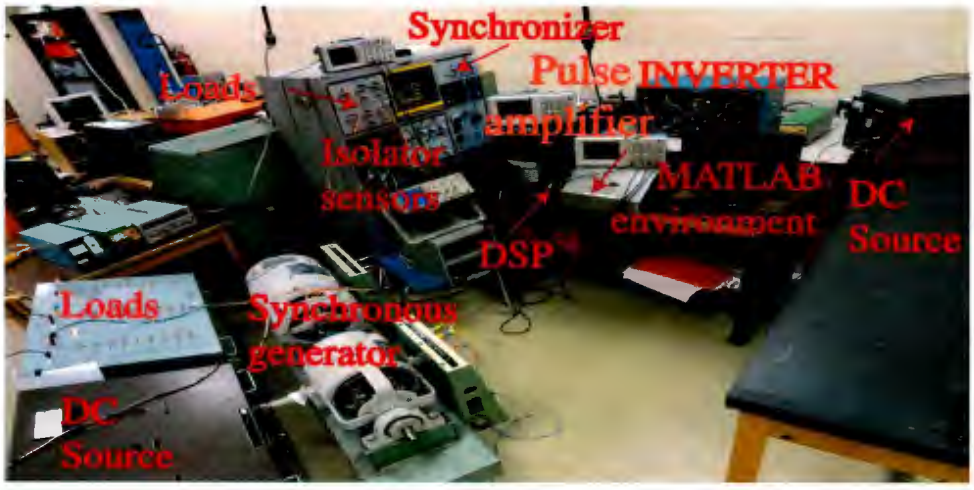

Figure 5.15: A photograph of the inverter interfaced micro-grid controller.

5.6 Test Results

5.6.1 Wind Turbine Emulator

The developed wind turbine simulator is tested in the laboratory environment based on the change in wind velocity. This is because the wind turbine starts to rotate and produces power at the rotor shaft whenever wind flows through a rotor plane and as long as the flow remains. The flow may either be constant or change

suddenly at any point of time. Therefore, a developed WTS should be able to follow the theoretical torque of the rotor for a specific wind speed or a sudden change in the wind speed at any point of time. To examine this performance, a wind pattern (Figure 5.16) following a series of step variations with equal duration was fed to the wind turbine model. Although the flow of the wind in practice does not follow the pattern utilized in this test, this pattern is a standard signal for laboratory testing that obviously explores the system behaviour.

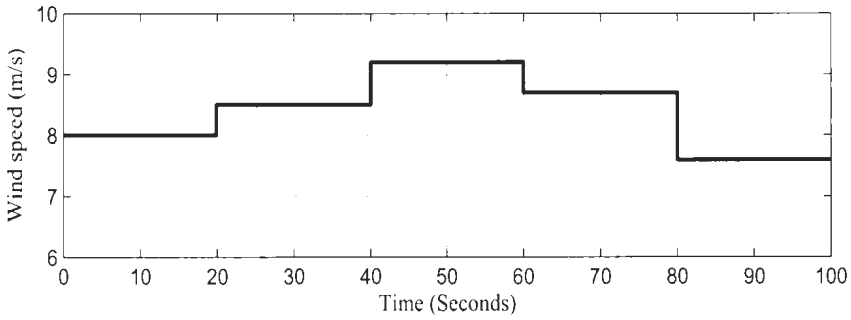

Figure 5.16: Wind speed variation fed into the wind turbine model

Figures 5.17 and 5.18 show the developed WTS test results which are obtained using a four channel Tektronix TDS 3014B digital phosphor oscilloscope. The actual and the corresponding reference torque produced by the turbine shaft due to the variation in the wind speed are shown in Figure 5.17. It can be seen from Figure 5.17 that the reference torque (the upper trace) of the wind turbine rotor is followed by the actual torque (the lower trace) of the system. Also, the step change in the reference torque reflects the change of the wind speed, and the actual torque also follows the reference torque during the step change and subsequently until the next change in wind speed. The almost exact fit of the DC motor actual torque and the reference torque produced by the wind turbine model shows accuracy and

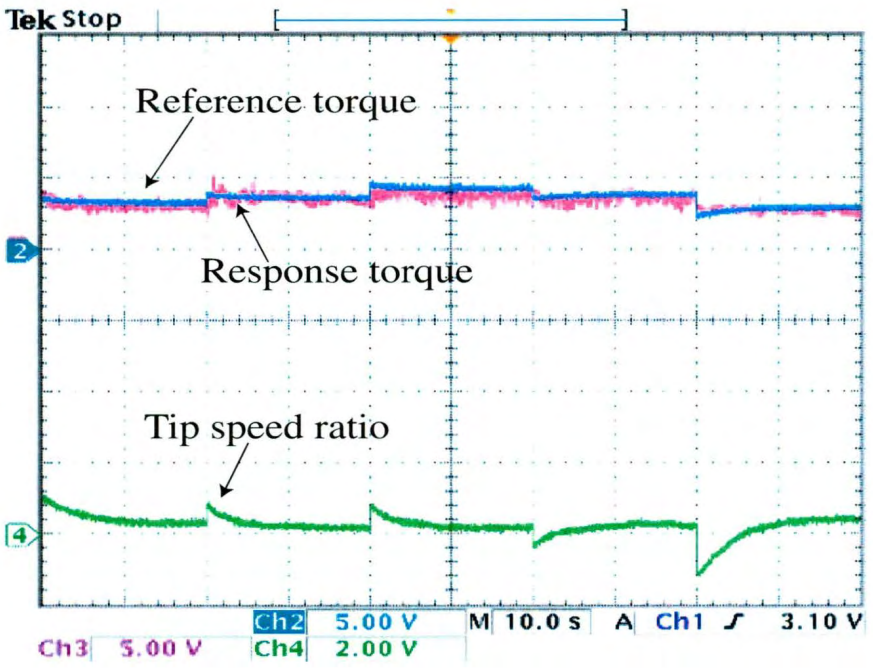

Figure 5.17: The experimental performances of the wind turbine emulator without optimum power controller

speed at every change in wind velocity. It is obvious from the result that the designed discrete torque controller has the significant ability to control the DC motor in such a way that its shaft behaves as a wind turbine rotor and provides a controllable torque. However, the developed WTE in conjuction with the generator is not featured with a maximum power extraction feature. This is because the error in tip speed ratio shown in Figure 5.17 is not zero yet.

Figure 5.18 shows experimental performances of the WTE when an optimal power extraction feature is included in the simulator. The tip speed ratio control technique described in section 5.2.1 is incorporated to maintain the operation of the simulator at the optimal tip speed ratio. It can be seen from Figure 5.17 that the WTE is operated at different tip speed ratios at different wind speeds which

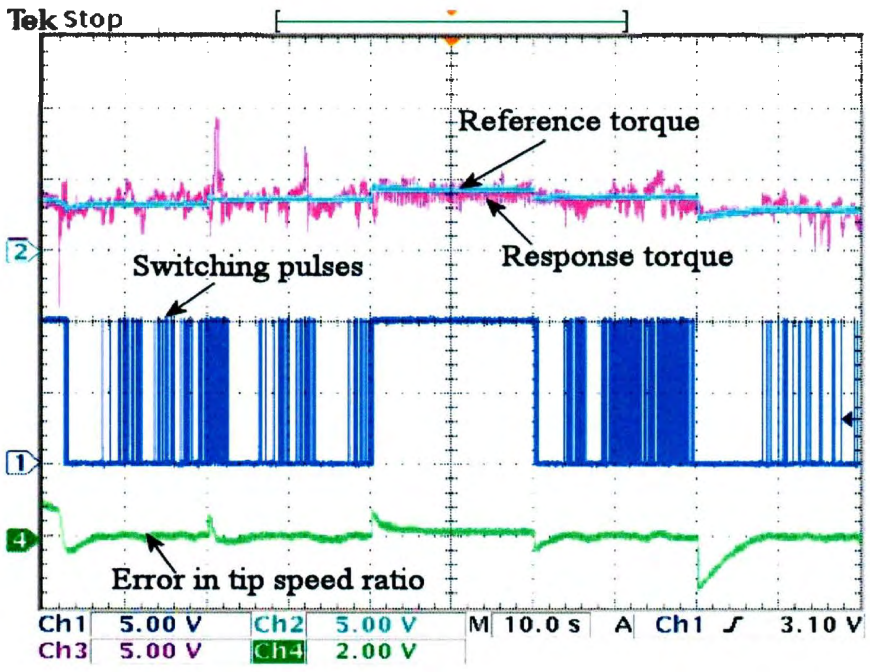

Figure 5.18: The experimental performances of the wind turbine simulator along with optimum tip speed ratio controller

causes an error in tip speed ratio. On the contrary, Figure 5.18 shows the close-to-zero error in the tip-speed ratio while the WTE is operated along with its optimal tip speed ratio controller. Note that there is a dip or shoot in the tip speed ratio error because of the step change in wind velocity. It also shows the good tracking between the reference torque and the actual torque of the WTS .

5.6.2 Testing of Micro-Grid Active Power Controller

The developed active power controller is tested to verify the performances of the controller in the micro-grid operation. It is worth mentioning here that this controller is enabled to engage during the operation of the isolated micro-grid with WPGS (Figure 3.2). Thus the performances of the developed controller are tested

only for an isolated micro-grid with WPGS. The experimental results with and without the application of the developed controller for an isolated micro-grid operation are presented to evaluate the performances of the controller. Figure 5.19 shows the experimental test results of the micro-grid system without the application of the active power controller.

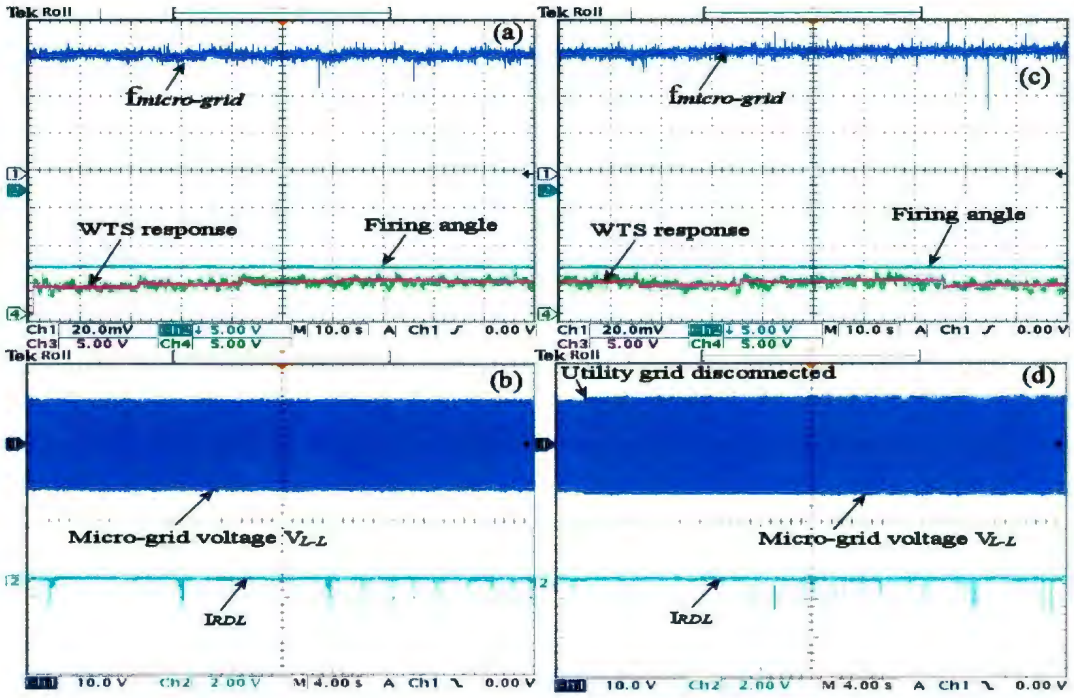

Figure 5.19: The experimental performances of the isolated micro-grid system without the application of the active power controller: (a) Frequency, firing angle and WTS response during grid connected operation, (b) Voltage and dump load current during grid connected operation, (c) Frequency, firing angle and WTS response at isolated condition, (d) Voltage and dump load current at isolated condition

Figures 5.19(a) and 5.19(b) show the micro-grid frequency, WTE simulator response, system voltage, firing angle and current flowing into the dump load. The zero value firing angle and also the zero current flow into the dump load indicate the disengagement of the controller during the utility-grid connected micro-grid

(Figure 2(a)) operation. Furthermore, the frequency and the voltage of the micro-grid system are at their nominal value. However, the utility grid is disconnected and the performance results of the isolated micro-grid system with wind power generator are shown in Figures 5.19(c) and 5.19(d). It can be seen from Figures 5.19(c) and 5.19(d) that the power controller is not activated yet because of the zero value of the firing angle and also the zero current flow into the dump load. Since the controller is not activated yet, the micro-grid frequency starts to deviate from the nominal value. This is because of the excess power in the micro-grid system generated by the wind power generator. In addition, the excess power in the system causes the micro-grid voltage to change to a higher value than the nominal value. It can also be noticed from the WTS response that fast and accurate tracking between the reference torque of the wind turbine and the actual torque are obtained from the system.

The experimental results of the isolated micro-grid system with the employment of the active power controller are shown in Figure 5.20. Micro-grid system frequency, firing angle, WTE response, micro-grid voltage, and current flowing into the dump load are presented in Figures 5.20(a) and 5.20(b). At the time of utility grid disconnection, the micro-grid frequency and voltage start to deviate. However, due to the involvement of the active power controller, the micro-grid frequency and voltage become their nominal values. The non-zero value of the firing angle and the current flowing into the dump load indicate the engagement of the controller in the system operation. Also, the WTE response indicates the variable speed operation of the WT generator in the micro-grid system.

Figures 5.20(c) and 5.20(d) present the performance results of the micro-grid system during a step increase in the micro-grid power demand. Since the power

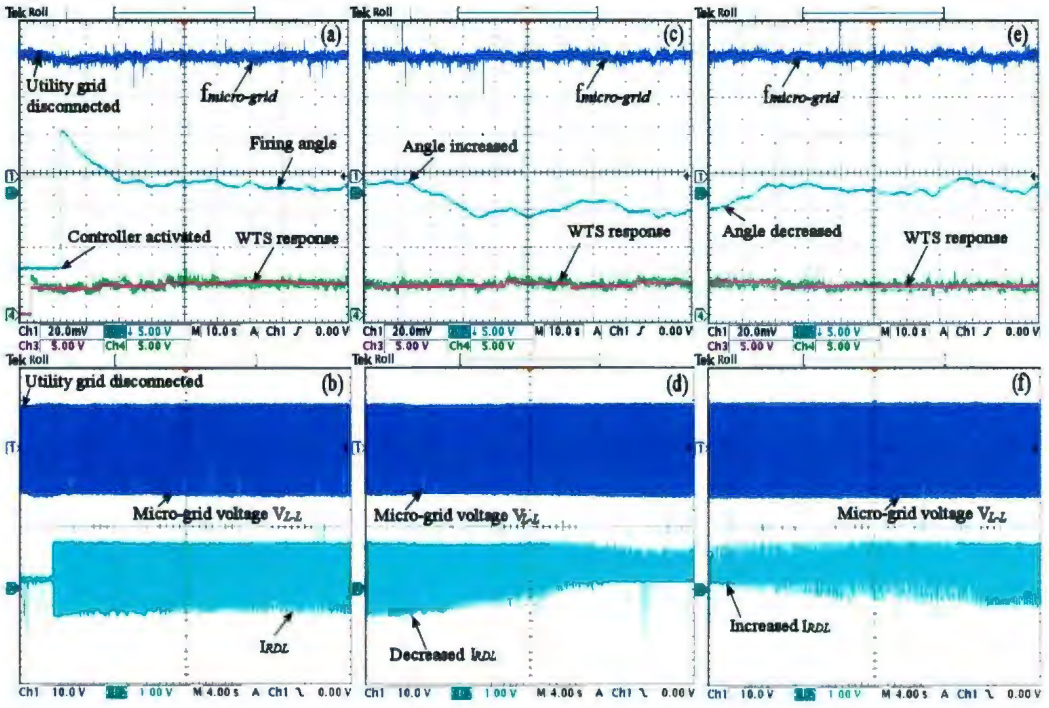

Figure 5.20: The experimental performances of the isolated micro-grid system with the application of the active power controller: (a) Frequency, firing angle and WTS response during isolated micro-grid operation, (b) Voltage and dump load current during isolated micro-grid operation, (c) Frequency, firing angle and WTS response at isolated condition with step increase in load demand, (d) Voltage and dump load current at isolated condition with step increase in load demand, (e) Frequency, firing angle and WTS response at isolated condition with step decrease in load demand, (f) Voltage and dump load current at isolated condition with step decrease in load demand

demand has increased in the micro-grid system, the controller adjusts the firing angle so that the current flowing into the dump load is accommodated to maintain the power balance in the micro-grid domain. Due to the accurate and fast action of the active power controller, the system frequency and voltage are maintained at their operating nominal value. Also the WT operates at a variable wind speed, which can be observed from the WTE response.

The experimental performances of the micro-grid system are also presented in

Figures 5.20(e) and 5.20(f), while a step decrease in micro-grid load demand is applied. Figure 5.20(e) shows the micro-grid frequency, firing angle for the power semiconductor switches, and WTE response. Due to the decrease in load demand, the controller provides necessary actions to harmonize the firing angle in order to maintain the power balance between power generation and consumption in the micro-grid domain. This can be noticed from the firing angle response and the current flowing into the dump load. This is because the firing angle is decreased to allow more current to flow into the dump load, which leads to fast and accurate balance in power generation and load demand. The fast and accurate balance between generation and load demand can be observed from the frequency and voltage responses shown in Figures 5.20(e) and 5.20(f).

The power quality performances of the isolated micro-grid system are also investigated and presented in Figure 5.21. The results are presented for a short duration to observe the changes closely. Figure 5.21(a) shows the voltage and current flowing into the dump load, while the frequency spectrum for the voltage harmonics is shown in Figure 5.21(b).The frequency spectrum only shows the fundamental component of the micro-grid voltage. Figure 5.21(c) shows micro-grid voltage and current flowing into the dump load while micro-grid load demand is increased. Due to the increase in micro-grid load demand, the current flowing into the dump load is also reduced. Moreover, the frequency spectrum during this operational condition also shows only the presence of the fundamental component of the micro-grid voltage. A similar frequency spectrum is also noticed, while the micro-grid load demand is decreased. The presence of only one fundamental frequency component in the micro-grid voltages ensures high quality power in the isolated micro-grid system.

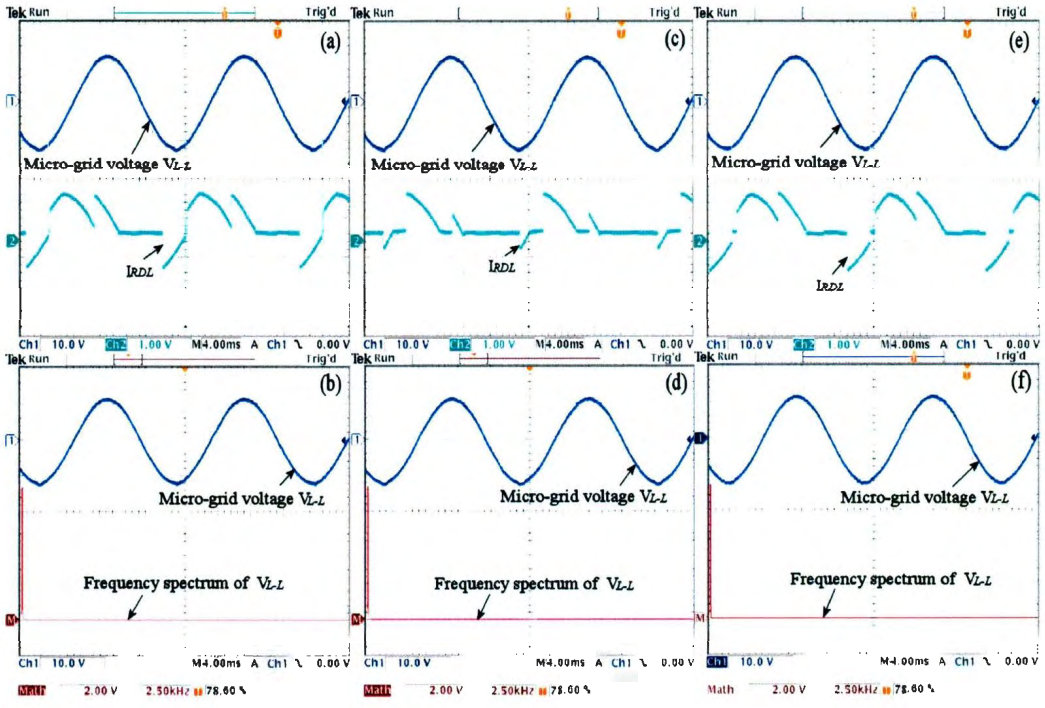

Figure 5.21: Power quality performances of the isolated micro-grid system with the application of the active power controller: (a) Voltage and current flowing into dump load, (b) Voltage and frequency spectrum of the voltage, (c) Voltage and current flowing into the dump load with a step increase in load demand, (d) Voltage and frequency spectrum of the voltage with a step increase in load demand, (e) Voltage and current flowing into the dump load with a step decrease in load demand, (f) Voltage and frequency spectrum of the voltage with a step decrease in load demand

5.6.3 Testing of Power Flow Based Micro-Grid Controller

The developed power flow based micro-grid controller is tested with a laboratory prototype to verify the performances of the controller in the micro-grid operation. It is worthwhile to mention here that this controller is enabled to engage during the operating mode of an isolated micro-grid without WPGS (Figure 3.3), where the inverter interfaced storage unit is considered. Thus the performances of the developed controller are tested under various conditions during the opera-

tion of an isolated micro-grid without WPGS. The considered operating conditions include varying the storage power generation and load demand for stand-alone modes. The variation of power generation is realized by changing the command values for the storage, which is connected at bus 1, and the variations of the load power demand is realized through timed connection of an additional load at bus 4. The experimental test results with the application of the developed controller during the operation of an isolated micro-grid are presented to evaluate the performances of the controller.

The experimental performance results are presented in Figure 5.22, when the micro-grid is operating in isolated mode and the WPGS is not in operation. During this operating condition, the micro-grid load demand is supplied by the HGS and the inverter interface storage unit connected to bus 1. The calculated power of various buses for the voltage equilibrium condition is utilized to generate the command power values for the converter controller. This command power is adjusted by the inverter controller and it can be seen from the measured and power flow calculated power at bus 1 in Figure 5.22(a). The close matches between the measured and calculated active and reactive powers indicate the effective and accurate adjustments in the generated power of bus 1 (the slack bus). Such an adjustment of command power values by the inverter controller also ensures the power balance in all other buses including the load buses in the system which can be seen from Figures 5.22(b), 5.22(c) and 5.22(d).

In addition, the stability of the active and reactive power generation and delivery can be observed through bus $d-q$-axis voltage components shown in Figures 5.23(a) and 5.23(b), where close-to-unity V_d and close-to-zero V_q values can be seen at all buses of the micro-grid test setup.

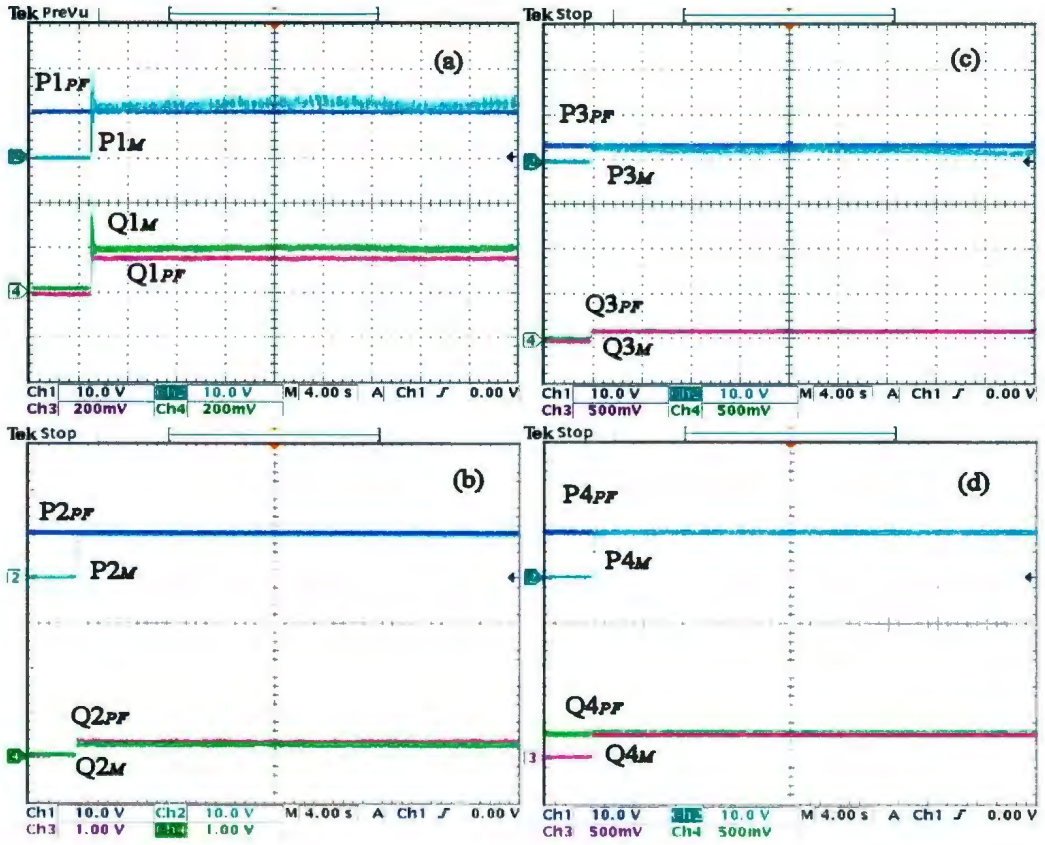

Figure 5.22: The experimental performances of the isolated micro-grid system with power flow based micro-grid controller: (a) Measured and command power calculated by power flow at bus 1 (1V = 200W), (b) Measured and calculated power at load bus 2 under equilibrium condition (1V = 100W), (c) Measured and calculated power at bus 3, (d) Measured and calculated power at load bus 4 under equilibrium condition (1V = 100W).

Figure 5.24 shows the experimental test performances of the developed power flow based micro-grid controller during the operating mode of an isolated micro-grid without WPGS along with a step change in micro-grid load demand. Such a change in load demand also reflects the effect of change in power generation by the storage unit. This is because the change in load demand needs to be adjusted by the change in the storage power generation. It can be seen from Figure 5.24(a)

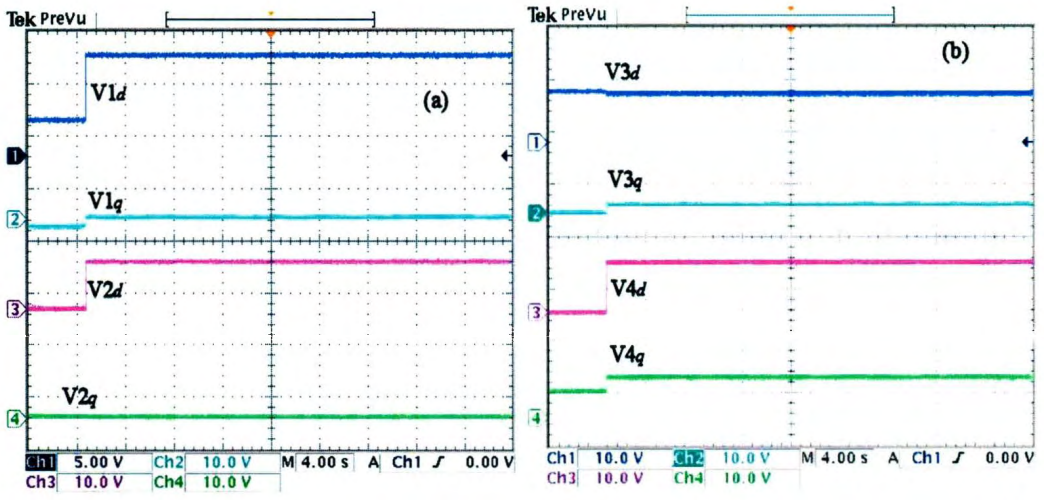

Figure 5.23: The experimental performances of the isolated micro-grid system with power flow based micro-grid controller: $d-q$-axis voltage components at various buses in the micro-grid test setup.

that the measured and power flow calculated power is the same in the isolated micro-grid because of the fact that the power flow calculates the bus powers under voltage equilibrium condition and sends the command values to the inverter controller. The current controlled inverter adjusts power from storage which results in the power balance in all buses in the micro-grid test setup. Afterwards, at time $t = 18.0\,\text{sec}.$, the power demands of bus 2 increase in a stepwise manner that can be seen from Figure 5.24(b). Due to the change in micro-grid power demand, the power flow solution recalculates the bus powers and generates new command power values for the inverter controller. This change causes the change in reference value of the inverter current controller. The inverter controller adjusts this change to ensure the command power flow from storage to the micro-grid. The impact of this adjustment can be observed from Figure 5.24(a), where the generated power at bus 1 is changed according to the variation in load demand. It can also be seen that the measured and power flow calculated power is the same even after the change

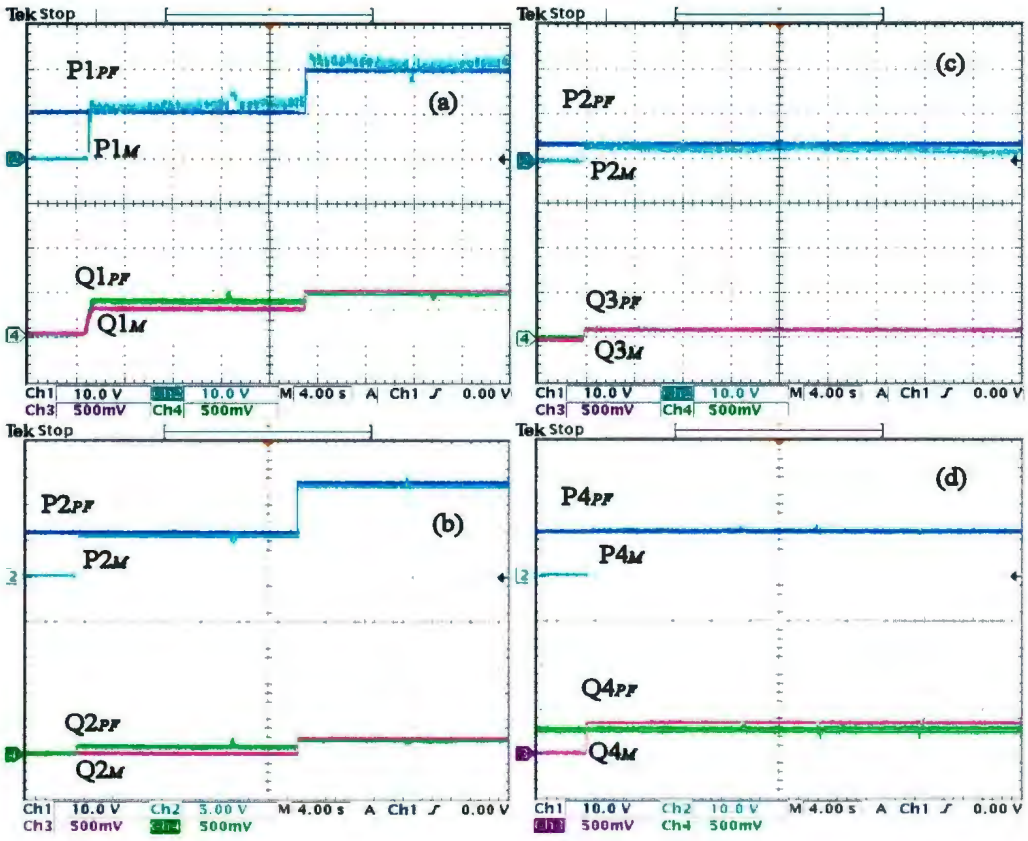

Figure 5.24: The experimental performances of the isolated micro-grid system with the application of power flow based micro-grid controller: (a) Measured and command power calculated by power flow at bus 1 with a change in command power (1V = 100W), (b) Measured and calculated power at load bus 2 under equilibrium condition with a step increase in load (1V = 50W), (c) Measured and calculated power at bus 3 with a step increase in load demand at bus 2, (d) Measured and calculated power at load bus 4 under equilibrium condition with a step increase in load at bus 2 (1V = 50W).

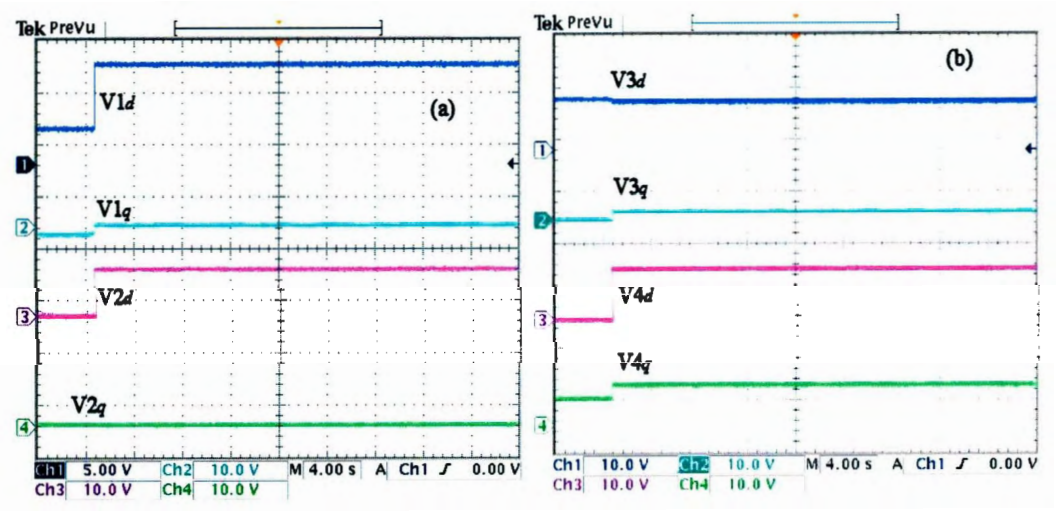

Figure 5.25: The experimental performances of the isolated micro-grid system with the application of power flow based micro-grid controller: $d-q$-axis voltage components at various buses in the micro-grid test setup with a step increase in load demand

in load demand. Moreover, measured and calculated active and reactive powers for all other buses in the micro-grid test setup are also the same before and after the load change and can be seen from Figures 5.24(c) and 5.24(d).

In addition, an indication of the stability of the micro-grid can be observed from the close-to-unity V_d and close-to-zero V_q values before and after the step increase in load demand from Figures 5.25(a) and 5.25(b). These indications are ingredients for stable power generation and delivery, as well as showing significant capability of the proposed power flow based control to initiate adjustments in response to an increase in power demands.

5.7 Summary

In this chapter, the performances of micro-grid control schemes along with a micro-grid test setup are investigated and presented. The micro-grid test setup

is comprised of renewable energy sources such as wind and hydro based micro-generation. The developed micro-grid test setup is represented as a scaled version laboratory prototype of the micro-grid system presented in chapter 3. The detailed hardware arrangement of the MTS is described and presented. A WTS is developed and incorporated in the MTS in order to reflect the impact of variable speed operation of a wind energy conversion system in micro-grid operation. The WTS simulator is also featured with an optimum power controller in order to extract maximum power from the wind. The experimental testing and results presented in this chapter reflect the satisfactory operation of the developed WTS in the laboratory. The implementation procedure of the developed micro-grid controller utilizing this MTS is also presented and discussed in this chapter. An active power controller based on the AC voltage control concept is tested for the operating mode of an isolated micro-grid with wind power generation. It is found that the active power controller is able to maintain the power balance between generation and load in isolated micro-grid operation under various operating conditions. An inverter interfaced storage control scheme that combines the power flow solution and current reference control of the inverter during the operating mode of an isolated micro-grid without wind power generation is tested. It is also found from the test results that this controller has the significant capability to maintain fast and accurate power balance in the system while the micro-grid needs to be supplied by the storage unit. The experimental development and performance testing of the micro-grid controllers presented in this chapter provide the technical viability to maintain power balance for stable and reliable operation of a micro-grid system that is comprised of renewable micro-generation.

Chapter 6

Micro-Grid Reliability Assessment

The aim of this chapter is to investigate the reliability of generating and supplying power using a micro-grid system consisting of renewable energy sources. This chapter concentrates on 1) development of the mathematical model for the reliability of the wind power generation system; 2) development of the mathematical model for the reliability of the various operational modes of the micro-grid system; 3) calculation of the reliability of the systems. A comparative study is also carried out in order to evaluate the reliability of generating and supplying power with such a micro-grid system at various locations in Newfoundland and Labrador.

6.1 Micro-Grid System Reliability

The one-line diagram of the proposed micro-grid system shown in Figure 6.1 consists of an HGU, a WPGS (Wind Farm), and two load areas represented as Load-I and Load-II. Also it has a connection link with the utility grid. The WPGS is connected to bus 7 through a TL2 (0.8 km) transmission line and a 12.5/66kV, 45 MVA power transformer. Each WT in WPGS is separated by a TLd (0.36 km) length line.

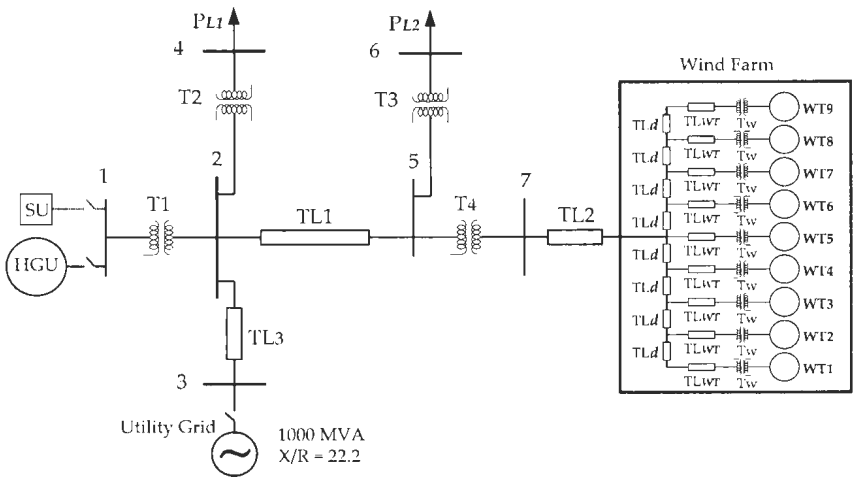

Figure 6.1: The single-line diagram of a micro-grid system at Fermeuse, Newfoundland, Canada.

Each WT is connected to the WPGS transmission line by a transformer, Twt (1/12.5 kV, 4MVA), and a line of length, TLwt (0.03 km). HGU and WPGS are separated from each other by a TL1 (20.12) km transmission line.

Micro-grid System Reliability (MSR) is a measurement of the system's overall ability to produce and supply electrical power. This measurement indicates the adequacy of power generation and supply of a micro-grid system for a given combination of DG units in the system as well as the sub-systems contained in a DG unit. In order to do a reliability study of the system shown in Figure 6.1, the combination of DG units and the sub-systems contained in a DG unit are represented by the concept of the reliability block diagram (RBD). Figure 6.2 shows the RBD of the case study micro-grid system. It is worth mentioning that the focus of this study is to evaluate the reliability of generating and supplying power using the micro-grid system; hence the other subsystems, except for DG units, are not considered. The simplified RBD of the micro-grid system can be represented as in

Figure 6.3, where all DG units are connected in parallel. However, according to the operational modes of the micro-grid system, the RBD of the micro-grid system at different operational modes can be shown in Figure 6.4.

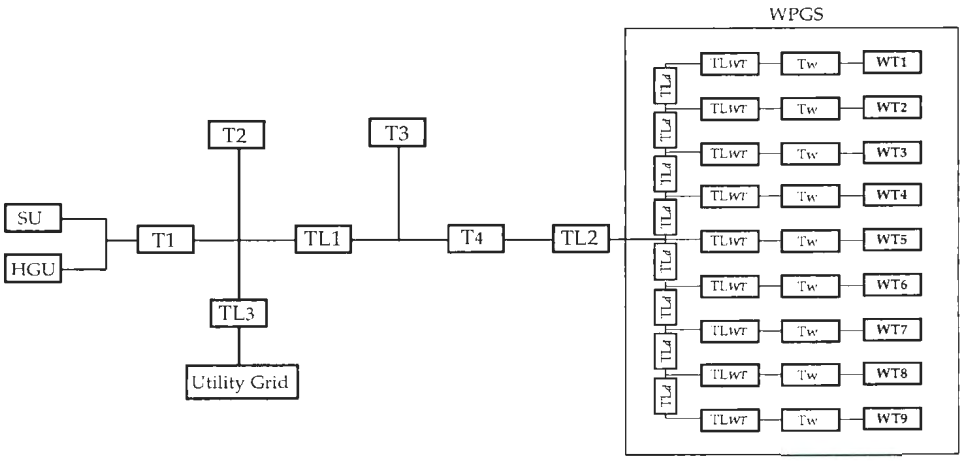

Figure 6.2: Detail reliability block diagram of the micro-grid system.

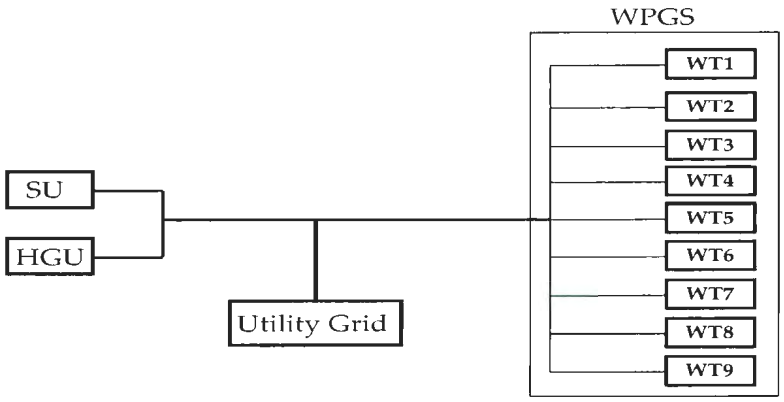

Figure 6.3: Simplified reliability block diagram of the micro-grid system.

Moreover, in order to estimate reliability of a DG unit, the various sub-systems in a DG unit can also be represented by the RBD. The RBD of a wind generator system is shown in Figure 6.5, which consists of a WT or WT rotor, gear box, generator

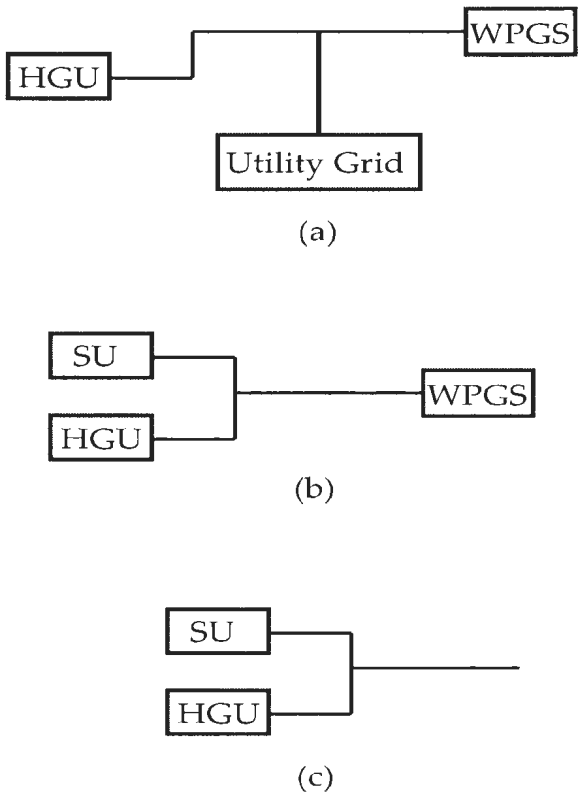

Figure 6.4: Reliability block diagram: (a) Grid connected mode, (b) Isolated micro-grid with wind power generation system, (c) Isolated micro-grid without wind power generation system.

and power electronics interfacing circuitry. In this study, the HGU and utility grid are assumed to be highly reliable generation sources. The reliability assessment of a storage unit (SU) is beyond the scope of this project; however, it is assumed for the sake of reliability calculation of an isolated micro-grid system without WPGS (Figure 5(c)).

Figure 6.5: Reliability block diagram of a wind turbine system.

6.2 Reliability Modeling

Two types of modeling approaches, deterministic and probabilistic approaches, can be considered to calculate the reliability of a system [114]. However, the deterministic approach in reliability analysis does not account for system uncertainties because the analysis is limited to a fixed set of values or a specific operating condition. Hence the probabilistic approach is a preferred method for evaluating reliability of any systems including power system networks. There are two main methodologies that can be used in the probabilistic reliability modeling approach namely, (1) Analytical method, and (2) Monte Carlo simulation method. The analytical method estimates system reliability based on analytical solutions of the system model that are derived mathematically. In order to derive such a model, the knowledge of the failure mechanisms and the root causes of failures are important and hence the developed models become very system specific [115]. An example is the analytical model developed to estimate the reliability for a light bulb. If the filament of the bulb is changed, the analysis will change. In this approach, failure is not considered as a stochastic event. Rather it is treated as the time to failure which is assumed to be deterministic [115]. On the contrary, Monte Carlo simulation treats the occurence of failures as a random event which mimics the wind speed distribution [116]. For example, in a time series of wind data, some of the wind data is not sufficient to produce power which can be considered as a

failure event and those events occur randomly. In addition, this study focuses on the estimation of the reliability of generating and supplying power of the micro-grid system with the wind speed considered as the main uncertainty in the system. Thus Monte Carlo simulation based reliability estimation for the micro-grid system is considered in this work.

6.2.1 Wind Speed Data Modeling

The relation between wind speed and a WT rotor power output is expressed as [83]

$$P_{ro} = 0.5\rho A_{SA} C_p(\lambda, \beta)\, v_w^3 \tag{6.1}$$

where A_{SA} is the swept area covered by the turbine rotor, C_p is the power coefficient, v_w is the wind velocity, β is the pitch angle of rotor blades, λ is the tip speed ratio and ρ is air density. For a given WT, A_{SA}, C_p, β, λ, ρ are constant. The relation in (6.1) can be expressed as:

$$P_{ro} \propto v_w^3 \tag{6.2}$$

Since wind speed is the main factor that creates uncertainty in the power output of a WECS system, wind speed is considered here as the key factor to estimate the MSR. In order to relate wind speed effects in reliability estimation, wind speed field data modeling is essential because the data itself varies not only from site to site but also varies according to the wind turbine hub heights. Wind speed data modeling for a typical wind turbine includes:

- Identifying best-fit distribution for one year wind field data
- Evaluating the goodness-of-fit test

- Estimating the distribution parameters

Identification of Best-Fit Distribution

Rather than believing that a time series wind data follows a specific distribution, it is better to identify the best-fit distribution of the available wind data for a given site and for a given wind turbine hub height. The probability plots method is used to evaluate the fit of one year wind speed field data to a distribution [115]. The following steps are taken to accomplish the fitting of the wind data to a distribution:

1. Obtain one year wind speed data from the site measurement.

2. Scale the wind data according to the hub height of the wind turbine using (6.3)

$$v_{w2} = v_{w1} \times \left(\frac{h_2}{h_1}\right)^{\alpha} \tag{6.3}$$

   where h_1 and h_2 are the height of the anemometer and hub, respectively, v_{w1} and v_{w2} are the wind velocity at the anemometer height and at the hub height, respectively, and α_s is the shear exponent that is expressed as:

$$\alpha_s = (0.096 \times \log(Z_0) + 0.016 \times \log(Z_0) + 0.24) \tag{6.4}$$

   where Z_0 is the surface roughness.

3. Use Matlab *Distribution Fitting Tool* to obtain probability plot of the scaled wind data.

4. Fit the probability plot of the scaled wind data for different distributions such as normal, log-normal, exponential and Weibull.

5. Identify the distribution corresponding to the best fit of the probability plots.

Goodness-of-Fit Test

After identifying the best-fit distribution, the goodness-of-fit test is performed to select the distribution for the reliability calculation. The identified distribution of wind speed data is Weibull. Hence, a specific test method called MANN'S test is selected for goodness-of-fit test of the Weibull distribution. The hypotheses for such a test are:

H_0: Wind speed data are Weibull

H_1: Wind speed data are not Weibull

The statistic for MANN'S test is expressed as [115]

$$M = \frac{k_1 \sum_{i=k_1+1}^{r-1} \left[\left(\ln v_{w_{i+1}} - \ln v_{w_i}\right)/M_i\right]}{k_2 \sum_{i=1}^{k1} \left[\left(\ln v_{w_{i+1}} - \ln v_{w_i}\right)/M_i\right]} \tag{6.5}$$

where $k_1 = \frac{r}{2}$, $k_2 = \frac{r-1}{2}$, $M_i = Z_{i+1} - Z_i$, and $Z_i = \ln\left[-\ln\left(1 - \frac{i-0.5}{n+0.25}\right)\right]$. If the test statistic $M < F_{crit}$ for n number of wind data, then H_0 is accepted.

Distribution Parameters Estimation

In order to determine Weibull distribution parameters, the least-squares technique is used because of its accuracy to fit a straight line in a given data point [115]. In this approach, the wind speed field data are transformed to Weibull distribution to fit a linear regression line as in (6.6)

$$y_i = a + bx_i \tag{6.6}$$

where

$$x_i = \ln v_{w_i} \tag{6.7}$$

$$y_i = Z_i \tag{6.8}$$

$$a = -\beta_{ws} \ln \theta \tag{6.9}$$

$$b = \beta_{ws} \tag{6.10}$$

The values of a and b are determined from the least-squares fit using (6.7) and (6.8). By knowing the values a and b, the Weibull parameters are determined as

$$\theta_{ws} = \exp\left(-\frac{a}{b}\right) \tag{6.11}$$

$$\beta_{ws} = b \tag{6.12}$$

where θ_{ws} and β_{ws} are defined as the scale and shape parameters for wind speed field data.

6.2.2 Wind Power Generation System

According to the micro-grid configuration, all nine WTs in WPGS are connected in parallel, which are also shown in the simplified RBD in Figure 6.3. In order to estimate the reliability of power generation by the WPGS, a single WT system is considered because they are all identical both in terms of topology and sub-systems context. A WT system comprised of different sub-systems is shown in Figure 6.5. The different sub-systems are connected in series because failure of power generation by any sub-system has to be considered as the WT system failure to generate power. The modeling of reliability estimation of different sub-systems

in a WT system is described in the following sub-sections.

Wind Turbine Rotor

The wind speed field data model provides information about the shape parameter and scale factor for Weibull distribution. Such parameters are used to generate a series of random wind speed data that follows Weibull distribution. Randomly generated data are then used to determine power generation by the WT using (6.1), which represents Weibull distribution of power generation. Weibull parameters for power distribution are determined using the parameter estimation technique described in the preceding section. The Weibull parameters for power distribution are defined as θ_{tp} and β_{tp}. So, the reliability of generating power using the WT rotor, R_{tp} can be expressed as

$$R_{tp} = \exp\left[-\left(\frac{P_{ciw}}{\theta_{tp}}\right)^{\beta_{tp}}\right] - \exp\left[-\left(\frac{P_{cow}}{\theta_{tp}}\right)^{\beta_{tp}}\right] \tag{6.13}$$

where θ_{tp} and β_{tp} are defined as shape parameter and scale factor for power distribution. P_{ciw} and P_{cow} are the power at cut-in and cut-out wind speed, respectively. The reliability of generating i^{th} wind speed power, R_{P_i} can be expressed as

$$R_{P_i} = \exp\left[-\left(\frac{P_i}{\theta_{tp}}\right)^{\beta_{tp}}\right] \tag{6.14}$$

where P_i is the power for i^{th} wind speed in between the cut-in and cut-out region.

Gear Box

Weibull parameters obtained from field data modeling are utilized to produce a set of random wind data. Such data are used to determine the wind turbine speed

using the following equation:

$$\omega_{wt} = \frac{\lambda v_w}{R_t} \tag{6.15}$$

where ω_{wt} is the wind turbine speed and R_t is the turbine radius, respectively. The wind turbine speed is also the speed ascertained by the gear box low speed shaft. Speed ascertained by the gear box can be represented as Weibull distribution of speed. This distribution is utilized to estimate shape parameter and scale factor for the reliability model of the gear box. The reliability of the gear box, R_{gb} can be expressed as

$$R_{gb} = \exp\left[-\left(\frac{\omega_{wt,s}}{\theta_{gb}}\right)^{\beta_{gb}}\right] - \exp\left[-\left(\frac{\omega_{wt,m}}{\theta_{gb}}\right)^{\beta_{gb}}\right] \tag{6.16}$$

where $\omega_{wt,s}$ is the starting speed of the wind turbine, θ_{gb} and β_{gb} are the shape parameter and scale factor for the speed ascertained by the gearbox, and $\omega_{wt,m}$ is the maximum operating speed of the wind turbine.

The reliability of the gear box for i^{th} speed recognized by the gear box, $R_{gb_{wt,i}}$ can be estimated as

$$R_{gb_{wt,i}} = \exp\left[-\left(\frac{\omega_{wt,i}}{\theta_{gb}}\right)^{\beta_{gb}}\right] \tag{6.17}$$

where $\omega_{wt,i}$ is the i^{th} speed of the WT seen by the gear box.

Generator

In order to consider the effect of wind speed in estimating the reliability of generating power using the wind generator, the estimation of Weibull parameters using field data are used. Such parameters are utilized to generate a set of random wind speed data. Power generated by the WT is then determined using (6.1). However, the power at the generator output depends on the gearbox efficiency and various

losses in the generator. Efficiency of the gear box and generator are considered as 90 percent, which is observed from system modeling and simulation. The power at the generator output can be determined as 90 percent of the power at the turbine output. Thus a power distribution at the generator output can be obtained, which also follows Weibull. This power distribution at the generator output is used to estimate Weibull distribution parameters using the least-squares parameter estimation technique. After identifying the generator output power distribution parameters, the reliability of generating power by the generator, R_g can be evaluated as

$$R_g = \exp\left[-\left(\frac{P_{g,ciw}}{\theta_{gp}}\right)^{\beta_{gp}}\right] - \exp\left[-\left(\frac{P_{g,cow}}{\theta_{gp}}\right)^{\beta_{gp}}\right] \tag{6.18}$$

where θ_{gp} and β_{gp} are considered as the shape parameter and scale factor for the generator power distribution. $P_{g,ciw}$ and $P_{g,cow}$ are the generator power at the cut-in and cut-out wind speed, respectively.

The reliability of generating power $P_{g,i}$ of the generator, $R_{P_{g,i}}$ can be expressed as

$$R_{P_{g,i}} = \exp\left[-\left(\frac{P_{g,i}}{\theta_{gp}}\right)^{\beta_{gp}}\right] \tag{6.19}$$

where $P_{g,i}$ is the generator power for i^{th} wind speed in between the cut-in and cut-out speeds.

Power Electronics Interfacing System

The Interfacing Power Electronics (IPE) system in a doubly-fed induction generator based WT consists of a back-to-back pulse width modulated (PWM) converter as shown in Figure 6.6. The components in the IPE system are diodes, IGBT switches and a DC bus capacitor. The reliability model of such a system can be developed

based on the relationship between the lifetime and failure rate of the components in the system. The lifetime of the components is determined considering junction temperature as a covariate [81]. The junction temperature, T_j of a semiconductor device can be calculated as [117].

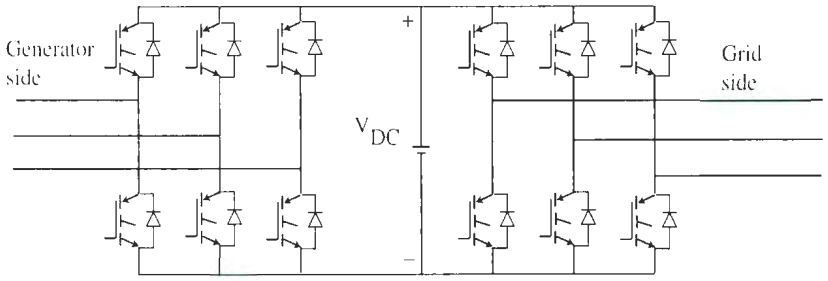

Figure 6.6: Interfacing power electronics system of a doubly-fed induction generator based wind turbine system.

$$T_j = T_a + P_l R_{ja} \tag{6.20}$$

where P_l is the power loss of a component, T_a is the ambient temperature and R_{ja} is the junction resistance. The power loss at a rated wind speed operating condition is considered in developing the reliability model in [81]. However, it is to be noted that power losses in the semiconductor components vary according to the wind speed variation at the wind turbine input. Thus power loss variation in the semiconductor components is important to consider as a stress factor to calculate the lifetime of the components instead of using power loss quantity for a single operating condition. Thus equation (6.20) can be expressed as

$$T_{j_i} = T_a + P_{l_i} R_{ja} \tag{6.21}$$

where P_{l_i} is the power loss of a component at the i^{th} wind speed, T_{j_i} is the component junction temperature at the i^{th} wind speed, and junction resistance is assumed to be constant for wind speed.

In the IPE system, there are two types of semiconductor components; namely, diode and IGBT switches. Two types of power losses, conduction losses and switching losses, occur in such components. The conduction loss, $P_{cl,d}$ and switching loss, $P_{sl,d}$ of a diode can be expressed as [118, 119]

$$P_{cl,d} = \left(\frac{1}{8} - \frac{m}{3\pi}\cos\phi\right) R_d I_{mo}^2 + \left(\frac{1}{2\pi} - \frac{m}{8}\cos\phi\right) V_{FO} I_{mo} \tag{6.22}$$

$$P_{sl,d} = \frac{1}{\pi} f_s E_{sr} \frac{V_{dc} I_{mo}}{V_{ref,d} I_{ref,d}} \tag{6.23}$$

Total power losses of diode, $P_{tl,d}$ in the IPE system can be expressed as the sum of the conduction loss, $P_{cl,d}$ for total number of diodes and the switching loss, $P_{sl,d}$ for the total number of switches in the system, and can be expressed as

$$\begin{aligned} P_{tl,d} = {} & 12\left[\left(\frac{1}{8} - \frac{m}{3\pi}\cos\phi\right) R_d I_{mo}^2 + \left(\frac{1}{2\pi} - \frac{m}{8}\cos\phi\right) V_{FO} I_{mo}\right] \\ & + 12\left[\frac{1}{\pi} f_s E_{sr} \frac{V_{dc} I_{mo}}{V_{ref,d} I_{ref,d}}\right] \end{aligned} \tag{6.24}$$

where m is the modulation index ($0 \leq m \leq 1$), I_{mo} maximum output current of the inverter, V_{F0} and R_d are the diode threshold voltage and resistance, respectively, f_s is the switching frequency, E_{sr} is the rated switching loss energy given for commutation voltage and current $V_{ref,d}$ and $I_{ref,d}$. V_{dc} and I_{dc} are the actual commutation voltage and current, respectively and ϕ is the angle between voltage and current.

The conduction loss, $P_{cl,IGBT}$ and switching loss, $P_{sl,IGBT}$ of a IGBT switch can

be expressed as [119, 121]

$$P_{cl,IGBT} = \left(\frac{1}{8} + \frac{m}{3\pi}\cos\phi\right) R_{ce} I_{mo}^2 + \left(\frac{1}{2\pi} + \frac{m}{8}\cos\phi\right) V_{CEO} I_{mo} \tag{6.25}$$

$$P_{sl,IGBT} = \frac{1}{\pi} f_s \left(E_{on} + E_{off}\right) \frac{V_{dc} I_{mo}}{V_{ref,IGBT} I_{ref,IGBT}} \tag{6.26}$$

Total power losses of switches, $P_{tl,IGBT}$ in the IPE system can be expressed as the sum of the conduction loss, $P_{cl,IGBT}$ for total number of diodes and the switching loss, $P_{sl,IGBT}$ for the total number of switches in the system, and can be exressed as

$$\begin{aligned} P_{tl,IGBT} = {} & 12\left[\left(\frac{1}{8} + \frac{m}{3\pi}\cos\phi\right) R_{ce} I_{mo}^2 + \left(\frac{1}{2\pi} + \frac{m}{8}\cos\phi\right) V_{CEO} I_{mo}\right] \\ & + 12\left[\frac{1}{\pi} f_s \left(E_{on} + E_{off}\right) \frac{V_{dc} I_{mo}}{V_{ref,IGBT} I_{ref,IGBT}}\right] \end{aligned} \tag{6.27}$$

where V_{CEO} and R_{ce} are the IGBT threshold voltage and on-state resistance, respectively. Reference commutation voltage and current are $V_{ref,IGBT}$ and $I_{ref,IGBT}$, while V_{dc} is the actual commutation voltage. E_{on} and E_{off} are the turn-on and turn-off energies of IGBT.

The lifetime, $L\left(T_{j_i}\right)$ of a component for i^{th} wind speed can be expressed as

$$L\left(T_{j_i}\right) = L_o \exp\left(-B\Delta T_{j_i}\right) \tag{6.28}$$

where L_o is the quantitative normal life measurement (assumed to be 10^6), $B = \frac{E_A}{K_B}$, where K_B is the Boltzmann constant (= 8.6×10^{-5} eV/K), E_A is the activation energy (= 0.2 eV) for typical semiconductor components [118]. ΔT_{j_i} is the variation in junction temperature for i^{th} wind speed and can be expressed as

$$\Delta T_{j_i} = \frac{1}{T_a} - \frac{1}{T_{j_i}} \tag{6.29}$$

The failure rate of a component for i^{th} wind speed can be defined as

$$\tau_i = \frac{1}{L\left(T_{j,}\right)} \tag{6.30}$$

Using (6.30), a distribution of failure rates for a set of wind speed data for a semiconductor component can be generated. Similarly, the failure rate for other components in the IPE system can be modeled using (6.30). The components in the IPE system are considered in series connection from the reliability point of view, because the IPE system fails if any one of the components fail in the IPE system. Thus the failure rates for different components are added to determine the failure rate of the IPE system for i^{th} wind speed. Hence a distribution of failure rates for the IPE system can be generated for a series of wind speed data. A least-squares technique is then used to determine the distribution parameters. By knowing the distribution parameters, the reliability of the IPE system, R_{IPE} can be modeled as

$$R_{IPE} = \exp\left[-\left(\frac{\tau_{ciw}}{\theta_{IPE}}\right)^{\beta_{IPE}}\right] - \exp\left[-\left(\frac{\tau_{cow}}{\theta_{IPE}}\right)^{\beta_{IPE}}\right] \tag{6.31}$$

where θ_{IPE} and β_{IPE} are defined as shape parameter and scale factor for failure rate distribution. τ_{ciw} and τ_{cow} are failure rates of the IPE system at cut-in and cut-out wind speed, respectively.

The reliability of a component in the IPE system, R_{IPE_C} can be expressed as

$$R_{IPE_C} = \exp\left[-\left(\frac{\tau_{ciw_C}}{\theta_{IPE_C}}\right)^{\beta_{IPE_C}}\right] - \exp\left[-\left(\frac{\tau_{cow_C}}{\theta_{IPE_C}}\right)^{\beta_{IPE_C}}\right] \tag{6.32}$$

where θ_{IPE_C} and β_{IPE_C} are defined as a shape parameter and scale factor for failure rate distribution of a component. τ_{ciw_C} and τ_{cow_C} are failure rates at the cut-in and

cut-out wind speed for a component, respectively.

The reliability of a WT system, R_{wts} can now be expressed as

$$R_{wts} = R_{tp} \times R_{gb} \times R_g \times R_{IPE} \tag{6.33}$$

In WPGS, all nine WTs are connected in parallel with identical configuration. Hence the reliability of the WPGS, R_{WPGS} can be expressed as

$$R_{WPGS} = \left[1 - (1 - R_{wts})^N\right] \tag{6.34}$$

where N is the number of WT systems in a WPGS.

6.2.3 Micro-Grid Reliability Model

Figure 6.3 shows the simplified RBD of the micro-grid system, where all DG units are connected in parallel. Assuming the reliability of the HGU as R_{HGU} and the utility grid as R_{UG}, the overall micro-grid system reliability, R_{MSR} can be modeled as

$$R_{MSR} = \left[1 - (1 - R_{wts})^N (1 - R_{HGU})(1 - R_{UG})\right] \tag{6.35}$$

However, the micro-grid system operates in three different modes which are shown in Figure 6.4. The MSR can also be modeled according to their operating modes. Figure 6.4(a) shows the grid connected mode of operation where all DG/-generation units are connected with the utility grid. Thus the MSR for the grid connected mode of operation, $R_{MSR_{M1}}$ can be expressed by the similar equation

presented in (6.35). Therefore,

$$R_{MSR_{M1}} = \left[1 - (1 - R_{wts})^N (1 - R_{HGU})(1 - R_{ug})\right] \tag{6.36}$$

Figure 6.4(b) represents the operating mode of an isolated micro-grid with WPGS, where the storage unit is not operating as a power generation unit. Thus the MSR during isolated operation with WPGS, $R_{MSR_{M2}}$ can be defined as

$$R_{MSR_{M2}} = \left[1 - (1 - R_{wts})^N (1 - R_{HGU})\right] \tag{6.37}$$

Furthermore, Figure 6.4(c) shows the operating mode of an isolated micro-grid without WPGS. During this operating mode, the SU generates and delivers power to the micro-grid load. Therefore, the SU is to be considered in the reliability model as a generating unit during this operating mode. Assume that the reliability of the SU is R_{SU}. Hence the MSR during this mode, $R_{MSR_{M3}}$ can be written as

$$R_{MSR_{M3}} = [1 - (1 - R_{HGU})(1 - R_{SU})] \tag{6.38}$$

6.3 Implementation of the Micro-Grid Reliability Model

In order to implement the developed MSR model to evaluate the reliability of generating power by the micro-grid system, numerical simulation is conducted using the Matlab/Simulink simulation package. The flow diagram for implementing the MSR model is shown in Figure 6.7. The steps taken to execute the flow diagram are described as follows:

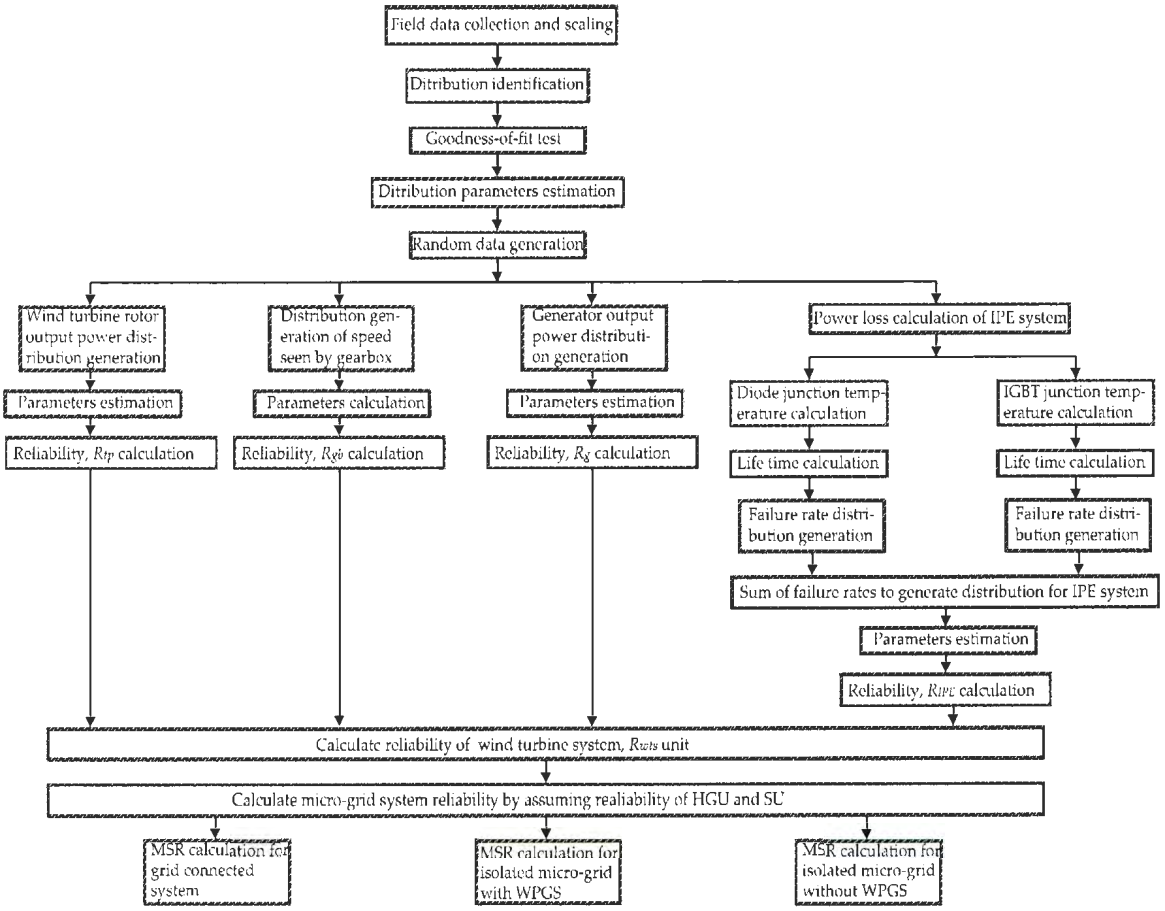

Figure 6.7: Flow diagram for calculation of micro-grid system reliability

STEP 1: Wind speed field data model

- identify the probability distribution using wind speed field data and probability plots
- select the distribution of the wind speed using goodness-of-fit test
- calculate distribution parameter using (6.11) and (6.12)

- generate a series of random data as the input for the next steps of the reliability flow diagram

STEP 2: Reliability of power generation by the WT rotor

- generate distribution of the WT rotor output power
- estimate parameters of the WT rotor output power distribution
- calculate reliability using (6.13)

STEP 3: Reliability of the gear box

- determine speed distribution ascertained by the gear box
- calculate speed distribution parameter using least-squares technique
- calculate reliability using (6.16)

STEP 4: Reliability of the generator

- generate the output power distribution of the generator
- determine the distribution parameter using the least-squares technique
- evaluate reliability of the generator output power using (6.18)

STEP 5: Reliability of interfacing power electronics

- calculate power loss of diodes and IGBTs in IPE system using (6.24) and (6.27)
- generate failure rate distributions for diodes and IGBT switches
- generate a failure rate distribution of IPE system by adding two distributions of the diode and IGBT

- estimate parameter of failure rate distribution of IPE system
- calculate reliability using (6.31)

STEP 6: Reliability of DG units

- calculate reliability of a WT system using (6.33)
- determine reliability of WPGS using (6.34)
- assume reliability for HGU and SU

STEP 7: Reliability of the micro-grid system

- calculate MSR using (6.35), (6.36), (6.37)and (6.38) for various operational modes

6.4 Simulation Results

The reliability model and its implementation procedure described in the preceeding sections are tested to determine probability distribution parameters, and consequently the reliability of the various sub-systems in the WT system for a stochastically varying wind speed condition. This reliability estimation is then utilized to determine MSR in various operating modes. The power generation wind speed region of the selected turbine is v_{ciw}= 4 m/s and v_{cow}= 25 m/s. The reliability of the HGU and utility grid are assumed as 85 percent, since they are assumed as highly reliable power generation sources. The reliability of the storage unit is assumed to be the same as the IPE system (= 0.8144), because the storage units are commonly interfaced through the power electronics inverter system. The IGBT module and diode parameters for loss calculation are obtained from [81]. One year wind speed

data is used for the field data modeling process. Assume that two WT systems can be connected to the isolated micro-grid system due to the stability issue.

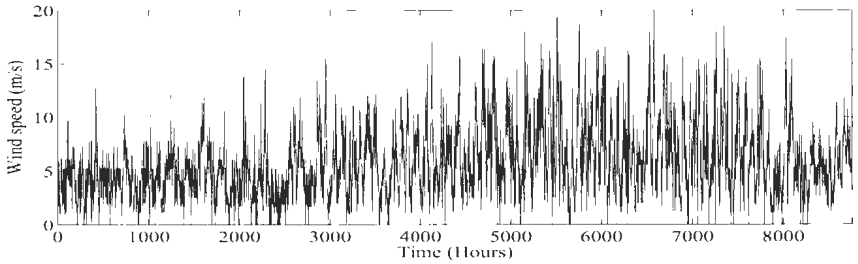

Figure 6.8: Wind speed field data

Figure 6.8 shows the hourly wind speed field data collected over an one year period. This data is utilized to identify the distribution using the probability plot technique. The probability plots of wind speed field data are shown in Figure 6.9. It can be seen from Figure 6.9 that the probability of wind speed follows Weibull and Rayleigh distributions closely; however, the Weibull distribution follows the probability of wind speed more closely than the Rayleigh distribution. Thus the Weibull distribution is identified as the best fit distribution for wind speed data in this study. In order to select Weibull distribution, a goodness-of-fit test is also carried out, where $M = 0.87 \leq F_{crit}$, and hence H_o is accepted. The probability density function of Weibull distribution is shown in Figure 6.10. A least-squares method is followed to estimate the Weibull distribution parameter, which is shown in Figure 6.11. The estimated Weibull parameters are as follows:
The shape parameter for wind speed, β_{ws} = 1.92, and the scale parameter, θ_{ws}=13.1. These parameters are used to generate random wind speed data for reliability evaluation of different sub-systems in a wind turbine system.

The results of reliability calculation for different sub-systems in a wind turbine system are presented in Table 6.1. The results reveal that the reliability of gener-

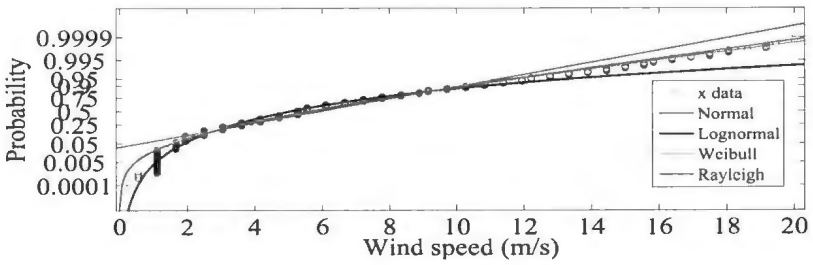

Figure 6.9: Probability plots for distribution identification

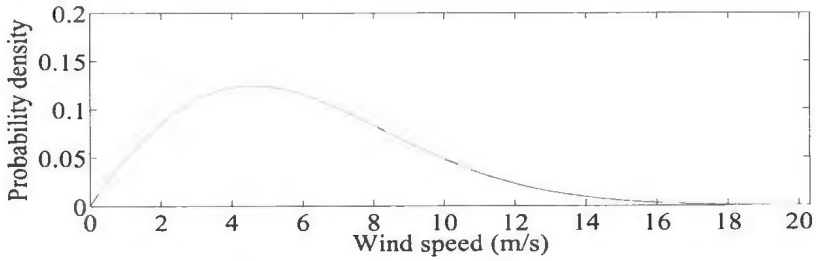

Figure 6.10: Probability density function of wind speed data

ating power by wind turbine rotor is 0.9068, while the reliability of gear box and generator are 0.9107 and 0.9266, respectively. However, the reliability of generating power for the IPE sub-system is only 0.8144. These results indicate that the IPE sub-system in a variable speed wind generator system is less reliable than the other sub-systems. Table 6.2 presents the reliability results of DG units such as a WT system, WPGS, HGU, SU and utility grid. The reliability of the WT system and WPGS is calculated based on the model derived in this work, however, the reliability of the HGU, SU and utility grid are assumed. The overall reliability of a wind turbine system is 0.6232. Since nine WT systems are connected in parallel in a WPGS, the calculated reliability of WPGS is significantly high.

Reliability estimation results of the micro-grid system during various operational modes are presented in Table 6.3. The MSR during grid connected mode is

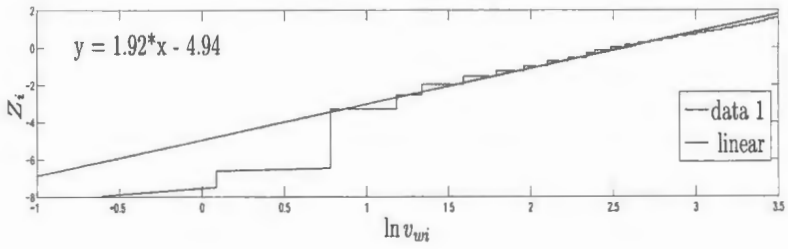

Figure 6.11: Least-squares plot for parameters estimation

Table 6.1: Reliability results of different sub-systems in a variable speed wind generator system

Sub-systems	Distribution parameters		Sub-system parameters		Reliability
WT rotor	θ_{tp}	β_{tp}	P_{ciw}	P_{cow}	R_{tp}
	1560.58	1.422	77	3000	0.9068
box	θ_{gb}	β_{gb}	$\omega_{wt,s}$	$\omega_{wt,m}$	R_{gb}
	13.73	3.33	4.1	18.4	0.9107
Generator	θ_g	β_g	$P_{g,ciw}$	$P_{g,cow}$	R_g
	1354	1.4142	73	2850	0.9266
IPE system	θ_{IPE}	β_{IPE}	τ_{ciw}	τ_{cow}	R_{IPE}
	1.158	2.658e-5	0.0202e-4	0.4821e-4	0.8144

higher than the other operational modes because during this mode all DG units are operating and they are in parallel. Moreover, this mode has two generation sources which are assumed as highly reliable in power generation and supply. On the other hand, MSR for an isolated micro-grid with WPGS varies depending on the number of WT systems operating in the WPGS. It is worth mentioning that in an isolated micro-grid, all WTs in the WPGS cannot be used because of the stability issue. This is because all the WTs in the WPGS consume reactive power from the utility grid during the grid connected mode; however, in an isolated mode there is no such reactive power generation source to provide sufficient reactive power for all nine WTs. Thus the reliability calculation is carried out for the different number

Table 6.2: Reliability results of distributed generation units

DG units	Reliability
WT system	R_{wts}
	0.6232
WPGS	R_{WPGS}
	0.9998
HGU	R_{HGU}
	0.85
SU	R_{SU}
	0.8144
Utility grid	R_{UG}
	0.85

Table 6.3: Reliability results of micro-grid system

Micro-grid operational modes	Reliability
Grid connected mode	$R_{MSR_{M1}}$
	.9999
Isolated micro-grid with WPGS:	$R_{MSR_{M2}}$
number of WT systems in WPGS (1, 2, 3, 4)	0.94, 0.97, 0.99, 0.997
Isolated micro-grid without WPGS	$R_{MSR_{M3}}$
	0.97

of WT systems in the WPGS. The reliabilities of generating and supplying power during the operating mode of an isolated micro-grid with WPGS are found to be 0.94 ((1 WTs in WPGS)), 0.97 (2 WTs in WPGS), 0.99 (3 WTs in WPGS) and 0.997 (4 WTs in WPGS). This result indicates that a higher reliability of generating and supplying power during this operating mode requires more WTs to be connected to the system. The reliability of the micro-grid without WPGS is also calculated as 0.97.

Table 6.4: Reliability results of the micro-grid system: Battle Harbour

Micro-grid operational modes	Reliability
Grid connected mode	$R_{MSR_{M1}}$
	.98
Isolated micro-grid with WPGS:	$R_{MSR_{M2}}$
number of WT systems in WPGS (1, 2, 3, 4)	0.92, 0.95, 0.98, 0.998
Isolated micro-grid without WPGS	$R_{MSR_{M3}}$
	0.97

6.5 Reliability Comparison of the Proposed Micro-Grid System

The reliability of generating and supplying power using the proposed micro-grid system is compared by assuming that this micro-grid can potentially be operated in various locations in Newfoundland and Labrador. The selection of the site for the micro-grid system is based on the availability of primary energy sources. Some of the locations which are considered in this study are Battle Harbour, St. Lawrence and Bonavista [71, 121]. The wind data for these three selected sites are collected from the Environment Canada website. In order to evaluate the reliability of the proposed micro-grid system for the selected sites, the procedure described in Section 1.3 is followed. The reliability calculation results obtained through numerical simulation in Matlab are presented in Tables 6.4, 6.5 and 6.6 for Battle Harbour, St. Lawrence and Bonavista, respectively.

It can be seen from the results that the MSR during grid connected mode is higher than the other operational modes for all three sites. This is because of the operation of all DG units operating in parallel in the micro-grid system. In addition, this operating mode has two generation sources which are assumed as highly

Table 6.5: Reliability results of the micro-grid system: St. Lawrence

Micro-grid operational modes	Reliability
Grid connected mode	$R_{MSR_{M1}}$
	.989
Isolated micro-grid with WPGS:	$R_{MSR_{M2}}$
number of WT systems in WPGS (1, 2, 3, 4)	0.928, 0.959, 0.988, 0.9998
Isolated micro-grid without WPGS	$R_{MSR_{M3}}$
	0.97

Table 6.6: Reliability results of the micro-grid system: Bonavista

Micro-grid operational modes	Reliability
Grid connected mode	$R_{MSR_{M1}}$
	.991
Isolated micro-grid with WPGS:	$R_{MSR_{M2}}$
number of WT systems in WPGS (1, 2, 3, 4)	0.94, 0.965, 0.992, 0.999
Isolated micro-grid without WPGS	$R_{MSR_{M3}}$
	0.97

reliable in power generation and supply. The MSR during the operating mode of an isolated micro-grid with WPGS varies for all three sites. This is because of the variation and the level of uncertainty in wind speed data for a particular site. The variation in MSR during the operating mode of an isolated micro-grid with wind power generation is also observed considering different numbers of wind turbines connected to the system. Such a variation in reliability is found for all three sites selected in this study. However, the reliability of the micro-grid system without WPGS is calculated as 0.97 for all three sites. This result comes from the fact that the reliability of generating and supplying power using the HGU and the SU are assumed to be the same at all three sites. The MSR reliability comparisons for these three sites provide the confidence level of generating and supplying reliable power

using a micro-grid system comprised of renewable micro-generation such as wind and hydro along with an inverter interfaced storage unit.

6.6 Summary

The reliability of generating and supplying reliable power by a micro-grid system comprised of variable-speed wind generator units is investigated and presented in this chapter. This investigation is carried out on a proposed micro-grid system. The mathematical model of micro-grid system reliability is derived and presented based on the best-fit probability distribution function. In addition, the reliability model of various sub-systems in a variable-speed wind generator unit is developed considering the impacts of stochastically varying wind speed. The developed micro-grid system reliability model is implemented through Monte Carlo simulation using the Matlab software tool. The reliability results obtained through simulation are presented and discussed. The reliability performance of generating and supplying reliable power with the proposed micro-grid system during its various operational modes is found encouraging and acceptable.

Chapter 7

Conclusions

Large scale integration and the diverse nature of micro-generation in a micro-grid system make the reliable operation and control of the system a remarkable challenge in isolated applications. A micro-grid system comprised of renewable micro-generation, wind and hydro, has been investigated in this work covering key aspects such as the system's dynamic behaviour analysis, continuous power balance between generation and load, micro-grid test setup and reliability assessment.

7.1 Concluding Summary

A micro-grid system consisting of renewable power sources was selected for this work based on a case study on the island of Newfoundland in the province of Newfoundland and Labrador, Canada. The major potential micro-generation in this system was a small hydro generation unit and a wind farm based on doubly-fed induction generator wind turbines. It was shown that in order to achieve stable and reliable operation of the selected system in a micro-grid, a pumped hydro storage

unit was a good candidate, along with fast and accurate power balance schemes. Therefore, a combination of a small hydro generator, variable speed wind power generator and a hydro based storage unit, which is a new system for a micro-grid operation, was introduced in this work.

Various issues related to the operation and control of the proposed micro-grid system were outlined and some of the issues were addressed throughout the thesis. An analytical approach was considered to identify the main operational modes of a micro-grid system comprised of renewable micro-generation. An analysis of the micro-grid system behaviour was carried out to observe the dynamic characteristics of the micro-generation and the micro-grid system as a whole. For this objective, an integrated dynamic model of the micro-grid system was developed. This model also includes the dynamic models of various systems and sub-systems of micro-generation within the system. A dynamic simulation of the developed micro-grid system model was carried out with the Matlab/Simulink software tool. It was found through simulation study that there were a number of key issues that affect the operation and control of the selected system in isolated micro-grid applications. Thus the research focus was on addressing the issues in order to achieve reliable and stable operation for the identified operating modes of the micro-grid contains renewable energy sources.

The control schemes during the operating modes of an isolated micro-grid with wind power generation and isolated micro-grid without wind power generation were developed. An active power controller was developed for the operating mode of an isolated micro-grid with wind power generation. The objective of this controller was to maintain an active power balance between the micro-grid generation and load. This objective was met by storing and shaping the excess power

of the micro-grid in a continuous fashion. The excess power was stored by pumping water to the upper reservoir, and the shaping was accomplished by dumping power to the dump or heating load. It was found that the developed active power controller is capable of maintaining a power balance between generation and load during the utility grid disconnection and in the subsequent operation of the micro-grid system. In addition, a conventional governor control based hydro storage unit was studied during the operating mode of an isolated micro-grid without wind power generation system. Although this control approach showed satisfactory performance, an effective and fast power adjustment by this control was limited. Therefore, a power flow based inverter interfaced control scheme for micro-grids in stand-alone and utility grid-connected modes of operation was developed. The power flow analysis was utilized to determine command values of active and reactive power for both generation and delivery under various changes in operating conditions. These command values were employed to calculate the reference current for the current controller of the inverter in this scheme. It was shown that the performance results of this control scheme for micro-grid systems demonstrate good abilities to initiate control actions, to quickly and effectively maintain stable and reliable operation of the micro-grid for various modes of operation, and to deal with changes in its operating conditions. The accuracy of this control scheme was also observed from the micro-grid system frequency response and bus voltages through all tested operating conditions, where close-to-unity V_d and close-to-zero V_q values were maintained.

An experimental investigation was carried out in order to verify the conclusions reached through simulation results. A scaled version micro-grid test setup (MTS) comprised of renewable micro-generations was developed. In order to re-

flect the variable speed operation of a wind turbine system, a wind turbine emulator was developed and incorporated in the MTS. An optimum power controller was also employed in the wind turbine emulator (WTE) to ensure the maximum power extraction from the wind. The implementation procedure and the testing of the developed micro-grid controllers utilizing this MTS was also described. The active power controller based on the alternating voltage control concept was tested for the operating mode of an isolated micro-grid with wind power generation. The experimental performance showed that the active power controller is able to maintain the power balance between generation and load in an isolated micro-grid operation in a continuous fashion. Experimental testing was also performed for an inverter interfaced storage control scheme that combines the power flow solution and current reference control of the inverter during the operating mode of an isolated micro-grid without wind power generation. It was found from the test results that this controller has the significant capability to maintain fast and accurate power balance in the system while the micro-grid needs to be supplied by the storage unit.

The adequacy of generating and supplying power using a micro-grid system comprised of renewable micro-generations was assessed through reliability analysis. The reliability models of various sub-systems in a variable-speed doubly-fed induction generator wind turbine were derived considering the effects of stochastically varying wind speed. Variable operating conditions of the wind energy conversion system (WECS) and the temperature were employed as the stress factors in the developed reliablity model. Also, the micro-grid system reliability model was developed based on the system reliability concept. A Monte Carlo simulation approach was taken to implement the developed models using the Matlab software

tool. It was found that the reliability performance of generating and supplying reliable power using the proposed micro-grid system during its various operational modes was encouraging (Tables 6.3, 6.4, 6.5 and 6.6). The developed model was also utilized to verify the reliability performance of the micro-grid system in various sites in Newfoundland and Labrador. It was shown that a micro-grid system consisting of renewable power sources had the ability to provide reliable power, if the system was installed in resourceful sites.

7.2 Contributions

Major contributions and achievements of this work toward developing and testing a micro-grid system based on renewable micro-generation are summarized as follows:

A. Micro-grid based on renewable micro-generation:

The combination of micro-generation in the existing micro-grid systems, their control strategies and the analysis of a case study in Newfoundland were investigated. As a result of this assessment, a micro-grid system comprised of renewable micro-generation, a variable speed wind turbine generator and a small hydro unit was selected. The dynamic behaviour of this micro-grid system was analysed using modeling and simulation with the Matlab/Simulink tool considering the variation in voltage and frequency of the system under the identified operating conditions.

The major contributions of the work include: a micro-grid system comprised of renewable micro-generation to maximize renewable power utilization, reduce fossil fuel dependency and transmission losses; addressing the challenging issue

of reliable and stable operation of the proposed system in isolated micro-grid applications. The publications resulting from these contributions are:

- R. Ahshan, M. T. Iqbal, George K. I. Mann, and John E. Quaicoe, "Modeling and Analysis of a Micro-grid System Powered by Renewable Eenergy Sources", Accepted, The Open Renewable Energy Journal, 2012.

- R. Ahshan, M. T. Iqbal, George K. I. Mann, and John E. Quaicoe, "Micro-grid System Based on Renewable Power Generation Units", in Proc. IEEE Canadian Conf. on Electrical and Computer Engineering, CCECE'2010, Calgary, AB, Canada, 2010.

- R. Ahshan, M. T. Iqbal, George K. I. Mann, and John E. Quaicoe, "Simulation of a 27 MW Wind Farm in Newfoundland", in Proc. IEEE Newfoundland Electrical and Computer Engineering Conf., NECEC'2010 St. John's, NL, Canada, 2010.

- R. Ahshan, M. T. Iqbal, George K. I. Mann, and John E. Quaicoe, "Wind, Hydro and Pumped Hydro Storage Based Micro-grid for Newfoundland", in Proc. IEEE Newfoundland Electrical and Computer Engineering Conf., NECEC'2010 St. John's, NL, Canada, 2010.

B. Active Power Controller:

The system was controlled during the operating mode of an isolated micro-grid with wind power generation to maintain the power balance between the generation and load. A combination of power storing and power shaping concepts was employed in the developed active power control scheme. The stable micro-grid system frequency during the grid disconnection and in subsequent operation is a

result of the combined action of storing and constantly smoothing the excess power available during this operating mode. Furthermore, the experimental testing was carried out with an MTS in the laboratory to verify the performance of the developed active power controller.

The major contributions of the work include: the introduction of new control concepts for the stable and reliable operation of the micro-grid system; design of an active power controller based on an alternating voltage control technique; the performance analysis of the controller for the operating mode of an isolated micro-grid with wind power generation; and the verification of the controller performance on the basis of experimentation. The following publications which arose from these contributions are:

- R. Ahshan, M. T. Iqbal, George K. I. Mann, and John E. Quaicoe, "Design and Performance Testing of an Active Power Controller for the Operation of a Micro-grid", Under review with the Renewable Energy Journal, 2012.

- R. Ahshan, M. T. Iqbal, George K. I. Mann, and John E. Quaicoe, "Frequency Regulation for a Micro-grid System Based on Renewable Power Generation", accepted, The Open Renewable Energy Journal, 2011.

- R. Ahshan, M. T. Iqbal, George K. I. Mann, and John E. Quaicoe, "Experimental Investigation of a Micro-grid Power Controller", in Proc. IEEE Electrical Power and Energy Conference, EPEC'2011, Winnipeg, MB, Canada, 2011.

C. Power Flow based Micro-Grid Controller:

A combination of power flow and current control inverter was investigated for the operation of the proposed micro-grid system. The command power signals for the

micro-generation/inverter were the result of the $d-q$-axis power flow calculation of the micro-grid system. The reference current signal was derived from the command power calculated using power flow. The inverter current controller ensured the reference current flow from micro-generation to the micro-grid. As a result, power balance was maintained in the system during the operating modes of an isolated micro-grid with wind power generation system and an isolated micro-grid without wind power generation system. Moreover, experimental testing was carried out with an MTS in the laboratory to verify the performance of the developed power flow based controller during the operating mode of an isolated micro-grid without wind power generator.

The major contributions of the work include: a novel power flow based micro-grid controller for the stable and reliable operation of the micro-grid system; formulation of the $d-q$-axis power flow; demonstration of command power control through a current control inverter; the performance analysis of the controller for the isolated micro-grid operation; and verification of the controller performance on the basis of experimentation during isolated micro-grid operation without the wind power generator. The publications resulting from these contributions are:

- R. Ahshan, S. Saleh, M. T. Iqbal, and George K. I. Mann, "Development of a Micro-grid Controller Employing a Load Flow Analysis", in Proc. IEEE Electrical Power and Energy Conference, EPEC'2011, Winnipeg, MB, Canada, 2011.

D. Micro-grid Reliability Assessment:

The reliability of generating and supplying power using a micro-grid system consisting of renewable power sources was investigated. The effect of variable oper-

ating conditions on various sub-systems in a wind based micro-generation was incorporated in the developed reliability model of a wind energy conversion system. The reliability models of the micro-grid system under various operating modes were derived based on the system reliability concept. The developed model was applied to evaluate the reliability of generating and supplying power using the proposed micro-grid for different locations in Newfoundland and Labrador.

The major contributions of the work include: a unique approach to model micro-grid system reliability; variable operating conditions and sub-systems reliability model employment in an overall reliability model of a wind energy conversion system; and the quantification of the reliability of the micro-grid system under various operational modes to observe the ability to generate and supply reliable power to the micro-grid load. The publications resulting from these contributions are:

- R. Ahshan, M. T. Iqbal, George K. I. Mann, and John E. Quaicoe, "Reliability Analysis of Micro-grid System Powered by Renewable Energy Sources", Under review with the IEEE Systems Journal, 2012.

- R. Ahshan, M. T. Iqbal, George K. I. Mann, and John E. Quaicoe, "Reliability Assessment of a Micro-grid System", in Proc. IEEE Electrical Power and Energy Conference, EPEC'2011, Winnipeg, MB, Canada, 2011.

7.3 Future Works

A micro-grid system based on renewable micro-generation is a novel way to maximize the utilization of renewable sources as well as to reduce the dependency on fossil fuel generation. However, it is important to point out that this investigation

is not one which has covered all aspects for the reliable, stable and robust operation of the proposed micro-grid, but rather is a starting point for further study. Based on this work, the following can be considered for further investigation in the micro-grid research area.

- Micro-grid system behaviour may be further investigated with the addition of other renewable micro-generation such as ocean and solar power generation. This investigation may explore the additional requirements and the appropriate storage for the selected micro-grid for a particular site. This effort will be worthwhile as important information on a preferred storage system is found.

- A voltage control scheme may be investigated for the operating mode of an isolated micro-grid with wind power generation so that the performance of the system can be analyzed while both the voltage and frequency controllers perform control actions during this operating mode. One aim could be to use the dynamic voltage restorer, and to evaluate the performance in controlling the micro-grid voltage.

- The micro-grid test setup may be improved by developing the hydro generation emulator and employing a back-to-back PWM voltage source converter in the rotor side of the induction generator. As a result the power flow based micro-grid controller could be tested for both the operating mode of an isolated micro-grid with wind power generation and an isolated micro-grid without wind power generation. Moreover, the effectiveness of the power flow based micro-grid controller may be further extended with the increased number of inverter interfaced micro-generation.

- The reliability assessment of the proposed micro-grid system may be improved by employing the reliability model of other micro-generation and sub-systems in the proposed micro-grid. Also the extended investigation may be carried out while other renewable source based micro-generations are added to the micro-grid system.

- Micro-grid protection is also an important research area which is not considered in the present work. Existing and new micro-grid protection techniques may be investigated in order to ensure secure and safe operation of the system.

Bibliography

[1] F. Blaabjerg, R. Teodorescu, M. Liserre and A. V. Timbus, "Overview of Control and Grid Synchronization for Distributed Power Generation Systems", *IEEE Trans. on Industrial Electronics*, Vol. 53, No. 5, pp. 1398–1409, 2006.

[2] T. Ackermann and V. Knyazkin, "Interaction between distributed generation and the distribution network: Operation aspects", *IEEE PES Transmission and Distribution Conference and Exhibition: Asia Pacific*, Yokohama, Japan, Oct. 2002, pp. 1357–1362.

[3] C. Abbey, F. Katiraei, and C. Brothers, "Integration of Distributed Generation and Wind Energy in Canada", Invited paper *IEEE Power Engineering Society General Meeting PES'06 Proceedings*, Montreal, CA, June, 2006, pp. 1–7.

[4] F. Katiraei, C. Abbey and R. Bahry, "Analysis of Voltage Regulation Problem for 25kV Distribution Network with Distributed Generation", *IEEE Power Engineering Society General Meeting PES'06 Proceedings*, Montreal, CA, June, 2006, pp. 8-16.

[5] R. H. Lasseter, "Micro-grids", *IEEE Power Engineering Society Winter Meeting PES'02 Proceedings*, New York, NY, January, 2002, pp. 146–149.

[6] F. Katiraei, M. R. Iravani and P. W. Lehn, "Small Signal Dynamic Model of a Micro-grid including Conventional and Electronically Interfaced Distributed Resources", *IET Gener. Transm. Distrib.*, Vol. 1, No. 3, pp. 369–378, 2007.

[7] M. Shahid Khan and M. R. Iravani, "Supervisory hybrid control of a micro-grid system", *IEEE Electrical Power Conference*, Montreal, CA, Oct. 2007, pp. 20–24.

[8] H. B. Puttgen, P. R. Macgregor and F. C. Lambert, "Distributed generation: semantic hype or the dawn of a new era?", *IEEE Power and Energy Magazine*, Vol. 1, No. 1, pp. 22–29, 2003.

[9] "Expert estimates, based on transmission losses published in Energy Statistics Handbook", *A joint publication of Statistics Canada and Natural Resources Canada.*

[10] T. Ackermann, G. Andersson and L. Soder, "Distributed generation: a definition", *Electric Power Systems Research*, Vol. 57, No. 3, pp. 195–204, 2001.

[11] P. Dondi, D. Bayoumi, C. Haederli, D. Julian and M. Suter, "Network integration of distributed power generation", *Journal of Power Sources*, Vol. 106, No. 1, pp. 1–9, 2002.

[12] N. Jenkins, R. Allan, P. Crossley, and G. Strbac, *Embedded Generation*, Bristol, U.K.: Inst. Elect. Eng., 2002.

[13] N. D. Hatziargyriou and A.P.S. Meliopoulos, "Distributed energy sources: technical challenges", *IEEE Power Engineering Society Winter Meeting PES'02 Proceedings*, New York, NY, January, 2002, pp. 1017–1022.

[14] J. A. P. Lopes, "Integration of dispersed generation on distribution network-impact studies", *IEEE Power Engineering Society Winter Meeting PES'02 Proceedings*, New York, NY, January, 2002, pp. 323–328.

[15] M. H. J. Bollen, *Understanding power quality problems,* Piscataway, NJ: IEEE press, Power Engineering, 2000.

[16] W. EI.-Khattam, M. M. A. Salam, "Distributed generation impact on the dynamic voltage restorer rating", *IEEE Transmission and Distribution Conference and Exposition*, Sept. 2003, pp. 595–599.

[17] C. L. Masters, " Voltage rise the big issue when connecting embedded generation to long 11kV Overhead lines", *Power Engineering Journal*, Vol. 106, No. 1, pp. 1–9, 2002.

[18] K. P. J. Macken, M. H. J. Bollen, R. J. M. Belmans " Mitigation of voltage dips through distributed generation systems", *IEEE Trans. on Industry Applications*, Vol. 40, No. 6, pp. 1686–1693, 2004.

[19] B. Renders, K. D. Gusseme, W. R. Ryckaert, K. Stockman, L. Vandevelde, M. H. J. Bollen, " Distributed generation for mitigating voltage dips in low-voltage distribution grids", *IEEE Trans. on Power Delivery*, Vol. 23, No. 3, pp. 1581–1588, 2008.

[20] M. A. Kashem and G. Ledwich, "Distributed generation as voltage support for single wire earth return system", *IEEE Trans. on Power Delivery*, Vol. 19, No. 3, pp. 1002–1011, 2004.

[21] M. A. Kashem, G. Ledwich, "Multiple distributed generators for distribution feeder voltage support", *IEEE Trans. on Energy Conversion*, Vol. 20, No. 3, pp. 676–684, 2005.

[22] J. W. Smith, D. L. Brooks, "Voltage impacts of distributed wind generation on rural distribution feeders", *IEEE Transmission and Distribution Conference and Exposition*, Sept. 2001, pp. 492–497.

[23] F. Iov, Hansen, F. Blaabjerg, and R. Teodorescu, "Modeling of soft-starters for wind turbine applications", *IEEE Power Quality Proceedings*, January, 2003, pp. 179–182.

[24] I. Boldea, L. Mihet-Popa, F. Blaabjerg, "Wind turbine generator modeling and simulation where rotational speed is the controlled variable", *IEEE Trans. on Industry Applications*, Vol. 40, No. 1, pp. 3–10, 2004.

[25] " IEEE Standard for interconnecting distributed resources with electric power systems", *IEEE Standard 1547*, July 2003.

[26] "IEEE Recommended practice for utility interface of photovoltaic systems", *IEEE Standard 929*, April 2003.

[27] H. Zeineldin, E. F. EI-Saadany and M. M. A. Salama, "Intentional islanding of distributed generation", *IEEE Power Engineering Society General Meeting PES'03 Proceedings*, July, 2003, pp. 2446–2451.

[28] P. Fuangfoo, W. Lee and M. Kuo, "Impact study on intentional islanding of distributed generation connected to a radial transmission system in Thailand's electric power system", *IEEE Trans. on Industry Applications*, Vol. 43, No. 6, pp. 1491–1498, 2007.

[29] M. H. J. Bollen, Y. Yang and F. Hassan, "Integration of distributed generation in the power system–a power quality approach", In *13th International Conference on Harmonics and Quality of Power Proceedings*, 2008, pp. 1–8.

[30] I. T. Papaioannou, A. S. Bouhouras, A.G. Marinopoulos, M. C. Alexiadis, C. S. Demoulias and D. P. Labridis, "Harmonic impact of small photovoltaic systems connected to the LV distribution network", In *5th International Conference on European Electricity Market*, Lisbon, Portugal, 2008, pp. 1–6.

[31] S. A. Gonzalez, R. Garcia-Retegui and M. Benedetti, "Harmonic computation technique suitable for active power filters", *IEEE Trans. on Industry Electronics*, Vol. 54, No. 5, pp. 2791–2796, 2007.

[32] M. Cirrincione, M. Pucci and G. Vitale, "A single-phase DG generation unit with shunt active power filter capability by adaptive neural filtering", *IEEE Trans. on Industry Electronics*, Vol. 55, No. 5, pp. 2093–2110, 2008.

[33] T. Pfajfar, I. Papi, B. Bletterie and H. Brunner, "Improving power quality with coordinated voltage control in networks with dispersed generation", In *9th International Confeence on Eletrical Power Quality and Utilization*, Barcelona, 2007, pp. 1–6.

[34] C. L. Smallwood, "Distributed generation in autonomous and non-autonomous micro-grid", In *IEEE Rural Electric Power Conference Proceedings*, Colorado, USA, 2002, pp. 1–6.

[35] M. Barnes, A. Dimeas, A. Engler, C. Fitzer, N. Hatziargyriou, C. Jones, S. Papathanassiou and M. Vandenbergh, "Micro-grid laboratory facilities", In *IEEE International Conference on Future Power System*, The Netherlands, 2005, pp. 1–6. Also find www.microgrids.eu.

[36] "MICROGRIDS-Large Scale Integration of Micro-Generation to Low Voltage Grids", *EU Contract ENK5-CT-2002-00610, Technical Annex*, May 2002. Also find http://microgrids.power.ece.ntua.gr.

[37] N. Hatziargyriou, H. Asano, R. Iravani and C. Marnay, "Micro-grids- an overview of ongoing research, development and demonstration projects", *IEEE Power and Energy Magazine*, LBNL–62937, pp. 78–94, 2007.

[38] S. Morozumi, "Overview of micro-grid research and development activities in Japan", In *IEEE A Symposium on Micro-grids*, Montreal, 2006, pp. 1–6.

[39] F. Katiraei and M. Iravani, "Transients of a micro-grid system with multiple distributed energy resources", In *IEEE International Conferences on Power Systems Transients*, Montreal, Canada, 2005, pp. 19–23.

[40] "IEEE Recommended Practice for Industrial and Commercial Power System Analysis", *IEEE Standard 399*, 1997.

[41] M. Shahabi, M. R. Haghifam, M. Mohamadian and S. A. Nabavi-Niaki, "Microgrid dynamic performance improvement using a doubly fed induction wind generator", *IEEE Trans. on Energy Conversion*, Vol. 24, No. 1, pp. 137–145, 2009.

[42] R. Majumder, A. Ghosh, G. Ledwich and F. Zare, "Load sharing and power quality enhanced operation of a distributed micro-grid", *IET Renew. Power Gener.*, Vol. 3, No. 2, pp. 109–119, 2009.

[43] C. Nayar, "Remote Area Micro-Grid System using Diesel Driven Doubly Fed Induction Generators, Photovoltaics and Wind Generators", *IEEE International Conferences on Sustainable Energy Technologies ICSET'2008 Proceedings*, Singapore, November, 2008.

[44] L. Ye, H. B. Sun, X. R. Song and L. C. Li, "Dynamic modeling of a hybrid wind/solar/hydro microgrid in EMTP/ATP", *Elsevier, Renewable Energy*, Vol. 39, No. 1, pp. 96–106, 2012.

[45] S. V. Papaefthymiou, E. G. Karamanou, S. A. Papathanassion and M. P. Papadopoulos, "A wind-hydro-pumped storage station leading to high RES penetration in the autonomous island system of Ikaria", *IEEE Trans. on Sustainable Energy*, Vol. 1, No. 3, pp. 163–172, 2010.

[46] P. Piagi, and R. H. Lasseter, "Autonomous control of micro-grids", *IEEE Power Engineering Society General Meeting PES'06 Proceedings*, July, 2006, pp. 8–16.

[47] D. Georgakis, S. A. Papathanasiou, N. Hatziargyriou, A. Engler and C. Hardt, "Operation of a prototype micro-grid system based on micro-sources equipped with fast-acting power electronics interfaces", *IEEE 35th Annual Power Electronics Specialists Conference PESC'04 Proceedings*, Aachen, Germany, June, 2004, pp. 2521–2526.

[48] Y. Kojima, M. Koshio, S. Nakamura, H. Maejima, Y. Fujioka and T. Goda, "A Demonstration Project in Hachinohe: Microgrid with Private Distribution Line", *IEEE International Conference on Systems Engineering Proceedings*, 2007, pp. 1–6.

[49] K. Kawasaki, S. Matsumura, K. Iwabu, N. Fujimuram and T. Iima, "Autonomous Dispersed Control System for Independent Micro-grid", *Journal of Electrical Engineering, Japan*, Vol. 166, No. 1, pp. 1121–1127, 2009.

[50] F. Katiraei and M. R. Iravani, "Power Management Strategies for a Microgrid With Multiple Distributed Generation Units", *IEEE Trans. on Power Systems*, Vol. 21, No. 4, pp. 1821–1831, 2006.

[51] R. Majumder, A. Ghosh, G. Ledwich and F. Zare, "Load Sharing and Power Quality Enhanced Operation of a Distributed Micro-grid," *IET Renew. Power Gener.*, Vol. 3, No. 2, pp. 109–119, 2009.

[52] T. Lin and P. Cheng, "Design of a new cooperative harmonic filtering strategy for distributed generation interface converters in an islanding network," *IEEE Trans. on Power Electronics*, Vol. 22, No. 5, pp. 1919–1927 2007.

[53] R. H. Lasseter, J. H. Eto, B. Schenkman, J. Stevens, H. Vollkommer, D. Klapp, E. Linton, H. Hurtado and J. Roy., "CERTS Microgrid Laboratory Test Bed," *IEEE Trans. on Power Delivery*, Vol. 26, No. 1, pp. 325–332, 2011.

[54] X. Li, Y. Song and S. Han, "Frequency Control in Micro-grid Power System Combined With Electrolyzer System and Fuzzy PI Controller," *Elsevier, Journal of Power Sources*, Vol. 180, No. 1, pp. 468–475, 2008.

[55] I. Şerban and C. Marinescu, "Aggregate load-frequency control of a wind-hydro autonomous micro-grid," *Renewable Energy*, Vol. 36, No. 12, pp. 3345–3354, 2011.

[56] J. A. P. Lopes, C. L. Moreira and A. G. Madureira, "Defining control strategies for micro-grids islanded operation," *IEEE Trans. on Power Systems*, Vol. 21, pp. 916–924, 2006.

[57] H. Dagdougui, R. Minciardi, A. Ouammi, M. Robba and R. Sacile, "A Dynamic Decision Model for the Real-Time Control of Hybrid Renewable Energy Production Systems," *IEEE Systems Journal*, Vol. 4, No. 3, pp. 323–333, 2010.

[58] S. Ahn, J. Park, I. Chung, S. Moon, S. Kang and S. Nam, "Power-Sharing Method of Multiple Distributed Generators Considering Control Modes and Configurations of a Microgrid," *IEEE Trans. on Power Delivery*, Vol. 25, No. 3, pp. 2007–2016, 2010.

[59] L. A. de S. Ribeiro, O. R. Saavedra, S. L. de Lima and J. G. de Matos, "Isolated Micro-Grids With Renewable Hybrid Generation: The Case of Lenis Island", *IEEE Trans. on Sustainable Energy*, Vol. 2, No. 1, pp. 1–11, 2011.

[60] A. Mehrizi-Sani, R. Iravani, "Potential-function based control of a micro-grid in islanded and grid-connected modes", *IEEE Trans. on Power Systems*, Vol. 24, No. 4, pp. 1883–1891, 2010.

[61] S. V. Iyer, M. N. Belur, M. C. Chandorkar, "Analysis and mitigation of voltage offsets in multi-inverter micro-grids", *IEEE Trans. on Energy Conversion*, Vol. 26, No. 1, pp. 354–364, 2011.

[62] A. Elmitwally and M. Rashed, "Flexible operation strategy for an isolated PV-diesel micro-grid without energy storage", *IEEE Trans. on Energy Conversion*, Vol. 26, No. 1, pp. 235–345, 2011.

[63] T. L. Vandoorn, B. Meersman, L. Degroote, B. Renders, L. Vandevelde, "A control strategy for islanded micro-grids with DC-link voltage control", *IEEE Trans. on Power Delivery*, Vol. 26, No. 2, pp. 703–713, 2011.

[64] R. Aghatehrani and R. Kavasseri, "Reactive power management of DFIG wind system in micro-grids based on voltage sensitivity analysis", *IEEE Trans. on Sustainable Energy*, Vol. 2, No. 4, pp. 451–458, 2011.

[65] L. Xu and D. Chen, "Control and Operation of a DC micro-grid with variable generation energy storage", *IEEE Trans. on Power Delivery*, Vol. 26, No. 4, pp. 2513–2522, 2011.

[66] Y. A. I. Mohamed and E. F. El-Saadany, "Adaptive Decentralized Droop Controller to Preserve Power Sharing Stability of Paralleled Inverters in Distributed Generation Micro-grids," *IEEE Trans. on Power Electronics*, Vol. 23, No. 6, pp. 2806–2816, 2008.

[67] A. Llaria, O. Curea, J. Jiménez and H. Camblong, "Survey on microgrids: Unplanned islanding and related inverter control techniques," *Renewable Energy*, Vol. 36, No. 8, pp. 2052–2061, 2011.

[68] Z. Miao, A. Domijan, Jr. and L. Fan, "Investigation of micro-grids with both inverter interfaced and direct AC-connected distributed energy resources," *IEEE Trans. on Power Delivery*, Vol. 26, No. 3, pp. 1634–1642, 2011.

[69] A. K. Basu, S. P. Chaowdhury, S. Chaowdhury, D. Ray, P. A. Crossley, "Reliability Study of A Micro-grid System", *IEEE Trans. on Power Systems*, Vol. 21, No. 4, pp. 1821–1831, 2006.

[70] R. Karki, P. Hu, and R. Billinton, "Reliability Evaluation Considering Wind and Hydro Power Coordination", *IEEE Trans. on Power Systems*, Vol. 25, No. 2, pp. 685–603, 2010.

[71] R. Billinton and D. Huang, "Incorporating wind power in generating capacity reliability evaluation using different models", *IEEE Trans. on Power Systems*, Vol. 26, No. 4, pp. 2509–2517, 2011.

[72] A. P. Leite and C. L. T. Borges, "Probability Wind Farms Generation Model for Reliability Studies Applied to Brazilian Sites", *IEEE Trans. on Power Systems*, Vol. 21, No. 4, pp. 1493–501, 2006.

[73] X. Liu, A. A. Chowdhury and D. O. Koval, "Reliability Evaluation of a Wind-diesel-battery Hybrid Power System", *IEEE Industrial and Commercial Power Systems Technical Conference ICPS 2008*,Clearwater Beach, FL, May 2008.

[74] L. Wang and C. Singh, "Adequacy Assessment of Power-generating Systems Including Wind Power Integration Based on Ant Colony System Algorithm", *IEEE Lausanne Power Tech*,Lausanne, Switzerland, July 2007.

[75] F. A. Bhuiyan and A. Yazdani, "Reliability Assessment of a Wind-Power System With Integrated Energy Storage", *IET Renewable Power Generation*, Vol. 4, Issue. 3, pp. 211–220, 2010.

[76] J. Choi, J. Park and M. Shahidehpour, "Probabilistic Reliability Evaluation of Composite Power Systems Including Wind Turbine Generators", In *IEEE International Conference on Probabilistic Method Applied to Power Systems*, pp. 802–807, Singapore 2010.

[77] F. Vallee, J. Lobry and O. Deblecker., "System Reliability Assessment Method for Wind Power Integration", *IEEE Trans. on Power Systems*, Vol. 23, No. 3, pp. 1288-1297, 2008.

[78] A. M. L. D. Silva and L. A. F. Manso, "Application of Monte Carlo Simulation to Generating System Well-being Analysis Considering Renewable Sources", In *IEEE International Conference on Probabilistic Method Applied to Power Systems*, pp. 439–444, 2004.

[79] K. Xie, Z. Jiang and W. Li, "Effect of wind speed on wind turbine power converter reliability", *IEEE Trans. on Energy Conversion*, Vol. 27, No. 1, pp. 96-104, 2012.

[80] J. Wen, Y. Zheng and F. Donghan, "A Review on Reliability Assessment for Wind Power," *Renewable and Sustainable Energy Reviews*, Vol. 13, pp. 2485–2494, 2009.

[81] M. Arifujjaman, "Performance and Reliability Comparison of Grid Connected Small Wind Turbine Systems," *Ph.D. Thesis*, Memorial University, Canada, 2010.

[82] C. Schauder and H. Mehta, "Vector analysis and control of the advanced static VAR compensators", *IEE Proceedings*, Singapore, July, pp. 299–306, 1993.

[83] J. G. Slootweg, S.W.H. De Haan, H. Polinder and L. W. Kling, "General Model for Representing Variable Speed Wind Turbines in Power System Dynamics Simulations, *IEEE Trans. on Power Systems*, Vol. 18, No. 1, pp. 144–151, 2003.

[84] S. Heier, *Grid Integration of Wind Energy Conversion System*, 2^{nd} Edition, Wiley-Chicester, U.K, 2006.

[85] P. C. Krause, O. Wasynczuk and S. D. Sudhoff, *Analysis of Electric Machinery and Drive Systems*, 2^{nd} Edition, IEEE Press, 2002.

[86] M. G. Simoes and F. A. Farret, *Alternative Energy Systems: Design and Analysis with Induction Generator*, 2^{nd} Edition, CRC Press, 2008.

[87] IEEE Working Group on Prime Mover and Energy Supply Models for System Dynamic Performance Studies, *Hydraulic turbine and turbine control models for dynamic studies, IEEE Trans. on Power Systems*, Vol. 7, No. 1, pp. 167–179, 1992.

[88] "Recommended Practice for Excitation System Models for Power System Stability Studies", *IEEE Standard 421.5*, August 1992.

[89] "MATLAB/SIMULINK 2008b User Guide Manual", *SimPowerSystems for use with simulink.*

[90] M. J. Khan and M. T. Iqbal, "Analysis of a Small Wind-Hydrogen Stand-Alone Hybrid Energy System", *Applied Energy*, Vol. 86, No. 11, pp. 2429–2442, 2009.

[91] "Mechanical Operating and Maintenance ", *Manual V90 - 3.0 MW, VCRS 60 Hz-Class II*, Item no.: 964106.R00, 2007.

[92] A. Gaillard, P. Poure, S. Saadate and M. Machmoum, "Variable Speed DFIG Wind Energy System for Power Generation and Harmonic Current Mitigation", *Elsevier, Renewable Energy*, Vol. 34, No. 6, pp. 1545–1553, 2009.

[93] F. Katiraei, M. R. Iravani and P. W. Lehn, "Micro-grid autonomous operation during and subsequent to islanding process", *IEEE Trans. on Power Delivery*, Vol. 20, No. 1, pp. 248–257, 2005.

[94] S. S. Choi and R. Larkin, "Performance of an autonomous diesel-wind turbine power system", *Journal of Electric Power System Research*, Vol. 33, No. 2, pp. 87–99, 1995.

[95] L. N. Hannett and B. Fardanesh, "Field test to validate hydro-turbine governor model structure and parameters", *IEEE Trans. on Power Systems*, Vol. 9, No. 4, pp. 1744–1751, 1994.

[96] I. Kamwa, D. Lefebvre and L. Loud, "Small signal analysis of hydro-turbine governors in large interconnected power plant", *IEEE Power Engineering Society Winter Meeting*, Vol. 2, pp. 1178–1183, 2002.

[97] M. H. Rashid, "Power Electronics: Circuits, devices and applications," *3rd Edition, Prentice-Hall*, India, New Delhi-2005.

[98] P. L. Dandeno, P. Kundur and J. P. Bayne, "Hydraulic unit dynamic performance under normal and islanding conditions-analysis and validation", *IEEE Trans. on Power Apparatus and Systems*, Vol. 9, No. 6, pp. 2134–2143, 1978.

[99] M. Dai, M. N. Marwali, J. W. Jung and A. Keyhani, "Power Flow Control of a Single Distributed Generation Unit," *IEEE Trans. on Power Electronics*, Vol. 23, No. 1, pp. 343–352, 2008.

[100] L. Wang, K. Wang, W. Lee and Z. Chen, "Power-Flow Control and Stability Enhancement of Four Parallel-Operated Offshore Wind Farms Using a Line-Commutated HVDC Link," *IEEE Trans. on Power Delivery*, Vol. 25, No. 2, pp. 1190–1202, 2010.

[101] X. H. Wu, S. K. Panda and J. X. Xu, "Analysis of the Instantaneous Power Flow for Three-Phase PWM Boost Rectifier Under Unbalanced Supply Voltage Conditions," *IEEE Trans. on Power Electronics*, Vol. 23, No. 4, pp. 1679–1691, 2008.

[102] F. Milano, Continuous Newtons Method for Power Flow Analysis, *IEEE Trans. on Power Systems*, Vol. 24, No. 1, pp. 50–57, 2009.

[103] M. Geidl, and G. Andersson, "Optimal Power Flow of Multiple Energy Carriers," *IEEE Trans. on Power Systems*, Vol. 22, No. 1, pp. 145–155, 2007.

[104] M. K. Ghartemani and H. Karimi, "Processing of Symmetrical Components in Time-Domain," *IEEE Trans. on Power Systems*, Vol. 22, No. 2, pp. 572579, 2007.

[105] A. K. Jain, A. Behal, X. T. Zhang, D. M. Dawson and N. Mohan, "Nonlinear Controllers for Fast Voltage Regulation Using STATCOMs, *IEEE Trans. on Control System Technology*, Vol. 12, No. 6, pp. 827–842, 2004.

[106] X. Yuan, F. Wang, D. Boroyevich, Y. Li, and R. Burgos, "DC-link Voltage Control of a Full Power Converter for Wind Generator Operating in Weak-Grid Systems," *IEEE Trans. on Power Electronics*, Vol. 24, No. 9, pp. 2178–2192, 2009.

[107] R. Teodorescu and F. Blaabjerg, "Flexible control of small wind turbines with grid failure detection operating in stand-alone and grid-connected mode," *IEEE Trans. on Power Electronics*, Vol. 19, No. 5, pp. 1323–1332, 2004.

[108] S. K. Chung, "Phase-locked loop for grid-connected three-phase power conversion systems", In *IEE Electrica Power Applications*, pp. 213–219, 2000.

[109] M. Liserre, A. Dell Aquila and F. Blaabjerg, "Design and control of a three phase rectifier under non-ideal operating conditions", In *IEEE 37th Industrial Application Society Meeting IAS'02*, pp. 1181–1188, 2002.

[110] H. M. Kojabadi, L. Chang, T. Boutot, "Development of a novel wind turbine simulator for wind energy conversion systems using an inverter-controlled in-

duction motor", *IEEETrans. on Energy Conversion*, Vol. 19, No. 3, pp. 547–552, 2004.

[111] R. Ahshan, M. T. Iqbal and George K. I. Mann , "Controller for a small induction-generator based wind turbine", *Applied Energy*, Vol. 85, No. 4, pp. 218–227, 2008.

[112] F. Castro Sayas and R. N. Allan, "Generation availability assessment of wind farms", In *IEEE Gener. Trans. Distrib. Proceedings*, 1996.

[113] R. Teodorescu, F. Iov, and F. Blaabjerg, "Flexible development and test system for 11 kw wind turbine", In *IEEE 34th Power Electronics Specialist Conference PESC'03*, pp. 67–72, 2003.

[114] J. Wen, Y. Zheng and F. Donghan, "A Review on Reliability Assessment for Wind Power," *Renewable and Sustainable Energy Reviews*, Vol. 13, pp. 2485–2494, 2009.

[115] C. E. Ebeling, "An Introduction to Reliability and Maintainability Engineering," *McGraw Hill*, Boston, 1997.

[116] S. Vittal and M. Teboul, "Performance and Reliability Analysis of Wind Turbines using Monte Carlo Methods based on System Transport Theory", In *Conference Proceedings on Structural Dynamics and Materials*, pp. 1–8, Austin, Texas, USA, 2005.

[117] F. F. Oettinger, D. L. Blackburn and S. Rubin, "Thermal Characteristics of Power Transistors," *IEEE Trans. on Reliability*, Vol. 23, Issue. 8 pp. 831–838, 1976.

[118] F. Casanellas, "Losses in PWM Inverter Using IGBT's", *IEE Electric Power Application*, Vol. 141, Issue. 5, pp. 235–239, 1994.

[119] M. H. Bierhoff, and F. W. Fuchs, "Semiconductor Losses in Voltage Source and Current Source IGBT Converters Based on Analytical Derivation", *IEEE Power Electrics Specialist Conference*, Vol. 4, pp. 2836–2842, Germany, 2004.

[120] L. K. Mestha and P. D. Evans, "Analysis of On-state Losses in PWM Inverter", *IEE Proceedings*, Vol. 136, Issue. 4, 1989.

[121] M. T. Iqbal and N. Bose, "Sizing a hybrid power system for Battle Harbour Island in Labrador", *Wind Engineering*, Vol. 31, Issue. 4, pp. 233–245, 2007.

[122] K. Ogata, "Modern Control Engineering," *Prentice Hall*, New Jersey, 1997.

[123] N. W. A. Lidula and A. D. Rajapakse, "Micro-grids research: A review of experimental micro-grids and test systems", *Renewable and Sustainable Energy Reviews*, Vol. 15, pp. 186–202, 2011.

Appendix A

The Micro-Grid System Parameters

The major sub-systems' parameters of a renewable sources based micro-grid system are given below:

A.1 Data of Micro-Grid Transmission Lines and Transformers

Table A.1: Fermeuse Micro-Grid System: Transmission Lines and Transformers

Component	V [kV]	Z [Ω]	S [MVA]
TL1	66	$0.0416 + j0.0663$	40
TL2	12.5	$0.0374 + j0.3741$	40
TL3	66	$0.002 + j0.0032$	50
TL_d	12.5	$0.00072 + j0.0012$	40
TL_{WT}	12.5	$0.00006 + j0.000096$	5
T1	6.9/66	$0.0854 + j0.8541$	10
T2	66/12.5	$0.0493 + j0.493$	5
T3	66/12.5	$0.061 + j0.62$	4
T4	66/12.5	$0.05 + j0.5$	40
T_W	1/12.5	$0.006 + j0.0625$	5

The single line diagram of the micro-grid system is shown in Figure 3.1. The data for the transmission lines and transformers are listed in Table A.1.

A.2 Wind Turbine Data

The micro-grid system is comprised of nine identical WTs. The manufacturer parameters of a WT for the rating of 3 MW is presented in Table A.2.

Table A.2: Wind turbine specification

Rated power	3MW
Rotor diameter	90m
Nominal speed	16.1 RPM
Rotor speed range	9.9-18.4 RPM
Number of blades	3
Blade length	44m
Gear ratio	1:109
Cut-in wind speed	4m/s
Cut-out wind speed	25m/s
Rotational direction and orientation	Clockwise upwind

A.3 Doubly-Fed Induction Generator Data

Each WT in the micro-grid system is based on a doubly-fed induction generator. The parameters for the induction generator are listed in Table A.3.

A.4 Synchronous Generator Data

A synchronous generator is used in the hydro generation unit. The parameters of a synchronous machine for the ratings of 7 MVA are given in Table A.4.

Table A.3: Induction generator paramters

Type	Asynchronous with wound rotor
Nominal power	3MW
Voltage	1000V
Rated speed	1758 RPM
Number of poles	4
Total inertia constant	3.02s
Friction coefficient	0.01
r_s, r'_r	2.35mΩ, 1.67mΩ
$L_{ls}. L'_{lr}$	0.151H, 0.1379H
L_m	2.47H

Table A.4: Synchronous generator paramters

Nominal power	7 MVA	2 MVA
Voltage	6.9 kV	6.9 kV
Rated speed	360 RPM	360 RPM
Number of poles	20	20
r_{ss}	0.02854 pu	0.00175 pu
x_d	1.305 pu	0.32 pu
x_q	0.474 pu	0.148 pu
x'_d	0.296 pu	0.0355 pu
x''_d	0.252 pu	0.027 pu
x''_q	0.243 pu	0.051 pu
x'_{ls}	0.18 pu	0.0268 pu
H	3.1 s	1.035 s
T'_d	3.34 s	2.1 s
T''_d	0.013 s	0.017 s
T''_q	0.052 s	0.01 s

Appendix B

Schematic Diagrams of the Matlab/Simulink Models

This appendix provides the schematic diagrams of the Matlab/Simulink models presented in this work for different operating modes of a micro-grid system that is comprised of renewable micro-generations.

B.1 The Micro-Grid System

The Matlab/Simulink model schematic of the renewable micro-generation based micro-grid system is shown in Figure B.1. Each wind turbine block, WTn (where n=1, 2, ...9.) contains the model of wind turbine rotor, induction generator, and their control. Hydro generation unit block, HGU, contains a hydro turbine, synchronous generator and govornor and excitation control models.

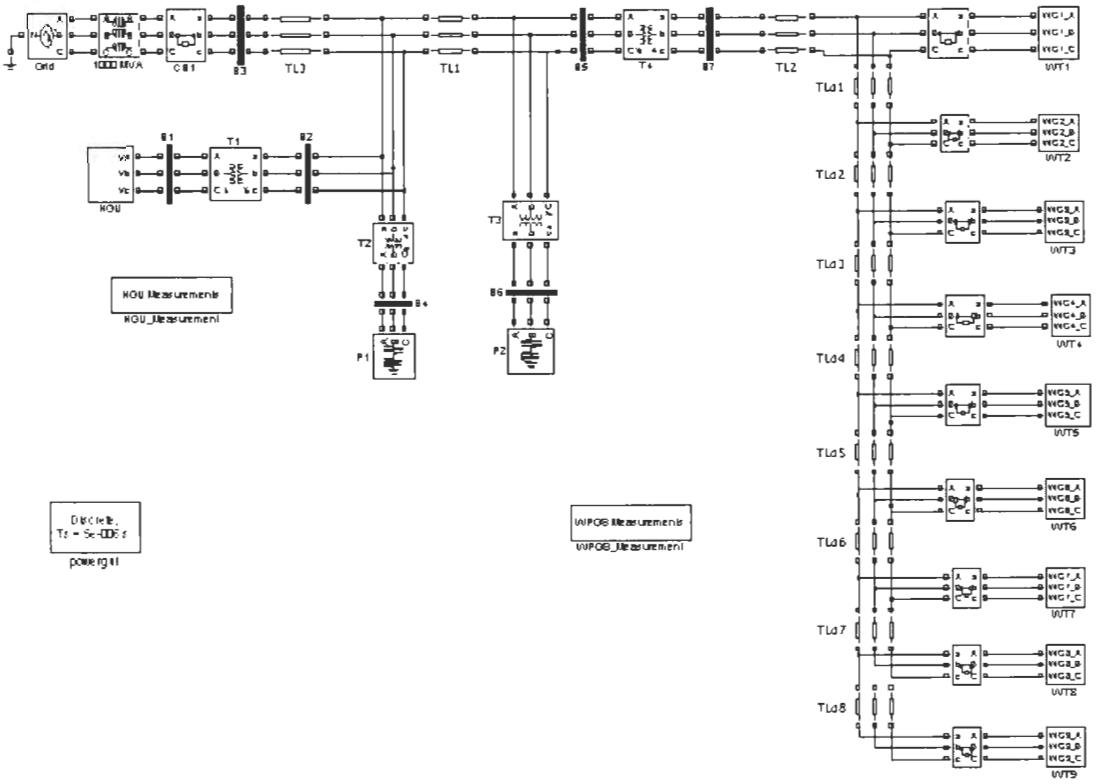

Figure B.1: The micro-grid system shown in Figure 3.1

B.2 The Micro-Grid System With Active Power Controller

Figure B.2 shows the Matlab/Simulink model schematic of the renewable micro-grid system along with an active power controller model. The active power controller block contains the model of a phase locked loop, a firing pulse generation unit, power variation coefficient, control signal and firing angle estimator.

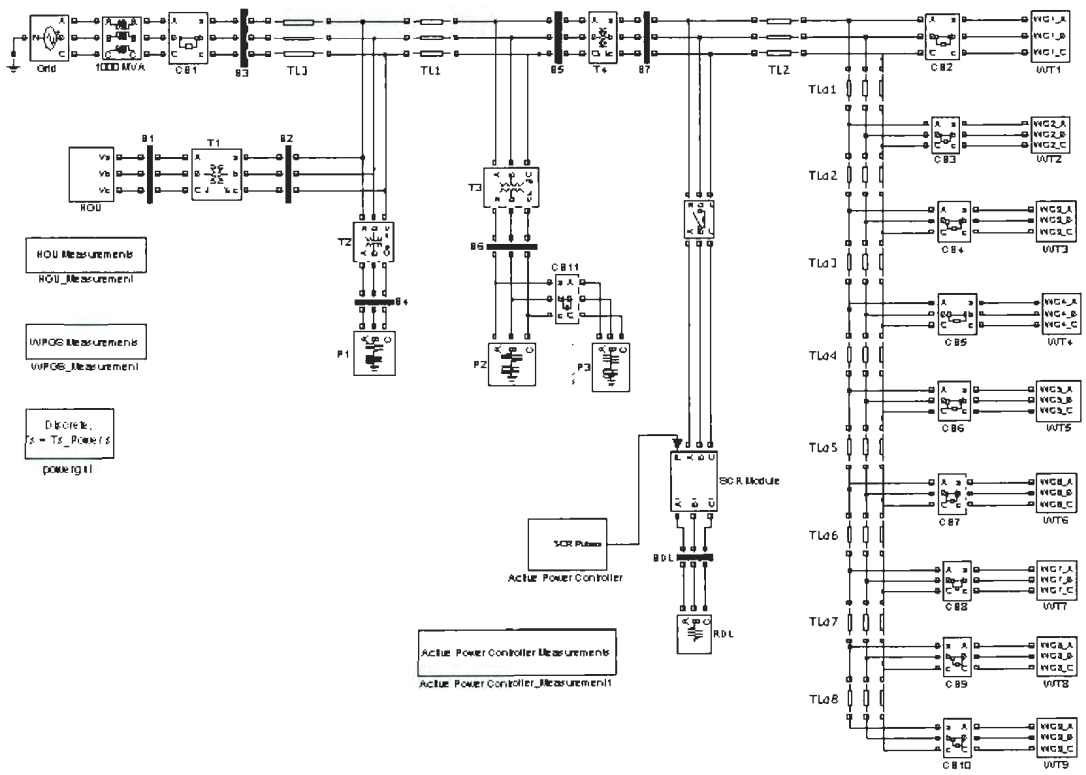

Figure B.2: Active power controller in the study micro-grid system

B.3 The Micro-Grid System With Storage System Controller

The Matlab/Simulink model schematic of a micro-grid system based on renewable micro-generations along with the storage control is shown in Figures B.3 and B.4. A hydro storage unit that is operated using conventional governor-excitation control is used to maintain the micro-grid voltage and frequency, and is presented in Figure B.3. The HSU block contains the model of the hydro turbine, synchronous generator and control of governor and excitation system. Figure B.4 shows the model of the micro-grid system along with a load flow based micro-grid controller

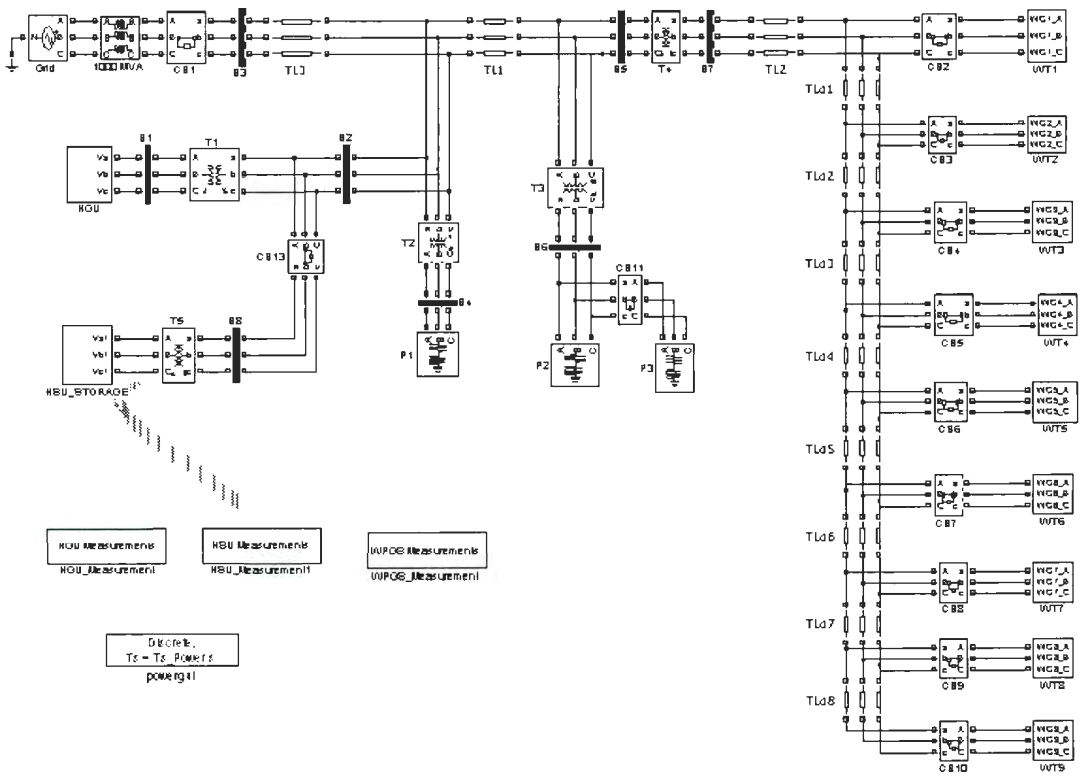

Figure B.3: Hydro Storage System in the study micro-grid system

for an inverter interfaced storage unit. The inverter interface storage unit block contains the model of the current control inverter presented in Figure 4.38. The power flow block contains the model of the $d-q$-axis power method formulated in section 4.4.2.

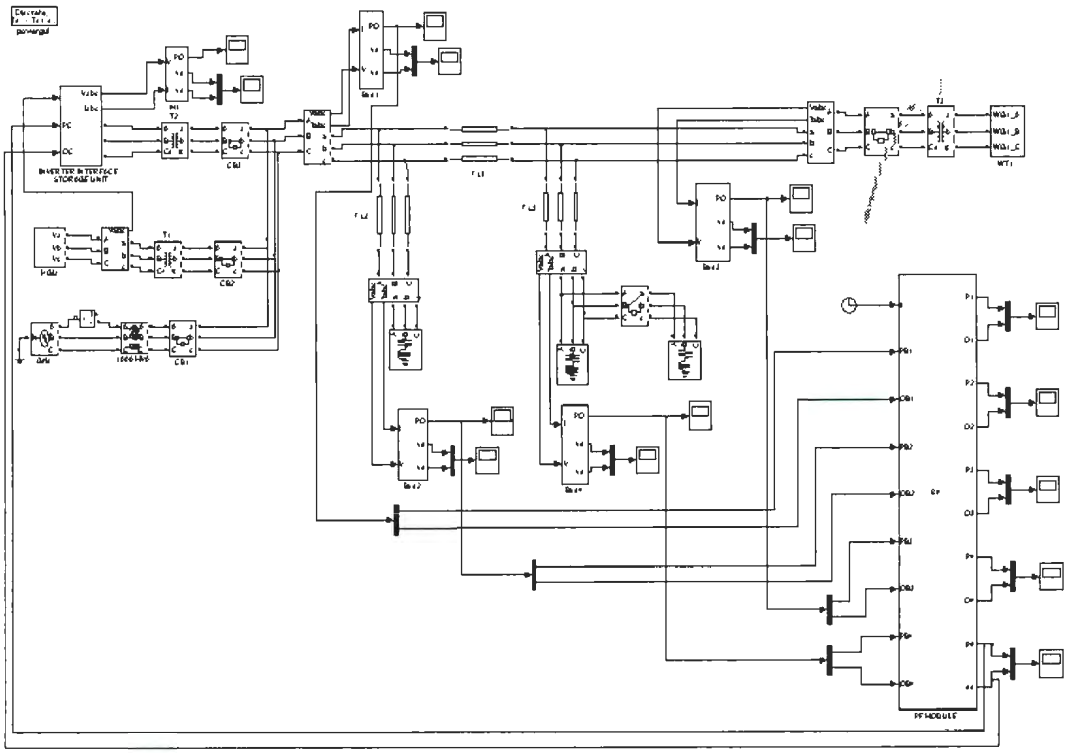

Figure B.4: Power flow based micro-grid controller

Appendix C

Micro-Grid Test Setup Parameters

This appendix provides the nameplate data for various sub-systems in the micro-grid test setup.

C.1 Separately-Excited DC Motor for Wind Turbine Emulator

The nameplate information for the separately-excited DC motor used for the wind turbine emulator is given in Table C.1.

Table C.1: Separately-excited DC motor used for wind turbine emulator

Type	DC Working Machine
Rated Power	3.75 kW
Maximum RPM	4000
Full Load Amps.	30
Volts	125
Field Volts	125
Company	Mawdleys Limited
Country	England

C.2 Separately-Excited DC Motor for Hydro Generation Unit

The nameplate information of a separately-excited DC motor that is used to drive the synchronous generator for hydro generator unit is listed in Table C.2.

Table C.2: Separately-excited DC motor used for hydro generation unit

Model No	M253AS-DBZ
Serial No	370-117301
Type	M-1670
Enclosure	OPEN
Rated Power	2.2 kW
Full Load RPM	1750
Full Load Amps.	18
Volts	125
Field Amps.	0.85
Field Volts	125
Ambient ^0C	40
^0C Rise	60
Company	Canron Limited
Country	Canada

C.3 Induction Generator Data

The nameplate information for the induction generator used for the wind turbine generation is listed in the following Table C.3.

Table C.3: Induction generator nameplate parameters

Type	Wound rotor induction generator
Rated Power	2.0 kW
Volt	125/208
RPM	1725
Number of poles	4
Phase	3
Full load current Amps.	8.2
Hertz	60
Rotor Volts	10
Rotor Amps.	8.2
Company	Mawdleys Limited
Country	England

C.4 Synchronous Generator Data

The nameplate information for the synchronous generator used for the hydro generation is listed in the following Table C.4.

Table C.4: Synchronous generator nameplate parameters

Type	SG-1480
Serial No.	360-214-215
Rated Power	2.0 kVA
Volt	125/208
RPM	1800
Phase	3
Amps.	5.5
Hertz	60
Ambient ^0C	40
^0C Rise	60
Company	Canron Limited
Country	Canada

Appendix D

Recursive PID Algorithm

This appendix provides the recursive PID algorithm formulation that is desiged and implemented for the wind turbine emulator.

The time domain PID controller equation can be expressed as [122]

$$\mathrm{u(t)} = \mathrm{K}\left[\mathrm{e(t)} + \frac{1}{\mathrm{T_I}}\int_0^t e(\tau)d\tau + T_D\frac{de(t)}{dt}\right] \tag{D.1}$$

where $u(t)$ is the output of the controller at any instant t, $e(t)$ is the error between expected and actual control variables, K is the gain which is equal to proportional gain of the PID controller, T_I is the integral time of the controller and T_D is the derivative time of the controller.

For small sampling time T_o, the above time domain controller equation can be converted to equivalent discrete form by approximating the integral and derivative term. The digitized form of PID controller equation can be written as

$$\mathrm{u(t)} = \mathrm{K}\left[\mathrm{e(k)} + \frac{\mathrm{T_o}}{\mathrm{T_I}}\sum_{i=0}^{k} e(i-1) + \frac{T_D}{T_o}(e(k) - e(k-1))\right] \tag{D.2}$$

where k is the discrete time step, and $e(k-1)$ is the error occuring in the previous step.

This is a non-recursive control algorithm. However, recursive algorithms are more suitable for programming on computers. Recursive algorithms are characterized by the calculation of the current manipulated variable $u(k)$ based on the previous manipulated variable $u(k-1)$ and correction terms. By considering the previous manipulated variable from k^{th} step, equation (D.2) can written as

$$u(k-1) = K\left[e(k-1) + \frac{T_o}{T_I}\sum_{i=0}^{k-1} e(i-1) + \frac{T_D}{T_o}(e(k) - e(k-1))\right] \tag{D.3}$$

Combining equation (D.2) and (D.3)

$$u(k)-u(k-1) = K\left[e(k) - e(k-1) + \frac{T_o}{T_I}e(k-1) + \frac{T_D}{T_o}(e(k) - 2e(k-1) - e(k-2))\right] \tag{D.4}$$

or

$$u(k) - u(k-1) = p_0 e(k) + p_1 e(k-1) + p_2 e(k-2) \tag{D.5}$$

where

$$p_0 = K(1 + \frac{T_D}{T_o}) \tag{D.6}$$

$$p_1 = K(\frac{T_o}{T_I} - 2\frac{T_D}{T_o} - 1) \tag{D.7}$$

$$p_2 = K\frac{T_D}{T_o} \tag{D.8}$$